University of Southampton

Energy Dispersive EXAFS and Quick EXAFS Studies of Homogeneous Nickel and Palladium Catalysts.

A Thesis submitted for the Degree of Doctor of Philosophy

By

Vijaya Laxmi Kambhampati

Department of Chemistry

July 1998

UNIVERSITY OF SOUTHAMPTON

ABSTRACT

FACULTY OF SCIENCE

CHEMISTRY

Doctor of Philosophy

ENERGY DISPERSIVE EXAFS AND QUICK EXAFS STUDIES OF HOMOGENEOUS NICKEL AND PALLADIUM CATALYSTS.

by Vijaya Laxmi Kambhampati

A study of homogeneous nickel alkene oligomerisation and palladium Heck reaction catalysts using Energy Dispersive EXAFS and Quick EXAFS is described.

Acquisition time and concentration studies were performed on three main nickel catalysts i.e. $Ni(acac)_2$, $NiCl_2(PEt_3)_2$, and $NiBr_2(PEt_3)_2$ in order to find out the best experimental conditions for obtaining data.

Ni-K-edge QUEXAFS was used to perform a time resolved study of the formation of nickel metal particles from a mixture of the $Ni(acac)_2$ catalyst and $AlEt_3$ cocatalyst at room temperature. The study showed a real time change in the white line features of the QUEXAFS spectra as the complex changed from the starting material to give colloidal nickel particles Further analysis of the final spectrum indicated the possible formation of 19 atom nickel metal clusters. At low temperature and in the presence of hex-1-ene, the QUEXAFS data indicated the formation of a mononuclear nickel species with only light atom coordination, possibly a square planar organometallic consisting of one acac group in addition to an ethyl group and a coordinated olefin.

Time resolved Ni-K-edge EDEXAFS spectroscopy (13 seconds per spectrum) was used to follow the formation of an organometallic intermediate from an in-situ reaction mixture of $Ni(acac)_2/AlEt_2(OEt)$/hex-1-ene at room temperature. The EDEXAFS spectra showed a real time change in the white line features of the spectra from that of the starting material, i.e. $Ni(acac)_2$, to that of the organometallic product over a period of six minutes.

Ni-K-edge and Br-K-edge EDEXAFS and QUEXAFS studies were performed on numerous mixtures of $NiX_2(PEt_3)_2$ (X=Cl, Br) /$AlEt_3$ at low temperatures and room temperature and in the presence and absence of hex-1-ene. The results indicated the formation of adducts of the nickel and aluminium species at low temperatures and also the loss of the halogen atom from the nickel coordination sphere at room temperature. Some evidence was also found for the alkylation of the nickel species after loss of the halogen atom.

QUEXAFS studies were also performed on the palladium-K-edge of the Heck reaction mixture, $Pd(OAc)_2$/ methallylalcohol/ iodobenzene/ tri-n-butylamine/ NMP. In situ QUEXAFS studies of the mixture showed the presence of carbon coordination around the palladium atom in addition to iodine atoms. In the presence of triphenylphosphine, bromobenzene was used as the aryl halide.The EXAFS of this reaction mixture showed the formation of $PdBr(OAc)(PPh_3)_2$, which on heating formed $PdBr_2(PPh_3)_2$. In the absence of bromobenzene, EXAFS studies showed the formation of palladium particles in the reaction mixture.

ACKNOWLEDGEMENTS

Firstly, I would like to thank my supervisor, Professor John Evans, for all the supervision, help, guidance and encouragement he has given me throughout the duration of this thesis. I would also like to thank him for giving me the opportunity of working with him on the topics of EXAFS and catalysis. I would like to thank him for the many hours he has spent with the the team collecting data at Daresbury and Grenoble, where he was always available to provide help as required. He has always been present to answer any questions and solve any problems I may have had on the thesis.

I would like to thank Dr. Andrew Dent for so much help without which most of the data in this thesis could not have been collected.

I would also like to acknowledge the E.P.S.R.C. for financial assistance and for enabling me to work at Daresbury and Grenoble. I would like to thank B.P. Research International for granting a C.A.S.E. award for this work. In particular, I would like to thank Dr. John Couves, for being ready to assist if necessary and for regular and helpful appraisal of the research work being carried out.

I must also thank Dr. W. Levason and Simon Pope for help with analysis of some of the UV/visible/NIR data in Chapter 6. I would like to thank Dr. Judith Corker for providing a very clear thesis which has provided the background for the nickel work in this thesis. Special thanks must also go to to Norman Binsted for helping to determine the size of the nickel metal clusters described in Chapter 4 and to Anthony Genge for solving the X-ray crystal data in Chapter 7.

I would like to thank Dr. Tony Masters, Michael, Dayan and John from the University of Sydney, for help with collecting data at Daresbury and for also providing the syringe drivers for the low temperature equipment.

I must thank my lab-mates, Malcolm, Chris and Basyar, for helping me settle in and for assistance whenever required. I would also like thank all the members of the seventh level, past including (Kathryn, Clive, and Darren) and present (Tony, Nick, Simon (Orchard), Simon, Shehla, Steve, Daryl, Julia, Julie, Maria, Lynn, Sarah and Sandra) who have provided such a friendly atmosphere to work in.

Last but not the least, I would like to thank my parents and all the members of my family, Chandra, Sarada, Vijay and Usha, for much support over the time.

ABBREVIATIONS

XAS	X-ray Absorption Spectroscopy
XANES	X-ray Absorption Near Edge Structure
EXAFS	Extended X-ray Absorption Fine Structure
EDEXAFS	Energy Dispersive EXAFS
QUEXAFS	Quick EXAFS
UV/visible	Ultra-Violet/visible
cod	1,5-cyclooctadiene
Et	Ethyl
acac	Acetylacetonate
Ph	Phenyl
OAc	Acetate
NMP	N-Methylpyrrolidinone

For the EXAFS spectra,

_____ Experiment

----- Theory

CONTENTS

To my parents, my family and numerous well-wishers.

CHAPTER 1 HOMOGENEOUS NICKEL ALKENE OLIGOMERISATION CATALYSTS.

1.1 Introduction to catalysis:

The I.U.P.A.C. has defined catalysis as the phenomenon in which a relatively small amount of a foreign material called a catalyst augments the rate of a chemical reaction without itself being consumed (Burwell, 1976)[1,2]. In practice, this means that a catalyst reduces the activation energy of a reaction which must itself be energetically favoured. This is shown below in Figure 1.1[3],

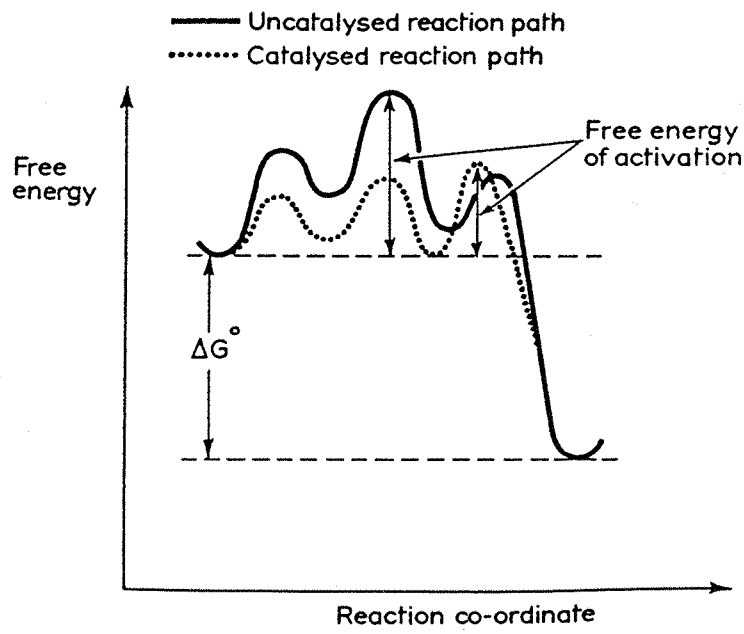

Figure 1.1. Free energy plot showing the effect of catalysis.[3]

A catalytic system can be seen as a cycle of reactions connected in such a way such that during one journey round the circle the substrates are converted to products without any net change occuring in the catalyst at the end of the cycle. The cycle can often consist of the catalyst being activated as the initial step to facilitating a reaction to take place and then being `deactivated' at the end of the reaction to release the original catalyst. An example of such a catalytic cycle is shown on Figure 1.2[3]:

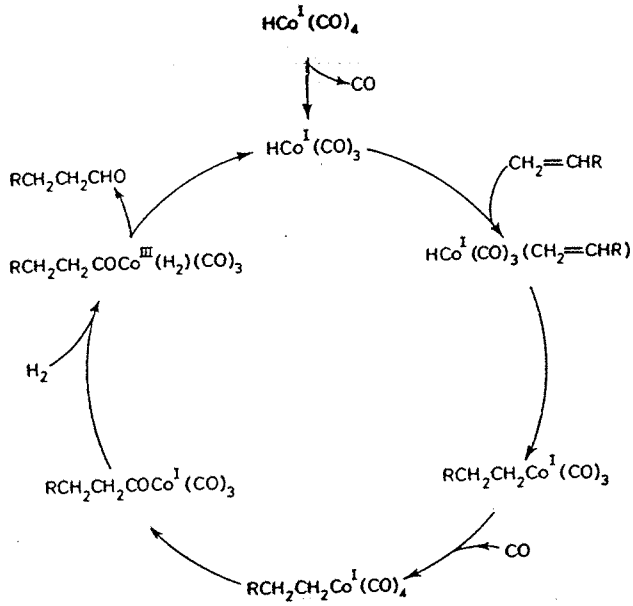

Figure 1.2. Catalytic cycle of the cobalt catalysed hydroformylation of a terminal alkene.[3]

As shown in the Figures 1.1 and 1.2, activation of one or more of the reactants in order to persuade them to react together is an essential part of catalysis. There are two main types of activation processes. These are: 'activation by coordination' and 'activation by addition'.

'Activation by coordination' is the process by which a substrate XY interacts with the catalyst centre in such a way that the integrity of XY is maintained. An example of the first type is the coordination of an olefin to cyclopentadienylcarbonyliron (Fp^+) which renders the olefin susceptible to attack by a wide range of nucleophiles under mild conditions as shown below in Figure 1.3[3]:

Figure 1.3. Addition of a nucleophile to a coordinated alkene.

A common example of 'activation by addition' is the oxidative addition reaction where a substrate XY adds to a metal complex such that both the formal oxidation state and the coordination number are increased by two in the resulting complex[3]. An example of such a reaction is shown in Figure 1.4 as the addition of H_2 to Rh(I):

$$Rh^{I}Cl(PPh_3)_x + H_2 \longrightarrow Rh^{III}ClH_2(PPh_3)_x$$

$$x = 2 \text{ or } 3$$

Figure 1.4. Addition of H_2 to $Rh(I)Cl(PPh_3)_2$.

Finally, a catalyst can be as simple as a proton or as complex as an enzyme. It can be purely inorganic in nature, purely organic or a mixture of the two. In this thesis we will mainly be concerned with transition metal catalysts containing nickel and palladium.

1.2 Transition metal catalysts:

There are numerous reasons[3] which explain popularity of transition metals as catalysts for reactions. These are:

a) *Variability of the oxidation state*: The ability to enter into redox cycles and to readily interchange between oxidation states is an important reason for the wide ranging catalytic activity of transition metals. In theory, a transition metal can have access to as many formal positive oxidation states as it has valence d and s electrons plus one. However, not all of the elements form stable complexes for all of their available oxidation states. π-bonding ligands such as CO stabilise low

oxidation states while small σ-bonding ionic ligands such as H^- and F^- coordinate to metals in high oxidation states.

b) *Variability of the coordination number*: Transition metals are able to adopt different coordination numbers and stereochemistries. The ability of a transition metal to accomodate several different ligands in its coordination sphere is important factor in its ability to catalyse reactions e.g. in the hydroformylation reaction in which an aldehyde is formed from an olefin, carbon monoxide and hydrogen, the transition metal must be able to accomodate olefin, carbonyl and hydride groups in its coordination sphere together with other non-participative groups.

c) *Choice of ligands*: Transition elements readily form linkages with almost every other element in the periodic table and with most organic molecules. This property allows them to have a very rich coordination chemistry and makes them very suitable for their role as catalysts.

d) *Bonding ability*: *d*-block elements can form bonds with a wide range of compounds. This is because they can form strong bonds with compounds containing π-electron systems or having orbitals of suitable symmetry or energy to form dπ-bonds. Transition metals are also able to form very strong σ-bonds with several highly reactive species e.g hydride and alkyl groups thus stabilising these species, which can then be used to act in a particular manner e.g. in the presence of an olefin $RhH_2Cl(PPh_3)_2$ readily gives up its hydride ligands to the olefinic double bond.

e) *Ligand effects*: A ligand can influence the behaviour of a transition metal catalyst by modifying the steric or electronic environment at the active site. Usually it is a combination of both effects.

The above properties of transition metals make them widely used catalysts.

1.3 Homogeneous vs Heterogeneous catalysis:

In homogeneous reactions, all the constituents of the reaction are present in the same phase i.e. the liquid phase. In heterogeneous catalysis, one or more of the constituents are present in different phases. In such cases, the catalyst is usually present as the solid phase and the reactants as liquids or more frequently as gases. While in homogeneous catalysis, the catalyst is often a discrete entity, in heterogeneous catalysis, the reaction takes place at the phase interface i.e. on the catalyst surface. It has been estimated that nearly three quarters of all industrial chemicals produced have involved the use of a catalyst during manufacture. 10% to 15% of these catalysts have been homogeneous catalysts. Besides cobalt, nickel is the most frequently used metal for reactions such as carbonylation, cyclic and linear oligomerisation[4].

The advantages of heterogeneous catalysts over homogeneous catalysts include the ease with which they can be separated from the reaction products assuming that these are liquids or gases. Also, being bulk solids, heterogeneous catalysts usually have higher thermal stability than homogeneous systems, thus allowing the reaction to be run at higher temperatures giving rise to higher reaction rates. In-situ regeneration of the catalyst is possible when using heterogeneous catalysts but less possible when using homogeneous catalysts.

In contrast, the advantages of homogeneous catalysts are that they are more selective than heterogeneous catalysts. They are also likely to be more active per metal centre than heterogeneous catalysts. This is because in heterogeneous catalysts there are numerous different sites of which only a proportion catalyses the reaction of interest unlike in homogeneous catalysts where there is only one site. Homogeneous catalysts are also more easy to study than heterogeneous catalysts as there are few physical techniques which allow accurate monitoring of reactions taking place on the catalyst surface. Ease of study also makes homogeneous catalysts more easy to modify than heterogeneous catalysts.

1.4 Oligomerisation:

This is a process by which mono-olefins can be converted into a mixture of, dimers, trimers, and higher oligomers in which the dimer predominates. This is shown below in Figure 1.5:

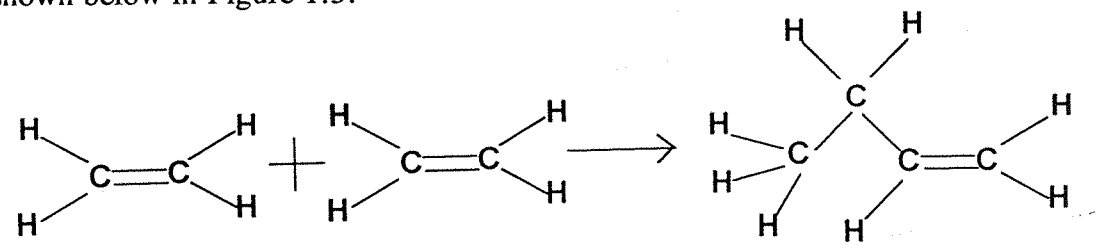

Figure 1.5. Oligomerisation of ethene.

The higher oligomers are probably formed as the result of co-oligomerisation with the monomer. In most cases, the reaction is accompanied by isomerization of the products. Alkene oligomerisation reactions are generally first order in catalyst concentration and second order in alkene concentration. The rate of oligomerisation decreases in the order ethene > propene > but-1-ene > cycloalkene[5]. Oligomerisation can be catalysed by numerous transition metal complexes of which nickel complexes are the most widely used[6,7,8].

1.5 The Nickel Effect:

In 1949, Ziegler and Gellert[9] discovered that long chain aluminium alkyls could be produced by repeated insertion of ethylene molecules into the Al-C bond. This growth reaction terminated, however, after the statistical insertion of approximately 100 molecules. Olefins insert into the metal-carbon bonds of monomeric aluminium alkyls at about 100°C - 160°C and 100 atm generating long chain derivatives. The chain length can be controlled by the temperature, pressure

and contact time. This "growth reaction" is used in the industrial synthesis of unbranched aliphatic alcohols containing about 14C in the chain, for use in biodegradable detergents. The alcohol results from controlled oxidation of the product of growth reaction.

It was discovered in 1952, by K.Ziegler and his co-workers[10,11] that ethylene reacts with triethylaluminium in the presence of nickel to produce 1-butene. Thus, in the presence of nickel salts, the polymerisation of ethylene by triethylaluminium is terminated after one insertion step. This is known as the "Nickel Effect" and the reaction involving only one insertion step is known as 'oligomerisation'.

The Shell Higher Olefin Process (SHOP)[12] was started in 1977 to produce a range of olefins using the oligomerisation process. SHOP has the capability of making considerable adjustments in output to suit market needs. This is accomplished by oligomerising ethylene in the presence of a nickel catalyst to a geometric distribution of olefins. Saleable olefins are recovered for distribution while those for which no ready market exists are recombined isomerised and metathesised to C_{11} to C_{14} internal olefins which are hydroformylated by the Shell process to linear detergent range alcohols used in the large surfactant market[12].

1.6 Nickel Alkene Oligomerisation Catalysts[13]:

Active homogeneous alkene oligomerisation catalysts can be prepared from almost every type of nickel compound. The nickel component in homogeneous systems is most frequently a Ni^{2+} salt such as nickel acetylacetonate[14] or a nickel halide. The activity depends to some extent on the nature of the nickel salt. Phosphines and phosphites are standard ligands. Other ligands include chelating phosphines[15,16]. The catalyst is also reported to have been formed from organonickel complexes and reactions have been reported involving a nickel hydride[17], nickel alkyls or aryls[18,19], nickel olefin[20] complexes and also π-allyl nickel complexes[21,22,23]. The full activity of the catalyst is normally only observed in the

presence of a Lewis acid. In the majority of the cases, the Lewis acid is an alkylaluminium sesquichloride or an aluminium trihalide. Systematic studies of the effect of varying the concentration of the Lewis acid are not common. The optimum value depends on the nature of both the Lewis acid and the nickel component[24]. Other metal halides may also be used and these include titanium(IV) chloride[25] and boron trihalide[19]. It has been thought that systems involving transition metal fluorides are more effective than the chlorides.

In this thesis, we have mainly been looking at various nickel complexes. In these cases, the generation of an active catalyst involves the addition of a Lewis acid/reducing agent, which may be present as an alkylaluminium sesquichloride or a dialkylaluminium alkoxide[24], trialkyl aluminium[15,16,24,27], butyllithium[24,26], diethyl zinc, or sodium borohydride[28]. Although the majority of catalysts consist of a combination of nickel complex- Lewis acid, the Lewis acid is not always essential e.g. ethene is slowly dimerised at moderate temperatures by $[(C_6H_5)_3P)_2NiBr(aryl)]$ complexes[29] and styrene is dimerised by π-allylNiX catalysts at room temperature[30,31]. However, the nickel complex on its own cannot catalyse the reaction at the moderate conditions of temperature and pressure used in the presence of the Lewis acid.

Organoaluminium compounds of low Lewis acidities, such as dialkyl aluminium alkoxides, are often used. Industrially, organoaluminium compounds are used on a large scale for the oligomerisation and polymerisation of olefins. Triethylaluminium is a common alkylating agent which is also a Lewis acid. Like all organoaluminium compounds, it has an extensive chemistry. Generally, trialkyls are colourless liquids or low melting solids which must be stored under an inert atmosphere because they are very sensitive to atmospheric oxidation and hydrolysis. The trialkyls inflame spontaneously when exposed to air. Stringent safety precautions should be observed during their manipulation[32].

Thus, a typical catalyst for alkene oligomerisaton can be made by mixing a nickel salt with triethylaluminium or an organoaluminium sesquichloride in a solvent such as toluene.

Besides the Lewis acid, the solvent also plays a role in the reaction. In general, aromatic or halohydrocarbons are preferred but individual cases are known where the reaction proceeds satisfactorily in saturated hydrocarbons[26] and alcohols, or even in the absence of solvent. The dimerisation of propylene using [η^4-$\{(CH_3)_4C_4\}NiCl_2]_2$-$(C_2H_5)_3Al_2Cl_3$-lig as catalyst proceeds five times faster in chlorobenzene than in benzene[33].

The nickel component used in supported catalysts is frequently nickel oxide. However, catalysts have also been prepared by reacting the support with an organonickel complex e.g $(COD)_2Ni$ and π-allylnickel complexes among others. The support or the nickel complex may be pretreated with diethylaluminium sesquichloride or triethylaluminium. The most frequently implemented support is silica-alumina, which may be activated by treatment with a sulphur containing ligand. The catalyst may also be prepared by hydrolysing the organonickel complex with the support[34,35,36]. Reactions involving anchoring of nickel species to various polymer supports are also known[37,38]. Other supports include activated charcoal, polystyrene[39], polyphosphinostyrene and polyvinylpyridine.

1.7 Reaction Mechanism:

It is known that oligomerisation can be catalysed by nickel atoms in the absence of aluminium atoms. In the presence of an aluminium cocatalyst, the catalysis by the nickel catalyst occurs more efficiently. In the presence of nickel catalyst and aluminium cocatalyst, it was found that the rate of dimerisation was the same as the rate of multiple insertion of ethylene molecules into the Al-C bond.[40] It is thought that an aluminium hydride intermediate is not involved because such compounds are effective catalyst poisons[13,41].In the absence of nickel, some aluminium complexes will catalyse the reaction to polymerisation.

One of the reaction mechanism proposed for alkene oligomerisation involves the reduction of the nickel(II) complex by trialkyaluminium to give nickel(0) which

then reacts with the olefins present in the reaction mixture to form an olefin complex e.g. tri(ethene)nickel. It is then thought that a multicentre bond is formed between the nickel(0) complex and the trialkylaluminium in which the α-carbon of the trialkylaluminium bridges the nickel and aluminium atoms. This is shown below in figure 1.6. In an arrangement of this type, the carbon atoms of the complexed olefinic double bond as well as the β-H of the alkyl group, approach the Al atom closely enough to permit an electrocyclic reorganisation[41].

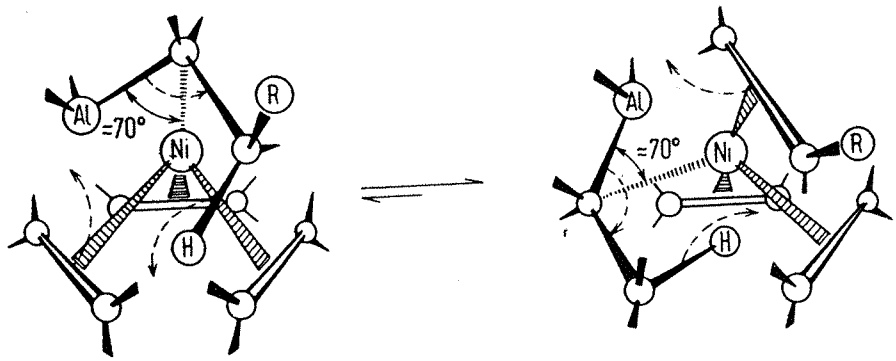

Figure 1.6. Interaction between tri(ethene)nickel and trialkylaluminium during the nickel catalysed oligomerisation of ethene.[41]

It is known that stereoregular polymerisation of olefins results from the use of nickel catalysts, prepared by mixing organoaluminum compounds with transition metal halides, alkoxides or other derivatives. The active state in such systems is believed to be a coordination complex containing the transition metal in a low oxidation state, partially alkylated, and affording vacant coordination sites for olefin to be taken up, subsequently to insert into an adjacent metal-carbon bond.

It has also been suggested[13] that the large variety of nickel catalyst systems discussed in the previous section involve a common active species. The comparable activity of the various systems supports this suggestion. Evidence has accumulated

that the active species is a nickel hydride.[42-45] It is thought that the nickel hydride species is generated by established organometallic reactions, such as β-hydride transfer from an intermediate alkyl species, the direct transfer of a hydrogen to the nickel centre from a coordinated alkene molecule, and oxidative addition of a Bronsted acid to a zero-valent nickel complex[42,43].

The abstraction of a hydrogen atom from the olefin has been demonstrated spectroscopically for propylene[44] and possibly accounts for the formation of the HNiX system in reactions involving zerovalent nickel systems like $[(C_6H_5)_3P]_2Ni(CO)_2$.

Attempts to isolate the catalytically active nickel hydride or alkyl complexes directly from oligomerisation reactions have generally been unsuccessful. This is likely to be because the hydride species exists in very small quantities when an excess of alkene is present. This is because the nickel hydride species is expected to react immediately with the olefin molecules also bonded to the nickel atom.

For nickel halogenophosphines, the catalytically active species can therefore be thought of as consisting of a square planar hybridized nickel atom interacting with a hydride (or alkyl), a phosphine, an electronegative group X, and olefin molecules as shown in Figure 1.7.[13]

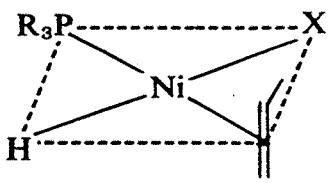

Figure 1.7. Possible active species during the nickel catalysed oligomerisation of olefins.[13]

It is probable that the Lewis acid interacts with the nickel through the group X. An understanding of the nature of this interaction can be obtained from an X-ray

structural study of the adduct formed by [η^3-C_3H_5NiCl-(P(*cyclo*-$C_6H_{11})_3$)] with CH_3AlCl_2; the nickel and the aluminium are bridged by a chlorine atom[22], as shown below in Figure 1.8:

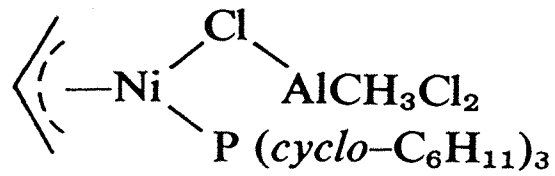

Figure 1.8. The structural formula of the adduct formed by [η^3-C_3H_5NiCl-(P(*cyclo*-$C_6H_{11})_3$)] with CH_3AlCl_2.

It is possible that the Lewis acid in these complexes decreases the charge on the metal. A second important function of the Lewis acid is to react with redundant phosphine molecules, thereby creating free coordination sites at the nickel. This is perhaps important for catalysts based on $(R_3P)_2NiX_2$ compounds.

Much of the evidence for the oligomerisation mechanism has been accumulated either through detailed studies on the nature of the products formed (e.g. labelling experiments) in catalytic reactions, or by the use of model systems and is therefore mostly circumstantial.

Recent evidence to support the nickel hydride mechanism in ethene oligomerisation has been obtained by Keim *et al.*[45] from in-situ NMR studies on a catalyst derived from $Ni(cod)_2$. ^1H NMR data recorded for a mixture of $Ni(cod)_2$ and the phosphine ligand (1) indicated the formation of a nickel hydride species by the formation of a triplet at δ 23.6. On treatment of the catalyst solution with

ethene, the hydride resonance disappears and a new signal appears attributable to an alkylnickel complex. Although the catalytic hydride complex could not be isolated, the reaction of $Ni(cod)_2$ with PCy_3 and (1) was shown to produce the hydride complex (2), shown below in Figure 1.9.

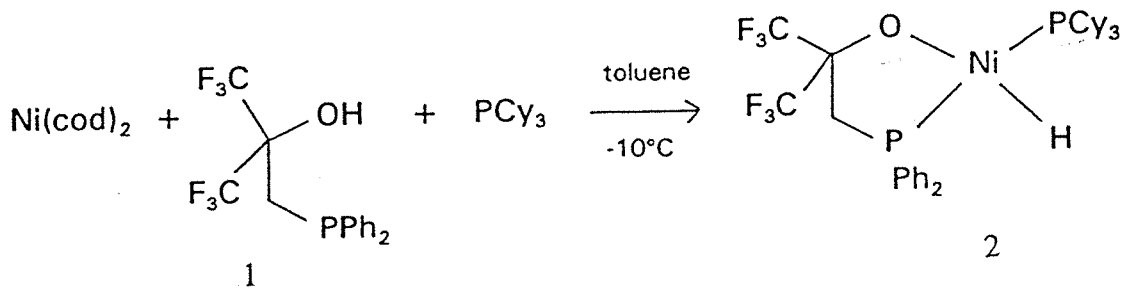

Figure 1.9. Formation of a nickel hydride species from the reaction of $Ni(cod)_2$ with $[C_2(CF_3)_2(OH)(PPh_2)]$ and PCy_3.

The effectiveness of halohydrocarbons as solvents for the oligomerisation reaction is probably associated with their polar, weakly basic nature, which enables them to act as effective solvents for polar species. It is also thought that the halohydrocarbon functions as a source of halide. This has never been substantiated, but may be of importance in those reactions involving trialkylaluminium[13].

A simple mechanism for the oligomerisation of ethylene[13] is shown in Figure 1.10 and consists of the following three distinctive steps: a) insertion into the Ni-H bond, b) insertion into the Ni-C bond, and c) olefin elemination.

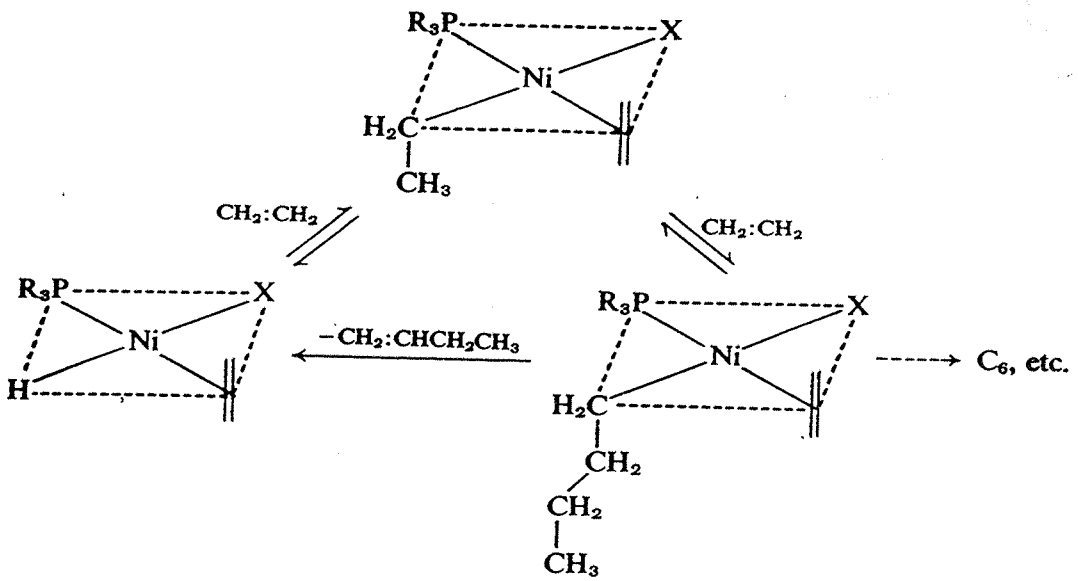

Figure 1.10. Schematic diagram showing a mechanism for the nickel catalysed oligomerisation of ethene[13].

The first step in Figure 1.10, involves the coordination of an ethene molecule to the nickel hydride species. This is followed by migration of the hydride

to the ethene to form an alkylnickel complex. A second ethene molecule coordinates and migration of the alkyl group to the ethene follows. Two pathways are available at this stage. The nickel hydride species can be regenerated via β-hydride elimination of the dimeric product or alternatively, higher oligomers may be produced by further alkene coordination/migration processes. The degree of oligomerisation is largely determined by the relative rates of the elimination and alkyl migration steps which are in turn influenced by the nature of the donor ligand present. Several reactions modelling the addition of a Ni-H to an alkene have been described by Wilke[46]. Tertiary phosphine ligands have been found to exert the most dramatic effect on products of oligomerisation reactions and have thus been studied in great detail[47,48]. In the case ethene oligomerisation, a preference for chain growth rather than product elimination is observed when bulky phosphines with large cone angles are present.

It has been suggested that the elimination reaction proceeds via the transition state shown in Figure 1.11[77], whereas the alkyl to alkene migration step proceeds through the less sterically hindered state shown in Figure 1.12[77].

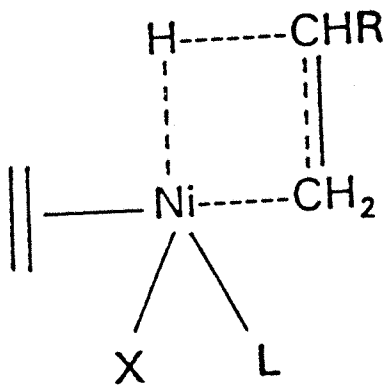

Figure 1.11. Transition state proposed during olefin elimination.[77]

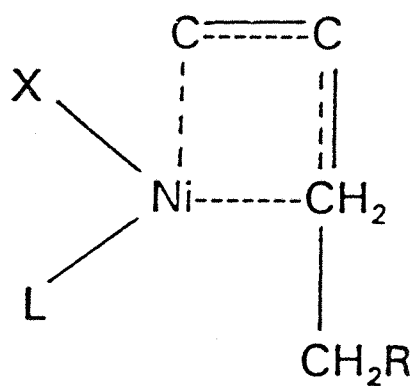

Figure 1.12. Transition state proposed during the alkyl to alkene migration step.[77]

In the case of propene, the situation is complicated by the asymmetry of the olefin. Results have confirmed that the first step is kinetically controlled and produces mainly a Ni-n-propyl species which rearranges to the thermodynamically more stable Ni-isopropyl species as shown in Figure 1.13.[13]

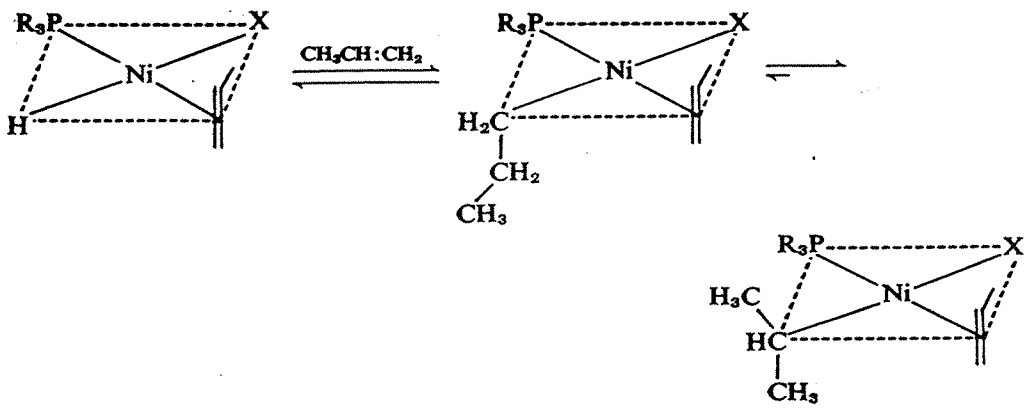

Figure 1.13 (i) Schematic diagram of the nickel catalysed oligomerisation of propene.[13]

The same choice exists in the second step and leads to the situation shown in Figure 1.13 (ii)[13]. The role of the Lewis acid in the catalytic reaction has received little attention. A recent study indicates that variation of the Lewis acid affects the first step in the dimerisation of propene but has no significant effect on the second, and it is suggested that the nature of the anion influences the rate at which the Ni-n-propyl species isomerises to the thermodynamically more stable Ni-isopropyl species[13].

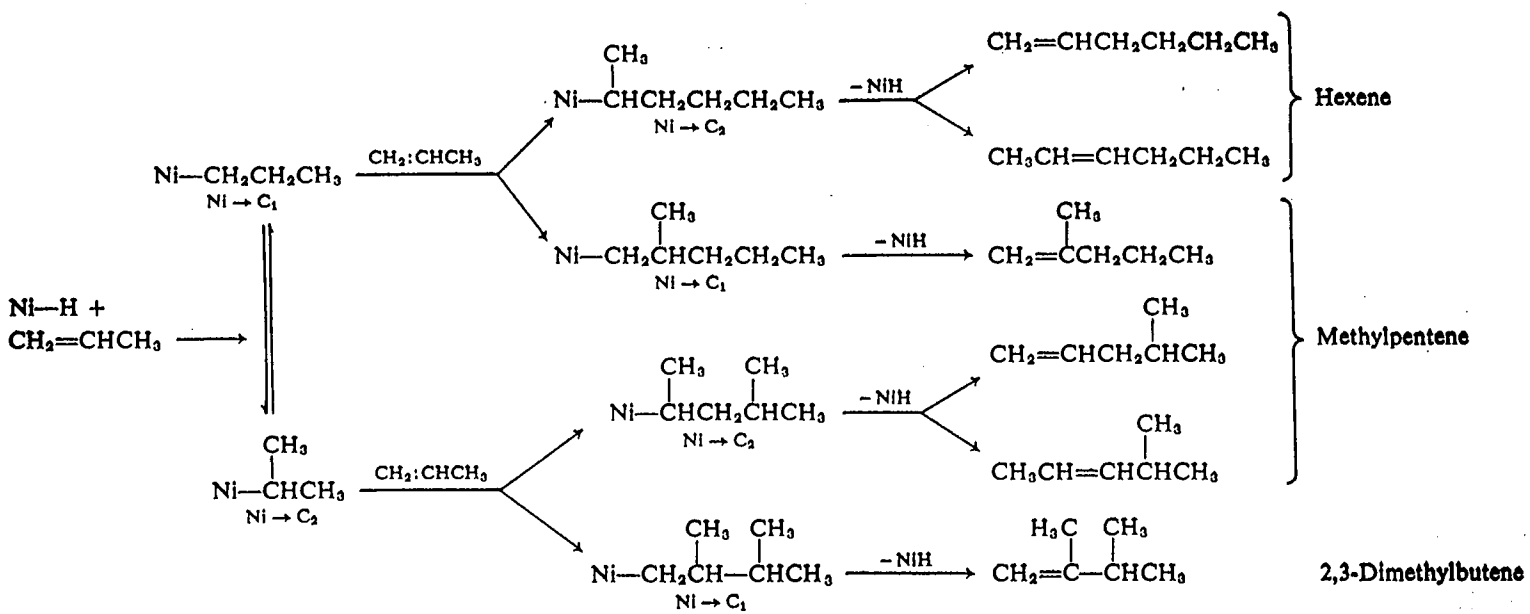

Figure 1.13(ii).[13] **Schematic diagram of the nickel catalysed oligomerisation of propylene**

Recently, theoretical studies have been performed by Fan *et al.*[49] on ethene oligomerisation by an organometallic nickel catalyst formed from $Ni(acac)_2$. The studies involved calculations based on density function theory and proposed that $(acac)NiCH_2CH_3$ was the actual catalyst while (acac)NiH was a precursor or precatalyst. The studies showed that the nickel hydride (acac)NiH is very active in the presence of ethylene and leads to $(acac)NiC_2H_5$ with an exothermicity of 44.7 kcal/mol. Thus a mechanism based on the regeneration of nickel hydride is not considered viable and a modified mechanism where (acac)NiH is a precursor or precatalyst while the actual catalyst is $(acac)NiC_2H_5$ was proposed.

1.8 Isomerisation of olefins:[50-66]

Some isomerisation is also thought to occur during the oligomerisation. This is because the isomerisation of olefins is also catalysed by some nickel catalysts and very similar nickel hydride intermediates may be involved in the oligomerisation and isomerisation of olefins. Some isomerisation must also therefore be occurring in oligomerisation reactions.

There are two mechanisms for isomerisations of olefins. These are,
1) Double bond migration and 2) Skeletal rearrangements.

1) *Double Bond migrations*: Double bond migration are often of the type shown below in Figure 1.14.

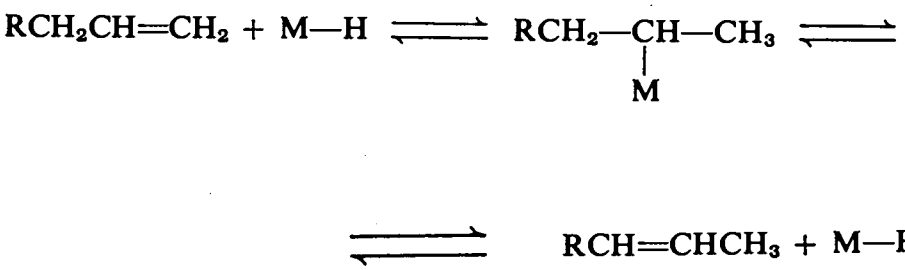

Figure 1.14. Rearrangement of an olefin through a η^3-allyhnetalhydride.

2) *Skeletal Rearrangements*: Two types of nickel catalysed skeletal rearrangements of dienes have been observed. These are shown below in Figure 1.15:

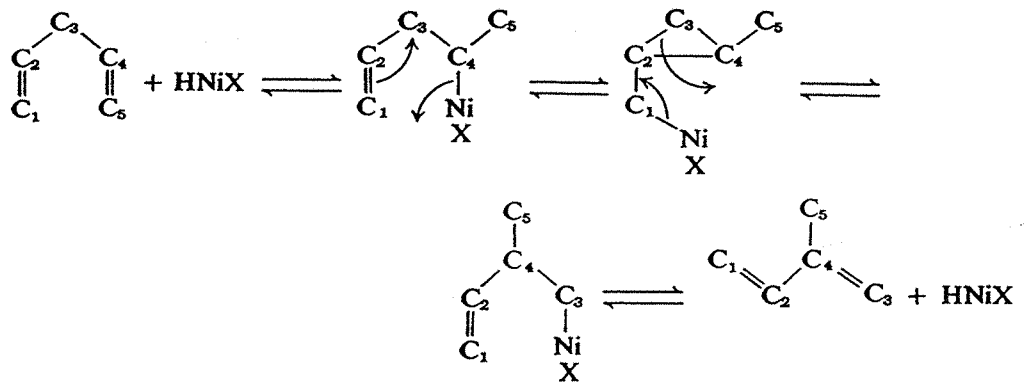

Figure 1.15. Formation of a cyclopropylcarbinyl intermediate during the rearrangement of a diene.

1.9 Analytical techniques to study nickel catalysts:

Various analytical and spectroscopic techniques may be applied to study the intermediates obtained during catalysis. It is not always possible to isolate reaction intermediates. It may be necessary to perform in-situ studies of the reaction mixture. This may require stabilisation of the intermediate stage by dropping the temperature of the reaction mixture e.g in the case of reactive alkyl species. Also varying the concentrations and ratios of various components of the reaction mixture will provide mixtures at different stages of the reaction which can then be studied. Kinetic studies as the reaction proceeds can provide some insight into the rates of the reaction, and also whether the reaction is a one stage or two stage process.

Sometimes a combination of techniques may be required to provide information on the intermediate.

EXAFS was the main technique which was used in this thesis to study the catalyst mixture both in the presence and absence of olefin. Further details about the EXAFS technique will be given in Chapter 2 of this thesis. In summary, this technique provided information on the identity of coordinating atoms around a central metal atom. The information provided usually consisted of the type of atom, coordination number, and distance from the central atom. EXAFS spectroscopy is usually carried out at the number of synchrotron radiation sources available around the world. These sources provide high intensity continuous radiation for use in spectroscopy. Until recently EXAFS spectroscopy required 40 minutes or more to acquire a spectrum. Over such a timescale, only species stable for over 40 minutes can be studied. This makes it difficult to study reactions as they happen in solution. Recent developments in EXAFS technology has made it possible to follow reactions which occur over minutes. These developments include the use of QUEXAFS which allows acquisition of spectra in minutes and EDEXAFS which allows acquisition of spectra in seconds. Further details of EXAFS, QUEXAFS and EDEXAFS are given in Chapter 2 of this thesis.

Among the various other techniques that can be used to study intermediates is electronic absorption spectroscopy which may be used to obtain information on oxidation states and also coordination geometry of various intermediate stages. This can act as complementary to EXAFS studies of most compounds as it provides information on the immediate environment of the metal atom.

^{1}H, ^{31}P, ^{13}C NMR studies of reaction mixtures at low and ambient temperatures can also provide information on the nature of species present in the mixture e.g. the presence of alkyl coordinated olefin and hydride species. In-situ solution infra-red spectroscopy can also be useful in indicating the formation of new functional groups. Two of the in-situ cells developed for infra-red spectroscopic studies were the ICI[67] and Moser[68] cells which both consist of reaction cells fitted with integral stirrers.

While, crystallisation of the material in the reaction mixture and subsequent X-ray crystallography can provide some insight into the general direction the reaction is taking, it is not the same as an in situ experiment, as numerous changes may happen to the reaction intermediates or products during the crystallisation process.

1.10 Recent EXAFS studies of homogeneous and heterogeneous catalysts:

Using EXAFS, it is possible to obtain information on the type and number of atoms surrounding the absorbing atom, up to a distance of about 4-5 Å as well as the average distance to these atoms. Interatomic distances can be obtained to an accuracy of 1% while coordination numbers of any particular shell can be determined to an accuracy of 20%. The fact that EXAFS can be used on solids (crystalline and amorphous), liquids, solutions and gases make this a very useful technique.

EXAFS provides information on the average environment of a metal atom. Like most other forms of spectroscopy, EXAFS should be used in combination with other techniques. EXAFS is often used in combination with protein crystallography in the study of bioinorganic systems[69].

In situ and other forms of characterisation of heterogeneous catalysts has often involved the use of EXAFS. This is because the metal centres of interest located on the surface of a solid support can be probed directly without interference from the surrounding matrix. EXAFS has been used to characterise nickel ion sites in zeolite catalysts[70,71,72]. Woolery *et al.*[70] and Sano *et al.*[71] have both shown that the nickel in zeolite Y (introduced by ion exchange is present initially as $[Ni(OH_2)_6]^{2+}$ and that calcination results in a reduced Ni-O coordination of 4. The formation of small nickel metal particles on silica and alumina supports have been investigated using EXAFS[73,74].

EXAFS studies have also been reported on homogeneous sytems. Ballivet-Tkatcenko *et al.*[75] carried out studies on active alkene polymerisation catalysts derived from dinitrosyl iron and cobalt complexes in solution. The inactive precursors $[M(NO)_2Cl_2]_2$ (M= Fe, Co), together with the $AgBF_4$ activated catalysts were investigated by EXAFS and reference compounds were used to assist the data analysis. For the iron catalyst species in acetonitrile, the results were consistent with a trigonal bipyramidal coordination of three solvent molecules (non-equivalent) and two slightly bent nitrosyl ligands.

Combined EXAFS and IR studies on an ethene hydroformylation catalyst system derived from $[H_3Ru_4(CO)_{12}]^-$ have been reported by Evans *et al.*[76]. The in situ formation of the cluster species $[HRu_3(CO)_{11}]^-$ was concluded from the Ru-K-edge EXAFS data; the results were supported with results obtained using IR measurements.

Ni-K-edge EXAFS studies on propene dimerisation catalysts[77,78], formed by the interaction of solutions of $NiCl_2(PEt_3)_2$ with $Al_2Me_3Cl_3$ and $AlEt_3$ at -40°C indicated a first coordination sphere of C and P atoms as opposed to a coordination sphere of chlorine and phosphorus atoms in the staring material. In addition, the catalytic intermediate showed Ni...Al shells at 2.97 Å suggesting Ni-C-Al interactions which stabilise the nickel centre. A possible structure is shown in Figure 1.16.[77]

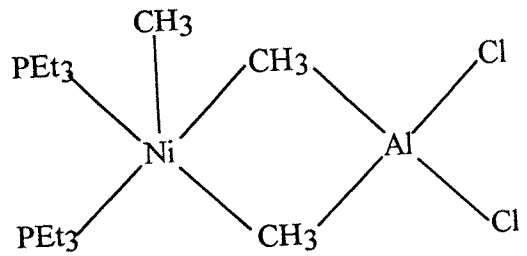

Figure 1.16. Figure showing a possible intermediate formed in a solution of $NiCl_2(PEt_3)_2/Al_2Me_3Cl_3/AlEt_3$ at -40°C.[77]

Studies of a $Ni(acac)_2$ precursor in the presence of phosphine and also a Lewis acid such as $AlMe_2(OEt)$ revealed the coordination of the phosphine followed alkylation and subsequent coordination of trialkylaluminium. This is shown schematically[78] in Figure 1.17.

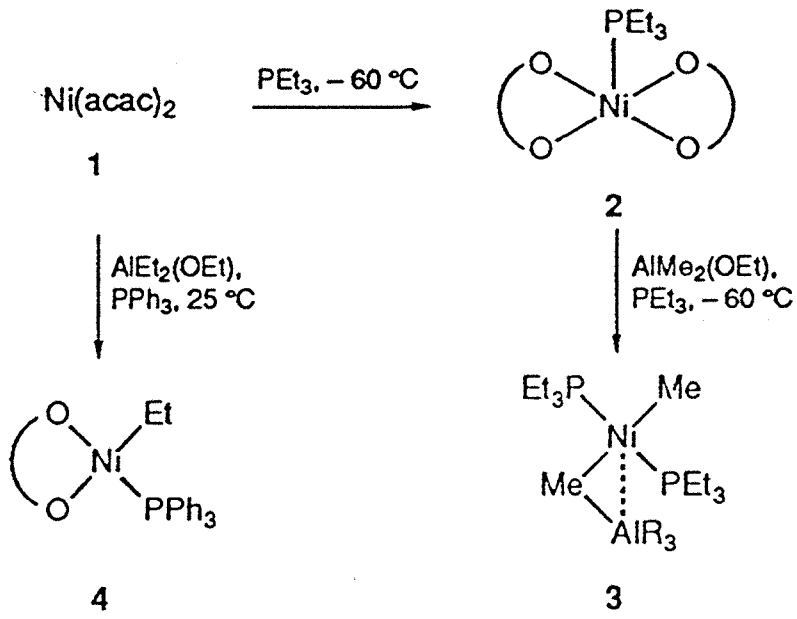

Figure 1.17. Schematic diagram showing the reaction of $Ni(acac)_2$ with $AlEt_2(OEt)$ and in the presence of phosphine[78].

Andrews and Evans[79,80] also performed in-situ NMR and EXAFS studies of homogeneous alkene oligomerisation catalyst $Ni(cod)_2$-$Ph_2PCH_2C(CF_3)_2OH$ formed on addition of $Ph_2PCH_2C(CF_3)_2OH$ to $Ni(cod)_2$ (cod= cycloocta-1,5-diene).

EXAFS was used by Goulon *et al.*[81,82] in the study of homogeneous hydrogenation catalysts prepared from the reduction of transition metal complexes by $AlEt_3$. The EXAFS spectrum of nickel octoate solution in benzene after reduction by $AlEt_3$ showed the formation of nickel metal clusters in solution.

Studies have also been performed on the bond angle determination at metal coordination centres from ligand K-edge EXAFS[83]. This was possible by triangulating the distances derived from both the ligand and metal absorption sites.

This has been possible with the extension of EXAFS into the soft X-ray region (S.O.X.A.F.S.) which has allowed access to common donor atoms such as phosphorus, sulphur and chlorine. This paper reports bond angles at nickel in phosphine complexes, some of which are precursors of alkene oligomerisation catalysts. The results were compared to those derived using X-ray crystallography.

1.11 Aims of the project:

The aims of this project include,

1) To perform concentration and acquisition time studies of the nickel catalysts using Ni-K-edge EDE and QUEXAFS spectroscopy.

2) To perform in situ studies of the nickel alkene oligomerisation catalysts using EDE and QUEXAFS spectroscopy at varying temperatures. This should provide some indication of the coordination sphere of the nickel atom in such catalyst solutions at varying temperatures in the presence and absence of the olefin.

3) To perform in situ studies of the palladium catalysts for the Heck reaction using QUEXAFS spectroscopy. This set of experiments would be useful in determining the nature of the coordination sphere around the central palladium atom during the vinylation of aryl halides.

1.12 REFERENCES

1. A.W.Parkins and R.C.Poller, 'An Introduction to Organometallic Chemistry', Macmillan Publishers Ltd, London, 1986.
2. R.L.Burwell, *Pure.Appl.Chem.*, 1976, **46**, 71.
3. C.Masters, 'Homogeneous Transition Metal Catalysis- A gentle art', Chapman and Hall, London, 1981.
4. W.Keim, *Angew.Chem.Int.Ed.Engl.*, 1990, **29**, 235.
5. O.-T.Onsager, H.Wang and U.Blindheim, *Helv.Chim.Acta.*, 1969, **52**, 196; 1969, **52**, 215; 1969, **52**, 224; 1969, **52**, 230.
6. G.Lefebvre and Y.Chauvin, *Aspects.Homog.Catal.*, 1970, **1**, 107.
7. J.R.Briggs, *J.Chem.Soc., Chem.Comm.*, 1989, 674.
8. T.Tsuji, *Adv.Organomet.Chem.*, 1979, **17**, 141.
9. K.Ziegler and H.G.Gellert, *Liebigs.Ann.Chem.*, 1950, **567**, 195.
10. K.Ziegler, *Angew.Chem.*, 1952, **64**, 323.
11. K.Ziegler, E.Holzkamp, H.Breil, H.Martin, *Angew.Chem.*, 1955, **67**, 541.
12. E.F.Lutz, *J.Chem.Ed.*, 1986, **63**, 202.
13. P.W.Jolly and G.Wilke, "The Organic Chemistry of Nickel", Academic Press, New York, Vol 1, 1974, Vol2, 1975.
14. W.Keim, A.Behr and G.Kraus, *J.Organomet.Chem.*, 1983, **251**, 377.
15. Y.Inoue, T.Kagawa, Y.Uchida and H.Hashimoto, *Bull.Chem.Soc.Jap.*, 1972, **45**, 1996.
16. Y.Inoue, T.Kagawa and H.Hashimoto, *Tetrahedron.Lett.*, 1970, 1099.
17. C.A.Tolman, *J.Am.Chem.Soc.*, 1970, **92**, 6777.
18. M.Uchino, A.Yamamoto and S.Ikeda, *J.Organomet.Chem.*, 1970, **24**, C63.
19. K.Maruya, T.Mizoroki and A.Ozaki, *Bull.Chem.Soc.Jpn.*, 1973, **46**, 993.
20. A.C.L.Su and J.W.Collette, *J.Organomet.Chem.*, 1972, **36**, 177.
21. B.Bogdanovic, B.Henc, A.Losler, B.Meister, H.Pauling, G.Wilke, *Angew..Chem.Int.Ed.Engl.*, 1972, **11**, 1023.
22. G.Wilke, B.Bogdanovic, P.Hardt, P.Heimbach, W.Keim, M.Kroner, W.Oberkirch, K.Tanaka, E.Steinrucke, P.Walter and H.Zimmermann, *Angew.Chem.Int.Ed.Engl.*, 1966, **5**, 151.

23. B.Bogdanovic, B.Henc, A.Losler, B.Meister, H.Pauling and G.Wilke, *Angew.Chem.Int.Ed.Engl.*, 1973, **12**, 954.

24. J.R.Jones and T.J.Symes, *J.Chem.Soc.C.*, 1971, 1124.

25. S.Abatowa, *Nefthikhimiya.*, 1973, **13**, 46.

26. C.Dixon, E.W.Duck and D.K.Jenkins, *Organomet.Chem.Syn.*, 1970/1971, **1**, 77.

27. J.R.Jones, *J.Chem.Soc.C.*, 1971, 1117.

28. S.Yoshikawa, S.Nishimura, J.Kiji and J.Furukawa, *Tetrahedron.Lett.*, 1973, 3071.

29. N.Kawata, K.-I.Maruya, T.Mizoroki and A.Ozaki, *Bull.Chem.Soc.Jap.*, 1971, **44**, 3217.

30. F.Dawans, *Tetrahedron.Lett.*, 1971, 1943.

31. G.Henrici-Olivé, S.Olivé, and E.Schmidt., *J.Organomet.Chem.*, 1972, **39**, 201.

32. 'Comprehensive Inorganic Chemistry'., Eds. J.C.Bailar, H.J.Emeleus, R.Nyholm, A.F.Trotman-Dickensen, Pergamon Press, 1973, Volume I, Chapter 12.

33. O.-T.Onsager, H.Wang and U.Blindheim., *Helv.Chim.Acta.*, 1969, **52**, 87.

34. W.Skupinski and S.Malinowski, *J.Organomet.Chem.*, 1975, **99**, 465; 1976, **117**, 183.

35. D.L.Bleach and T.P.Kobylinski, *J.Chem.Soc., Chem.Commun.*, 1980, 933.

36. Y.I.Yermakov and B.N.Kuznetsov, *J.Mol.Catal.*, 1980, **9**, 13.

37. N.Kawata, T.Mizoroki and A.Ozaki, *J.Mol.Catal.*, 1976, **1**, 275.

38. F.Dawans and D.Morel, *J.Mol.Catal.*, 1977, **3**, 404.

39. N.Kawata, T.Mizoroki, A.Ozaki and M.Ohkawara, *Chem.Lett.*, 1973, 1165.

40. K.Ziegler, H.-G.Gellert, E.Holzkamp, G.Wilke, E.W.Duck and W.-R.Kroll, *Justus.Liebigs.Ann.Chem.*, 1960, **629**, 172.

41. K.Fischer, K.Jonas, P.Misbach, R.Stabba and G.Wilke, *Angew.Chem.*, 1973, **12**, 943.

42. C.A.Tolman, *J.Am.Chem.Soc.*, 1970, **92**, 4217; 1970, **92**, 6777; 1970, **92**, 6785.

43. C.A.Tolman, *Inorg.Chem.*, 1972, **11**, 3128.

44. H.Bonnemann, *Angew.Chem.Int.Ed.Engl.*, 1970, **9**, 736.

45. W.Keim, U.Muller, C.Kruger, and P.Betz, *Angew.Chem.Int.Ed.Engl.*, 1989, **28**, 1011.

46. G.Wilke, *Angew.Chem.Int.Ed.Engl.*, 1988, **27**, 186.

47. B.Bogdanovic, B.Henc, H.-G.Karmann, H.-G.Nussel, D.Walter and G.Wilke, *Ind.Eng.Chem.*, 1970, **62**, 34.

48. B.Bogdanovic, *Adv.Organomet.Chem.*, 1979, **17**, 105.

49. L.Fan, A.Krzywicki, A.Somogyvari and T.Ziegler, *Inorg.Chem.*, 1996, **35**, 4003.

50. R.Cramer and R.V.Lindsey, *J.Am.Chem.Soc.*, 1966, **88**, 3534.

51. R.G.Miller, P.A.Pinke and D.J.Baker, *J.Am.Chem.Soc.*, 1970, **92**, 4490.

52. L.W.Gosser and G.W.Parshall, *Tetrahedron. Lett.*, 1971, 2555.

53. D.Bingham, D.W.Webster and P.B.Wells, *J.Chem.Soc., Dalton Trans.*, 1972, 1928.

54. B.Corain, *Chem.Ind.*, 1971, 1465.

55. B.Corain, *Gazz.Chim.Ital.*, 1972, **102**, 687.

56. B.Corain and G.Puosi, *J.Catal.*, 1973, **30**, 403.

57. C.A.Tolman, *J.Am.Chem.Soc.*, 1972, **94**, 2994.

58. G.Strujul, M.Bonivento, R.Ros, and M.Graziana, *Tetrahedron.Lett.*, 1974, 1791.

59. R.Cramer and R.V.Lindsey, *J.Am.Chem.Soc.*, 1966, **88**, 3534.

60. R.G.Miller and P.A.Pinke, *J.Am.Chem.Soc.*, 1968, **90**, 4500.

61. P.A.Pinke and R.G.Miller, *J.Am.Chem.Soc.*, 1974, **46**, 4221.

62. P.A.Pinke, R.D.Stauffer and R.G.Miller, *J.Am.Chem.Soc.*, 1974, **96**, 4229.

63. R.G.Miller, H.J.Golden, D.J.Baker and R.D.Stauffer, *J.Am.Chem.Soc.*, 1971, **93**, 6308.

64. R.G.Miller, *J.Am.Chem.Soc.*, 1967, **89**, 2785.

65. R.G.Miller, P.A.Pinke, R.D.Stauffer, H.J.Golden and D.J.Baker, *J.Am.Chem.Soc.*, 1974, **96**, 4211.

66. H.J.Golden, D.J.Baker and R.G.Miller, *J.Am.Chem.Soc.*, 1974, **96**, 4235.

67. K.A.Hunt, R.W.Page, S.Rigby and R.Whyman, *J.Phys.E.*, 1984, **17**, 559.

68.. W.R.Moser, J.E.Cnossen, A.W.Wang, S.A.Krouse, *J.Catal.*, 1985, **95**, 21.

69. C.D.Garner, "Applications of Synchrotron Radiation", Editors: C.R.A.Catlow and G.N.Greaves, Chapman and Hall, New York, 1990.

70. G.Woolery, G.Kuehl, A.Chester, T.Bein, G.Stucky and D.E.Sayers, *J.Physique.*, 1986, **47**, C8-28.

71. M.Sano, T.Maruo, H.Yamatera, M.Suzuki and Y.Saito, *J.Am.Chem.Soc.*, 1987, **109**, 52.

72. T.Bein, S.J.McLain, D.R.Corbin, R.D.Farlee, K.Moller, G.D.Stucky, G.Woolery and D.E.Sayers, *J.Am.Chem.Soc.*, 1988, **110**, 1801.

73. K.Tohji and Y.Udagawa, *Jpn.J.Appl.Phys.*, 1983, **22**, 882.

74. K.Tohji, Y.Udagawa, S.Tanabe and A.Ueno, *J.Am.Chem.Soc.*, 1984, **106**, 612.

75. D.Ballivet-Tkatchenko, C.Esselin and J.Goulon, *J.Physique.*, 1986, **47**, C8-343.

76. J.Evans, G.Jingxing, H.Leach and A.C.Street, *J.Organomet.Chem.*, 1989, **372**, 61.

77. J.M.Corker, PhD Thesis, Southampton University, 1991.

78. J.M.Corker and J.Evans, *J.Chem.Soc.,Chem.Commun.*, 1991, 1104.

79. P.Andrews and J.Evans, *J.Chem.Soc., Chem.Commun.*, 1993, 1246.

80. P.Andrews, PhD Thesis, Southampton University, 1993.

81. J.Goulon, E.Georges, C.Goulon-Ginet, Y.Chauvin, D.Commereuc, H.Dexpert and E.Freund, *Chem.Phys.*, 1984, **83**, 357.

82. C.Esselin, E.Bauer-Grosse, J.Goulon, C.Williams, Y.Chauvin, D.Commereuc and E.Freund, *J.Physique.*, 1986, **47**, C8-243.

83. J.M.Corker, J.Evans, H.Leach and W.Levason, *J.Chem.Soc.Chem.Commun.*, 1989, 181.

CHAPTER 2 EXTENDED X-RAY ABSORPTION FINE STRUCTURE SPECTROSCOPY.

2.1 Introduction:

X-ray absorption spectroscopy is concerned with the changes in the absorption spectrum observable on interaction of X-rays with matter. The wavelength of X-rays that are absorbed by a particular element are a characteristic of that element. This is because X-rays are only absorbed when they have the same energy as the energy required for an electron in the atom to make a quantum leap to another energy level or to be ejected from the atom. Thus, the wavelengths of X-rays absorbed depend on the energy levels available in the atom. The extent to which X-rays of a particular wavelength are absorbed depends on the absorption coefficient at that wavelength.

Absorption Edges: As the wavelength λ of the X-rays is decreased (or equivalently as the energy of the photons is increased), the absorption coefficient, μ, generally decreases until a certain critical wavelength is reached where the absorption coefficient increases abruptly by several-fold. This discontinuity in the absorption coefficient corresponds to the ejection of a core electron from an atom and is called an absorption edge. Further decrease in wavelength causes a similar decrease in absorption coefficient but at a somewhat different rate until another absorption edge is reached. There is one absorption edge for the K- shell, three for the L- shell, and five for the M- shell. This shown in the Figure 2.1.[1]

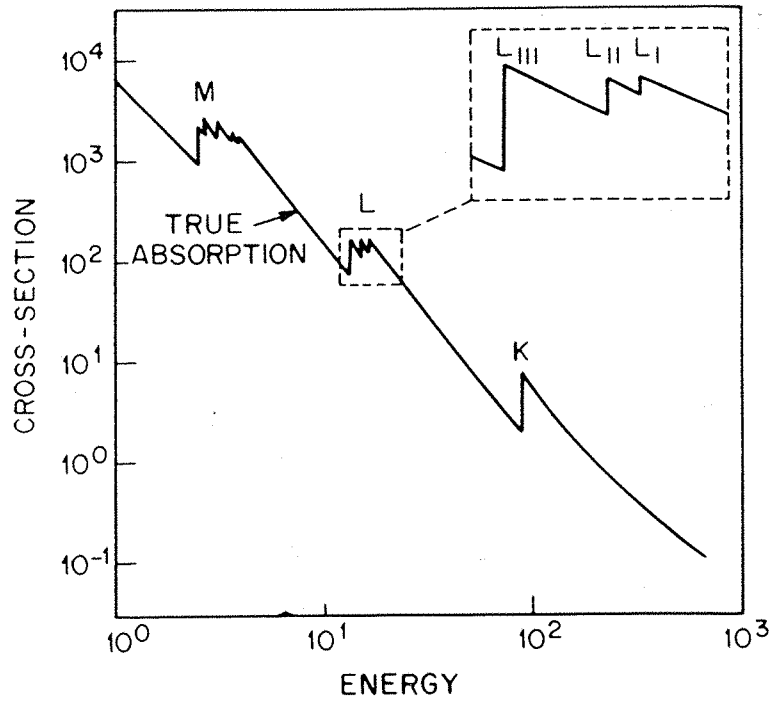

Figure 2.1.[1] Cross-section of absorption against photon energy showing the K, L, and M absorption edges.

Post-Edge Oscillations (XANES AND EXAFS): Small post-edge oscillations can be observed in the X-ray absorption spectrum of an element surrounded closely or bonded to other atoms. These oscillations can be divided into two overlapping regions called the XANES region and the EXAFS region. See Figure 2.2.

The EXAFS region consists of oscillations in the region 30 eV above the edge upto typically 1000 eV above the edge. These oscillations are caused by the backscattering of the ejected photoelectron by the neighbouring atoms back to the central atom. The constructive interference between the incoming (backscattered) and outgoing photoelectron leads to sinusoidal oscillations in the EXAFS region of the X-ray absorption spectrum.

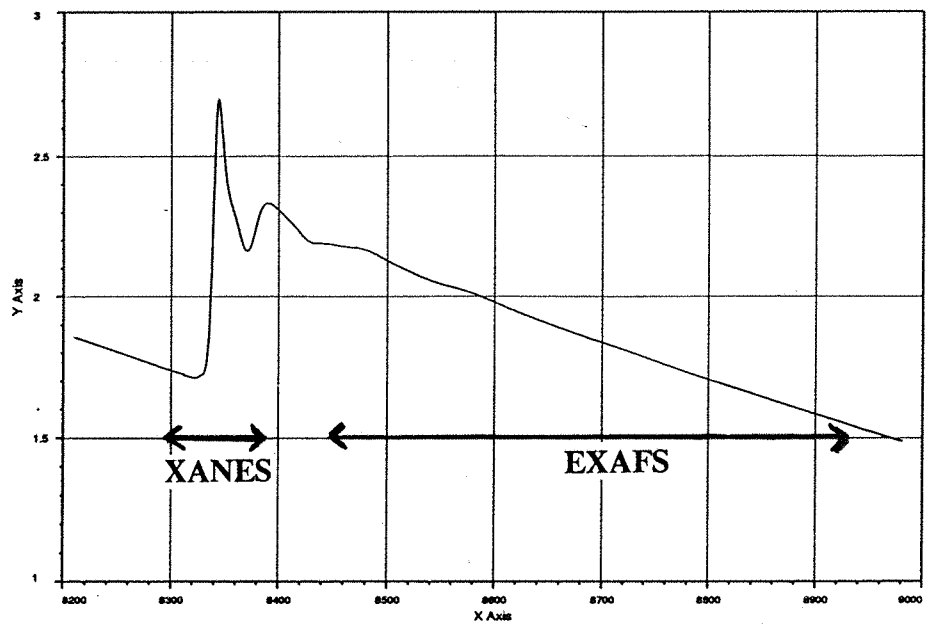

Figure 2.2. Ni-K-edge X-ray absorption spectrum of $Ni(acac)_2$ (70mM in toluene), showing the absorption edge, the XANES region and the EXAFS region.

The XANES region extends from approximately 30 eV before the edge to upto 70 eV past the edge. The oscillations in the XANES region are caused by multiple scattering resonances of the ejected photoelectron in the continuum.

In this thesis, we will mainly be concerned with EXAFS spectroscopy as a means to obtain chemical information.

2.2 Extended X-ray absorption fine structure spectroscopy[1]:

EXAFS spectroscopy involves the measurement of the X-ray absorption coefficient, μ, as a function of photon energy E above the threshold of an absorption edge. EXAFS spectra generally refer to the region 40 - 1000 eV above the absorption edge. Near or below the edge, there are absorption peaks due to excitation of core electrons to some bound states e.g. 1s to nd, (n+1)s, or (n+1)p orbitals for the K-edge. The edge position also contains information about the charge on the absorber. In between the pre-edge and the EXAFS region is the XANES region which is only now being understood. It arises from effects such as many-body interactions, multiple scatterings, distortion of the excited state wavefunction by the Coulomb field, band structures etc.

Transmission and fluorescence are two of the several modes of EXAFS measurements. Fluorescence has an advantage for dilute systems as it removes the background absorption due to other constituents, thereby improving sensitivity by orders of magnitude.

2.3 Theory of EXAFS spectroscopy:

EXAFS was first detected experimentally by Fricke[2] and Hertz[3] in 1920, although its capacity for structure has only been appreciated recently. One of the first physical explanations of EXAFS was provided by Kronig[4](1931). This was the long range theory formulated in terms of Bloch waves in crystalline material. However, he later formulated a short range theory (Kronig[5], 1932) based on the modification of the final state of the photoelectron by atoms surrounding the excited atom which was found to be more accurate. This theory of EXAFS was further developed by Hartree *et al.*[6] in 1934, Petersen[7] (addition of phaseshifts to the photoelectron wavefunction), Kostarev[8] (application of the theory to condensed matter), Schairawa *et al.*[7], Sawada[10] (inclusion of the lifetime of the core hole

state), and Shmidt[11] (inclusion of Debye Waller factors into the theory). A review of all the previous work on EXAFS was carried out by Azaroff[12] in 1963. Schaich (1973)[13] made a comparision of the short range and long range order theories based on Bloch waves in crystalline materials. He concluded that the two were formally identical provided inelastic damping effects are taken into acount.

EXAFS is the final state interference effect involving scattering of the outgoing photoelectron from the neighbouring atoms. The initial state is the localised core level corresponding to the absorption edge. The final state is of the ejected photoelectron which can be represented as an outgoing spherical wave originating from the X-ray absorbing atom. When the absorbing atom has a neighbouring atom, the outgoing photoelectron wave will be backscattered by the neighbouring atom producing an incoming electron wave. The final state is the sum of the outgoing and all the incoming waves, one from each neighbouring atom. It is the interference between the outgoing and the incoming waves which gives rise to the sinusoidal variation of X-ray absorption coefficient, μ, with photon energy E above the threshold of the absorption edge. This is known as EXAFS.

In the case of a monoatomic gas such as krypton, the μ vs E curve follows the λ^3 decay as shown in Figure 2.3. As can be seen from the figure the curve shows no post edge oscillations as there are no neighbouring atoms.

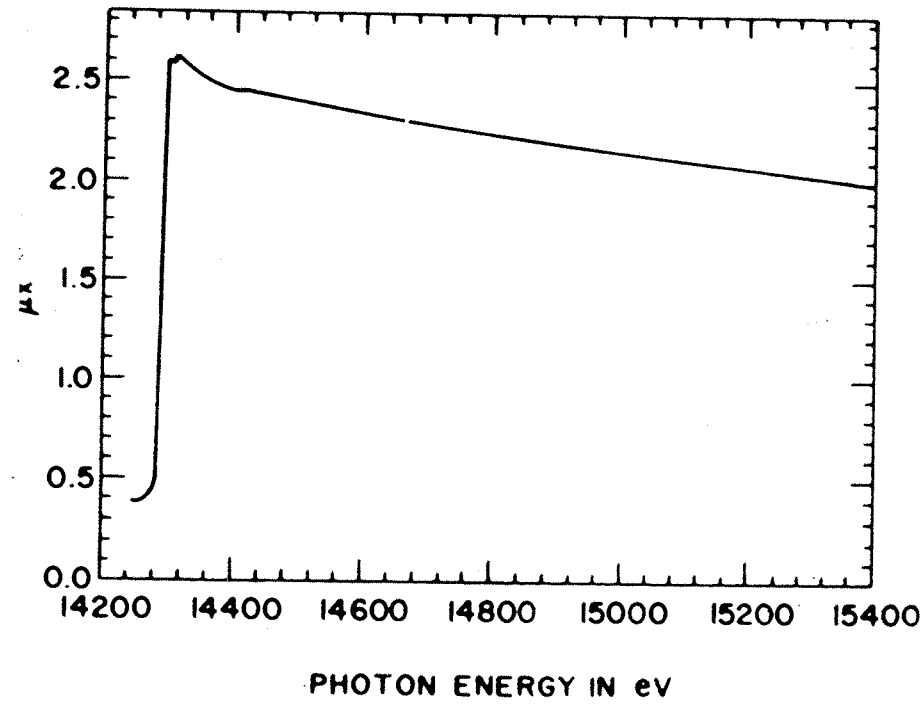

Figure 2.3.[1] X-ray absorption spectrum of the monoatomic gas krypton showing few oscillations in the EXAFS region.

In the presence of neighbouring atoms e.g in Br_2, the outgoing photoelectron can be backscattered from the neighbouring atoms thereby producing an incoming wave which can interfere constructively or destructively with the outgoing wave near the origin, resulting in the oscillatory behaviour of the absorption rate. This can be seen in Figure 2.4[1]. The amplitude and frequency of this sinusoidal modulation of μ vs E depends on the type (and bonding) of the neighbouring atoms and their distances away from from the absorber respectively.

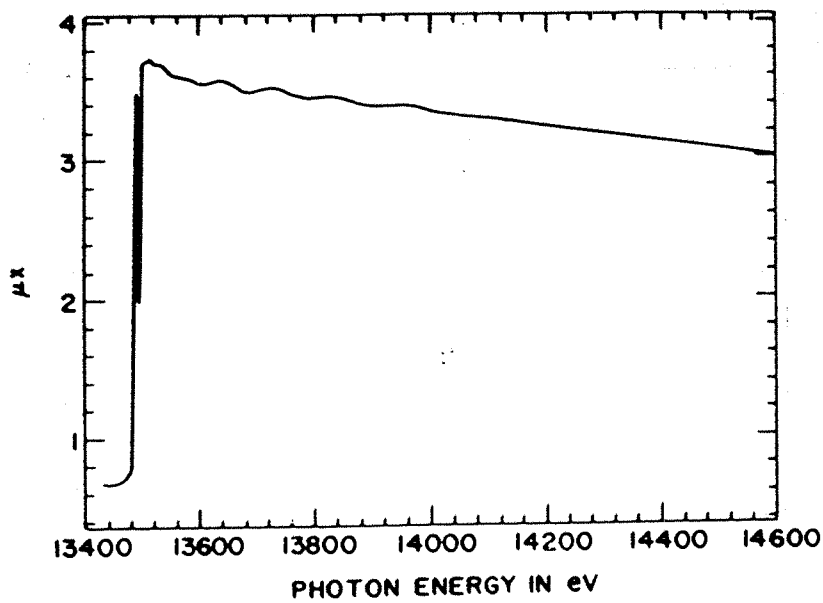

Figure 2.4.[1] X-ray absorption spectrum of bromine showing well defined oscillations in both the XANES and the EXAFS region.

In a transmission experiment, the absorbance is given by,

$$\mu x = \ln (I_0/I) \qquad (2.1)$$

where μ= X-ray absorption coefficient, x= sample thickness, and I_o and I are the intensities of the incident and transmitted beams respectively.

For a monoatomic gas such as krypton, with no neighbouring atoms, a photoelectron ejected by absorption of an X-ray photon will travel as a spherical wave with a wavelength $\lambda = 2\pi/k$ where,

$$k= \sqrt{2m(E-E_0)/h^2} \qquad (2.2)$$

Here E is the incident photon energy and E_o is the threshold energy of that particular absorption edge.

The modulation of the absorption rate in EXAFS, normalised to the background absorptions (μ_0) is given by,

$$\chi(E) = [\mu(E) - \mu_0(E)]/\mu_0(E) \qquad (2.3)$$

There are two main theories of EXAFS which use the amplitude and frequency of the sinusoidal modulation of μ vs E in order to obtain equations which enable information to be obtained on the type (and bonding) of the neighbouring atoms and their distances away from the absorber respectively. These are the plane wave theory e.g the short range single electron single scattering theory and the curved wave theory. The short range single electron single scattering theory makes the plane wave approximation which assumes that atomic radii are much smaller than the interatomic distance such that we can approximate the outgoing or incoming spherical electron waves by plane waves. This is true at sufficiently large kr i.e. high energy or at larger distances, r being the distance of the neighbouring atom from the absorbing atom. At lower energies, the plane wave approximation breaks down. This can be a problem in the case of light atom scatterers which scatter only low energy electrons and also in the case of multiple scatterings where low k data are needed. For such situations the curved wave theory is more appropriate.

The Plane Wave Single Electron Single Scattering Theory: In 1970, Sayers *et al.*[14,15] produced the basic plane wave EXAFS expression. Sayers *et al.*[14,15] pointed out that the Fourier transform of the EXAFS once corrected for the phaseshifts produces peaks at distances corresponding to the shell radii of the coordination shells of the neighouring atoms. This was a key point in the development of EXAFS as a technique for structural determinations. Sayers *et al.*[14,15] made the assumption that atoms are point scatterers. In 1974, Stern[23] developed the EXAFS theory further.

More formal derivations of the EXAFS equation based on Green's function and generalisation to Muffin tin scattering potentials can be found in Ashley and

Doniach[16], Lee and Pendry (1975)[17], Lee (1976)[18] and Grosso and Parravicini (1980)[19]. Adjustments were made in the theory for any amplitude reduction caused by multiple excitations by Rehr *et al.*[20] and Stern *et al.*(1980)[21]. A recent derivation of single and multiple scattering formalisms of EXAFS was obtained from Boland; Crane and Baldeschwieler (1982)[22].

Considerable work was done on the plane wave single electron single scattering theory by Stern[23], Stern Sayers and Lytle[24], Ashley and Doniach[16]; Lee *et al.*[17,25].

In summary, according to the plane wave theory EXAFS in k space is described by the following equation:

$$\chi(k) = \sum_j N_j S_i(k) F_j(k) e^{-2\sigma_j^2 k^2} e^{-2r_j/\lambda_j(k)} \frac{\sin(2kr_j + \phi_{ij}(k))}{kr_j^2} \qquad (2.4)$$

Here $\mathbf{F_j(k)}$ is the backscattering amplitude from each of the N_j neighbouring atoms of the jth type with a Debye Waller factor of σ_j (to account for thermal vibration (assuming harmonic vibration) and static disorder,(assuming Gaussian pair distribution) and at a distance r_j away).

$\mathbf{\phi_{ij}(k)}$ is the total phaseshift experienced by the photoelectron.

$\mathbf{e^{-2rj/\lambda j}}$ is due to inelastic losses the scattering process (due to neighbouring atoms and the medium in between) λ_j being the electron mean free path.

$\mathbf{S_i(k)}$ is the amplitude reduction factor to many-body effects such as shake up/off processes at the central atom (denoted by i).

Each EXAFS wave is determined by the backscattering amplitude ($N_jF_j(k)$), modified by the reduction factors $S_i(k)$, $e^{-2\sigma_j^2 k^2}$ and e^{-2r_j/λ_j} and $1/kr_j^2$ distance dependence, and the sinusoidal oscillation which is a function of interatomic distances ($2kr_j$) and the phase shift ($\phi_{ij}(k)$).

While N, is a linear term, $e^{-2\sigma^2 k^2}$ is an exponential damping which reduces the amplitude at increasing k values. The sinusoidal EXAFS oscillation is caused by the interference sin(2kr) term with a frequency 2r in k space. Distance r also reduces the EXAFS amplitude by $1/r^2$ which implies that the larger the distance, the weaker will be the EXAFS signal (assuming other things are equal). Finally, the effect of the total phase shift $\phi(k)$ in shifting the sine wave in k space is such that it not only changes the origin but also the frequency of the sine wave. It has relatively little effect on the amplitude.

The amplitude function $F_j(k)$ depends mainly on the type of backscatterer and also to some extent on the reduction factor $S_i(k)$ which is mainly a function of the absorber. The phase function contains information from both the absorber and the backscatterer.

The Debye Waller factor contains important structural and chemical information. It has two components- σ_{stat} and σ_{vib} due to static disorder and thermal vibrations respectively.

There are two categories of inelastic scattering processes which tend to reduce the EXAFS amplitude. The first is caused by multiple excitations at the central atom while the second is caused by excitation of the neighbouring atoms and the intervening medium by the photoelectron. In the equation 2.4, the inelastic losses due to multiple excitations (many body effects such as shake-up and shake-off processes) at the absorber are approximated by an amplitude reduction factor $S_i(k) < 1$, whereas, the inelastic losses due to an excitation of the neighbouring environment is approximated by $e^{-2r/\lambda(k)}$ where $\lambda(k)$, which depends on k, is the electron inelastic mean free path.

In EXAFS, multiple scattering can become important when atoms are arranged in a colinear array. Here the outgoing photoelectron is strongly forward scattered by the intervening atom, resulting in a significant amplitude enhancement. In fact, both the amplitude and the phase are modified by the intervening atom(s) for bond angles ranging from 180° to 75°. The effect however drops off very rapidly for bond angles below ca 150°. For these systems it is necessary to rewrite

the equation 2.4 to take into account the multiple scattering involving the intervening atoms.

Curved-wave theory: The exact curved wave theory can be found in Lee and Pendry (1975)[17] and Gurman and Pettifer (1979)[26]. This theory is mathematically complicated and difficult to apply in analysis. Gurman *et al.*[27,28] developed a rapid curved wave theory which can save upto 40 times in computation time.

2.4 Data Acquisition:

2.4.1 Synchrotron radiation:

A schematic representation of the S.R.S. at Daresbury is shown in Figure 2.5[29]. Synchrotron radiation is produced via the acceleration of an electron beam (in an ultra high vacuum chamber) to close to the speed of light. The electrons are accelerated using a radiofrequency booster and injected into a storage ring. The electron trajectory is maintained within the storage ring for several hours by constant magnetic fields and as the electrons travel at a fixed energy around the circular path and at relativistic speeds, synchrotron radiation is emitted. The radiation is in the form of a narrow cone that sweeps around the orbit as the electrons rotate,and beamlines located at tangents to the ring enable the wide band radiation produced (hard X-rays to far infra-red) to be utilised.

The Daresbury Synchrotron Radiation Source

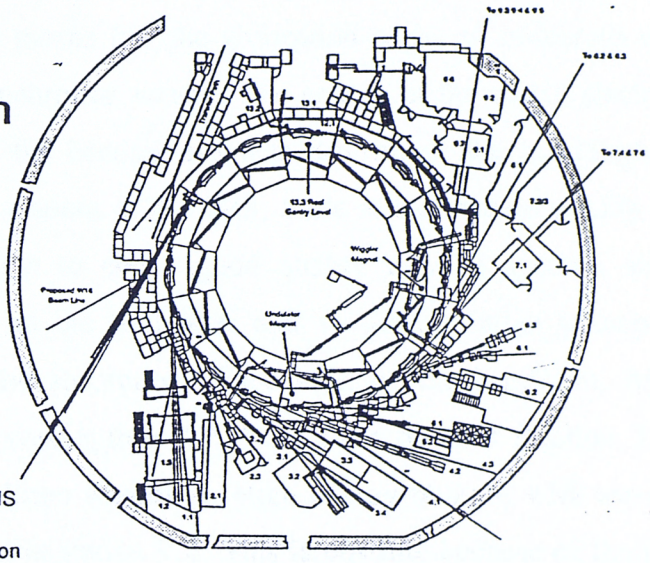

SRS EXPERIMENTAL STATIONS

1,1 Surface Spectroscopy
1,2 Spin-Resolved Photoemission
2,1 Time Resolved X-Ray Diffraction
2,2 Ultra Small Angle Scattering
3,1 Fluorescence Spectroscopy/Ion Spectrometry/Circular Dichroism
3,2 High Resolution Molecular Spectroscopy
3,3 Angle Resolved Photoelectron Spectroscopy
3,4 Soft X-Ray EXAFS/Soft X-Ray Spectroscopy Development Work
4,1
4,2 } Interdisciplinary Research Centre for Surface Science
4,3
5,1 Soft X-Ray grating Spectrometer
5,2 X-Ray Microscopy
6,1
6,2 } Angle Resolved Photoemission
6,3
7,1 Surface EXAFS
7,2/3 EXAFS
7,4 Protein Crystallography/High Angle Diffraction
7,6 Energy Dispersive EXAFS
X-Ray Topography
8,1 EXAFS
8,2 Small Angle Scattering
8,3 Powder Diffraction / Test
9,1 Powder Diffraction
9,2 EXAFS
9,3 Materials Science (EXAFS / X-Ray Diffraction)
9,4 X-Ray Surface Diffraction / Topography
9,5 Protein Crystallography (Laue)
9,6 Protein Crystallography
9,7 Laue / Energy Dispersive Diffraction
10,1 Mirror Materials Test Port
12,1
13,1 } Time Resolved Spectroscopy
13,2 Confocal Microscopy
13,3 Infra-Red Interferometry
16,1 Fixed Wavelength High Intensity
16,2 General Purpose Diffraction
16,3 Materials and Magnetic Diffraction
16,4 White Beam Station
16,5 Ultra-Dilute Spectroscopy

Figure 2.5. Schematic representation of the S.R.S at Daresbury.[29]

The advantages of synchrotron radiation over conventional sources can be summarised as follows:

1) Tuneability over a wide energy range with a continuous spectrum (i.e a broad spectral bandwidth) : This means that the absorption edges of numerous elements can be reached with the synchrotron source. The energy of the stored electrons and the radius of curvature of the bending magnets determines the maximum photon energy available. On most stations at the SRS, there is insufficient quality of light below ca. 0.9 Å wavelength to obtain good quality EXAFS spectra. Beryllium windows are also present on the beamlines and so the minimum photon energy available is governed by the absorption of the light by the beryllium, hence the photons with wavelengths greater than 3.2 Å may not be used (Station 3.4 is an exception as it has no beryllium windows). High energy photons with wavelengths as low as 0.3 Å are utilised in station 9.2. This is possible because of the presence of a Wiggler magnet. The Wiggler magnet (a niobium - titanium alloy embedded in copper and cooled in liquid helium) consists of three successive poles of alternating polarity and causes the electron beam to undergo a localised "wiggle". This has the effect of shifting the critical energy of the radiation to a higher level (See figure 2.6). Thus shorter wavelengths (higher energies) can be used.

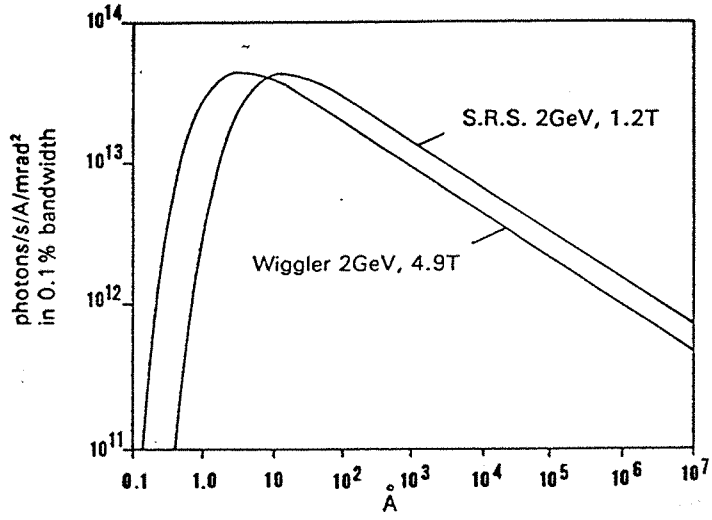

Figure 2.6. The synchrotron radiation spectrum obtainable from the S.R.S at Daresbury, showing the broad spectral bandwidth.

2) High Intensity: The intensity of the radiation produced is a factor of 10^3 to 10^6 times greater than that produced by the most powerful laboratory source. This means that spectra can be recorded in a shorter time and on more dilute samples.

3) High Collimation: As mentioned earlier, the radiation is not isotropic but is folded forwards by relativistic effects into a narrow cone (See Figure 2.7). High resolution can be achieved because the small vertical angle of emission of the beam ensures that the height of the beam is small (*ca.* 2mm) many metres away from the source.

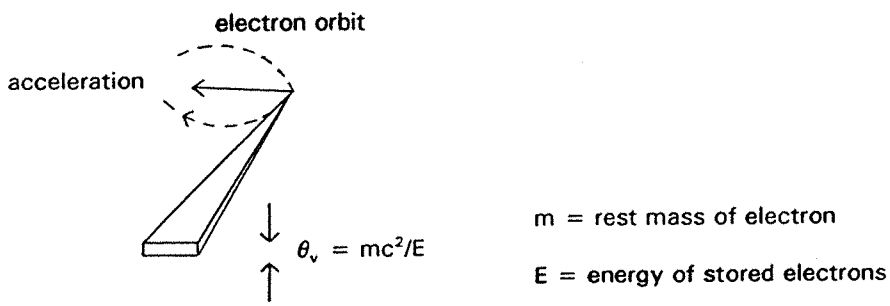

Figure 2.7.[47] Figure showing the emission of synchrotron radiation.

2.4.2 Three types of EXAFS spectroscopy: EXAFS, QUEXAFS, and EDE:

There are three main types of EXAFS based on the mode of acquisition. These are scanning EXAFS, Quick EXAFS (QUEXAFS), and Energy Dispersive EXAFS (EDE). While scanning EXAFS and QUEXAFS can be run in both the transmission and fluorescence modes, EDE can only be run in the transmission mode. In order to understand the latter two some understanding of the mechanism of operation of the first i.e. scanning EXAFS is required. Although the bulk of this thesis is based on data from EDE spectroscopy and some QUEXAFS, a few representative spectra have also been obtained using scanning EXAFS spectroscopy.

a) Transmission Scanning EXAFS:

The experimental set up for EXAFS spectroscopy in the transmission mode is shown below in Figure 2.8.

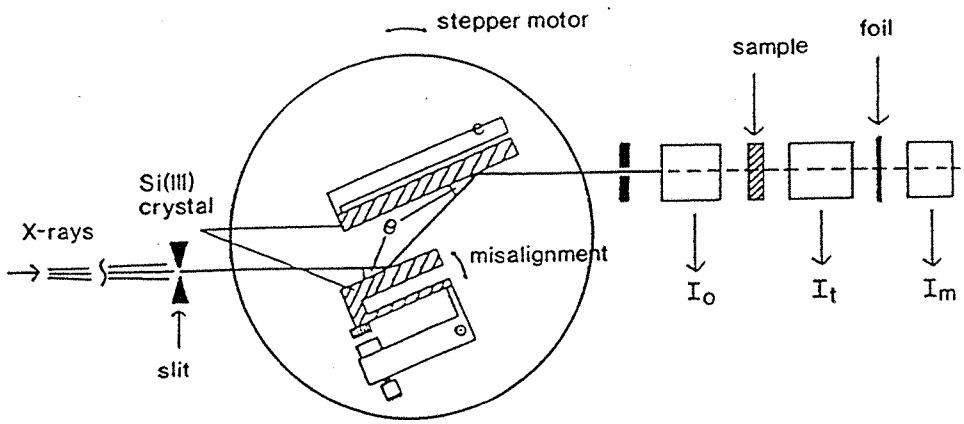

Figure 2.8. The experimental set-up for transmission EXAFS.

X-rays from the synchrotron source are collimated and the wavelength selected by the monochromator. Slits before and after the monochromator control the size of the beam hitting the sample, the vertical height of the beam being important in determining the energy resolution of the spectrum. The double crystal

monochromator on station 9.3 consists of two Si(220) crystals, that are connected to a stepper motor to enable angle θ to be varied and hence the desired energy range to be scanned. However, the light reflected off the second crystal is not perfectly monochromatic as it not only consists of the fundamental reflection (n=1 in the Bragg equation, $n\lambda = 2d\sin\theta$) but contains higher order harmonics as well. The higher order harmonics, which are not absorbed by the element under study, can cause significant contamination of the fine structure as they pass through the sample unattenuated. The rejection of the higher order harmonics is an important experimental consideration and is achieved by misaligning the first crystal off parallel with respect to the second crystal. On misaligning the crystal, the contribution to the signal from the higher order harmonics diminishes because the rocking curves for these harmonics are much narrower compared to that of the fundamental, and are also angularly displaced.[30] Hence, it is important to remain on one side of the curve during the scan. A pic20 motor is used to maintain the misalignment and therefore a constant degree of harmonic rejection as the scan proceeds. On Station 9.2, the double crystal monochromator consists of two Si(220) crystals.

Ion Chambers: For each wavelength selected by the monochromator, intensities of the incident and the emergent rays are measured by use of ion chambers before and after the sample. Each ion chamber contains two plates, one being at -400 V and the other having a Keithley amplifier attached. Transmittance values of around 80% and 20% for I_0 and I_t respectively are required and this is achieved by filling the ion chambers with various mixtures of rare gases, depending on the edge being studied. A relative absorbance (relative to the real absorbance $\ln I_0/I_t$) is measured by taking the log of the ratio of currents in each detector. The absorbance is relative due to being superimposed on the baseline of the spectrometer, which is itself energy dependent. A metal foil placed after second ion chamber but before a third ion chamber (I_m) may be used to calibrate the spectrum in the event of monochromator drift.

b) QUEXAFS[31,32]

This stands for Quick EXAFS. As mentioned earlier scanning EXAFS spectroscopy involves using a double crystal monochromator which is moved in small angular steps to vary the output energy of the monochromator.[31] At each of these positions, the monochromator is held fixed and the absorption of the sample is measured. The measurement time is varied to ensure a sufficiently accurate measurement of the absorption. The process is repeated at many energies until a spectrum of absorption against energy is complete. The time taken to complete such a scan is 30-90 minutes. Considerable reductions in total scan time can be achieved by moving the monchromator at a constant angular speed and measuring the absorption `on the fly'. This reduces considerably, as the time taken to wait while the monochromator moves and while it settles from the acceleration and decelaration of the move are reduced when the monochromator is scanned at constant speed. Under these circumstances, it becomes important to synchronise the data collection to monochromator movement by recording absorption (in transmission or fluorescence) at regular time intervals.[33,34.35] Thus, it is possible by these means to collect spectra in times as low as 20-30 seconds.

The experimental set up for the QUEXAFS was at Station 9.3 on the 5T wiggler at the SRS at Daresbury.[36.37] The station was equipped with a vertically focussing mirror, which in addition to providing extra flux also performs harmonic rejection due to due to the critical angle cutoff of the mirror reflectivity. Also, there is a very stable water-cooled monochromator.The monochromator is similar to that for scanning EXAFS spectroscopy and is made up of two crystals. The crystals are water cooled to prevent heating of the crystal. The advantage of the water cooled crystal is that d-spacing does not vary as the temperature changes with heat from the X-ray beam. The second crystal is long and flat and placed in a 'channel cut' position, thus allowing the monochromator to be moved through the required energies with the diffracted beam from the first crystal 'walking' up and down the second crystal. The second crystal is mounted on three piezoelectric 'Inchworm'

drivers, which have a travel distance of 25mm with a smallest step of 2 nm. The drivers are used to align the two crystals, in order for the crystal planes to be parallel with each other. To enhance the harmonic rejection, the second crystal is misaligned slightly. Unlike the monochromator on Station 9.2 (scanning EXAFS), where the second crystal is operated by a servo system to maintain the misalignment, the monochromator on Station 9.3 is operated without much movement of the second crystal position. This is because of the perfection of the second crystal, enabling almost exact alignment of the two crystals, the stability of the inchworm drivers and the monochromator set-up. If a servo system was used a settling time would be introduced to the system, which would lead to noise in the QUEXAFS scan. A dc servo motor which is controlled by the output from an encoder capable of encoding the Bragg angle position to 0.1 mdeg, and a shaft encoder on the drive motor drives the monochromator. The disadvantage of using stepper motors as on Station 9.2 to do QUEXAFS is that they move in a series of sharp steps, forming a series of high frequency pulses, causing intensity fluctuations in the monochromator output and giving rise to noise in the detection. The dc servo motor moves in smooth continuous movements and can also be turned or swung out at high speed whilst still achieving a static positional accuracy of 0.1 mdeg. monochromator Bragg angle is driven by a DC stepper motor system encoded by a 0.1mdeg encoder.[36,37] The high flux on the sample together with the use of a high count rate 13 element solid state germanium fluorescence detector (3) make it possible to obtain quality data on dilute solutions in less than 2 minutes.

Thus, although QUEXAFS was developed initially as a time resolved tool to investigate time dependent events it is nowadays lending itself to replace the more time consuming conventional point by point procedure, thus permitting a more efficient use of beam time at synchrotron sources.[32] A recent critical evaluation of the speed limit of the QUEXAFS technique was made by Frahm and Wong[32] who determined that with current technology a 1000 eV EXAFS scan can be measured in 5-20 seconds and a 100 eV XANES spectrum in 1-2 seconds depending on the crystal monochromator used and the energy range scanned. Further development

would be needed to achieve sub-second time resolution. Applications of QUEXAFS to time resolved studies include an investigation into the particle growth of PtRh clusters supported on NaY[38], combination with XRD to perform in-situ studies of a solid state production of cordierite from a precursor zeolite[39] and studies of high temperature solid combustion reactions[40] , among others.

c) Energy Dispersive EXAFS:

EDE is a technique developed for time resolved studies of chemical systems.[41,42] Unlike scanning EXAFS and QUEXAFS it does not involve scanning over the range of photon energies but involves measuring them all simultaneously by using an experimental setup which uses a bent crystal monochromator and a photodiode array detector. EDE is a technique that is currently employed at Daresbury for the study of dynamic experiments. This has involved the development of a high performance VME-based detector system using a photodiode array.[43]

Figure 2.9 shows the experimental set-up for the EDE station at Daresbury.[44] A bent silicon crystal monochromator selects the appropriate range of X-ray energies from the synchrotron radiation white beam which are spacially dispersed and brought to a focus at the sample. A linear photodiode array (PDA) is placed behind and registers the transmission spectrum across its active length.

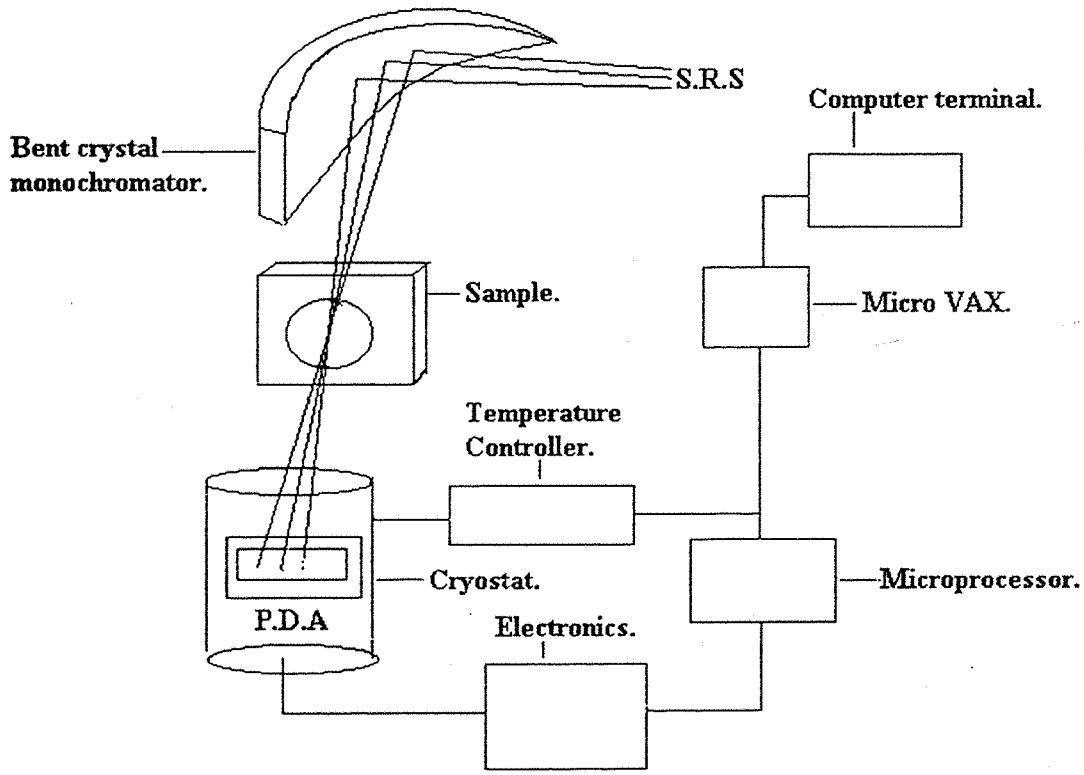

Figure 2.9. Schematic diagram showing the experimental setup for energy dispersive EXAFS at Station 9.3 at the S.R.S in Daresbury.

Four different photodiode arrays were used during the course of this thesis. They were as follows: The Reticon RL1024S, the Reticon 512T, the Reticon 512SB, and the Hamamatsu S3904. Daresbury Laboratory staff carried out separate investigations into each of these arrays and subsequently developed optimised drive and signal processing electronics to suit each of thse systems. Over the range of studies by Daresbury Laboratory,[42,45] the following characteristics of each of the photodiode arrays were determined.

Table 2.1 Characteristics of the 4 evaluated arrays:[42,45]

Device Type:	Ret1024S	Ret512T	Hama S3904	Ret 512SB
Active Length and	1"	1"	1"	1/2"
number of pixels	1024	512	1024	512
Pixel Size (microns)	25	50	25	25

Reticon RL1024S: The problems encountered by the Daresbury laboratory[42,45] included fixed pattern noise, poor linearity of response, low readout speed and signal to noise ratio. Most of these problems were in part due to the early metal oxide semiconductor technology.

Reticon 512T: This device gave much reduced fixed pattern noise, an improvement of x4 in linearity and of x2 in charge saturation. It is a 512 pixel device with 50μm spatial resolution.

Hamamatsu S3904: This device showed an increase in speed by x8, an increase in linearity of x4 better than the 512T and better energy resolution due to its 25 μm spatial pitch. However, it was x5 less efficient in photon capture than the r512T, possibly due to a thinner active area. It was, however, one of the best devices tested.

Reticon 512SB: This device exhibited excellent linearity similar to the S3904 and it is thought that readout speed could be increased by x5. Although this device gave very good measuring parameters, its reduced sensing area of 12.5mm limited the EXAFS range.

Calibration: Calibration of the EDE detector once again involved changing the angle of the bent crystal monochromator to search for the edge signal from a metal foil placed in the path of the beam. The degree of bend in the crystal was then varied to get a better focus at the sample followed by further fine tuning. Once the edge signal was found, this point of the detector is assigned the known energy value of the edge. The same monochromator position was maintained for the rest of the experiments based on this calibration. Post-edge energy values were assigned relative to this edge position. These values were assigned by obtaining a well

calibrated spectrum of the same foil using scanning EXAFS. The uncalibrated EDE spectrum was then aligned with the scanning EXAFS spectrum of the foil. The offset required to perfectly align all regions of the spectra was calculated. The energy values in eV from the scanning EXAFS spectrum were then assigned to the pixel numbers of the EDE spectrum, using the equation $y=mx+c$ where y= calibration, x= pixel number, m=energy value in ev per pixel number, c= offset required to align the spectra. The calibration at the ESRF in Grenoble was performed using a more complicated quadratic equation such as $y= ax^2+bx+c$, where x= pixel number, c= offset and y= calibrated value in ev.

Setup of cells for I_0 and I_t measurements in EDE: See figure 2.10.

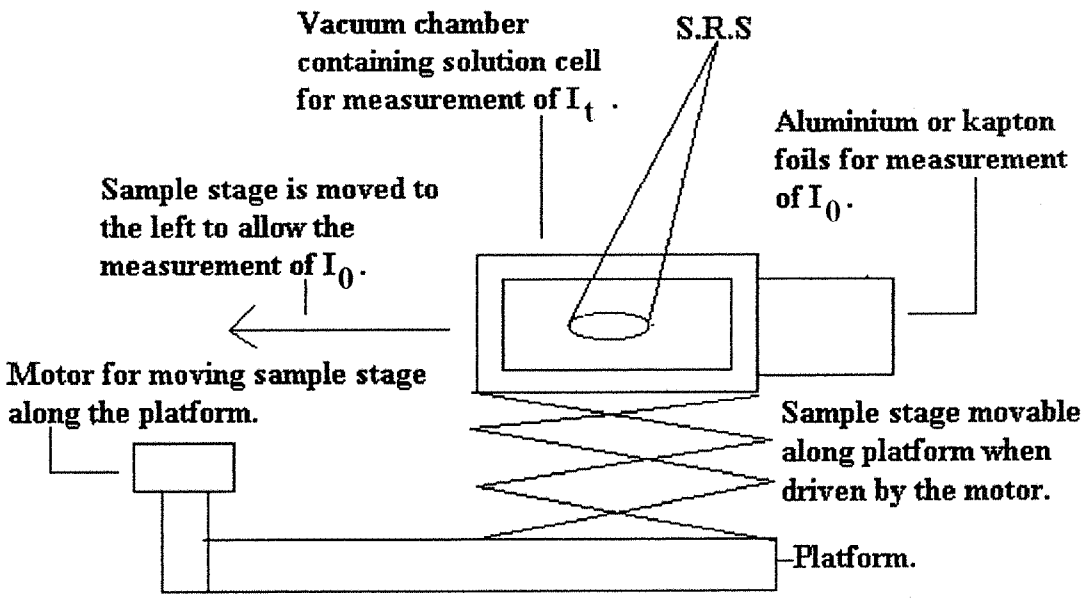

Figure 2.10. The motorised set-up of cells for the sequential measurement of I_t and I_0 as required for recording a complete EDE spectrum.

EDE Setup at the ESRF at Grenoble Station ID24: While EDE experiments at Daresbury usually involve silicon monochromator crystals in the Bragg geometry, it is possible at the Grenoble ESRF also to use silicon monochromator crystals in the Laue geometry. The difference between these two is that in the Bragg case there is asymmetric broadening of the reflectivity profile leading to strong distortions of the near edge structure and to a reduction in spectral resolution. In contrast the reflectivity profile of the crystal in the Laue case are hardly affected by the crystal bending and essentially preserves a rectangular shape.[46]

Figure 2.11 shows the experimental set-up using a Laue crystal in transmission mode.

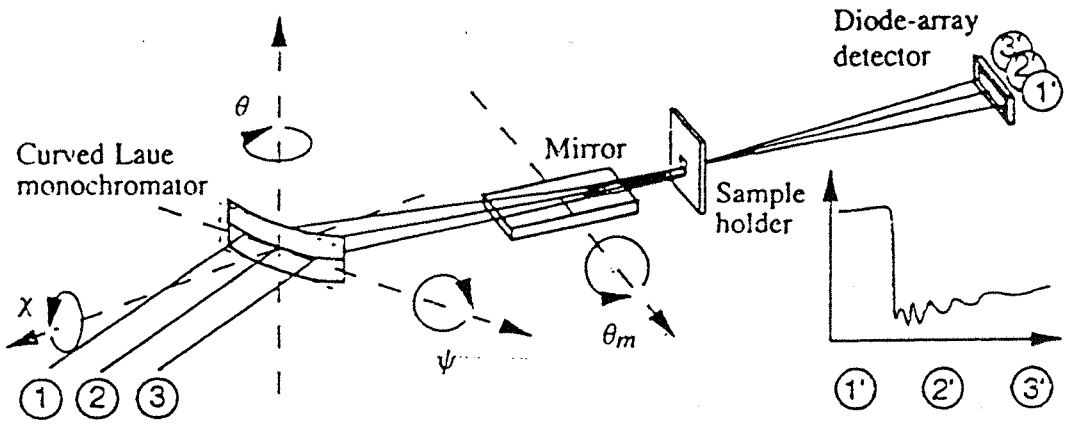

Figure 2.11. Schematic diagram of the EDE spectrometer DEXAFS at Hasylab employing transmission monochromator optics. [46]

A schematic diagram of the experimental setup of the optics and the experimental hutches at station ID24 at the ESRF at Grenoble used for obtaining EXAFS spectra is shown in Figure 2.12.

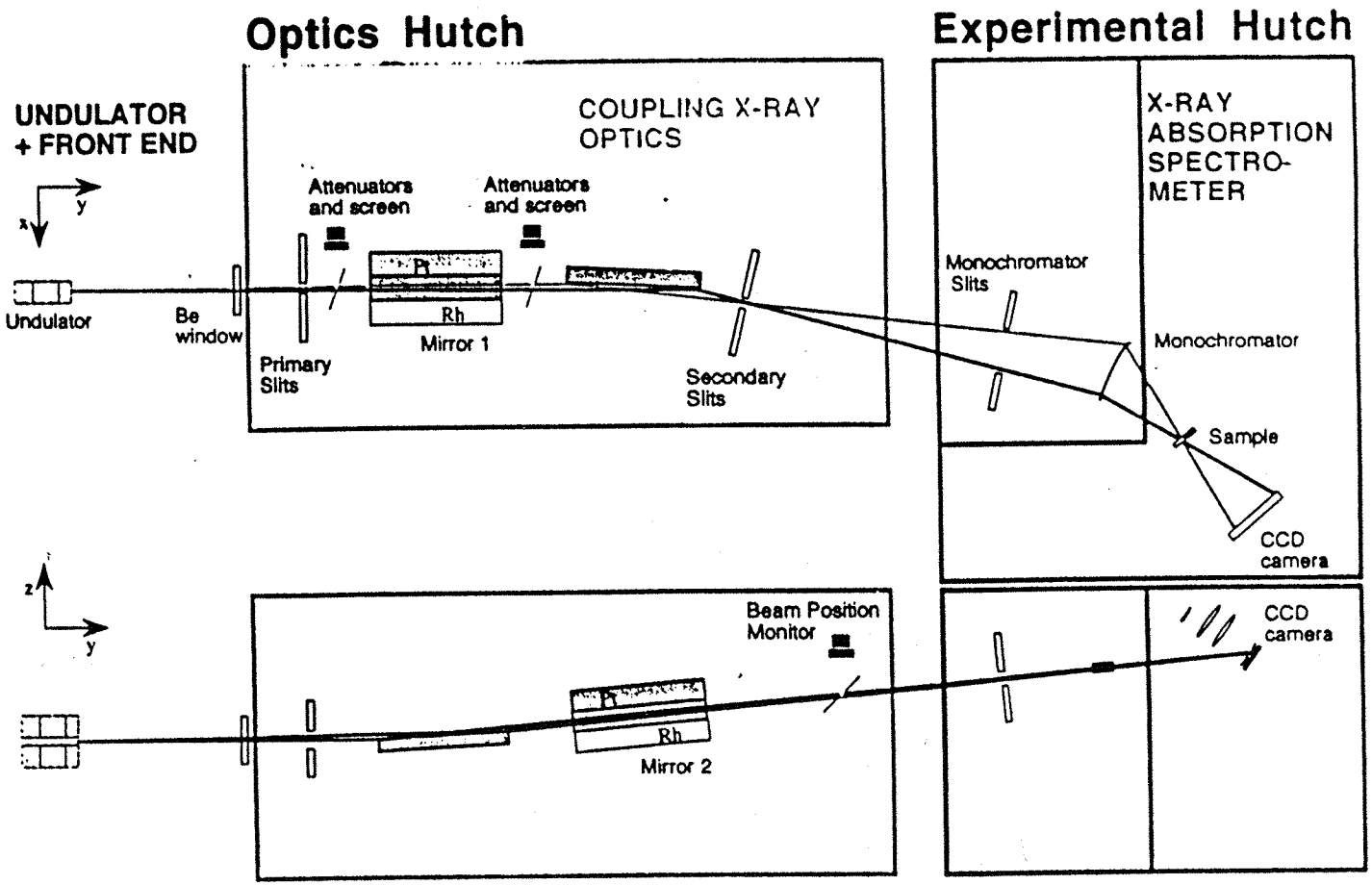

Figure 2.12. A schematic diagram of the experimental set-up of the optics and experimental hutches at station ID24 at the ESRF at Grenoble used for obtaining EXAFS spectra.

d) Fluorescence EXAFS:

Measuring fluorescence intensity provides an alternative means of obtaining relative values for μ. Fluorescence detection is required when the element under study is present in a low concentration, or when the sample is so thick that nearly all the beam is absorbed. This method of recording EXAFS is essential for dilute solutions since the fluorescence is of that of the absorber directly and so the contribution from the solvent is effectively removed. For dilute solutions, the fluorescence intensity obtained is a direct measure of the k-shell absorption probability. Thus, an excitation spectrum (I_f/ I_0 versus photon energy) is equivalent to an absorption spectrum (μ versus the photon energy).

Fluorescence detectors often consist of a thallium doped NaI detector, comprising of a collimator, scintillator and photomultiplier or a 13 element solid state germanium detector for very dilute samples. Experimentally, the sample is placed at 45° to the beam. Scattering of the radiation also occurs from the sample in this configuration but placing the detector in the horizontal plane at 90° to the beam ensures that the scatter count is minimised, since the radiation from the S.R.S. is polarised. Filters placed in front of the scintillation detector are used to further reduce the scattered radiation accompanying the fluorescence radiation. The choice of filter is dependent on the edge being studied; typically a (Z-1) foil is used for first row transition elements so that the K-edge of the filter is at a higher energy compared to the fluorescence.

Both scanning EXAFS and QUEXAFS spectroscopies can be carried out in the fluorescence mode, but EDE can only be carried out in the transmission mode.

2.4.3 Sample Preparation for XAS studies:

The experiments for this thesis were carried out on Station 9.3 of the S.R.S at Daresbury and at Station ID24 of the E.S.R.F at Grenoble.

a) Room temperature samples:

Solid precursor samples were diluted with boron nitride to give 10% of the element under study. Samples were held between kapton sellotape in aluminium sample holders. Room temperature solutions of the precursors were prepared under air sensitive conditions using dried and degassed solvents. Samples were contained in air tight aluminium cells (path length= 1cm) with kapton windows (Figure 2.13) held between clamping plates.

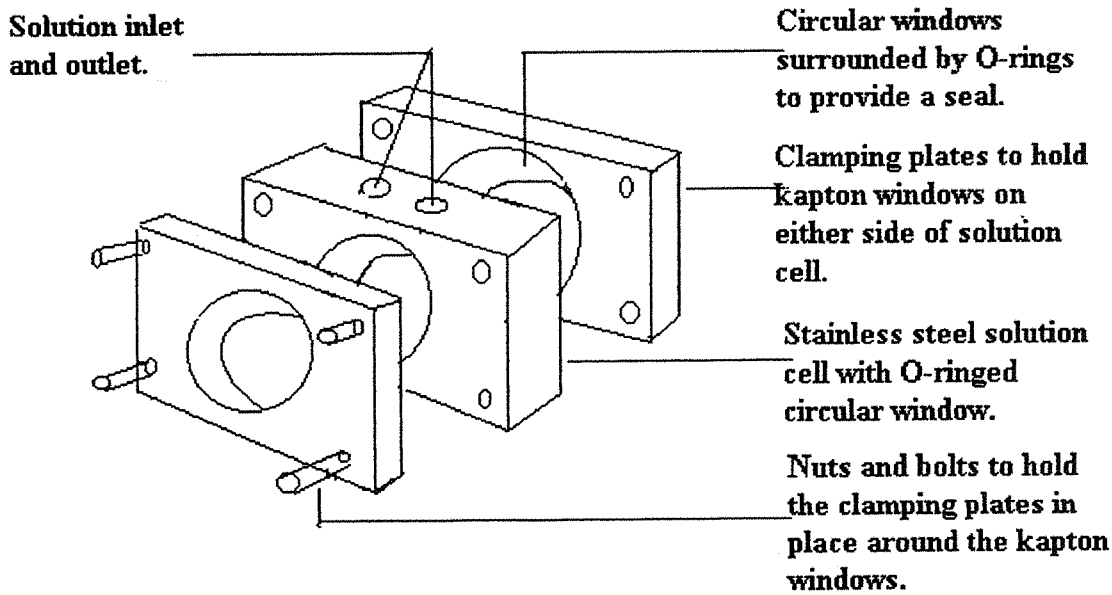

Figure 2.13. Room temperature cells for use in solution studies.

A cell filled with solvent was used for the blank or I_0. Figure 2.14 shows a photograph of the room temperature solution cells prior to, during and after assembling.

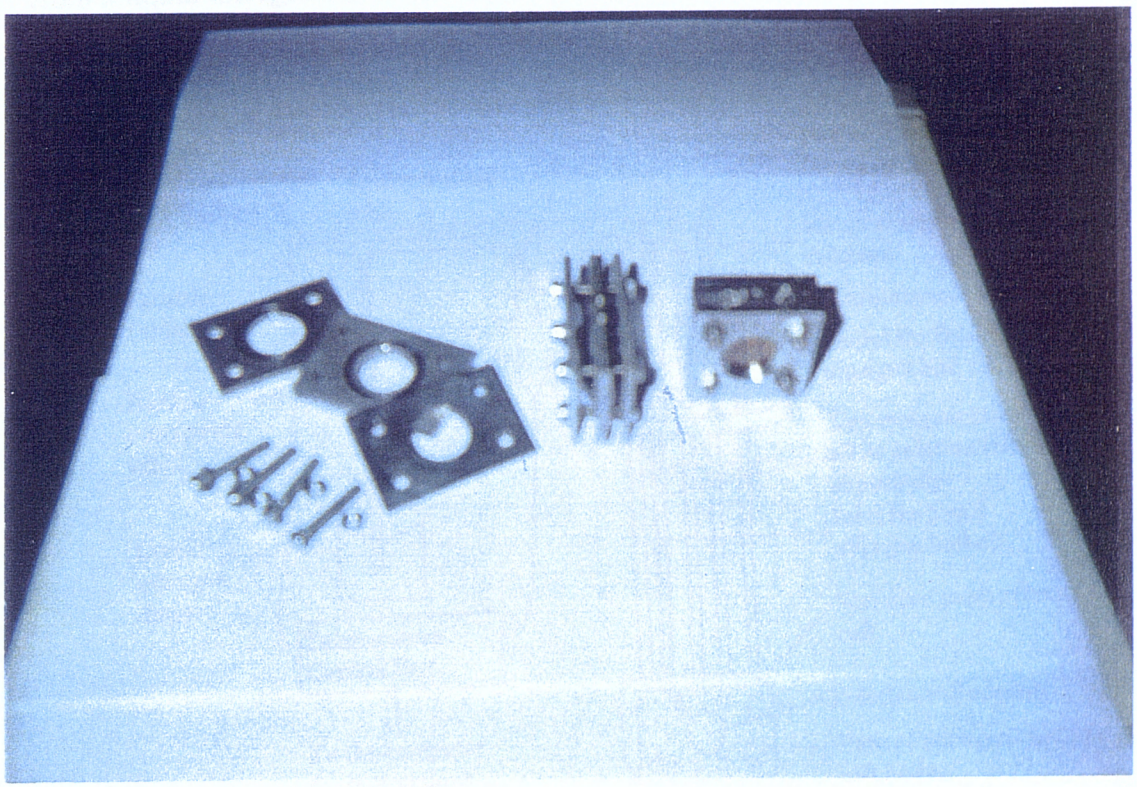

Figure 2.14. Figure showing a photograph of the room temperature solution cells prior to assembling.

b) Low Temperature Studies:

A schematic diagram of the equipment used for the low temperature studies of reaction mixtures is shown in Figure 2.15. **This equipment was used for all the Ni-K-edge and Br-K-edge variable temperature (i.e. room temperature and low temperature) studies in this thesis except where otherwise specified.** As can be

seen from Figure 2.15, the prepared reagent solutions were placed in the reagent syringes which were clamped into electronically driven syringe drivers. These syringe drivers pumped the reagent solutions into a cooled observation cell where mixing could take place at low temperatures. The cell was cooled using boil-off from a liquid nitrogen dewar as shown in Figure 2.15.

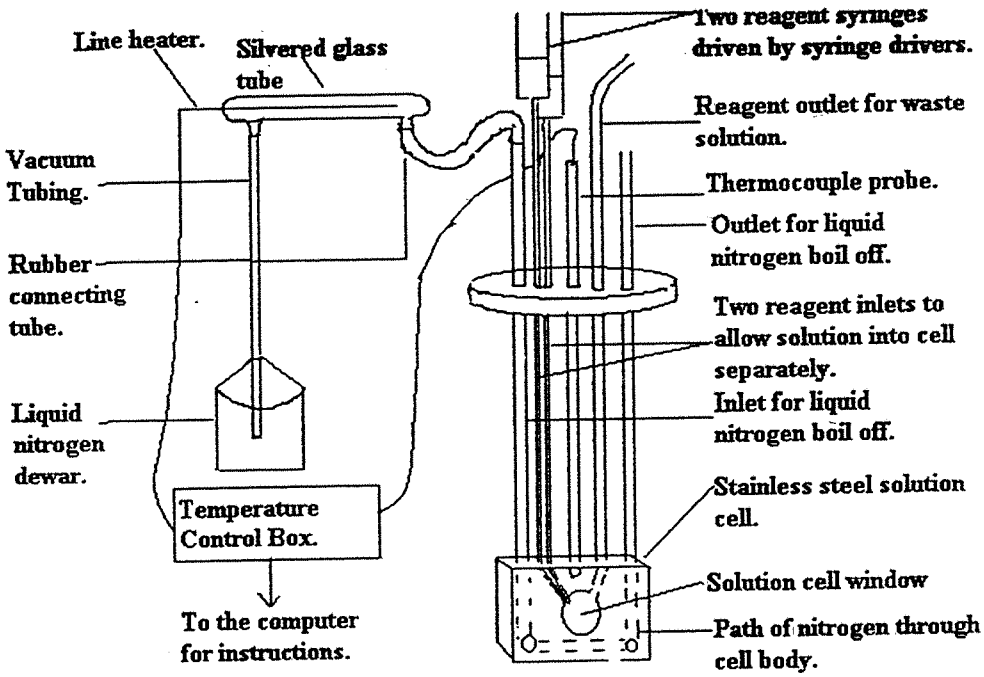

Figure 2.15. Schematic diagram showing the experimental set-up (not to scale) used for low temperature studies of reaction mixtures at the S.R.S in Daresbury.

As can be seen from the Figure 2.15, the observation cell had needle connections to the two reagent syringes to enable solutions to be driven separately in to the cell and mixed in situ. There is a single outlet or reagent waste tube out of the cell. The cell has kapton windows clamped to either side of it.

The solution cell was enclosed in a vacuum chamber[47] which prevented ice formation on the kapton windows as the cell was cooled. Figure 2.16 shows a photograph of 1) the vacuum chamber 2) the solution cell on its side 3) the temperature control box and 4) pressurised liquid nitrogen dewar as required for the low temperature solution studies.

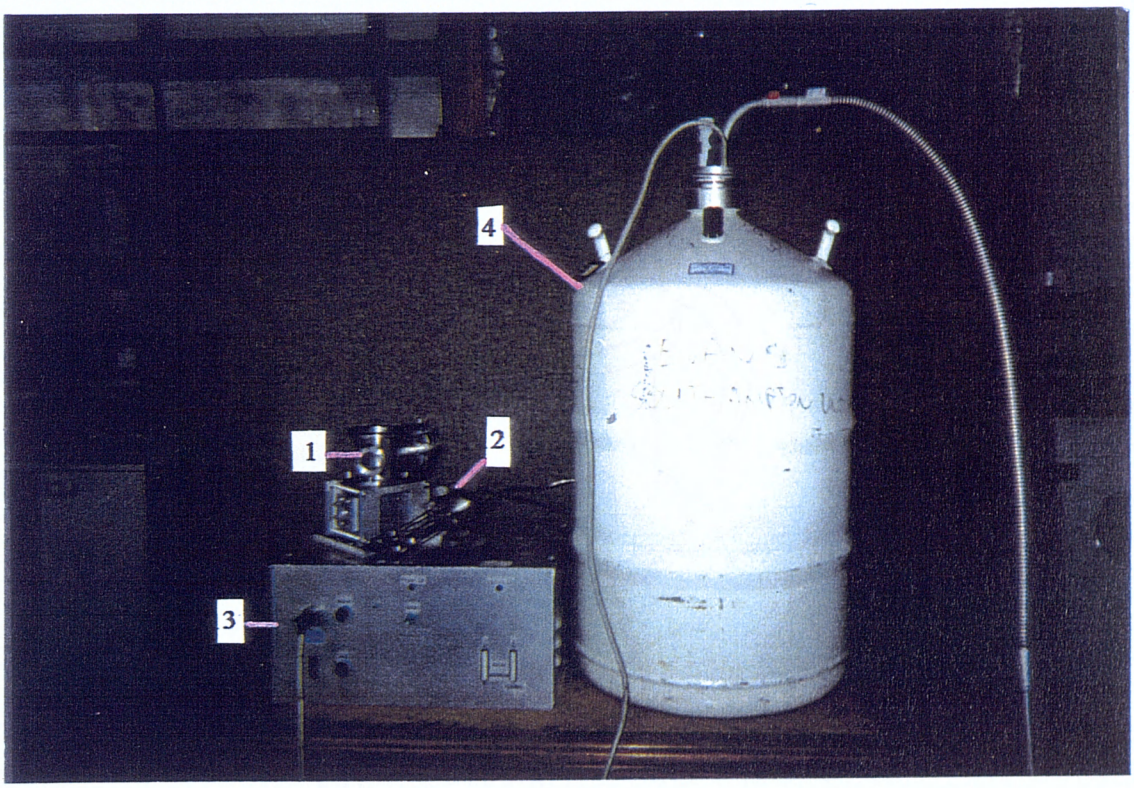

Figure 2.16. Figure showing a photograph of the low temperature equipment required for solution studies consisting of 1) a vacuum chamber 2) a solution cell on its side 3) a temperature control box and 4) a pressurised liquid nitrogen dewar.

The schematic arrangement of the items shown in the above Figure 2.16 has been given in Figure 2.15. Temperature control of the observation solution cell is achieved by regulating the flow of the boil off from the pressurised liquid nitrogen dewar in to a silvered glass tube where it is heated gently by a line heater to the

required temperature before being passed via steel tubes in and out of the steel body of the observation solution cell as shown in Figure 2.15. A thermocouple probe placed inside the cell body detects the temperature of the cell. This is relayed back to the computerised temperature control box which adjusts the flow of the liquid nitrogen boil off accordingly.

A more detailed drawing of the vacuum chamber[47] is shown in Figure 2.17. The vacuum chamber has beryllium windows which enable the X-rays to pass through to the reaction cell inside the vacuum chamber. The beryllium windows are placed on three sides of the box allowing for both transmission and fluorescence experiments.

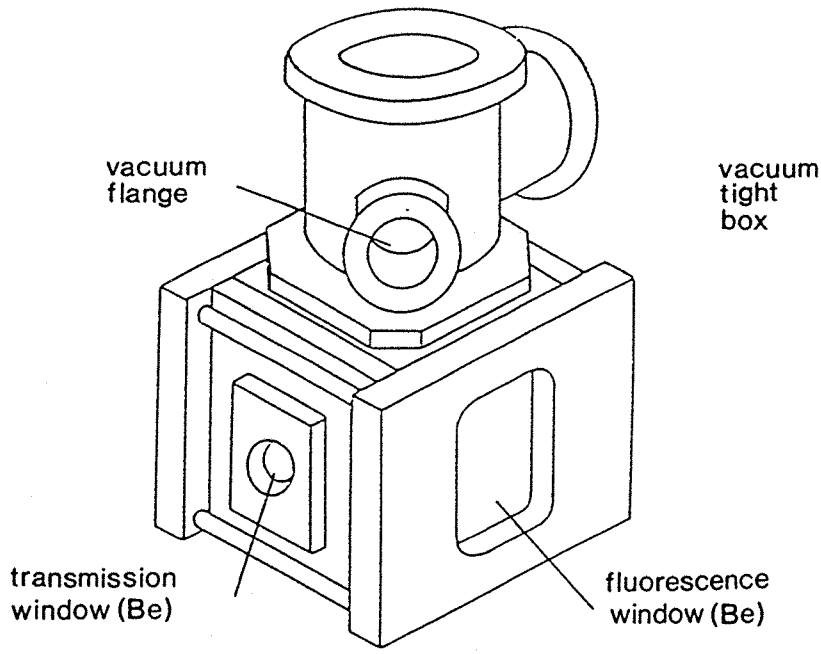

Figure 2.17.[47] Vacuum chamber used for low temperature EXAFS studies of reaction mixtures.

The chamber also has flanges for fitting vacuum pump tubing to evacuate the vacuum chamber after the cell is placed in the chamber and prior to lowering the temperature of the cell. The solution cell is secured to the chamber using vacuum tight Edwards fittings or locks. The kapton windows of the observation cell were

kept in line with the beryllium windows of the chamber so that the X-rays pass through the beryllium windows of the chamber through the windows of the observation cell and out through the next beryllium window of the chamber to reach the detector for analysis.

Figure 2.18 shows a photograph of the stopflow equipment[48] required to deliver solutions to the solution observation cell. As can be seen from the photograph the equipment consists of two syringe drivers holding the two reagent syringes, and their respective control boxes which control the speed with which solution from each syringe will be delivered to the observation cell where the mixing occurs. The photograph also shows two remote control boxes for starting and turning off the syringe drivers from outside the X-ray hutch.

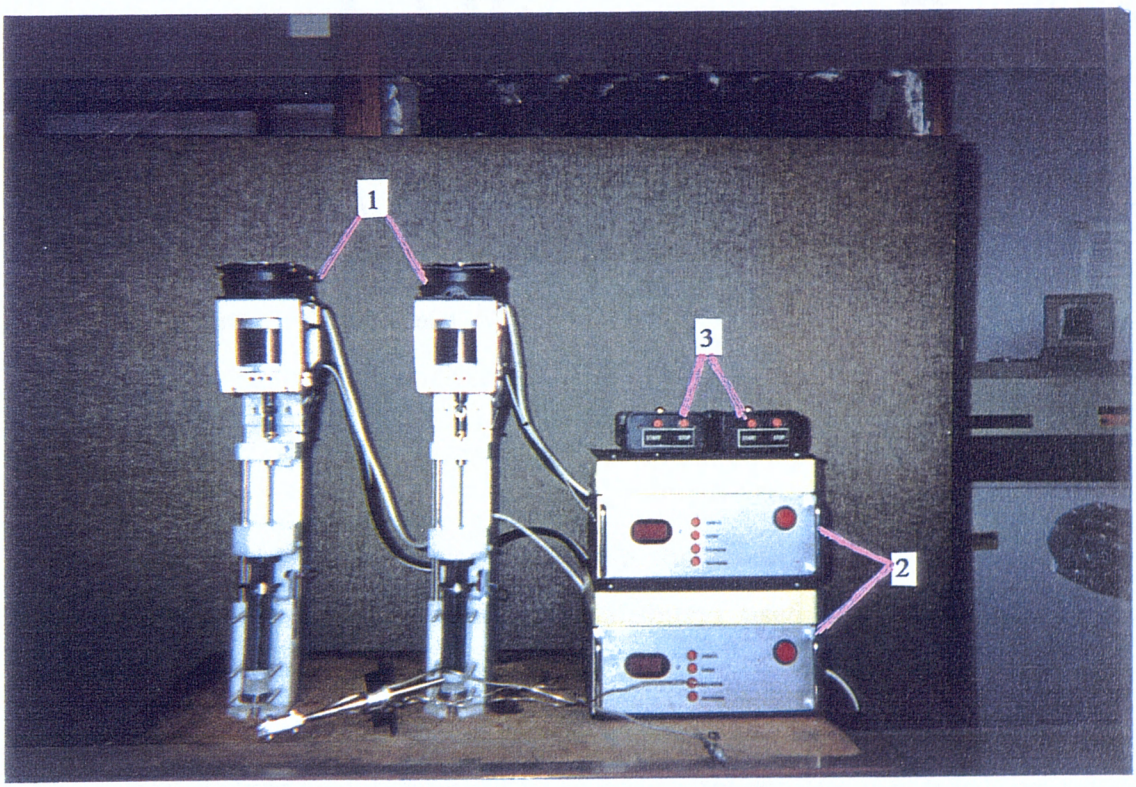

Figure 2.18. Figure showing a photograph of the stop flow equipment[48] consisting of 1) two syringe drivers, 2) two control boxes and 3) two remote control boxes for starting and turning off the syringe drivers from outside the X-ray hutch.

c) *Stopped flow studies:*

These were carried out using a modified SFA-20 by Hi-Tech Scientific, Salisbury, U.K. A schematic diagram of the modified SFA-20 stopped-flow system for room temperature EXAFS studies is shown in Figure 2.19.

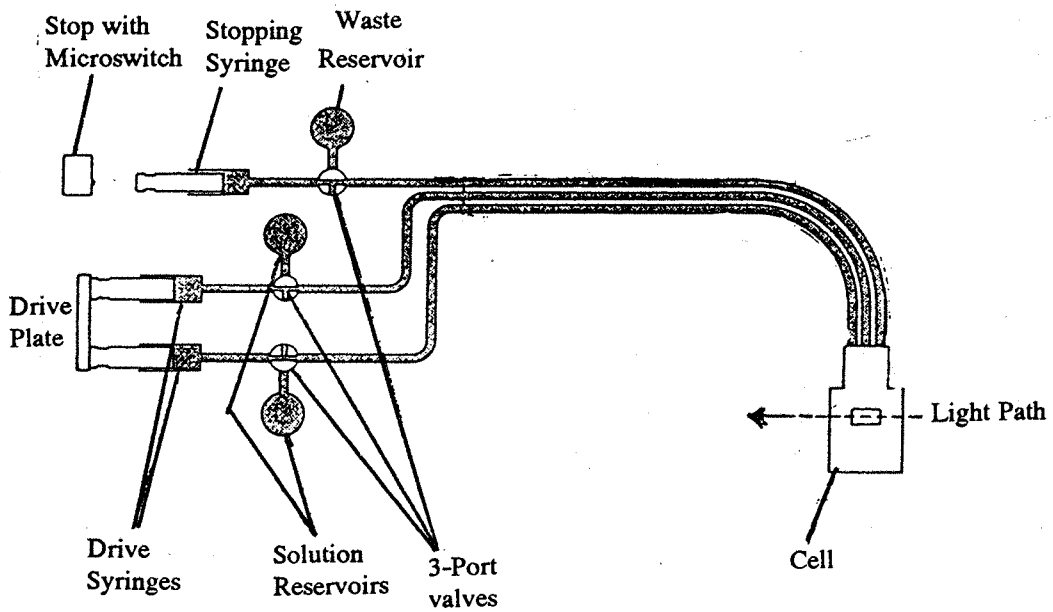

Figure 2.19. Schematic diagram showing the modified SFA-20 stopped-flow system (made by Hi-Tech Scientific, Salisbury) used for room temperature EXAFS studies of reaction mixtures.

The stopped-flow system consisted of two reagent syringes filled and driven by two syringe drivers which were controlled by a control box. On pressing the start button on the control box, the solutions from the two reagent syringes are released into a mixing chamber after which they enter an observation cell with kapton windows to allow X-rays to pass through. Simultaneously, any waste or old solution

in the observation cell is released into a waste syringe by the same mechanism which drives the reagent solutions ino the reaction cell. A photograph of the modified SFA-20, its control box, and the observation cells for sample and blank, is shown in Figure 2.20.

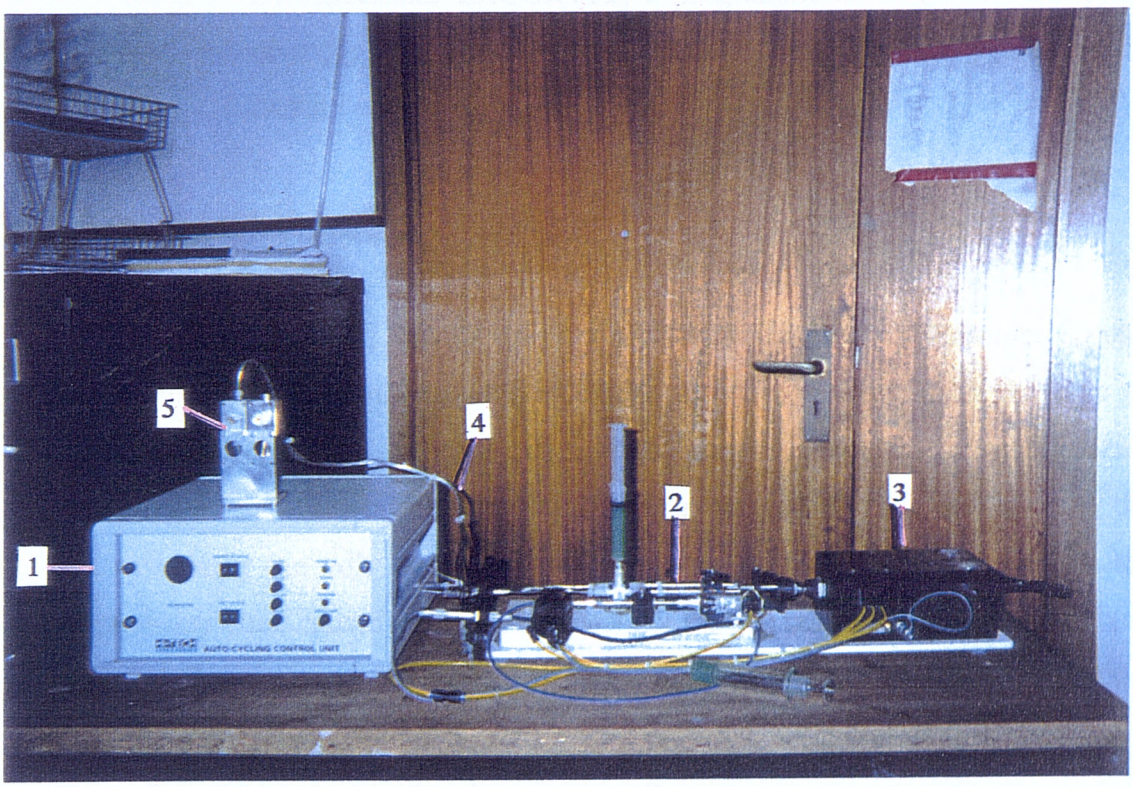

Figure 2.20. Photograph of the SFA-20 stopped-flow system (made by Hi-Tech Scientific, Salisbury, U.K) used for room temperature EXAFS studies of reaction mixtures. The different components labelled on the photographs are 1) control box 2) reagent syringes 3) syringe driver 4) steel tubes to the observation cells 5) observation cells (I_0 and I_t) .

2.5 Data Analysis:

In order to extract useful information from the raw spectrum it was necessary to process the data. Two separate programs were used to process the data. These were PAXAS[47,49] and EXCURVE92[50]. PAXAS is a PC program developed by N.Binsted at Southampton, and was used to subtract the background absorption from the raw XAS spectrum. EXCURV92, a programme developed in Daresury, was used subsequently, to generate a theoretical model to be fitted to the experimental EXAFS.

2.5.1 PAXAS:[47,49]

The first step in PAXAS was to calibrate the transmission or fluorescence spectra with reference to a monitor spectrum of the relevant metal foil. In the case of scanning EXAFS spectra, the data was collected as absorbance versus monochromator. The next step involved editing out any glitches or spikes in the spectrum using the edit facility of the programme. Glitches and spikes in the spectrum are often caused by beam movements, sample inhomogeneity or additional reflections from the monochromator. These were edited out of the spectrum, in the case of sharp spikes, by moving the points of the spike down in the y-direction. Where the glitch coverered a larger area, the relevant points were deleted and replaced by a polynomial to fit the rest of EXAFS spectrum. However, care was exercised when editing spectra by these methods as the spectrum may be corrupted. It was therefore often preferable to edit these artefacts on the k^3 weighted background subtracted spectrum than on the raw spectrum.[47]

In order to reduce the signal to noise ratio, spectra were sometimes averaged using PAXAS after they were aligned using the edit facility.

The spectrum now contained the background absorption of the spectrometer together with the residual absorption by any other element within the sample. In order that these effects were removed so that only absorption due to the central atom

remains, pre-edge and post-edge background subtraction were performed. The result of this background subtraction was a spectrum of $\chi(k)$ versus k.

Pre-edge background subtraction:[47] Removal of the pre-edge background was achieved by fitting the pre-edge absorption trend with a polynomial of order 2 or 3. The points U1 and L1 were defined by the program and then an extra point P1 is chosen (Figure 2.21). By altering the position and weighting of P1 satisfactory pre-edge subtraction was obtained. The background subtracted absorption (BSA) can be flat or gently sloping downwards. Poor pre-edge background subtraction can result in very low frequency terms in the EXAFS spectrum, thus leading to incorrect EXAFS amplitudes.

Post-edge background subtraction:[47] This was performed by defining the points U2, L2 and an extra point P2 and fitting these with either a polynomial of order 6 or 7 or an inverse polynomial or a linked cubic polynomial (splines), such that the amplitude of the EXAFS was divided equally (Figure 2.21). Various weighting parameters were also used as part of the post-edge background subtraction. These parameters were related by the equation,

$$W_i = W_c + ki^{wn} + e^{wek}$$

where w_i was the total weighting, W_n was varied in the range 0-5 and W_e was varied in the range 0-2. W_c can be taken as 0,-1, or -2. As the amplitude of the oscillations diminishes at high energy, the EXAFS was multiplied by a power of k, normally 3, in order to compensate for this (Figure 2.21).

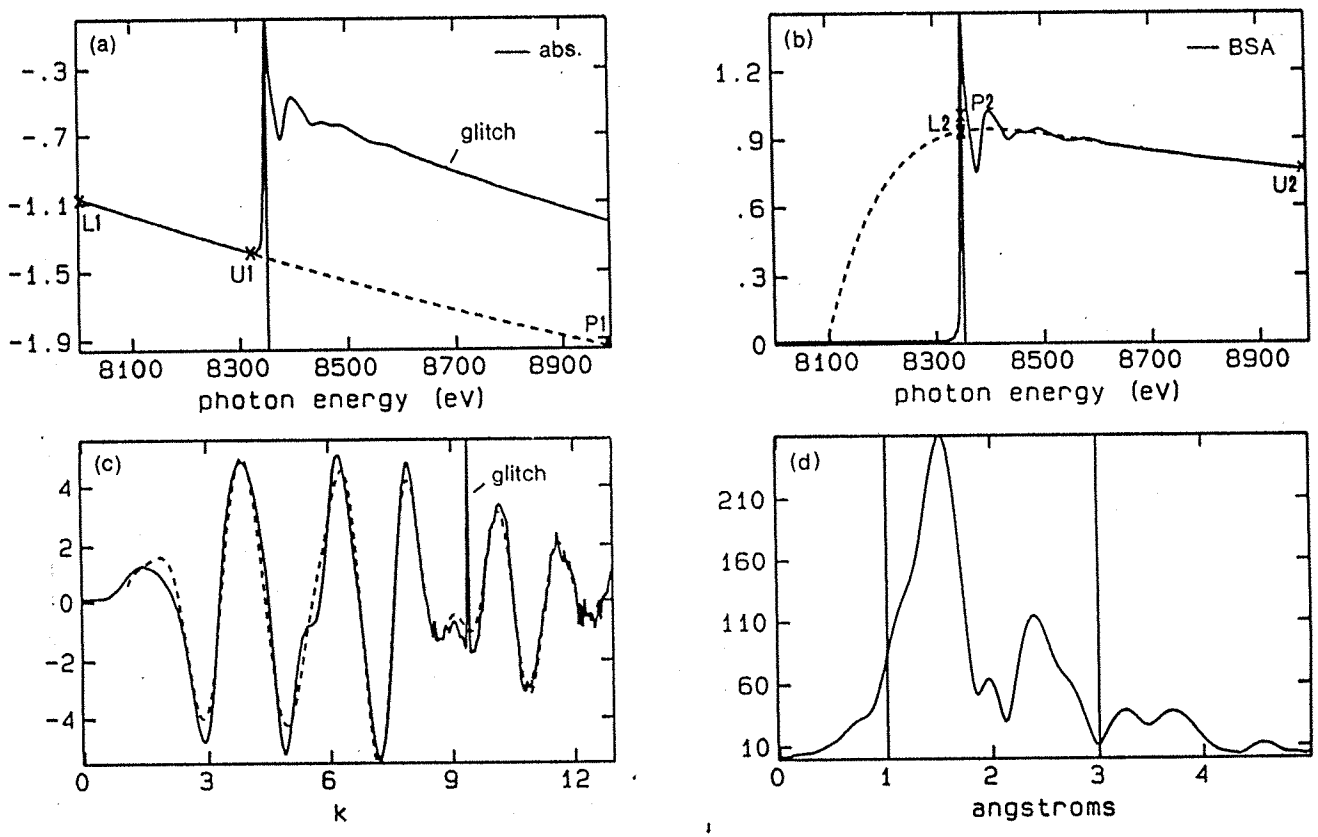

Figure 2.21.[47] Background subtraction in PAXAS. a) pre-edge background subtraction, b) post-edge background subtraction, c) k^3-weighted EXAFS together with the back transformation of the R-space spectrum (limits 1-3 Å). The R-space spectrum, or Fourier transform of the EXAFS is shown in (d).

2.5.2 EXCURV92:[50,51]

The rapid curved-wave theory of Gurman et al[27,28] has been used by this program to fit the experimental data to a calculated theoretical spectrum. In order to obtain a theoretical spectrum, firstly, the phase shifts were calculated for the elements present by ab initio methods. Von-Barth ground state potentials and Hedin Lundqvist exchange potentials were used by the calculation for this purpose. The parameters used to generate the theoretical spectrum are given below in Table 2.2. These parameters were used to generate a theoretical spectrum. The parameters of the theoretical spectrum were adjusted and refined by a least squares iteration to optimise the fit of the theoretical spectrum to the experimental spectrum.

Table 2.2 Parameters for generating a theoretical EXAFS spectrum.

NS	The number of shells for which the theory is calculated.
Nn	The number of atoms in shell N.
Rn	The distance of shell n from the central atom.
Tn	The atom type for shell N.
An	The Debye-Waller factor for shell n, defined as 2
Ef	The difference between calculated Fermi-level energy and the known value for the element.
Eo	The magnitude of the photoelectron energy at zero wave vector. This is not under user control when using Hedin-Lundqvist potentials.

Table 2.2 Parameters for generating a theoretical EXAFS spectrum (Cont'd).

AFAC	The energy independent amplitude factor intended to take care of reduction in amplitude due to multiple excitations. This is different for each absorbing element, and is obtained from analysis of model compounds.
Emin	The minimum energy value for calculations or plots.
Emax	The maximum energy value for calculations or plots.
Kmin	Wave vector corresponding to (Emin+E0).
Kmax	Wave vector corresponding to (Emax+E0)
Lmax	The maximum angular momentum usedin theory calculations.
WPI	Used to allow for experimental broadening when using Hedin-Lundqvist potentials, as the imaginary part of the potential (VPI) is not specified by the user.

In order to obtain the theoretical spectrum, it was necessary to input starting values for the coordination numbers, shell distances, Debye-Waller factors and Ef. The atom type of each shell was also defined. These variables were then refined together, except the coordination numbers, as they are highly correlated with the Debye-Waller factor. The co-ordination numbers were then refined separately without the Debye-Waller factors to obtain the optimum fit. Refinement takes place using an iterative procedure.

The goodness of fit between the theoretical spectrum and the experimental spectrum was measured in two ways. The first was by calculating the R-factor[52]. The R-factor was calculated as the sum total of the errors between all the data points given as a percentage of the experimental.

$$R=\int[\chi^T-\chi^E]k^3dk * 100 / \int\chi^E(k)k^3dk \qquad (2.5)$$

The R-factor should not exceed *ca.*30% or standard compounds, although with dilute samples and noisy data this can be difficult to achieve.

The goodness of fit was also measured using the Fit Index[53]. The fit index calculates the sum of the square of the differences between the theoretical and experimental data points.

$$FI = \Sigma_1 [(\chi^T - \chi^E)k_i^3]^2 \qquad (2.6)$$

A satisfactory fit index has a value of less than $8*10^{-4}$, with good fits being less than $5*10^{-4}$. Statistical errors and correlation coefficients[54] for the final values of each parameter are also calculated using standard techniques within the EXCURV92 program.

There are many factors which restricted the number of shells that could be fitted to a particular spectrum or data set. The most important factor was the length of the data set. This also placed a limitation on the resolution obtained from a given data set. The resolution determined the ease with which different shells could be distinguished. It is given[55] by the equation shown below.

$$\Delta R = \pi/2\Delta k \qquad (2.7)$$

Δk is determined by the length of the data set starting from $3Å^{-1}$. This is because EXAFS spectra are not fitted below *ca.* $k = 3Å^{-1}$, as this region is dominated by XANES, and requires a different theoretical treatment. Thus, the resolution obtained from a data set of length $14Å^{-1}$ is 0.14 Å. This would mean that shells separated by more than 0.14 Å apart can be distinguished by the data analysis. Thus, the length of the data affects the number of shells that can be distinguished in a given data set.

The length of the data was also important in determining the number of independent variables that can be iterated at one time when calculating the best

theoretical spectrum[51]. The number of independent variables is given by the following equation[55]:

$$N_{idp} = 2\Delta k\Delta r/\pi \qquad (2.8)$$

where Δr is the difference between the closest and the most distant shells being fitted. The number of refined variables must not exceed the calculated N_{idp}.

Various tests have also been designed to determine the statistical significance of shells and whether too many parameters have been included. The statistical test of Joyner *et al.*[56] suggests that if a reduction in the fit index is satisfied by FI_{n+1}/FI_n 0.96, then the new shell is significant. In this test, only shells that are significant at the 99% probability level are included.

The calculation of χ^2, provided an alternative test for determining the significance of an additional shell. This is calculated using the equation given below.

$$\chi^2 = (FI * N_{idp}) / [(N_{idp} - N_{pars}) * N_s] \qquad (2.9)$$

where, FI= The fit index,

N_{pars}= The number of refined variables

N_{idp}= The number of independent parameters,

N_s= The number of shells fitted according to equation 3

In order for a shell to be statistically significant, the value of χ^2 must be lower than its value before the new shell was introduced.

2.6 REFERENCES

1. EXAFS: Basic principles and data analysis, B.K.Teo, 1986, Springer Verlag, New York.
2. H.Fricke, *Phys.Rev.*, 1920, **16**, 202.
3. G.Hertz, *Z.Phys.*, 1920, **3**, 19.
4. R.deL.Kronig, *Z.Phys.*, 1931, **70**, 317.
5. R.deL.Kronig, *Z.Phys.*, 1932, **75**, 468.
6. D.R.Hartree, R.deL.Kronig, H.Petersen, *Physica.*, 1934, **1**, 895.
7. H.Petersen, *Z.Phys.*, 1936, **98**, 569.
8. A.I.Kostarev, *Zh.Eksp.Teor.Fiz.*, 1949, **19**, 413.
9. T.Schiraiwa, T.Ishimura, M.Sawada, *J.Phys.Soc.Jpn.*, 1958, **138**, 848.
10. M.Sawada, Rep.Sci.Workshop, Osaka.Univ., 1959, **7**, 1.
11. V.V.Shmidt, *Bull.Acad.Sci.USSR, Phys.Ser.*, 1963, **27**, 392.
12. L.V.Azaroff, *Rev.Mod.Phys.*, 1963, **35**, 1012.
13. W.Schaich, *Phys.Rev.B.*, 1973, **8**, 4078.
14. D.E.Sayers, F.W.Lytle and E.A.Stern, *Adv.X-ray.Anal.*, 1970, **13**, 248.
15. D.E.Sayers, E.A.Stern and F.W.Lytle, *Phys.Rev.Lett.*, 1971, **27**, 1204.
16. C.A.Ashley and S.Doniach, *Phys.Rev.B.*, 1975, **11**, 1279.
17. P.A.Lee and J.B.Pendry, *Phys.Rev.B.*, 1975, **11**, 2795.
18. P.A.Lee, *Phys.Rev.B*, 1976, **13**, 5261.
19. G.Grosso and P.G.Pastori, *J.Phys.C.*, 1980, **13**, 2919.
20. J.J.Rehr, E.A.Stern, R.L.Martin and E.R.Davidson, *Phys.Rev.B.*, 1978, **17**, 560.
21. E.A.Stern, B.A.Bunker and S.M.Heald, *Phys.Rev.B.*, 1980, **21**, 5521.
22. J.J.Boland, S.E.Crane and J.D.Baldeschwieler, *Phys.Rev.B*, 1983, **77**, 142.
23. E.A.Stern, *Phys.Rev.B.*, 1974, **10**, 3027.
24. E.A.Stern, D.E.Sayers and F.W.Lytle, *Phys.Rev.B.*, 1975, **11**, 4836.
25. P.A.Lee, B.K.Teo and A.L.Simon, *J.Am.Chem.Soc.*, 1977, **99**, 3856.
26. S.J.Gurman and R.F.Pettifer, *Phil.Mag.B.*, 1979, **40**, 345.
27. S.J.Gurman, N.Binsted and I.Ross, *J.Phys.C.*, 1984, **17**, 143.

28. S.J.Gurman, N.Binsted and I.Ross, *J.Phys.C.*, 1986, **19**, 1845.

29. Reproduced with kind permission from the Daresbury Laboratory photographic services group.

30. M.Hart and A.R.D.Rodrigues, *J.Appl.Cryst.*, 1978, **11**, 248.

31. B.R.Dobson, S.S.Hasnain, M.Neu, C.A.Ramsdale and L.M.Murphy, *Jpn.J.Appl.Phys.*, 1993, **32**, 32-2, 192.

32. R.Frahm and J.Wong, *Jpn.J.Appl.Phys.*, 1993, **32**, 32-2, 188.

33. R.Frahm, *Rev.Sci.Instr.*, 1989, **60**, 2515.

34. R.Frahm: X-ray Absorption Fine Structure, Eds. S.S.Hasnain, Ellis Horwood, 1991, 731.

35. R.Frahm, *Nucl.Instrum.Meth.*, 1988, **A270**, 578.

36. N.A.Cruise, PhD Thesis, University of Southampton, 1994.

37. B.R.Dobson, *Sync.Rad.News.*, 1994, **7**, 21.

38. F.Cimini and R.Prins, *J.Phys.Chem.B.*, 1997, **101**, 5277.

39. G.Sankar, P.A.Wright, S.Natarajan, J.Meurig Thomas, G.N.Greaves, A.J.Dent, B.R.Dobson, C.A.Ramsdale and R.H.Jones, *J.Phys.Chem*, 1993, **97**, 9550.

40. R.Frahm, J.Wong, J.B.Holt, E.M.Larson, B.Rupp and P.A.Waide, *Phys.Rev.B.*, 1992, **46**, 9205.

41. N.Allinson, G.Baker, G.N.Greaves and J.N.Koll, *Nucl.Instr.Meth.*, 1988, **A266**, 592.

42. G.Salvini, D.Bogg, A.J.Dent, G.Derbyshire, R.C.Farrow, A.Felton, C.Ramsdale, *Physica B.*,1995, **209**, 229.

43. G.E.Derbyshire, D.Bogg, A.J.Dent, R.C. Farrow, G.N.Greaves, W.I.Helsby, C.Morrell, C.A.Ramsdale, M.P.Wells, *Rev.Sci.Instr.*, 1992, **63**, Pt2A, 790.

44. G.E.Derbyshire, W.I.Helsby, A.J.Dent, S.A.Wright, R.C.Farrow, G.N.Greaves, C.Morrell and G.J.Baker, *Adv.X-ray.Analysis.*, 1990, **34**.

45. D.Bogg, A.J.Dent, G.E.Derbyshire, R.C.Farrow, C.A.Ramsdale, G.Salvini, *Nucl.Instr.Meth.*, 1993, **390**, 461.

46. M.Hagelstein, C.Ferrero, U.Hatje, T.Ressler and W.Metz, *J.Synchr.Rad.*, 1995, **2**,174.

47. J.M.Corker, PhD Thesis, University of Southampton, 1991.

48. Prepared at the Electronics Workshop, University of Sydney, Australia- By M.Conyngham, A.Masters, D.Niles McLeod, 1994.

49. N.Binsted, PAXAS, Program for the analysis of X-ray Absorption Spectra, University of Southampton, 1988.

50. N.Binsted, S.J.Gurman, J.W.Campbell, EXCURV92, SERC, Daresbury Laboratory Program, 1992.

51. K.Tearle, PhD Thesis, University of Southampton, 1995.

52. N.Binsted, S.J.Cook, J.Evans, G.N.Greaves and R.J.Price, *J.Am.Chem.Soc.*, 1987, **109**, 3669.

53. A.D.Cox, EXAFS for Inorganic systems, C.D.Garner and S.S.Hasnain, Eds., DL/SCI/R17, 1981.

54. S.Brandt, "Statistical and Computational Methods in Data Analysis", North Holland, Amsterdam, 1970.

55. S.S.Hasnain, (Editor), X-ray absorption Fine Structure, Ellis Horwood, New York, 1991, 195.

56. R.W.Joyner, K.J.Martin and P.Meehan, *J.Phys.C.*, 1987, **20**, 4005.

CHAPTER 3. CONCENTRATION AND ACQUISITION TIME STUDIES ON MODEL NICKEL COMPLEXES.

3.1 Introduction:

EDE[1,2] is a technique which allows fast acquisition of EXAFS data and is therefore suitable for time resolved studies of chemical systems.[3] It can also be used for studies of model compounds. The experimental set-up required for EDE is given in section 2.4.2.c and usually involves a dispersive focussing triangle shaped bent crystal monochromator with a position sensitive detector which is able to achieve fast recording of the energy dependent X-ray absorption spectrum.[4,5,6,7,8]

Three EDE detectors were used at the SRS at Daresbury during the course of this study. These were the Reticon 512T, Hamamatsu S3904, Hamamatsu S4874 detectors. The Reticon is a 500 pixel detecor with a 50μm spatial pitch, while the two Hamamatsu detectors are 1000 pixel detectors with 25 μm spatial pitch. The characteristics of the PDA (photo-diode arrays) in each of these detectors was evaluated by a range of studies carried out by Daresbury Laboratory staff.[9,10]

QUEXAFS (Quick EXAFS), like EDE, is also a technique for fast recording of EXAFS spectra to allow some time resolved work.[11,12,13,14,15] The experimental set-up required for QUEXAFS is detailed in 2.4.2.b and involves using a double crystal monochromator which is moved in small angular steps to vary the output energy of the monochromator. Data collection is synchronised to monochromator movement by recording the absorbance at regular time intervals.[16,17,18,19] Thus, spectra can be collected in minutes.

3.2 Objectives in this section:

The main objective of this section was to run spectra of the complexes ($NiBr_2(PEt_3)_2$, $NiCl_2(PEt_3)_2$, and $Ni(acac)_2$) using different dilutions of analyte and also to check the acquisition times required to optimise the EDE signal. This is because EDE is a developing technique and like all spectroscopic technique requires the appropriate concentrations and acquisition times to be used.

This section will compare EDE with QUEXAFS data and will also be concerned with the effect of the type of EDE detector and QUEXAFS on the quality of data obtained e.g. Reticon 512T, Hamamatsu S3904, Hamamatsu S4874, and QUEXAFS. ,

The data obtained from one of the EDE detectors and QUEXAFS was solved and is presented, in this chapter, to see the comparability of the parameters obtained. In all instances, tests were carried out to test the significance of a new shell[20] and to avoid overfitting of data to short data sets[21].

3.3 Experimental Details:

Details of the experimental set-up used for EDE and QUEXAFS spectroscopy are given in Section 2.4. Three main types of EDE detectors were used for the model studies in this chapter. These were the Reticon 512T 500 pixel (spatial pitch per pixel= 50μm) detector, the Hamamatsu S3874 1000 pixel (spatial pitch per pixel= 25μm) detector and the Hamamatsu S4874 1000 pixel detector. Upto 10k or 381eV of data can be obtained currently using EDE.

The Ni-K-edge EDE spectra of the three nickel complexes ($Ni(acac)_2$, $NiCl_2(PEt_3)_2$, and $NiBr_2(PEt_3)_2$) were obtained on the Reticon 512T detector using varying concentrations (10mM, 25mM, 50mM, 100mM) of analyte, and using varying numbers of scans (10, 100, 1000, 9000 scans). A comparision of these results is presented in Sections 3.4 and 3.5. A comparision of the results obtained from the three different EDE detectors and also QUEXAFS is presented in Section 3.7.

All the studies were carried out at room temperature, using the room temperature cells detailed in Section 2.4.3. The $NiX_2(PEt_3)_2$ (X= Br, Cl) solutions were prepared in dried and degassed *p*-fluorotoluene. The $Ni(acac)_2$ solution was prepared in dried and degassed toluene.

3.4 Introduction to the structures of the $NiBr_2(PEt_3)_2$, $NiCl_2(PEt_3)_2$, and $Ni(acac)_2$:

The three nickel complexes used for catalyst studies in this project were $NiBr_2(PEt_3)_2$, $NiCl_2(PEt_3)_2$ and $Ni(acac)_2$. Data from X-ray crystallography and other sources suggests that both $NiBr_2(PEt_3)_2$ and $NiCl_2(PEt_3)_2$ both adopt a trans square-planar structure in the solid state.[22-25] The square-planar structure of the complex along with some of the relevant parameters obtained from X-ray crystallography are shown in Figure 3.1.

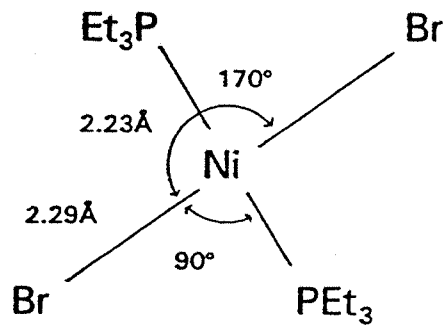

Figure 3.1. Square Planar $NiBr_2(PEt_3)_2$ complex.

Unlike the diamagnetic halogenophosphines of nickel, anhydrous $Ni(acac)_2$ which is paramagnetic adopts a trimeric structure in the solid state[26] and in most non-coordinating solvents. The nickel atoms are bound together in symmetrical linear chains of three by the acetylacetanato-oxygen atoms such that a distorted octahedron of oxygens surrounds each nickel atom (Figure 3.2).

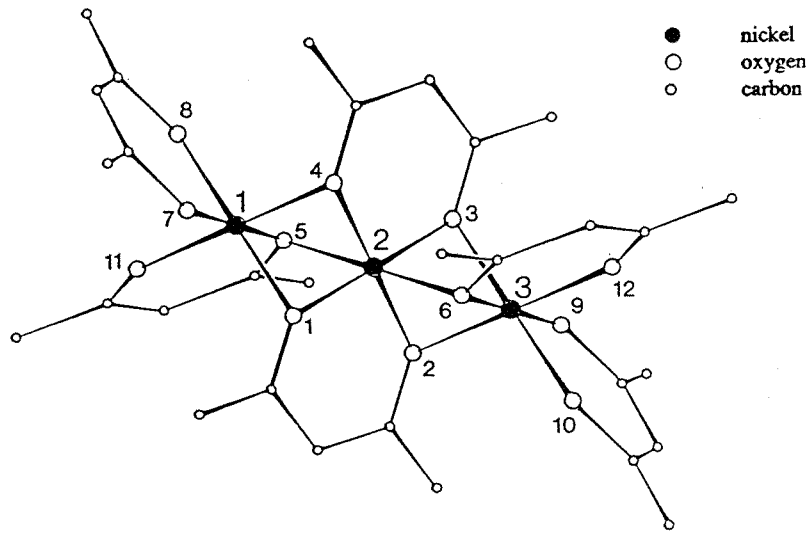

Figure 3.2 Trimeric structure of anhydrous $Ni(acac)_2$.[28]

Table 3.1[27] shows neighbouring atom distances to each nickel atom in the anhydrous $Ni(acac)_2$, calculated from the atomic coordinates for the X-ray crystal structure[28]. Each nickel atom is crystallographically unique and the distorted structure results in a wide range of Ni-O distances. The terminal oxygen atoms, for example, form short Ni-O bonds (1.89Å- 2.08Å) whereas the bridging Ni-O bonds are on average longer, with some of the bridges being asymmetric (distances ranging from 2.08Å- 2.40Å).

Table 3.1[27] Table showing the neighbouring atom distances from each nickel atom, calculated from the X-ray crystal structure for anhydrous $Ni(acac)_2$.[27]

Ni(1)		Ni(2)		Ni(3)	
atom	distance/Å	atom	distance/Å	atom	distance/Å
O(7)	1.976	O(6)	1.961	O(10)	1.887
O(11)	2.026	O(5)	1.966	O(12)	2.000
O(8)	2.062	O(4)	2.037	O(3)	2.070
O(5)	2.142	O(3)	2.051	O(9)	2.081
O(1)	2.148	O(1)	2.076	O(6)	2.146
O(4)	2.267	O(2)	2.180	O(2)	2.400
C(16)	2.763	C(2)	2.821	C(27)	2.794
Ni(2)	2.882	C(7)	2.831	Ni(2)	2.896
C(21)	2.894	Ni(1)	2.882	C(26)	2.902
C(22)	2.971	Ni(3)	2.896	C(11)	2.933
C(20)	3.175	C(22)	2.954	C(2)	3.063
C(17)	3.176	C(1)	2.987	C(30)	3.147
C(1)	3.234	C(6)	3.049	C(12)	3.246
C(25)	3.504	C(12)	3.109	C(8)	3.433
C(7)	3.611	C(10)	3.328	C(6)	3.478

A plot of the EXCURVE calculated radial distribution function for the X-ray crystal structure Ni-O distances for $Ni(acac)_2$ (assuming a value for the Debye Waller parameter of 0.003 $Å^2$ for each Ni-O interatomic distance)[27] shows that the spread of distances is non-Gaussian in nature (Figure 3.3). However, a Gaussian distribution of distances is assumed in the calculation of EXAFS theory and deviations from this type of distribution can lead to an apparent shortening of an EXAFS derived average distance.[29] Thus, the complicated structure of $Ni(acac)_2$ presents several potential problems where EXAFS analysis is concerned.

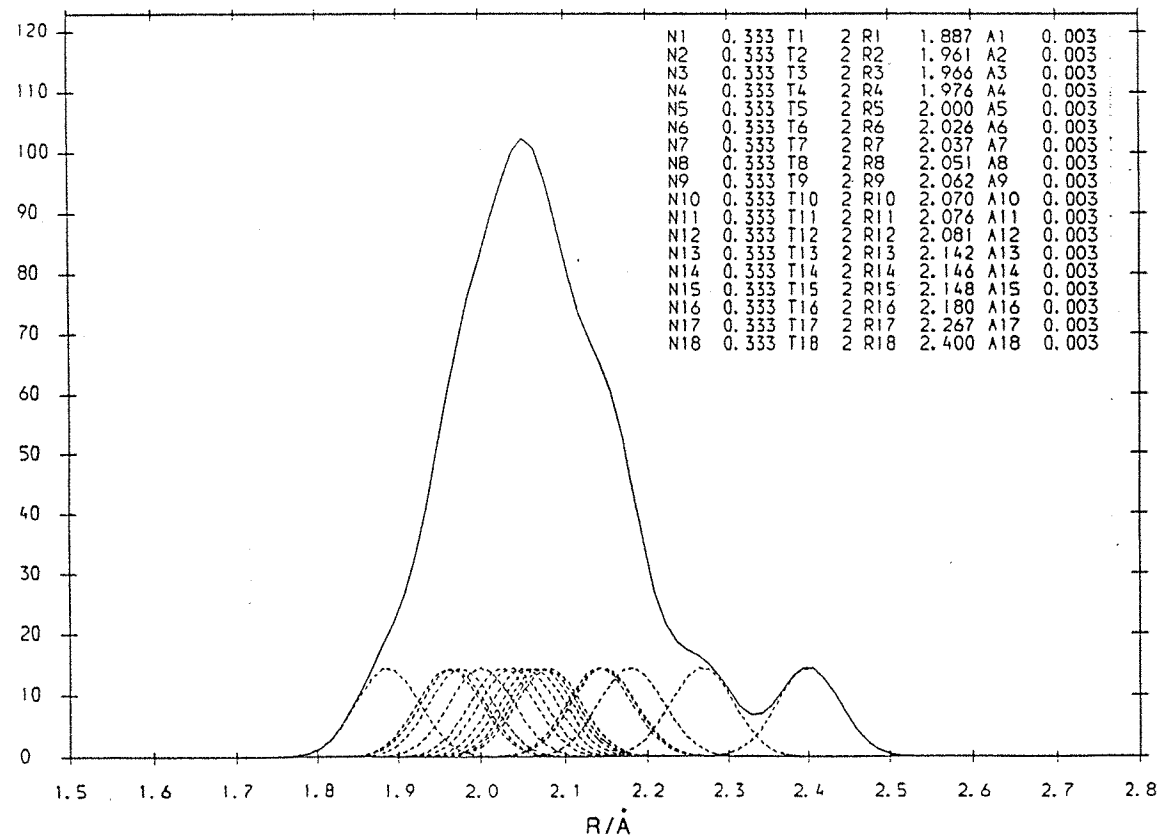

Figure 3.3. The EXCURVE calculated radial distribution function for the X-ray crystal structure Ni-O distances for $Ni(acac)_2$ (assuming a Debye-Waller factor of $0.003Å^2$ for each Ni-O interatomic distance).

In model EDE and QUEXAFS studies of the above mentioned three compounds, the nickel K-edge was studied and in the case of $NiBr_2(PEt_3)_2$, even the bromine K-edge EXAFS was studied, for chemical changes during and prior to the reaction taking place. The EDE and QUEXAFS data obtained was compared to the structures and parameters obtained from X-ray crystallography and previous EXAFS studies[27,30,31]. A comparision of the raw spectra from each of these nickel complexes is shown below in Figure 3.4. As expected there are some similarities between the raw spectra of the two $NiX_2(PEt_3)_2$ (X= Cl,Br).

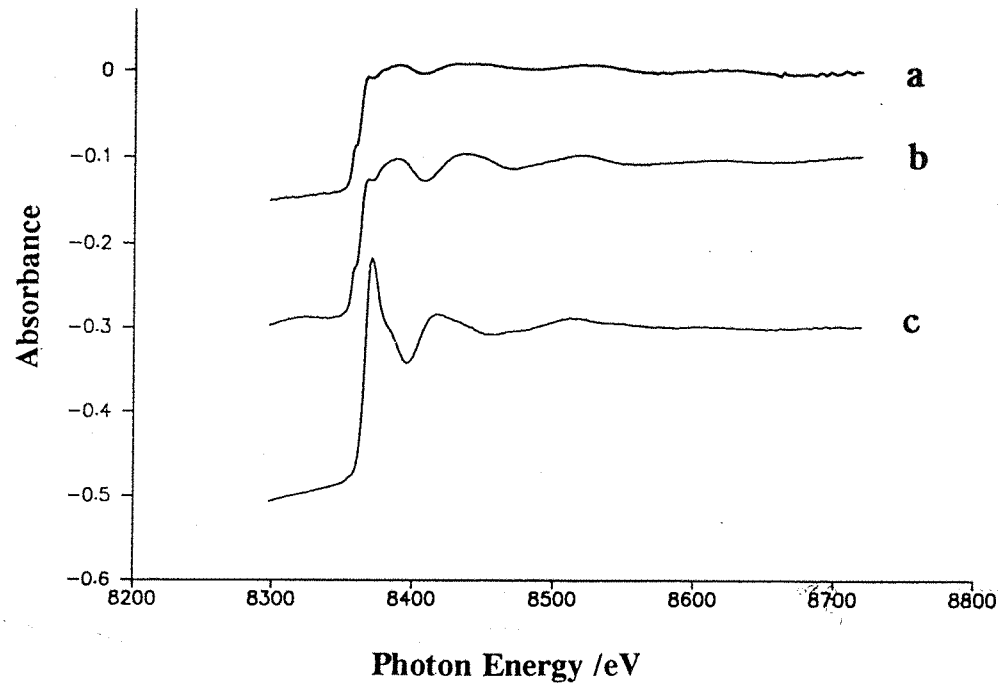

Figure 3.4. Comparision of the Ni-K-edge EDE spectra (Reticon 512T detector) of a) $NiBr_2(PEt_3)_2$ (100mM solution in p-fluorotoluene, 1000 scans, Each scan= 31 ms) b) $NiCl_2(PEt_3)_2$ (100mM solution in p-fluorotoluene, 1000 scans, Each scan= 28 ms) c) $Ni(acac)_2$ (100mM solution in toluene, 1000 scans, Each scan= 33 ms).

3.5 Comparision of EDE spectra of three nickel catalyst complexes obtained using different concentrations of the analyte:

Nickel-K-edge EDE spectra of the $NiBr_2(PEt_3)_2$ complex in *p*-fluorotoluene were obtained at concentrations of 10mM (1000 scans, each scan= 9.0ms), 25mM (1000 scans, each scan= 10 ms), 50mM (1000 scans, each scan= 25 ms), and 100mM (1000 scans, each scan= 31 ms) using 1000 scans. The results are shown in Figure 3.5.

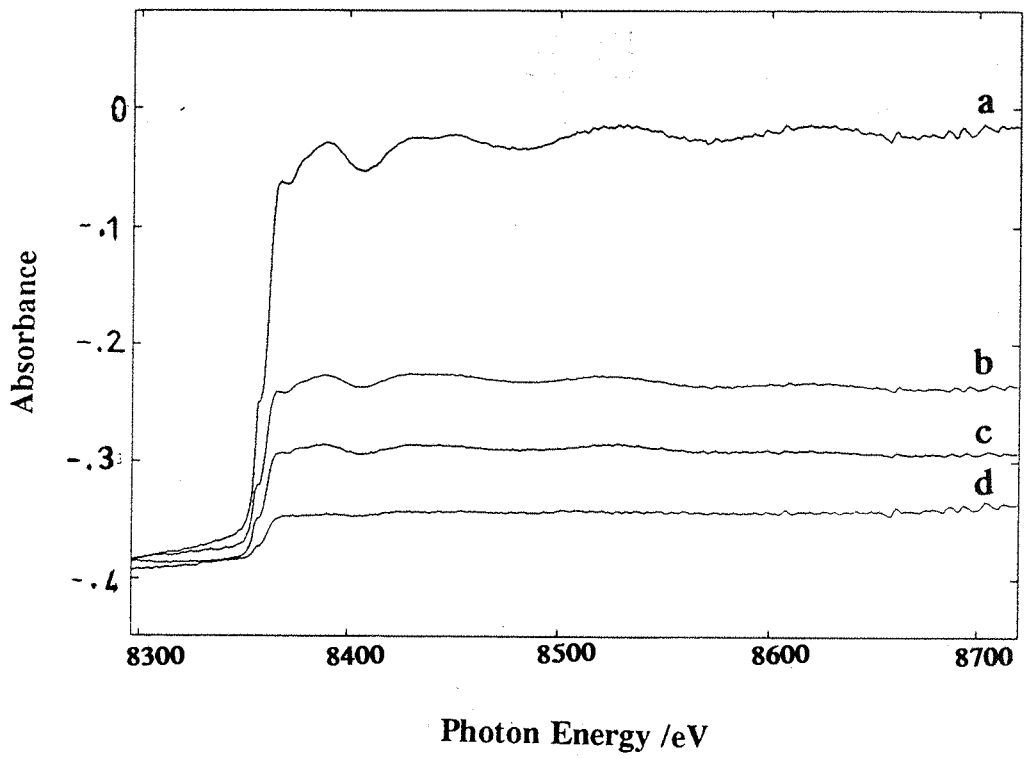

Figure 3.5. Comparision between the Ni-k-edge EDE (Reticon 512T) spectra of solutions with varying concentrations of $NiBr_2(PEt_3)_2$ in *p*-fluorotoluene a) 100mM (1000 scans, each scan= 31 ms), b) 50mM (1000 scans, each scan= 25 ms), c) 25mM (1000 scans, each scan= 10 ms), d) 10mM (1000 scans, each scan= 9 ms).

As the concentration of the nickel complex increased, the absorbance (edge height) increased according to Beer's law, $A = \varepsilon Cl$ (i.e. where ε = molar extinction coefficient). The law applies under dilute conditions until the point that the detector is saturated by the absorbance. The concentrations looked at in this study were lower than required for saturation of the detector.

Figure 3.5 shows that, given that the path length and absorption coefficient are kept constant, the edge height of the spectra is proportional to the concentration of the nickel complex.

A closer look at the k^3 weighted EXAFS regions of spectra of solutions of increasing concentrations of $NiBr_2(PEt_3)_2$ in *p*-fluorotoluene and $Ni(acac)_2$ in toluene are shown in Figure 3.6 a and b, respectively. As expected, the results show that the signal to noise ratio improved on increasing the concentration of the nickel complex. It may have helped to increase scan times in order to obtain longer data sets. However, this is not always the case. Also, longer scan times result in poorer time resolution during real time studies of a reaction involving this complex.

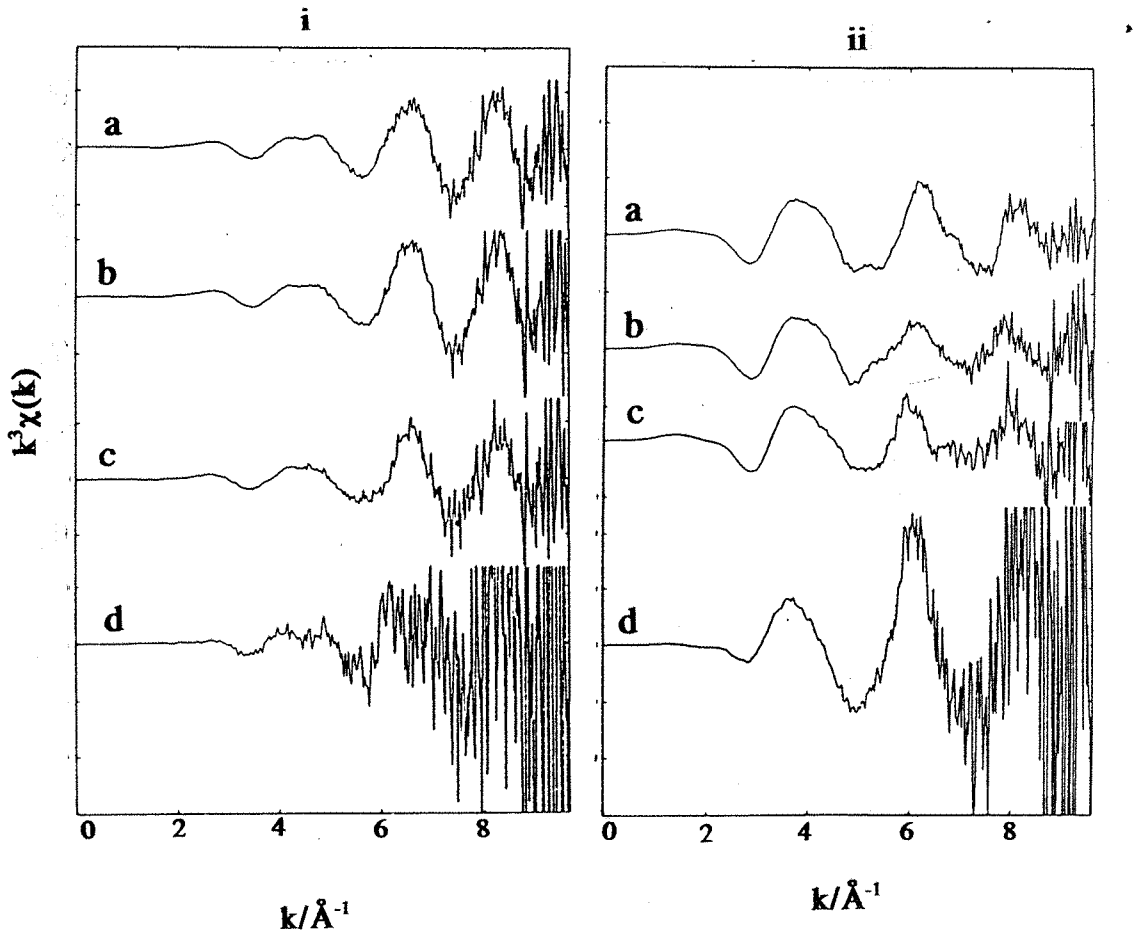

Fig.3.6 i) Comparision between k^3 weighted Ni-K-edge EDE (Reticon 512T) spectra (1000 scans) of solutions of varying concentrations a) 100mM (each scan= 31 ms) b) 50mM (each scan= 25ms) c) 25mM (each scan= 10 ms) d) 10mM (each scan= 9ms) of $NiBr_2(PEt_3)_2$ in p-fluorotoluene. ii) Comparision between k^3 weighted Ni-K-edge EDE (Reticon 512T detector) spectra (1000 scans) of solutions of varying concentrations a) 100mM (each scan= 32 ms) b) 50mM (each scan= 26 ms) c) 25mM (each scan= 11 ms) d) 10mM (each scan= 10 ms) of $Ni(acac)_2$ in toluene.

3.6 Comparision of the EDE spectra of three nickel catalyst complexes using varying numbers of scans:

The signal at any given concentration is optimised by increasing the integration time of the signal so that the background absorption can be removed accurately. Further improvement in the signal to noise ratio can be obtained by increasing the number of scans appropriately. It is expected that the signal to noise ratio should improve as a square root of the number of scans.

EDE spectra of $NiBr_2(PEt_3)_2$ (100mM in *p*-fluorotoluene) obtained using varying numbers of scans are shown in Figure 3.7a. EDE spectra of $Ni(acac)_2$ (100mM in toluene) using varying numbers of scans are shown on Figure 3.7b.

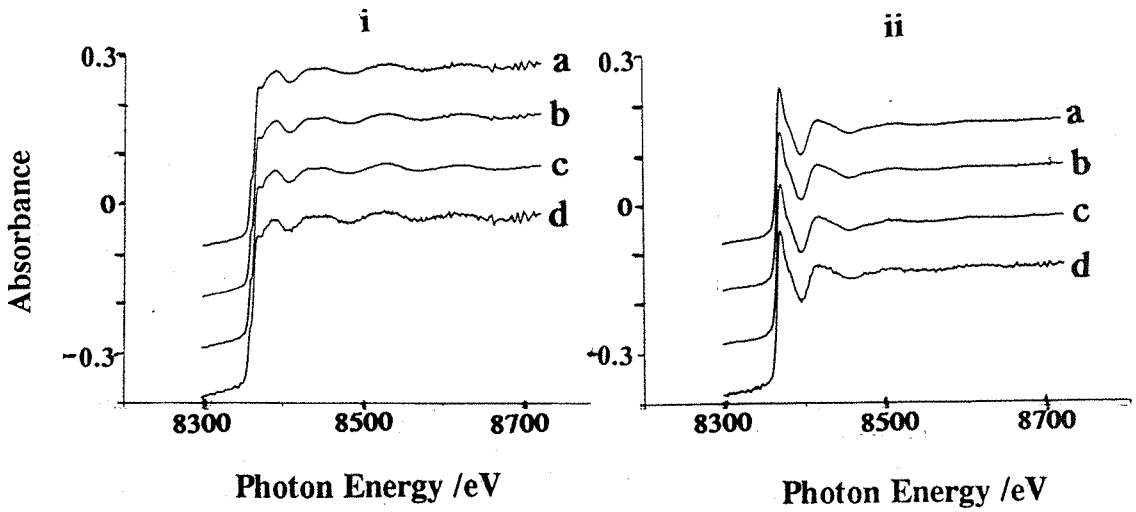

Figure 3.7. i) Comparision between EDE spectra obtained with varying numbers of scans, a) 9000 scans, b) 1000 scans, c) 100 scans, d) 10 scans; scan duration= 31 ms, of $NiBr_2(PEt_3)_2$ (100mM in p-fluorotoluene). ii) Comparision between EDE spectra obtained with varying numbers of scans, a) 9000 scans, b) 1000 scans, c) 100 scans, d) 10 scans, scan duration= 32 ms, of $Ni(acac)_2$ (100mM in toluene).

A closer look at the k^3-weighted EXAFS data of the same spectra can be seen on Figure 3.8 a and b. As expected, the signal to noise ratio improved as the number of scans was increased from 10 scans to 100 scans to 1000 scans. However, on increasing the number of scans further to 9000 scans the S/N ratio worsenned. This is thought to be related to the stability of the beam because movement of the beam can cause a misalignment of the I_0 with respect to I_t and thus cause greater noise in the data.

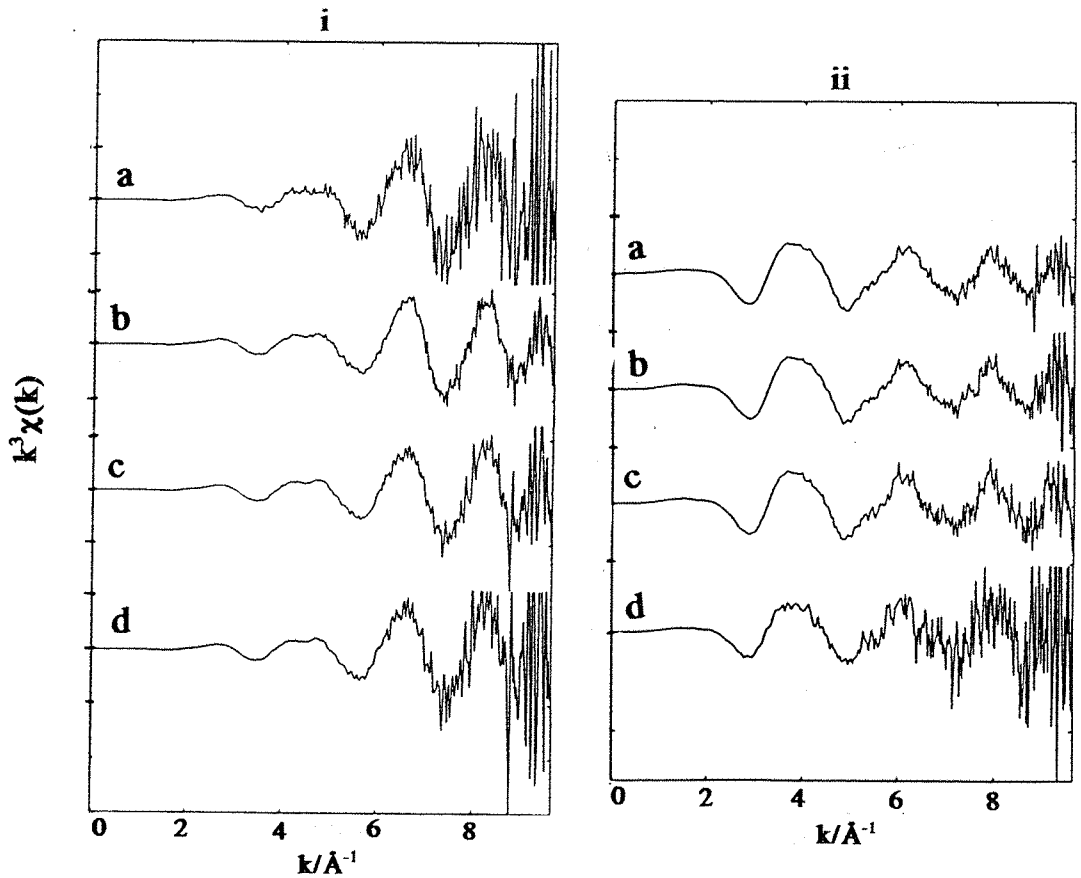

Figure 3.8 i) Comparision between k^3-weighted Ni-K-edge EDE data of $NiBr_2(PEt_3)_2$ (100mM in toluene) obtained using a) 9000 scans, b) 1000 scans, c) 100 scans, d) 10 scans; scan duration= 31 ms. ii) Comparision between k^3-weighted Ni-K-edge EDE data of $Ni(acac)_2$ (100mM in toluene) obtained using a) 9000 scans, b) 1000 scans, c) 100 scans, d) 10 scans; scan duration= 32 ms.

3.7 Comparision of the results obtained from various EDE detectors and QUEXAFS:

a) i) Comparision of Ni-K-edge EDE and QUEXAFS data obtained from $NiBr_2(PEt_3)_2$ in p-fluorotoluene:

Figure 3.9 shows a comparision of the data obtained using a Reticon 512T EDE detector and QUEXAFS from $NiBr_2(PEt_3)_2$ (100mM solution in *p*-fluorotoluene).

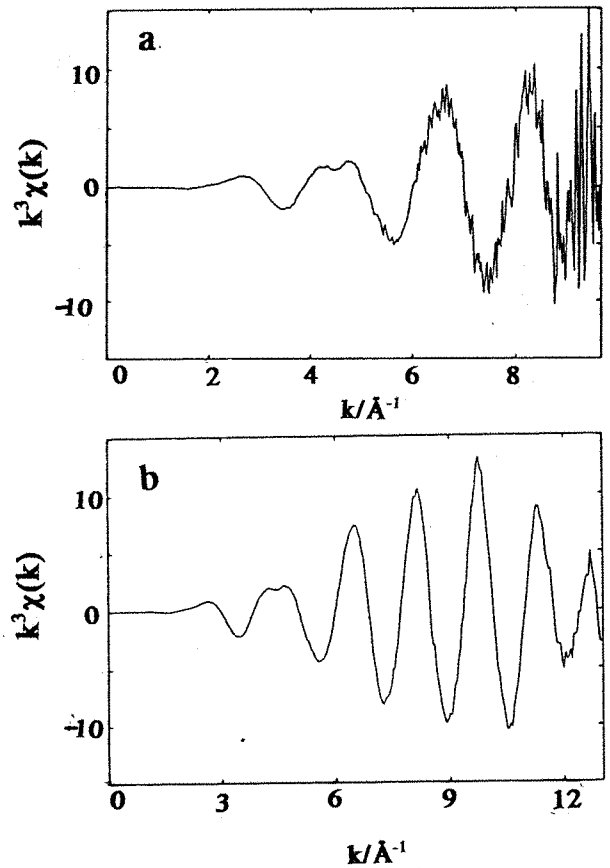

Figure 3.9. Figure showing a comparision between k^3-weighted Ni-K-edge EXAFS data obtained on a solution of $NiBr_2(PEt_3)_2$ (100mM in *p*-fluorotoluene) using a) Reticon 512T EDE detector (1000 scans, scan duration= 31 ms) and b) QUEXAFS (total acquisition time= 2 minutes).

The EDE data obtained using the Reticon 512T was obtained in 31 seconds. The QUEXAFS data was obtained in two minutes. As can be seen upto 12k of noise free data was obtained using the QUEXAFS. The EDE data is noisy but can be used upto 9k. The fitted data is presented in Figure 3.10 and Table 3.2.

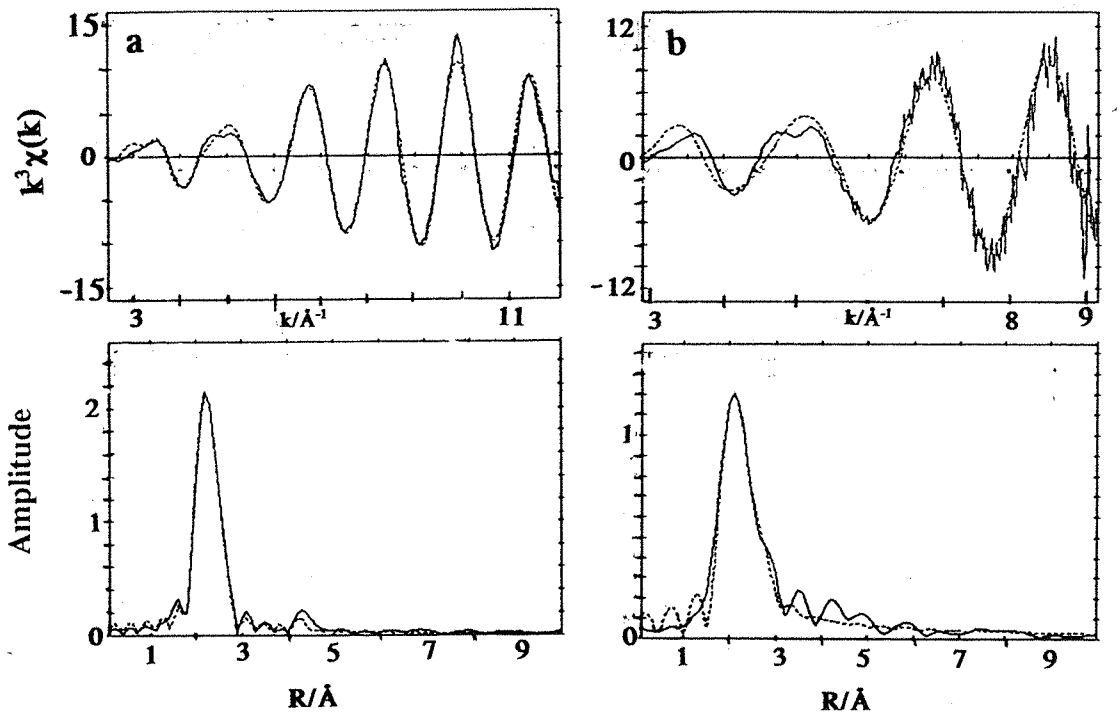

Figure 3.10. Figure showing a comparision between a) Fitted Ni-K-edge, k^3 - weighted QUEXAFS data (above) and its Fourier transform (below) and b) Fitted Ni-K-edge k^3-weighted EDE data (above) and its Fourier transform (below), of a solution of $NiBr_2(PEt_3)_2$ (100mM in *p*-fluorotoluene).

Table 3.2. Table showing the parameters obtained from the fitted Ni-K-edge EDE and QUEXAFS spectra, of $NiBr_2(PEt_3)_2$ (100mM in *p*-fluorotoluene), as shown on Figure 3.10. A comparision with scanning EXAFS data[30] is also made.

EDE Data: AFAC= 0.9, EF= 1(1), R= 30.0%.

QuE Data: AFAC= 0.9, EF= -1.5(4), R= 13.9%.

EXAFS Data: AFAC= 0.82, EF= 13.3 eV, VPI= -3.0 eV, R= 19.4%.

Type of coordinated atom	P	Br
EDE C.N	2.0 (2)	2.0 (1)
QuE C.N	1.97 (8)	2.08 (8)
EXAFS C.N	2	2
EDE R/Å	2.18 (2)	2.273 (5)
QuE R/Å	2.276 (4)	2.315 (2)
EXAFS R/Å	2.3 (9)	2.3 (3)
X-Ray R/Å	2.26	2.30
EDE $\sigma/Å^2$	0.012 (3)	0.009 (1)
QuE $\sigma/Å^2$	0.008 (1)	0.004 (1)
EXAFS $\sigma/Å^2$	0.01 (2)	0.0055 (5)

It is clear from Table 3.2, that both the EDE and QUEXAFS data supported the presence of two shells consisting of i) 2 phosphorus atoms at 2.2 Å from the central nickel atom and ii) 2 bromine atoms at 2.3 Å from the central nickel atom. This data

supports previous scanning EXAFS data and also X-ray crystallography data. The data supports the structure shown in Figure 3.1

The poorer resolution between shells obtained from the shorter EDE data is clear from Figure 3.10 a and b, which show the broadening of the Fourier transform peaks for the EDE data as compared to the Fourier transform peaks from the longer QUEXAFS data. This is expected as resolution is proportional to $\pi/2\Delta k$ where k= length of the data set.

a)ii) Comparision of bromine-K-edge EDE and QUEXAFS data using $NiBr_2(PEt_3)_2$ in p-fluorotoluene:

Figure 3.11 shows the k^3 weighted EXAFS data obtained from the bromine-K-edge spectrum of $NiBr_2(PEt_3)_2$ (140mM in *p*-fluorotoluene) using the Hamamatsu S3904 using 4000 scans (each scan= 190 ms). It also shows the bromine-K-edge spectrum of $NiBr_2(PEt_3)_2$ (140mM in *p*-fluorotoluene) using the Hamamatsu *S4874* using 4000 scans (each scan= 30.5 ms).

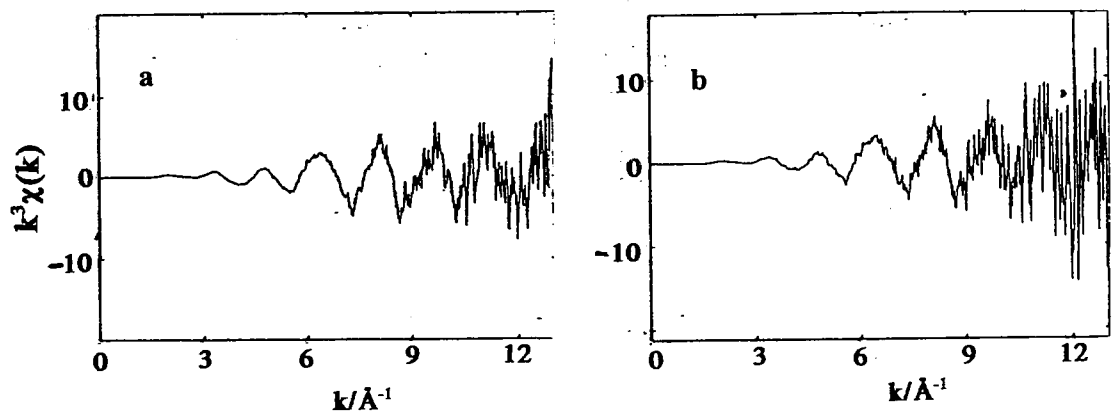

Figure 3.11. Figure showing the k^3-weighted Br-K-edge EDE data obtained on a) solution of $NiBr_2(PEt_3)_2$ (140mM in *p*-fluorotoluene) using the Hamamatsu S3904 EDE detector (4000 scans, each scan 190 ms) b) solution of $NiBr_2(PEt_3)_2$ (70mM in *p*-fluorotoluene) using the Hamamatsu S4874 EDE detector (4000 scans, 30.5 ms)

The fitted data from the Hamamatsu S3904 and its Fourier transform are shown on Figure 3.12. The parameters obtained from this fit are shown on Table 3.3.

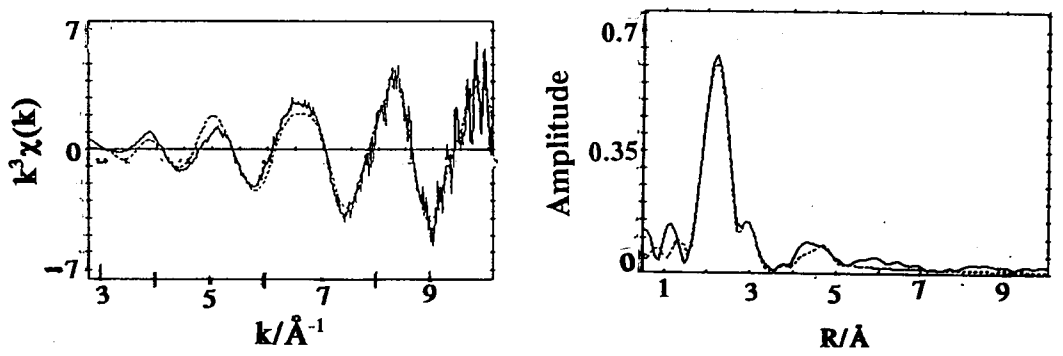

Figure 3.12. Figure showing the fitted k^3-weighted Br-K-edge EDE EXAFS data of $NiBr_2(PEt_3)_2$ (70mM in *p*-fluorotoluene) obtained using the Hamamatsu S3904 EDE detector (Figure 3.11 a) and its Fourier transform.

Table 3.3: Table showing the Br-k-edge parameters obtained from the fitted k^3 weighted EDEXAFS spectrum (Figure 3.12) of $NiBr_2(PEt_3)_2$ (70mM in *p*-fluorotoluene) and the fitted k^3 weighted scanning EXAFS data of $NiBr_2(PEt_3)_2$ (25mM in *p*-fluorotoluene).[30]

EDE parameters: AFAC= 0.80, EF(S.D)= -8.2 (0.9), R= 32.8%.

EXAFS parameters: AFAC= 0.81, E0= 13.9eV, VPI= -3.6 eV, R= 21.1%.

Type of atom	Ni	P	Br
EDE C.N	1.01 (2)	1.80 (3)	1.0 (2)
EXAFS C.N	1	2	1
EDE R/Å	2.294 (4)	3.206 (4)	4.44 (1)
EXAFS R/Å	2.29 (1)	3.17 (4)	4.57 (2)
X-ray R/Å	2.30	3.24	4.60
EDE σ/Å^2	0.0039 (4)	0.028 (4)	0.008 (2)
EXAFS σ/Å^2	0.0082 (6)	0.004 (1)	0.022 (3)

Thus, the data obtained from the EDE detector (Hamamatsu S3904 detector, total scan time= 12.6 minutes) does compare well to the data obtained using scanning EXAFS spectroscopy (total scan time= more than 40 minutes).

b) Comparision of nickel-K-edge EDE and QUEXAFS data from $Ni(acac)_2$ in toluene:

The Figure 3.13 shows a comparision of the data obtained from the Reticon 512T EDE detector, the Hamamatsu S3904 detector and also some QUEXAFS data using $Ni(acac)_2$ (100mM in toluene). While the Reticon data was obtained in 33 seconds, the Hamamatsu data was obtained in 1.8 minutes, the QUEXAFS data was obtained in two minutes.

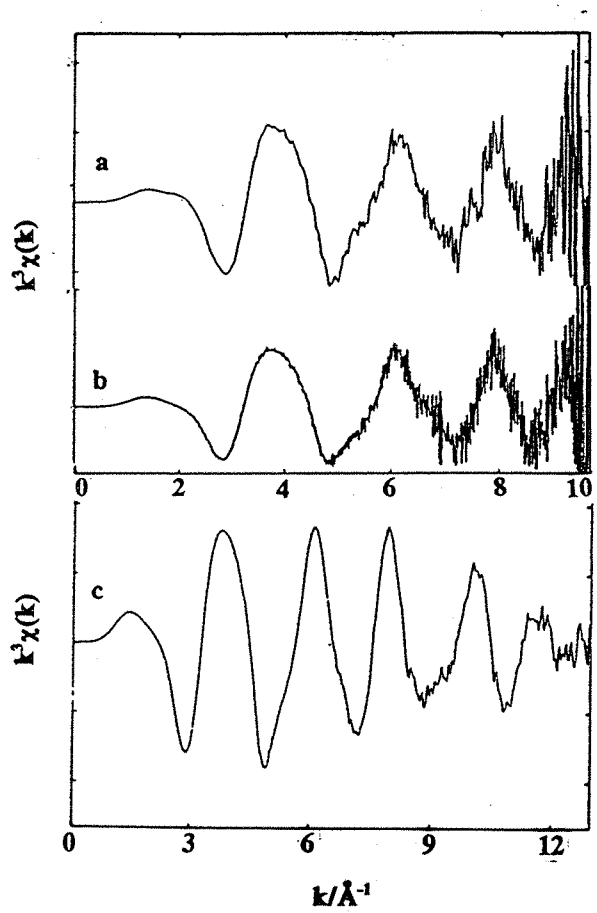

Figure 3.13. Figure showing a comparision between the k^3-weighted Ni-K-edge EXAFS data of $Ni(acac)_2$ (100mM in toluene) using a) EDE (Reticon 512 T detector, 1000 scans, scan duration= 32 ms) and b) Hamamatsu S3904 detector (1000 scans, scan duration= 105 ms) c) QUEXAFS (total acquisition time= 2 minutes).

Once again, the Reticon gave data upto 10k in 32 seconds, the Hamamatsu S3904 gave the same in 1.8 minutes, while QUEXAFS gave data upto 12k in two minutes. The data from the Reticon and QUEXAFS studies were subjected to curve fitting analysis and the results can be seen in Figure 3.14.

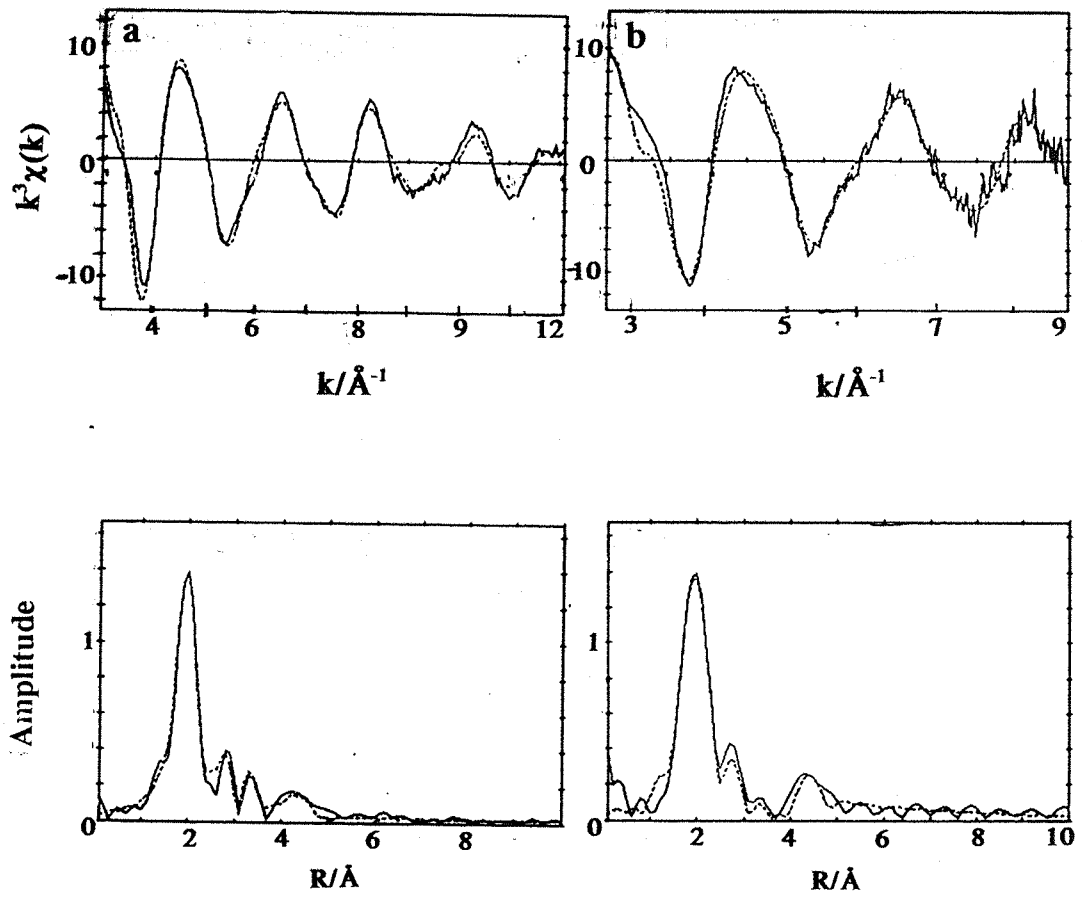

Figure 3.14. Figure showing the fitted k^3-weighted EXAFS data and Fourier transform of $Ni(acac)_2$ (100mM in toluene) obtained using a) QUEXAFS scan (scan duration= 2 minutes) b) EDE (Reticon 512T detector) scan (1000 scans, each scan= 31 ms).

The effect of shorter data lengths can also be seen from the broadenning of the Fourier transform peaks shown in figure 3.14, which leads to poorer resolution between shells.

Table 3.6 Table showing a comparision of the k^3-weighted Ni-k-edge parameters from EDE and QUEXAFS (See Figure 3.14) of $Ni(acac)_2$ (100mM in toluene) and scanning EXAFS data[27];

EDE data: AFAC= 0.9, EF(S.D)= 3.32 (0.29), R= 23.48%.

QUEXAFS data: AFAC= 0.9, EF(S.D)=2.38(0.56)), R= 20.28%,

EXAFS data: AFAC= 0.82, E_0= 28.8 eV, VPI= -2.0 eV, R= 18.8 %.

Type of atom	O	C	Ni	C
EDE C.N	6.4 (1)	____	1.4 (3)	11 (1)
QuE C.N	5.8 (1)	2.5 (3)	1.1 (2)	12.1 (8)
EXAFS C.N	6.1	3.8	1.3	8.2
EDE R/Å	2.009 (3)	____	2.86 (1)	4.45 (1)
QuE R/Å	1.999 (2)	2.874 (12)	3.158 (9)	4.42 (1)
EXAFS R/Å	1.98	2.85	3.09	4.33
EDE $\sigma/Å^2$	0.017 (1)	____	0.029 (4)	0.010 (3)
QuE $\sigma/Å^2$	0.015 (1)	0.021 (4)	0.019 (2)	0.012 (3)
EXAFS $\sigma/Å^2$	0.015	0.010	0.022	0.017

A comparision can be made between the EDEXAFS, QUEXAFS and scanning EXAFS data. Some discrepancies do arise due to the complicated structure being looked at, but overall the data remains comparable.

Both the QUEXAFS and EDEXAFS data could be fitted to a first coordination shell of six oxygen atoms at 2.0 Å which is as expected from the trimeric structure of $Ni(acac)_2$ and from X-ray crystallography data and scanning EXAFS data. QUEXAFS parameters solved the data to a second shell of 3 carbon atoms at 2.9 Å which was supported by scanning EXAFS data. However, EDEXAFS data did not achieve the resolution required to distinguish between the carbon shell at 2.9 Å and the nickel shell at 3.1 Å. QUEXAFS (data length= 12k), EDEXAFS (data length= 9k) and scanning EXAFS (data length= 14k) data were fitted to show the presence of a nickel shell of 1.3 atoms at 3.1Å to within statistical error. This supports the expected coordination number and spatial distance for this shell as per X-ray crystallography. QUEXAFS, EDEXAFS and scanning EXAFS data were all fitted to show the presence of a carbon shell at 4.4Å. However, the coordination number of the atoms in this shell varied between the methods used although the spatial distance from the central nickel atom was comparable within statistical error. Thus, despite being a complicated structure QUEXAFS, EDEXAFS and scanning EXAFS provided similar data for $Ni(acac)_2$.

c) Comparision of nickel-K-edge EDEXAFS and QUEXAFS data from $NiCl_2(PEt_3)_2$ in p-fluorotoluene:

Figure 3.15 shows a comparision between EDEXAFS data obtained using the Reticon 512T, the Hamamatsu S3904 and QUEXAFS data using $NiCl_2(PEt_3)_2$ (100 mM in *p*-fluorotoluene). It is quite clear from this figure that the Reticon EDE data is far better than the Hamamatsu data both as it is less noisy and also that it requires less acquisition time.

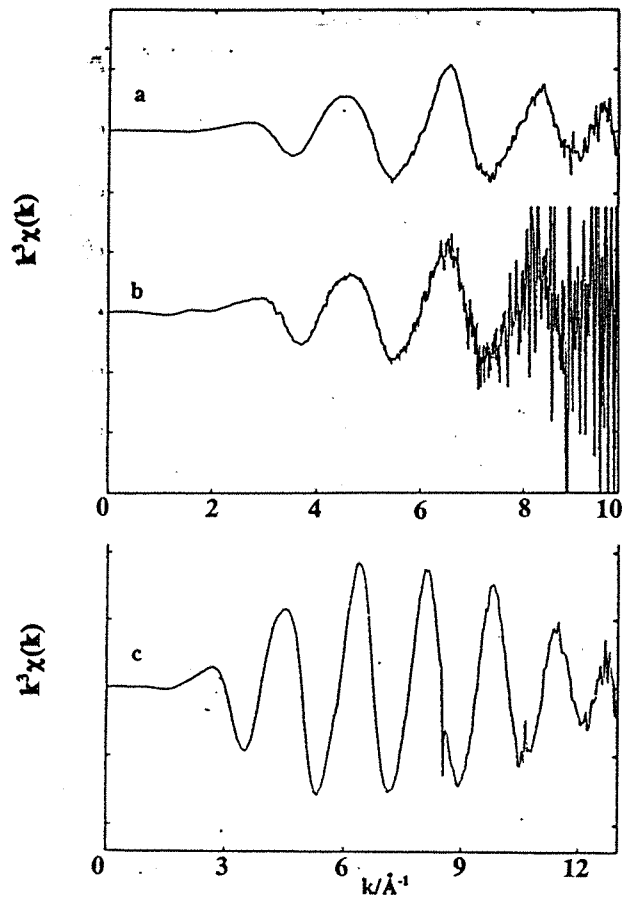

Figure 3.15. Figure showing a comparision between the k^3-weighted Ni-K-edge EXAFS data of $NiCl_2(PEt_3)_2$ (100mm in *p*-fluorotoluene) obtained using a) Reticon 512T EDE detector (1000 scans, each scan= 28 ms) b) Hamamatsu S3904 EDE detector (1000 scans, each scan= 105 ms) c) QUEXAFS (one scan, scan time= 2 minutes).

The Reticon and QUEXAFS data were solved to obtain a comparision between the parameters obtained using EDE and QUEXAFS. This is shown in Figure 3.16 and Table 3.8. It was decided not to solve the Hamamatsu data as it was too noisy compared to the Reticon 512T.

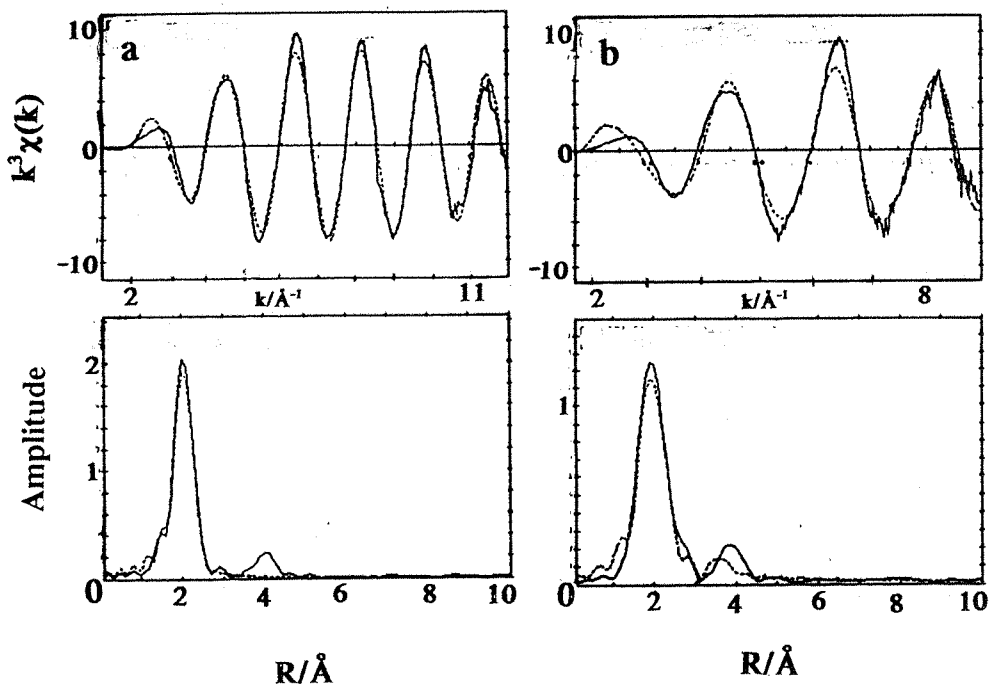

Figure 3.16. Figure showing the fitted k^3-weighted Ni-K-edge EXAFS data and the respective Fourier transforms of $NiCl_2(PEt_3)_2$ (100 mm in *p*-fluorotoluene) using a) QUEXAFS (one scan, scan time= two minutes), and b) EDE (Reticon 512T EDE detector, 1000 scans, each scan= 28 ms)

The Fourier transform data (Figure. 3.16) show quite clearly that the resolution between shells was poorer with the shorter EDE data. This can be seen by the broadenning of the peaks with shorter data sets. The parameters for the fitted data sets shown above in Figure 3.16 are shown in Table 3.8. Previous results obtained from transmission scanning EXAFS spectrum of $NiCl_2(PEt_3)_2$ (0.18M in *p*-fluorotoluene)[5] are also shown Table 3.8.

Table 3.8. Table showing the Ni-K-edge EDE, QUEXAFS parameters obtained for $NiCl_2(PEt_3)_2$ (100mM in *p*-fluorotoluene), using the fitted spectra shown on Figure 3.19. The table also shows the parameters obtained from the scanning EXAFS spectrum of $NiCl_2(PEt_3)_2$ (0.18M in toluene).[30]

EDE data: AFAC=0.9, EF= 1.47(0.55), R= 23.33%.
QUEXAFS data: AFAC= 0.9, EF= -1.31(0.32), R= 17.01%.
EXAFS data: AFAC= 0.82, E_0= 14.2eV, VPI= 3.0eV, R= 19.2%.

Type of coordinated atom	P	Cl	C
EDE C.N	4.12 (7)	___	___
QuE C.N	4.12 (4)	___	6.8 (7)
EXAFS C.N	2	2	___
EDE R/Å	2.192 (3)	___	___
QuE R/Å	2.204 (1)	___	4.295 (7)
EXAFS R/Å	2.14 (2)	2.21 (1)	___
EDE $\sigma/Å^2$	0.0093 (4)	___	___
QuE $\sigma/Å^2$	0.0052(1)	___	0.006 (1)
EXAFS $\sigma/Å^2$	0.0012 (4)	0.004 (1)	___

The fitted parameters in Table 3.8 show that due to the similarities between the phase-shifts of the phosphorus and the chlorine atoms and the fact that the two shells are at roughly the same radial distance from the central nickel atom, it was not possible to distinguish between the two shells. Thus, it was only possible to fit the spectrum to a

single shell of 4 phosphorus atoms at 2.192 (3)Å rather than to two shells of 2 phosphorus atoms at 2.14 (2)Å and two atoms of chlorine at 2.21(1) Å. This was true for both, the EDE and QUEXAFS data. It was possible to fit the scanning EXAFS data to two shells, one of chlorine and one of phosphorus.

3.8 Conclusion:

The results on the whole indicate that both EDE and QUEXAFS provide analysable data although the latter still provides longer data sets that therefore provides better resolution between shells. 8k-9k of data can be obtained using EDE within 35 seconds and 12k of data using QUEXAFS in two minutes. Conventional scanning EXAFS spectra usually provides 12k-14k of data within 40 minutes. Thus, a considerable saving in acquisition time has been made with EDE and QUEXAFS although there is still room for improvement of data lengths using EDE. A number of new EDE detectors are being developed and promoted at the SRS in Daresbury which should eventually lead to better quality data. Previous studies [9,10] have shown that the Hamamatsu has better energy resolution than the Reticon 512T due to its 25μm spatial pitch and also better linearity than the Reticon 512 T. The Hamamatsu is however less efficient at photon capture and takes longer to acquire a spectrum. Despite this, in our comparisions we found that the Reticon provided data with a better signal to noise ratio than the Hamamatsu using a smaller acquisition time.

Further, the studies have shown that with the current state of technology, the quality of EDE data can best be obtained at concentrations above 50mM of the analyte and 1000 scans. Increasing the number of scans to much more than 1000 scans results in noisier data due to instability of the beam. Also, increasing the number of scans and therefore the acquisition time of data results in poorer time resolution for real time studies of chemical reactions.

The studies with the model compounds also show that the EDE and QUEXAFS spectra both provide parameters that are comparable to scanning EXAFS and X-ray

crystallography parameters on the same compounds. However, when two shells are close together and the length of the data becomes important for the resolution of the two shells, then EDE is at a disadvantage compared to QUEXAFS and scanning EXAFS. However, EDE is still at a developmental stage and improvements in data quality are expected in a few years.

3.9 REFERENCES

1. N.Allinson, G.Baker, G.N.Greaves and J.N.Koll, *Nucl.Instr.Meth.*, 1988, **A266**, 592.
2. G.Salvini, D.Bogg, A.J.Dent, G.E.Derbyshire, R.C.Farrow, A.Felton, C.Ramsdale, *Physica B.*, 1995, **209**, 1-4, 229.
3. T.Matsushita, H.Oyanagi, S.Saigo, H.Kihara, and U.Kaminaga, 'EXAFS and Near Edge Structure III', 1984, Springer-Verlag, Editors; K.O.Hodgson B.Hedman, J.E.Penner-Hahn.
4. E.Dartgye, A.Fontaine, A.Jucha and D.Sayers, 'EXAFS and Near Edge Structure III', 1984, Springer Verlag, Editors, K.O.Hodgson, B.Hedman, J.E.Penner-Hahn.
5. G.E.Derbyshire, W.I.Helsby, A.J.Dent, S.A.Wright, R.C.Farrow, G.N.Greaves, C.Morrell and G.J.Baker, *Adv.X-ray.Analysis.*, 1990, **34**.
6. T.Matsushita and R.P.Phizackerley, *Jpn.J.Appl.Phys.*, **20**, 2223, 1981.
7. R.P.Phizackerley, Z.U.Rek, G.B.Stephenson, S.D.Conradson, K.O.Hodgson, T.Matsushita and H.Oyanagi, *J.Appl.Cryst.*, **16**, 220, 1983.
8. M.Hagelstein, C.Ferrero, U.Hatje, T.Ressler and W.Metz, *J.Synchr.Rad.*, 1995, **2**, 174.
9. D.Bogg, A.J.Dent, G.E.Derbyshire, R.C.Farrow, C.A.Ramsdale, G.Salvini, *Nucl.Instr.Meth.*, 1993, **390**, 1-3, 461.
10. G.Salvini, D.Bogg, A.J.Dent, G.E.Derbyshire, R.C.Farrow, A.Felton, C.Ramsdale, *Physica B.*, 1995, **209**, 1-4, 229.
11. R.Frahm and J.Wong, *Jpn.J.Appl.Phys.*, 1993, **32**, 32-2, 188.
12. R.Frahm, T.W.Barbee.Jr and W.Warburton, *Phys.Rev.*, 1991, **B44**, 2822.
13. F.Cimini and R.Prins, J.Phys.Chem.B., 1997, 101, 5277.
14. G.Sankar, P.A.Wright, S.Natarajan, J.Meurig Thomas, G.N.Greaves, A.J.Dent, B.R.Dobson, C.A.Ramsdale and R.H.Jones, J.Phys.Chem., 1993, 97, 9550.

15. R.Frahm, J.Wong, J.B.Holt, E.M.Larson, B.Rupp and P.A.Waide, *Phys.Rev.B.*, 1992, **46**, 9205.

16. B.R.Dobson, S.S.Hasnain, M.Neu, C.A.Ramsdale and L.M.Murphy, *Jpn.J.Appl.Phys.*, 1993, **32**, 192.

17. R.Frahm, *Rev.Sci.Instr.*, 1989, **60**, 2515.

18. R.Frahm: X-ray Absorption Fine Structure, Eds. S.S.Hasnain, Ellis Horwood, 1991, 731.

19. R.Frahm, *Nucl.Instrum.Meth.*, 1988, **A270**, 578.

20. R.W.Joyner, K.J.Martin, and P.Meehan, *J.Phys.C.*, 1987, **20**, 4005.

21. S.S.Hasnain, (Editor), 'X-ray absorption Fine Structure', Ellis Horwood, New York, 1991, 195.

22. W.Levason, 'The Chemistry of Organophosphorus Compounds', F.R.Hartley, ed., Wiley, New York, Vol I, 1990.

23. P.L.Goggin and R.J.Goodfellow, *J.Chem.Soc.A.*, 1966, 1462.

24. K.Shobotake and K.Nakamoto, *J.Am.Chem.Soc.*, 1970, **92**, 3332.

25. K.A.Jensen, P.H.Nielsen, and C.Pedersen, *Acta.Chem.Scand.*, 1963, **17**, 1115.

26. F.A.Cotton and J.P.Fackler, *J.Chem.Soc.*, 1961, **83**, 2818.

27. J.M.Corker, PhD Thesis, University of Southampton, 1991.

28. G.J.Bullen, R.Mason, and P.Pauling, *Inorg.Chem.*, 1965, **4**, 456.

29. B.K.Teo, 'EXAFS: Basic Principles and Data Analysis', Springer-Verlag, Berlin, 1986.

30. H.Leach, PhD Thesis, University of Southampton, 1990.

31. J.M.Corker, J.Evans, H.Leach and W.Levason, *J.Chem.Soc.,Chem.Commun.*, 1989, 181.

32. V.Scatturin and A.Turco, *J.Inorg.Nucl.Chem.*, 1958, **8**, 447.

CHAPTER 4. ELECTRONIC ABSORPTION AND QUEXAFS SPECTROSCOPIC STUDIES OF $Ni(acac)_2$/ $AlEt_3$ CATALYST MIXTURES.

4.1 Introduction:

The mechanism of nickel alkene oligomerisation catalysis has been studied by numerous workers.[1-7] A number of nickel complexes have been used as the catalyst with alkylaluminium cocatalysts.

This section of the thesis is devoted to a study of in situ mixtures of $Ni(acac)_2/AlEt_3$ where $Ni(acac)_2$ is the catalyst and $AlEt_3$ is the cocatalyst. As mentioned in the introduction, $AlEt_3$ is a strong Lewis acid and alkylating agent.[8] On addition of triethylaluminium to nickel acetylacetonate, alkylation of the nickel centre occurs with consequent loss of acac groups to the aluminium ion. The nickel alkyls are unstable and undergo homolytic cleavage of coordinated alkyl groups by coupling or by loss of an olefin molecule (in cases where the alkyl group has β-hydrogens) to give metallic nickel as shown in Figure 4.1.[2,3]

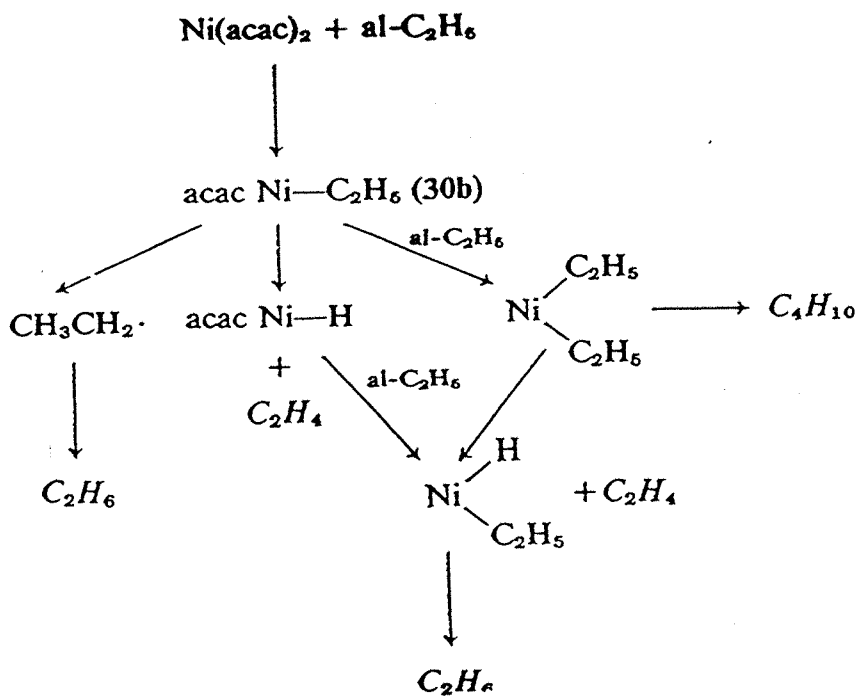

Figure 4.1. Figure showing the mechanism by which a nickel diethyl species may decompose to give alkene products and nickel metal.[2]

The $Ni(acac)_2/AlEt_3$ mixture is known to catalyse the oligomerisation of alkenes such as hex-1-ene. In-situ experiments of the nickel/aluminium catalyst mixture would have to be in the presence of hex-1-ene. Previous EXAFS studies of a similar catalyst mixture (i.e. $Ni(acac)_2/AlEt_2(OEt)$, in the presence of hex-1-ene have indicated the formation of an organometallic involving a coordinated olefin and alkyl species[9,10] as shown below.

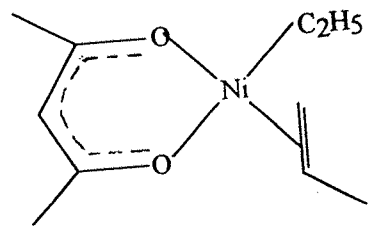

Figure 4.2. Figure showing the organometallic indicated to be present in mixtures of $Ni(acac)_2/AlEt_2(OEt)$/hex-1-ene (Ni:Al:hex-1-ene 1:2:20, [Ni]= 70mM in toluene) at 0°C using scanning EXAFS.

Studies involving $AlEt_3$ have shown that this cocatalyst is a much stronger Lewis acid and it has been difficult to isolate the organometallic species. It will be shown in this chapter that an organometallic as shown in Figure 4.2 is also formed when $AlEt_3$ is used as a cocatalyst. However, this organometallic can only be studied at low temperatures as at higher temperatures the reaction leads to nickel metal precipitation. Time-resolved studies of nickel metal particle formation will also be covered.

IR studies[16] of this reaction mixture, based on a drop in absorbance at $1261cm^{-1}$, showed that there is incomplete exchange of acetylacetonate groups for alkyl groups at the point where catalytic activity is the highest. The same study also showed that the nickel atom in the catalytic species still retains one acetylacetonate ligand even after some alkylation and during catalysis.

For the experiments in this chapter, the solvent used was toluene. This allowed the catalyst to be studied with limited interference from any coordinating solvent groups. Otherwise, the oligomerisation reaction is thought to occur faster and more efficiently in the presence of halogenated solvents.

The reaction was studied primarily using QUEXAFS spectroscopy with a scan duration of two minutes to allow for some time resolution in the studies of any reaction.[11,12] Preliminary electronic absorption spectroscopic studies of the reaction mixtures were also carried out.

4.2 Objectives:

a) To perform preliminary electronic absorption spectroscopy studies of the catalyst mixtures in the presence and absence of hex-1-ene.
b) to use Ni-K-edge QUEXAFS to study the formation of nickel metal particles in the $Ni(acac)_2/AlEt_3$ solution in the absence of hex-1-ene.
c) to use Ni-K-edge QUEXAFS to study the nickel/aluminium mixture in the presence of hex-1-ene i.e. $Ni(acac)_2/AlEt_3$/hex-1-ene (Ni:Al:hex-1-ene 1:2.5:20, [Ni]= 70mM) in toluene at -5°C and again at room temperature.

4.3 Preliminary electronic absorption spectroscopy studies of the catalyst mixture $Ni(acac)_2/AlEt_3$:

i) Spectrum of $Ni(acac)_2$, the starting material:

A spectrum of the starting material is presented in Figure 4.3.

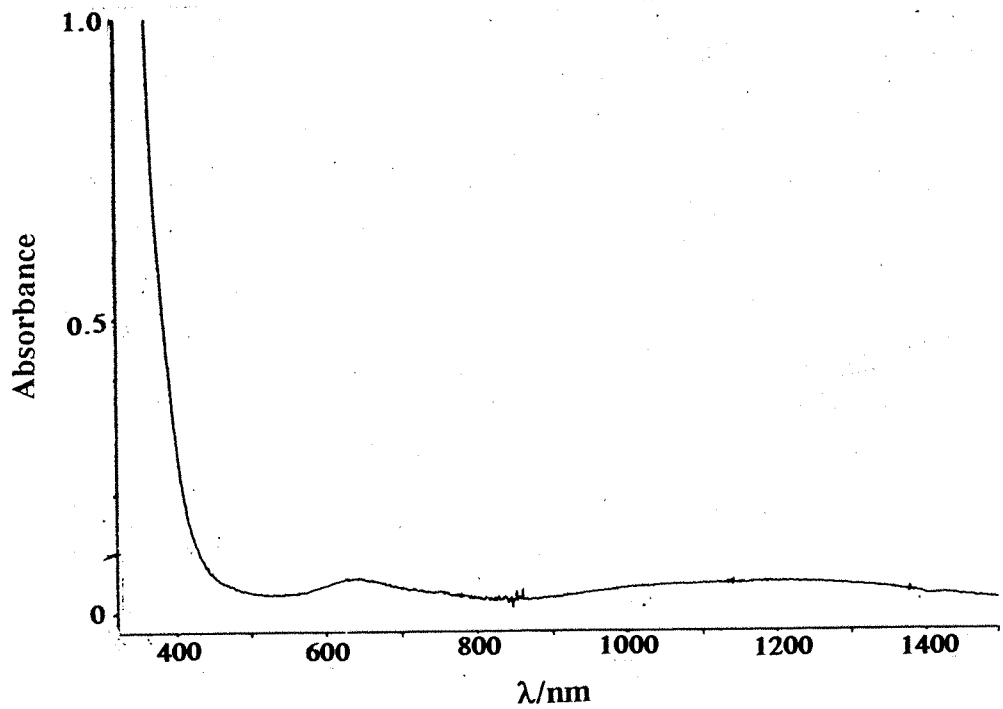

Figure 4.3. Figure showing the electronic absorption spectrum (scan duration= 4 minutes) of $Ni(acac)_2$ (10mM in toluene).

A detailed analysis of the electronic absorption spectrum of $Ni(acac)_2$ was carried out by G.Maki in 1958.[13] This showed that the peak at 1135 nm (ε= 4 l mol^{-1} cm^{-1}) is caused by a $^3A_{2g}$ to $^3T_{2g}$ transition and the peak at 655nm (ε= 5 l mol^{-1} cm^{-1}) is caused by a $^3A_{2g}$ to $^3T_{1g}$ transition.

ii) In the absence of hex-1-ene:

An electronic absorption spectroscopic study of the $Ni(acac)_2/AlEt_3$ mixture was carried out, in toluene, at room temperature, using varying ratios of Ni:Al e.g. 1:1, 1:2.5. In all instances, the concentration of nickel acetylacetonate in the

reaction mixture was 10mM. The studies were carried out in a spectrometer cell (See Appendix) under an atmosphere of argon. Each reaction was first scanned from half a minute after mixing reagents. Scans were then taken every five minutes.

Figure 4.4 shows the spectra of the reaction mixture (Ni:Al 1:1, [Ni]= 10mM in toluene).

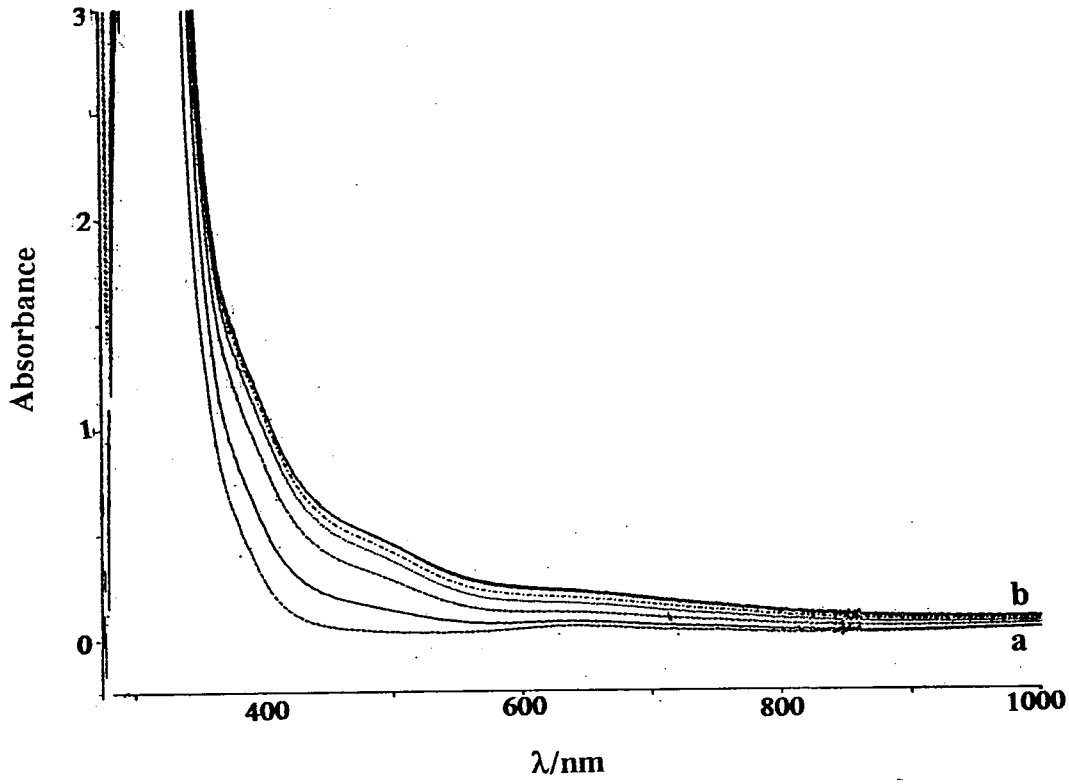

Figure 4.4. Figure showing the electronic absorption spectra (scan duration= 4 minutes) of $Ni(acac)_2/AlEt_3$ (Ni:Al 1:1, [Ni]= 10mM) mixture in toluene at room temperature taken a) 0.5 minutes after mixing reagents up to b) 25 minutes after mixing.

The spectra clearly show the appearance of two new bands at 400 nm (ε= 100 l $mol^{-1}cm^{-1}$) and at 500 nm (60 l $mol^{-1}cm^{-1}$) as the reaction proceeded. These bands are not caused by any product or starting material in the reaction mixture e.g.

aluminium acetylacetonate, $AlEt_3$, or even toluene. Spectra of all of these species show absorbances below 350 nm, while the bands concerned appear at higher wavelengths than that. From the low molar extinction coefficients, these bands are likely to be *d-d* transitions. Square planar complexes usually exhibit a band (ε= 50 - 500 l mol^{-1} cm^{-1}) at 430- 670 nm and a second band at 370- 430 nm.[14,15] The spectrum of the reaction mixture showed bands at 500 nm and 400 nm. The species in the reaction mixture was therefore likely to be square planar.

As mentioned before the reaction should lead to alkylation of the nickel species. However, the alkyl species are unlikely to be stable enough for observation. It is therefore likely that an alkyl species stabilised by aluminium interactions could be involved. A likely species is shown below in Figure 4.5.

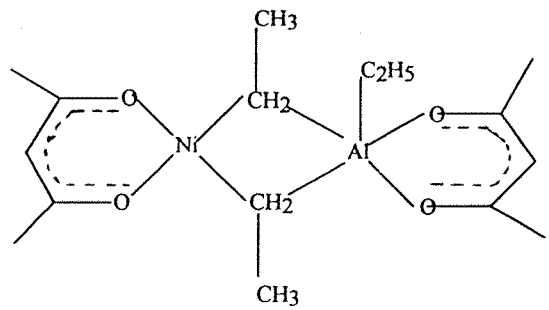

Figure 4.5. Figure showing a possible alkylated apecies stabilised by aluminium interactions.

Such a species with Ni-C-Al bridges has previously been implicated in the reactions between other nickel complexes and alkylaluminium.[1,9] The Ni-C-Al interaction is thought to be one stabilising factor retarding β-hydride or reductive elimination to afford metal.

Previous studies[16] have also shown the formation of $AlEt_2$(acac) as a product of the reaction. Such a product can easily be formed from the alkylated species shown in Figure 4.5 leading to a nickel diethyl species which then decomposes to give nickel metal.

Figure 4.6 shows the electronic absorption spectra of the catalyst mixture $Ni(acac)_2/AlEt_3$, using (Ni:Al 1:2.5, [Ni]= 10mM in toluene). Due to the higher Ni:Al ratio, the reaction here occurred to give nickel metal very fast. As nickel metal particles formed, they gave rise to a colloidal mixture which led to the high absorbance or scattering at lower wavelengths which also obscured changes in the visible region of the spectrum. It was not possible to observe any changes in the charge transfer region after this.

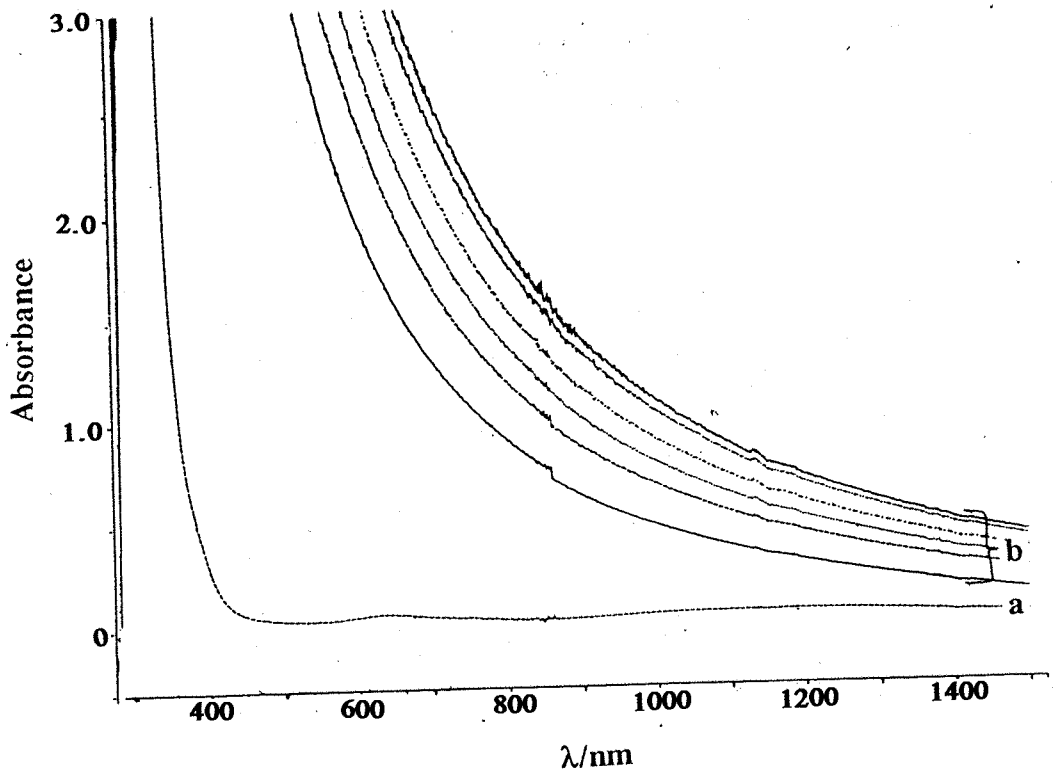

Figure 4.6. Figure showing the electronic absorption spectra of a) the catalyst $Ni(acac)_2$ (10mM in toluene) and b) Six consecutive scans of the mixture $Ni(acac)_2/AlEt_3$ (Ni:Al 1:2.5, [Ni]= 10mM) in toluene taken at 4 minute intervals with the first scan being taken 0.5 minutes after mixing of reagents) .

ii) In the presence of hex-1-ene:

Next, electronic absorption spectra of $Ni(acac)_2/AlEt_3$/hex-1-ene (Ni:Al:hex-1-ene 1:1:20, [Ni]= 10mM) were obtained at room temperature. The results are presented in Figure 4.7. The first spectrum was taken at half a minute after mixing the reagents. The changes in the region 400-600 nm are less clear than in the absence of hex-1-ene.

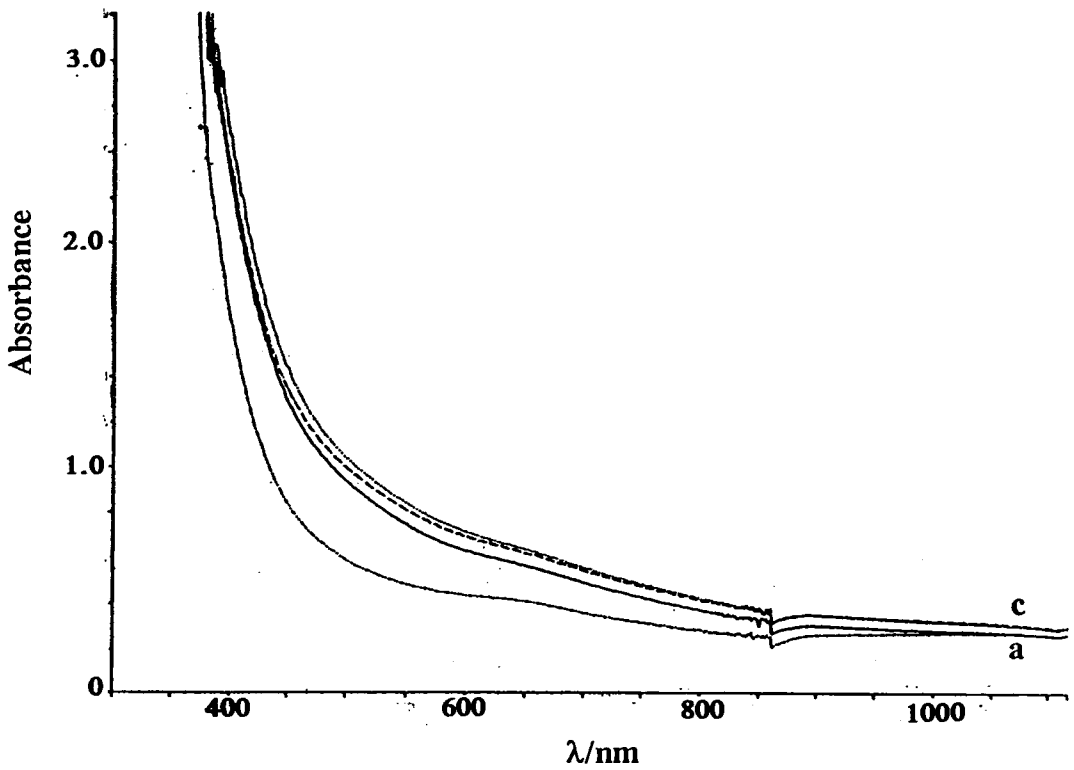

Figure 4.7. Figure showing the room temperature electronic absorption spectra of $Ni(acac)_2/AlEt_3$/hex-1-ene (Ni:Al:hex-1-ene 1:1:20, [Ni]= 10mM) taken at a) t= 0.5 b) 3.5 c) 6.5 minutes after mixing of reagents.

These were only preliminary experiments of the reaction using electronic absorption spectroscopy. Due to the lower concentrations of both the reagents, the reaction proceeded at a rate slow enough to be observed using room temperature electronic absorption spectroscopy. The exact experiments were not directly repeatable using EXAFS because the concentrations required for EXAFS were much higher (70mM- 80mM) than used for electronic absorption spectroscopy (10mM).

The next few sections of this chapter will be concerned with the QUEXAFS spectra of the $Ni(acac)_2/AlEt_3$ mixtures in the presence and absence of hex-1-ene. A spectrum of the metal foil will also be studied. All the mixtures in these sections were studied at the SRS at the Daresbury Laboratory on Station 9.3. They were studied in the transmission mode as detailed in Chapter 2. The variable temperature equipment (with the vertically held syringe drivers) as detailed in Section 2.4.3 b, was used for all these experiments. In all the cases, the two reagent syringes were used to pump solution into the observation cell (volume= 0.7ml) at the same rate (119 ml/hr) each. Thus, fresh solution entered the cell every 10.6 seconds. One of the syringes would contain the $Ni(acac)_2$ solution at twice the concentration required in the cell mixture (as it would be diluted by half using the other reagent solution) and the other syringe contained $AlEt_3$/hex-1-ene solution in toluene at twice the concentration required in the observation cell. **(The figures given in the brackets of the mixture throughout the rest of this chapter are of those of the mixture composition in the observation cell after mixing.).**

The EXAFS experiments were therefore carried out, using the variable temperature equipment, to study any organometallic intermediates formed at low temperatures. The EXAFS experiments were carried out at a range of temperatures ($-16^{o}C$, $0^{o}C$, and $20^{o}C$) to see the effect of changing the temperature on the reaction mixture. As mentioned above, the formation of colloidal nickel metal particles could also be studied using EXAFS.

4.4 QUEXAFS spectrum of nickel metal foil:

Figure 4.8 shows a fitted QUEXAFS spectrum of nickel metal foil and its Fourier transform. The data confirms the theoretical parameters obtained based on the FCC structure of the metal.

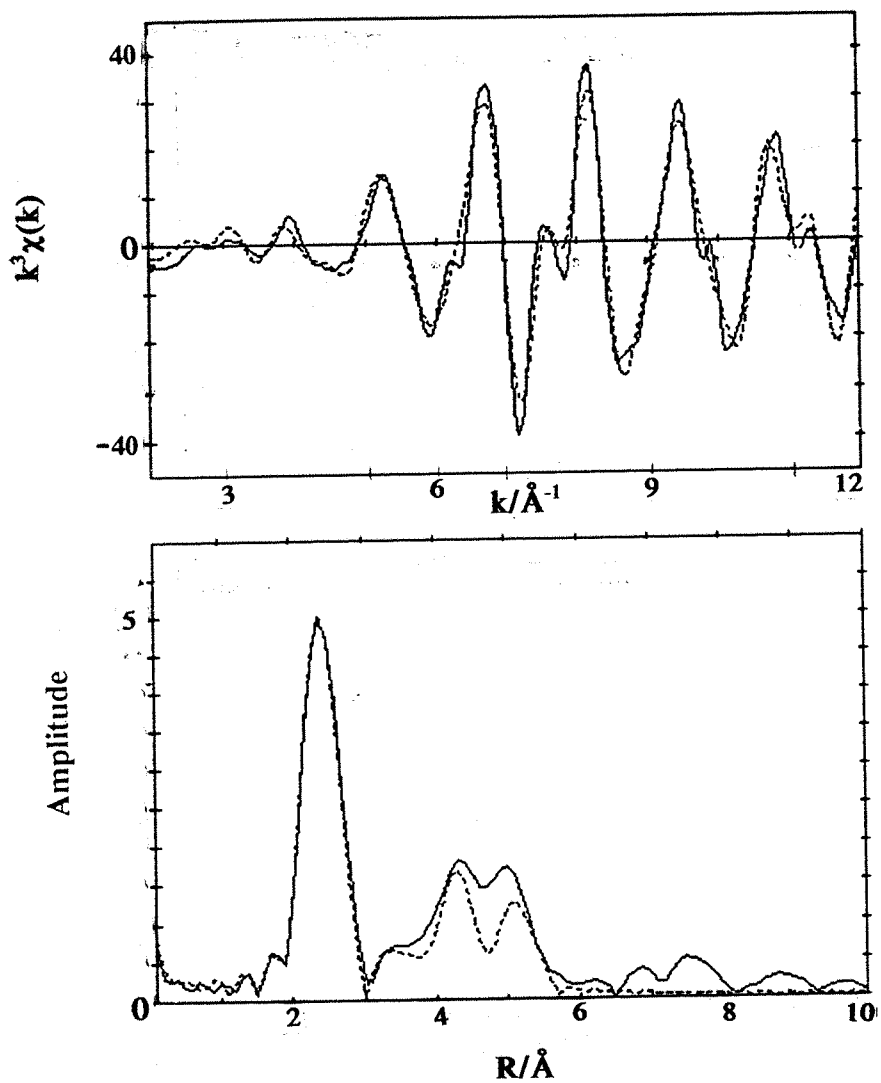

Figure 4.8. Figure showing fitted QUEXAFS data (one scan, scan time= 2 minutes) of nickel metal foil and its Fourier transform.

Table 4.1. Table showing the parameters obtained from the fitted QUEXAFS spectrum (one scan, scan time= 2 minutes) of nickel metal foil shown in Figure 4.8.

EF= -13.2(4) , AFAC= 0.9, R=28.87%.

Atom type	Coordination number	FCC Value	R/Å	FCC Value R/Å	$\sigma^2/Å^{-1}$
Ni	12.0 (2)	12	2.471 (2)	2.492	0.0106 (2)
Ni	6.5 (8)	6	3.478 (9)	3.524	0.019 (2)
Ni	28.0 (1)	24	4.320 (5)	4.316	0.0186 (8)
Ni	14 .4(8)	12	5.144 (4)	4.984	0.0062 (7)

The parameters in the Table 4.1 show a first shell of 12 nickel atoms at 2.471(2)Å, and second shell of six nickel atoms at 3.478(9)Å as expected from the FCC structure of the metal. However, coordination numbers for the third and fourth shells were higher than expected. This could be because not all multiple scattering paths were taken into account. In future experiments involving $Ni(acac)_2/AlEt_3$ mixtures, the appearance of nickel shells at 2.471 Å and 3.478 Å could indicate the formation of nickel metal particles in solution i.e. colloidal nickel.[17]

The particles of nickel that are likely to form in a Ni/Al mixture are more likely to be small and dispersed clusters rather than foil.

Numerous workers have studied the chemical nature of nickel metal clusters in the vapour state and in organic media.[18-20] EXAFS studies of nickel metal clusters in the vapour state have also been carried out.[21] These studies indicate a substantial

contraction of the nearest neighbour distances in vapour phase nickel clusters as compared to metallic nickel. The contraction in the nearest neighbour distances have been thought to increase as the size of the clusters decreases. A similar contraction has been seen in solvated nickel particles, but to a lesser extent. The observed bond, length contraction was explained by a redistribution of charge.[21] It was thought that in a cluster the total number of nearest neighbour atoms would be significantly less than in bulk. This would lead to a reduction in the repulsive interactions between non-bonded electron pairs. A contraction of nearest neighbour distances was therefore thought to be the result.

It has also been seen that the contraction of nearest neighbour distances was accompanied by an increase in the Debye Waller factors of the first shell in the case of small metal clusters compared to the foil or even bulk metal. This was due to the large vibrational amplitude at the surface of the clusters and arises from the relaxation of coordinatively unsaturated surface nickel atoms at certain faces of the fine particle.[29]

4.5 QUEXAFS spectra of $Ni(acac)_2/AlEt_3$ (Ni:Al 1:5, [Ni]= 70mM) mixture at varying temperatures:

a) Comparision of the raw spectra at varying temperatures:

Figure 4.9 shows a comparision of the raw Ni-K-edge QUEXAFS spectra of $Ni(acac)_2/AlEt_3$ (Ni:Al 1:5, [Ni]= 70mM) mixture in toluene taken at different temperatures (-16°C, 0°C, 20°C). At -16°C, the spectrum retained the white line features of the starting material i.e. $Ni(acac)_2$, showing that the reaction had proceeded little at these temperatures. At 0°C, the white line features of the spectrum are softened, as the alkylation proceeded resulting in the octahedral structure of the $Ni(acac)_2$ breaking down. Finally, at room temperature, there was

further change in the EXAFS spectrum of the reaction mixture as the reaction has proceeded towards the formation of nickel metal particles. Thus, the spectra show that the reaction proceeded to different extents at the different temperatures as expected.

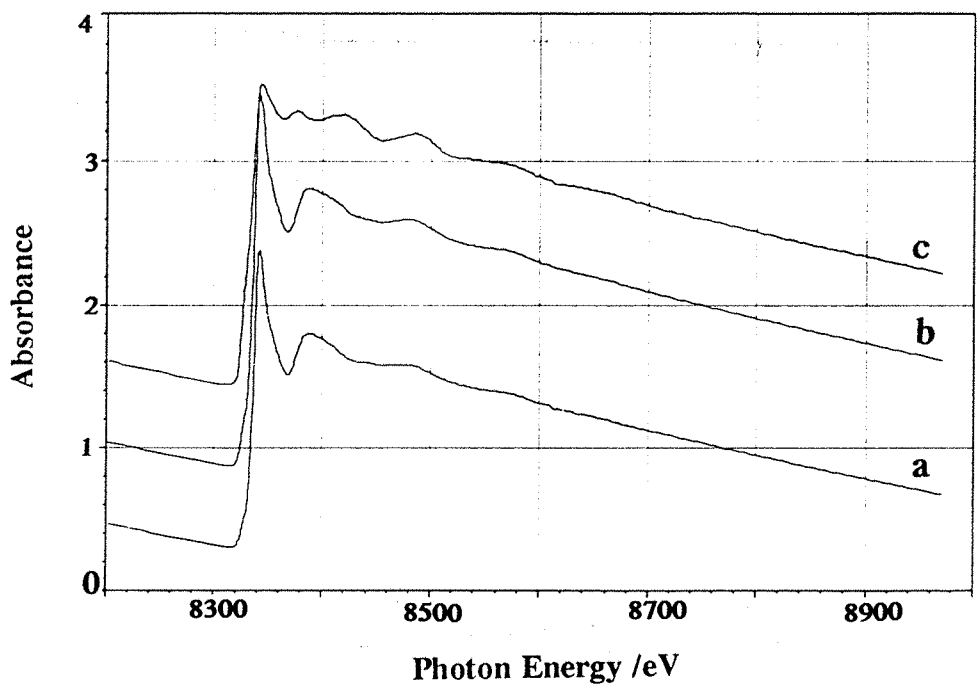

Figure 4.9. Figure showing a comparision of the white line features of the Ni-K-edge QUEXAFS spectra of the $Ni(acac)_2/AlEt_3$ (Ni:Al 1:5, [Ni]= 70mM) mixture in toluene taken at different temperatures a) -16°C b) 0°C c) 20°C

b) QUEXAFS spectra of $Ni(acac)_2/AlEt_3$ (Ni:Al 1:5, [Ni]= 70mM) mixture in toluene at room temperature:

Figure 4.10 shows ten spectra (scan time= 2 minutes) of the $Ni(acac)_2/AlEt_3$ (Ni:Al 1:5, [Ni]= 70mM) mixture in toluene at room temperature taken following one another starting from t= 0 minutes i.e. from the mixing of the reagents, up to 20 minutes after mixing. The figure shows quite clearly the change in the white line features of the solution from that of $Ni(acac)_2$ to that of nickel metal particles.

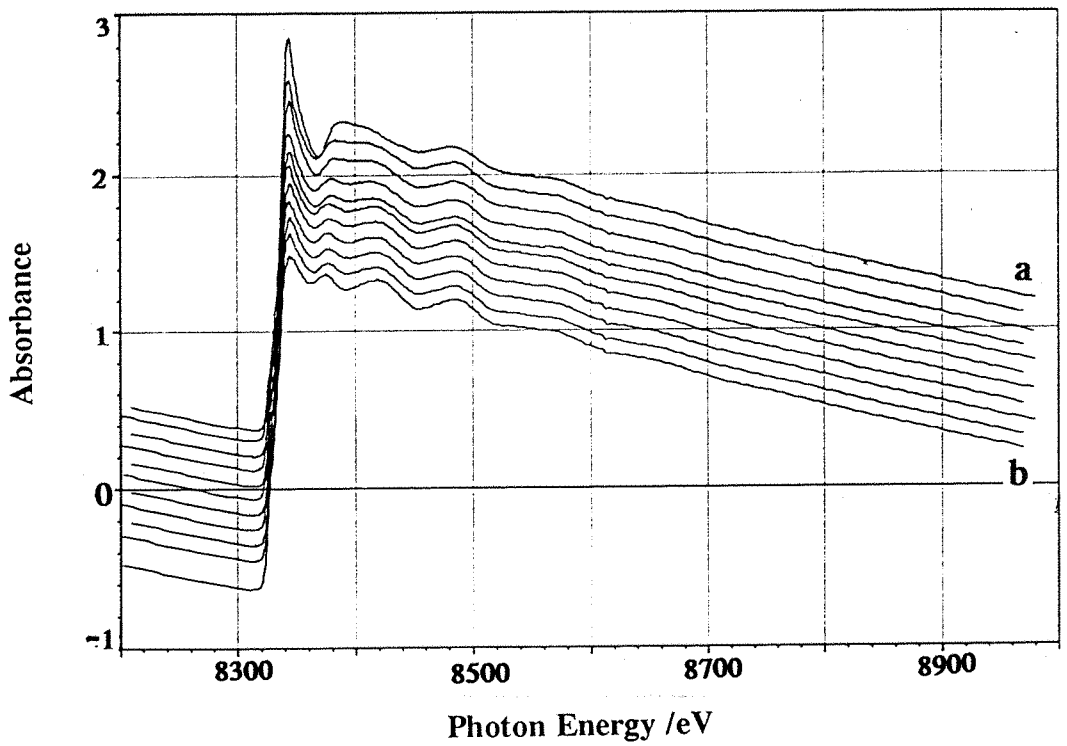

Figure 4.10. Figure showing ten consecutive QUEXAFS spectra (scan time = 2 minutes) taken of a room temperature solution of $Ni(acac)_2/AlEt_3$ (Ni:Al 1:5, [Ni]= 70mM) mixture in toluene starting from a) t= 0 minutes, i.e. point of mixing of the reagents in-situ up to b) 20 minutes after mixing reagents.

The spectrum at t= 20 minutes, i.e. the last spectrum in the series shown in Figure 4.10 was subjected to curve fitting analysis using EXCURV92. The results are shown in Figure 4.11 and Table 4.2.

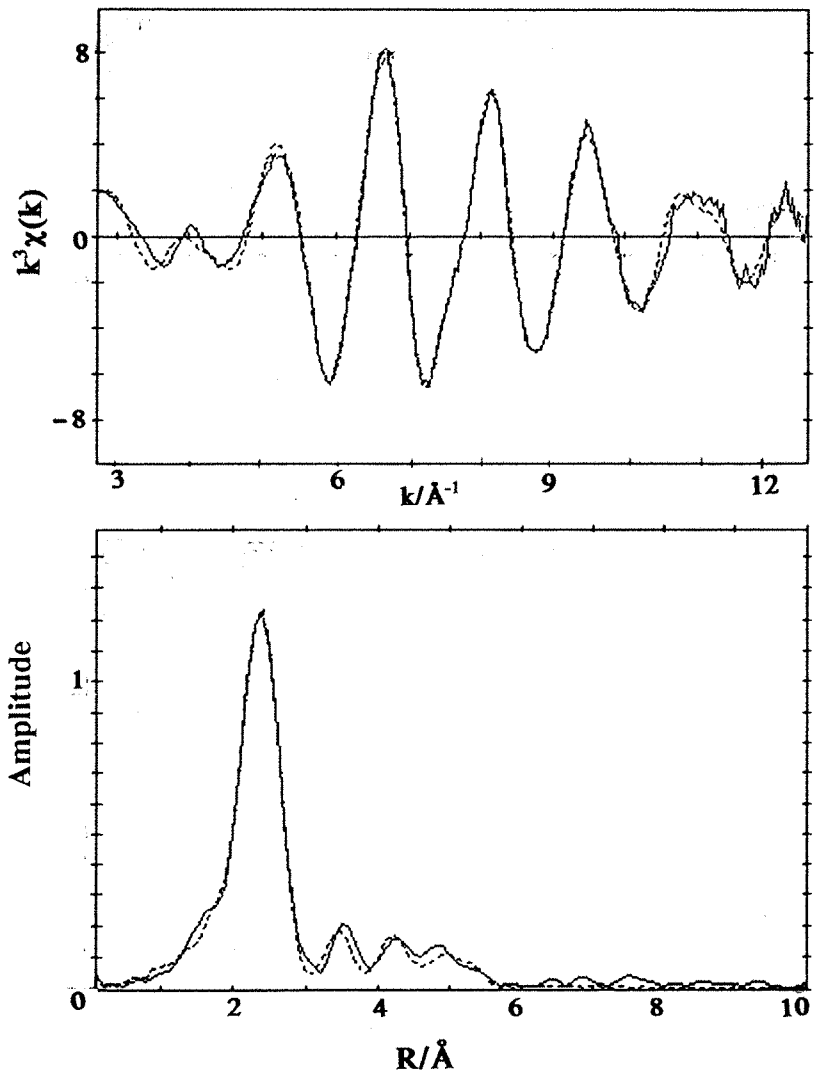

Figure 4.11. Figure showing the fitted QUEXAFS data (one scan, scan time= 2 minutes) of a room temperature solution of $Ni(acac)_2/AlEt_3$ (Ni:Al 1:5, [Ni]= 70mM) mixture in toluene and its Fourier transform taken 20 minutes after mixing the reagents.

Table 4.2. Table showing the parameters obtained from the fitted QUEXAFS spectrum of $Ni(acac)_2/AlEt_3$ (Ni:Al 1:5, [Ni]= 70mM) mixture in toluene taken at room temperature and 20 minutes after the reagents were mixed in situ at this temperature.

EF= 5.1 (3), AFAC= 0.9, R= 15.2%.

Atom Type	Coordination Number	R/Å	σ^2 /Å^{-1}
Ni	5.5 (1)	2.454 (1)	0.022 (0)
Ni	1.5 (1)	3.472 (6)	0.021 (1)
Ni	2.6 (2)	4.309 (6)	0.021 (1)
Ni	3.7 (4)	5.136 (8)	0.022 (2)
O	0.8 (1)	1.955 (8)	0.027 (3)

Thus, the parameters obtained from the fitted spectrum show that nickel metal particles were formed as upto four shells of nickel atoms could be fitted. However, the fit was also significantly improved on adding an oxygen shell of 0.82 atoms at 1.955 Å suggesting the presence of a mononuclear nickel species with some Ni-O distances. This shell may also have resulted from the formation of an oxygen or carbon shell on the surface of the nickel particles leading to the formation of a micro-heterogeneous catalyst.[17]

Numerous workers[22-27] have tried to determine the size of metal clusters using EXAFS based on the first shell occupation number which has been known to vary systematically with size since EXAFS samples the environment of low coordination outer shells as well as the 12 coordinate central atom. The clusters in these methods have been often assumed to be icosahedra.

The following table shows the average atomic coordination numbers for an FCC structure for up to 3 shells.[23]

Table 4.3. Table showing the average coordination numbers for FCC clusters of 13-55 atoms.[23]

Number of atoms in cluster	First shell	Second shell	Third shell
13 atoms	5.54	1.85	3.69
19 atoms	6.32	1.89	5.05
43 atoms	7.26	3.07	8.93
55 atoms	7.85	3.27	9.6

Based on the first shell occupancy of 5.5 atoms from the EXAFS parameters (Table 4.2), the data in the above table would indicate an average cluster size of 13 atoms. However, it is known that with EXAFS analysis, there is an experimental error of $\pm$ 20% on the first shell occupancy number. This would make it difficult to decide if we have a 13 atom or 19 atom structure.

Also, the occupancy numbers obtained from EXAFS spectroscopy are not accurate because not all multiple scattering paths are included and there is a high correlation between Debye Waller factors and the coordination number. Other problems are caused by the presence of discrete closely spaced shells which would make it difficult to obtain accurate coordination numbers and nearest neighbour distances.

To overcome the problem of extracting a nearest neighbour occupancy figure from the EXAFS spectrum, another method was devised by Mr.N.Binsted (Southampton University) to estimate the sizes of metal particles in solution. This method involved using a program to generate 1,2,3,4 shell model FCC clusters with octahedral symmetry. The program generated the expected EXAFS spectrum of the cluster by taking into account all the multiple scattering paths at each atom in the

FCC cluster. An EXAFS curve was generated for each of the atoms in the cluster and these were summed to give the final expected scattering pattern for the cluster. The expected fine structure was compared to the experimental spectrum of the nickel particle and the Ef and Debye temperature were refined. The core widths, phase shifts and amplitude factor were obtained from nickel foil data. The fits obtained for the spectra from each of these 1,2,3,4 shell clusters were then compared. As many clusters were generated as there were shells in the EXAFS spectrum plus one. This program was a development on a combined powder diffraction and EXAFS package to determine crystal structure in powder samples previously written by N.Binsted *et al.*[30]

The results from the new program were calculated for the experimental spectrum of nickel particles, shown in Figure 4.11. The results indicated that on average the data could best fit to a two-shell nickel cluster containing 19 atoms. However, the fit was improved by a provision made for the presence of a small quantity of a mononuclear nickel complexes containing Ni-O bonds. This preference for a two-shell 19 atom cluster had to be interpreted with caution. It is very possible that a variety of cluster sizes and symmetries were present in the sample and the preferred two-shell model containing 19 nickel atoms was just an average form of all the clusters. It could also merely be the dominant cluster of all the cluster sizes present. **If it was a mean structure it still provided some idea of the sizes of the clusters present in the solution.** Such a 19 atom cluster is shown below in Figure 4.12.

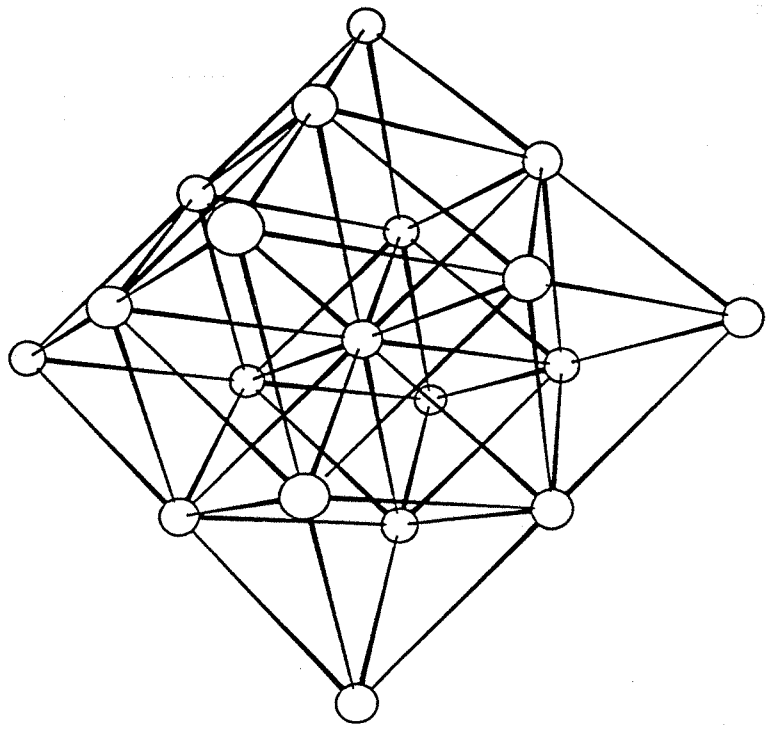

Figure 4.12. Figure showing the 19 atom two shell FCC structure of a cluster which could represent the mean of all the nickel metal clusters present in a sample solution of $Ni(acac)_2/AlEt_3$ (Ni:Al 1:5, [Ni]= 70mM) mixture in toluene at room temperature.

It should be noted that numerous Ni(0) complexes have been implicated as the main catalytic species in the Ni/Al mixtures.[1,3] The nickel metal clusters formed in this mixture could, in the presence of hex-1-ene be responsible for catalysing the oligomerisation reaction. Such catalysis would be possible by the coordination of olefin molecules to the nickel particles as they form[31] with catalysis occurring microheterogeneously. This does not preclude the participation of the aluminium reagent during the catalysis. However, the metal particles may also be a result of decomposition of the active organometallic catalyst.

c) QUEXAFS spectra of $Ni(acac)_2/AlEt_3$ (Ni:Al 1:5, [Ni]= 70mM) mixture in toluene taken at 0°C:

Figure 4.13 shows ten consecutive QUEXAFS spectra (scan time= 2 minutes) of $Ni(acac)_2/AlEt_3$ (Ni:Al 1:5, [Ni]= 70mM) mixture in toluene at 0°C taken from the point of mixing of the reagents upto 20 minutes after mixing. The white line features of the spectra look very similar to that of $Ni(acac)_2$, although there are some differences which become apparent in the next part of this section i.e. on analysing the data.

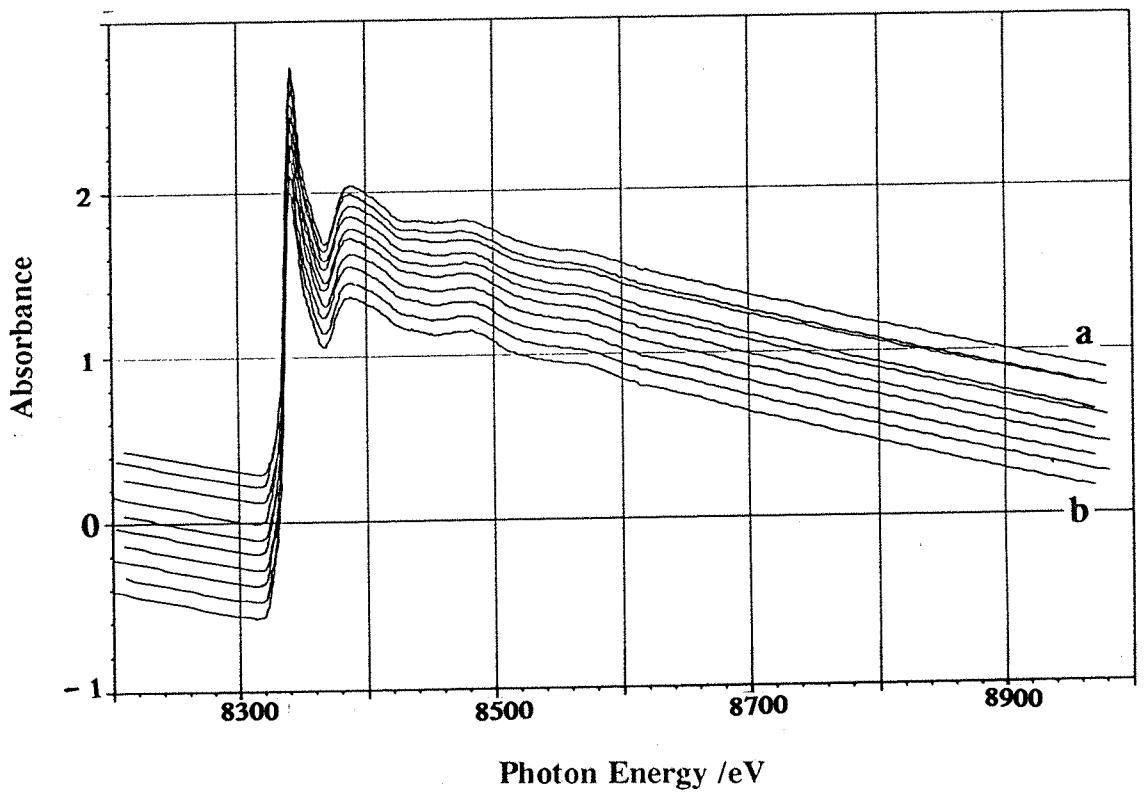

Figure 4.13. Figure showing ten consecutive QUEXAFS spectra (scan time= 20 minutes) of $Ni(acac)_2/AlEt_3$ (Ni:Al 1:5) mixture in toluene taken at 0°C starting a) from the time of mixing the reagents up to b) twenty minutes after the reaction.

The last spectrum of the series of spectra shown in Figure 4.13 (i.e. spectrum taken at twenty minutes after mixing), was subjected to curve fitting analysis. The fitted curve and its Fourier transform are shown in Figure 4.14.

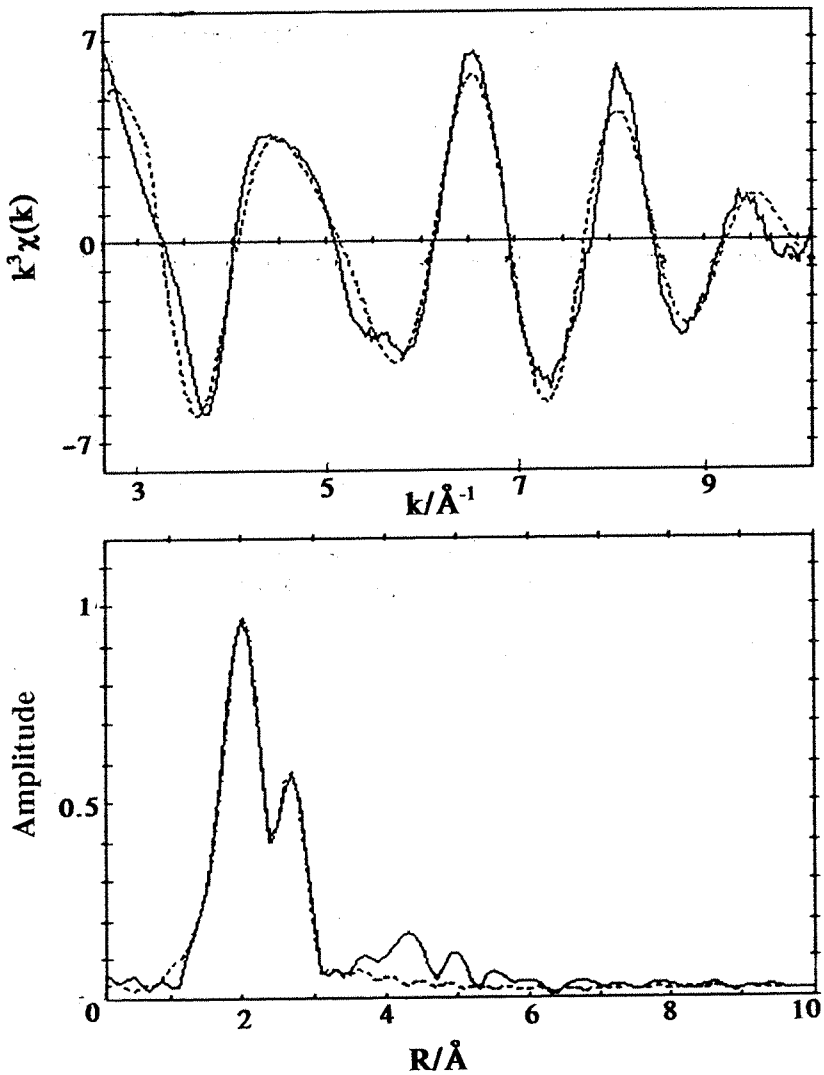

Figure 4.14. Figure showing the fitted QUEXAFS data (one scan, scan time= 2 minutes) of $Ni(acac)_2/AlEt_3$ (Ni:Al 1:5, [Ni]= 70mM) mixture in toluene at 0°C and its Fourier transform.

Table 4.4. Table showing the parameters obtained from the fitted QUEXAFS data (one scan, scan time= 2 minutes) of $Ni(acac)_2/AlEt_3$ (Ni:Al 1:5, [Ni]= 70mM) mixture in toluene at 0°C and its Fourier transform as shown in figure 4.14.

EF= 3.8(3), AFAC= 0.9, R= 24.4%.

Atom type	Coordination number	R/Å	$\sigma^2/Å^{-1}$
O	4.3 (1)	2.011 (4)	0.024 (1)
Ni	3.3 (1)	2.454 (3)	0.025 (1)

The parameters reveal that despite an original white line similar to that of the starting material the reaction had in fact proceeded to result in a mixture with some nickel particles in it. This is clear from the shell of nickel atoms at 2.454 Å. The data also fitted to a first shell of four oxygen atoms at 2.011 Å. Since the oxygen coordination of the starting material, $Ni(acac)_2$ is 6, it would seem that the mixture contained 4.3/6 = *ca.* 2/3 of the nickel as $Ni(acac)_2$ i.e. starting material. The solution had a nickel coordination of 3.3 nickel atoms. Since 2/3 of the nickel in the solution was present as $Ni(acac)_2$, therefore from the data in the above table, it would seem that the rest of the nickel present as nickel particles must have an average coordination number of 10.

The Ni-Ni distance of 2.454(3) Å obtained is smaller than the expected distance of 2.471(2) Å from the metal foil. As mentioned before, this is thought to be due to the reduction in repulsion interactions between non-bonded electron pairs in small clusters as compared to the metal foil or bulk metal because of the larger ratio of surface atoms in clusters. Also, the Debye Waller factor from this shell is larger (0.0245) as compared to the metal foil (0.010). This is explained as being due to the larger vibrational amplitude and surface relaxation possible in small clusters compared to the metal foil or bulk metal.

d) QUEXAFS spectra of the $Ni(acac)_2/AlEt_3$ (Ni:Al 1:5, [Ni]= 70mM) mixture in toluene at -16°C.

Figure 4.15 shows a comparision of ten consecutive spectra of the $Ni(acac)_2/AlEt_3$ (Ni:Al 1:5, [Ni]= 70mM) mixture in toluene at -16°C taken from the point of mixing the reagents in situ at -16°C upto 20 minutes after mixing. The results show that the reaction had not proceeded very far at these temperatures as the white line features of the spectra are very similar to that of $Ni(acac)_2$.

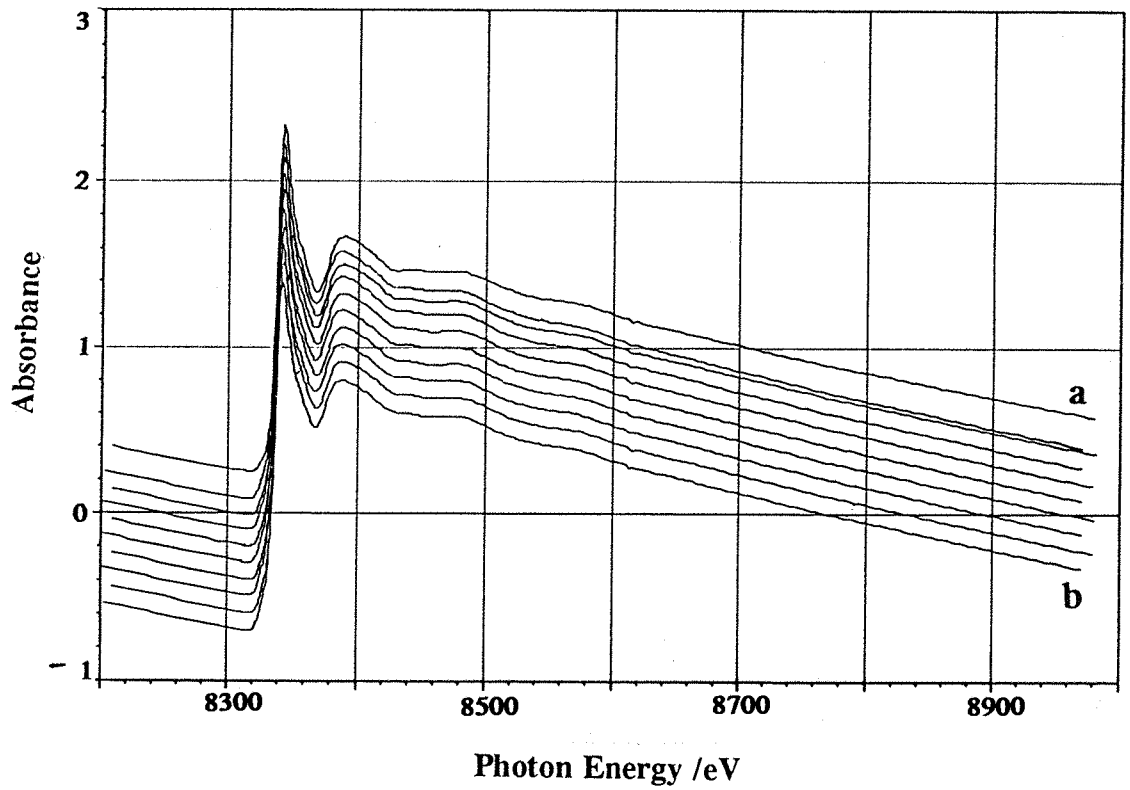

Figure 4.15. Figure showing a comparision of ten consecutive QUEXAFS spectra of $Ni(acac)_2/AlEt_3$ (Ni:Al 1:5, [Ni]= 70mM) mixture in toluene at -16°C taken from a) the point of mixing the reagents in situ at -16°C up to b) 20 minutes after mixing.

Although the white line features look very similar to that of the $Ni(acac)_2$ starting material it was still necessary to analyse the spectrum to find out if the reaction had proceeded at all. Figure 4.16 shows the fitted QUEXAFS spectrum and Fourier transform of $Ni(acac)_2/AlEt_3$ (Ni:Al 1:5, [Ni]= 70mM) mixture in toluene at -16°C taken at 20 minutes after mixing the reagents.

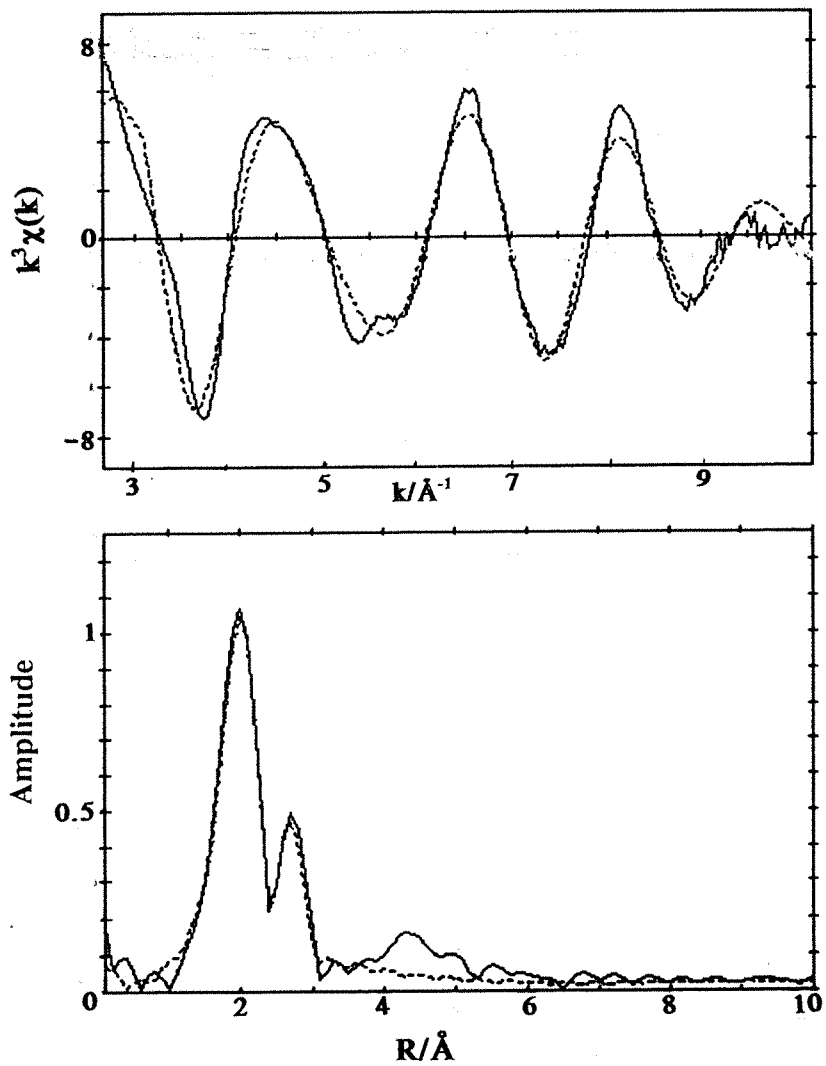

Figure 4.16. Figure showing the fitted QUEXAFS data and its Fourier transform of $Ni(acac)_2/AlEt_3$ (Ni:Al 1:5, [Ni]= 70mM) mixture in toluene at -16°C taken at 20 minutes after mixing the reagents.

Table 4.5. Table showing the fitted QUEXAFS spectrum and Fourier transform of $Ni(acac)_2/AlEt_3$ (Ni:Al 1:5, [Ni]= 70mM) mixture in toluene at -16°C taken at 20 minutes after mixing the reagents.

EF= 3.8 (3), AFAC= 0.9, R= 24.80%.

Atom Type	Coordination Number	R/Å	σ^2 /Å^{-1}
O	4.7(1)	2.010 (4)	0.0209 (9)
Ni	2.0 (0)	2.443 (4)	0.021 (1)

As with the previous mixture, the oxygen coordination of 4.7 atoms suggests that 4.7/6 i.e 78.3% of the nickel present in the mixture was in the form of the $Ni(acac)_2$ starting material. This is because a solution of the $Ni(acac)_2$ starting material would have an oxygen coordination shell of 6 atoms. The rest of the nickel in the solution must have existed as nickel metal clusters. From the nickel coordination of 2 nickel atoms at 2.443 Å, it would seem that the rest of the nickel (21.7%) existed as nickel particles with an average nickel coordination of 8. As expected from such small nickel clusters, there is a contracted Ni-Ni distance and larger Debye Waller factor than expected from the metal foil data shown in Table 4.1.

4.6 Ni-K-edge QUEXAFS spectra of $Ni(acac)_2/AlEt_3$ in the presence of hex-1-ene at varying temperatures:

a) Comparision of the raw spectra at varying temperatures:

Figure 4.17. shows a comparision of the white line features of the QUEXAFS spectra of the $Ni(acac)_2/AlEt_3$/hex-1-ene (Ni:Al:hex-1-ene

1:2.5:20, [Ni]= 70mM) mixture taken at varying temperatures (-16°C, 0°C).

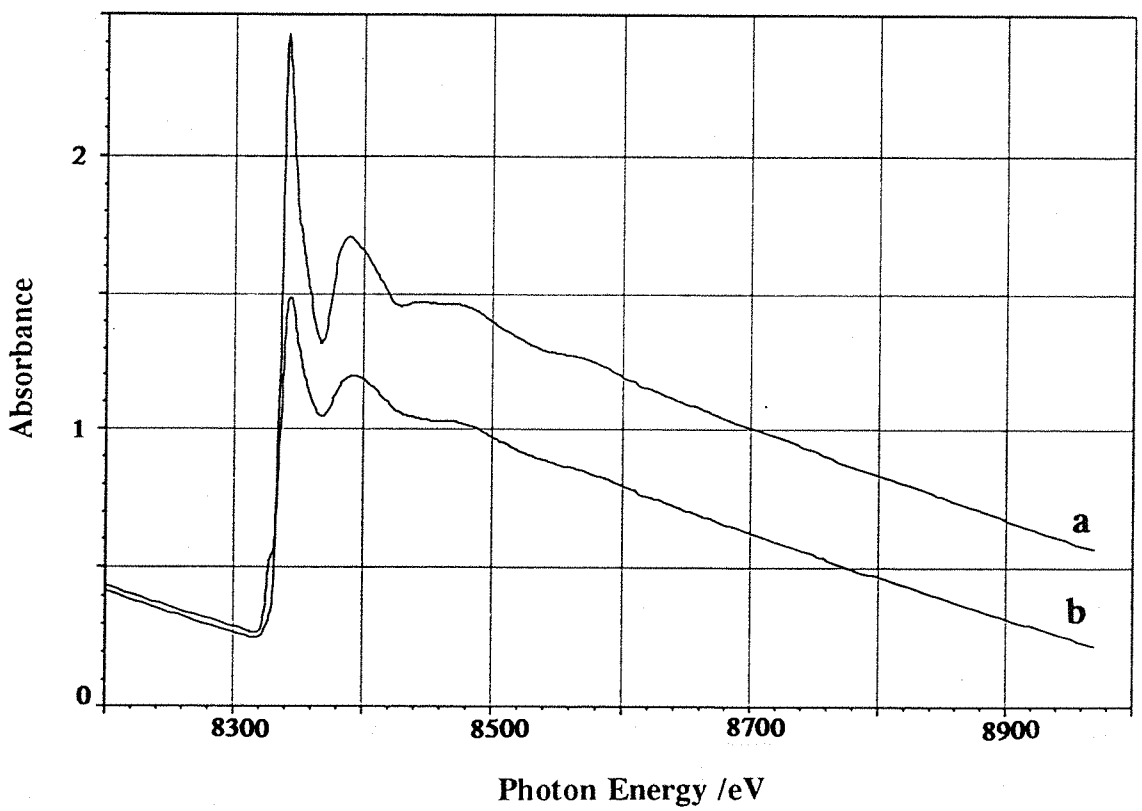

Figure 4.17. Figure showing a comparision of the Ni-K-edge QUEXAFS spectra of $Ni(acac)_2/AlEt_3$/hex-1-ene (Ni:Al:hex-1-ene 1:2.5:20, [Ni]= 70mM) at varying temperatures a) -16°C and b) 0°C.

b) Ni-K-edge QUEXAFS spectra of $Ni(acac)_2/AlEt_3$/hex-1-ene (Ni:Al:hex-1-ene 1:2.5:20, [Ni]= 70mM) at 0°C:

Figure 4.18 shows nine consecutive Ni-K-edge QUEXAFS spectra of $Ni(acac)_2/AlEt_3$/hex-1-ene (Ni:Al:hex-1-ene 1:2.5:20, [Ni]= 70mM) mixture at 0°C taken from the point of mixing the reagents in situ up to twenty minutes after

mixing the reagents. The white line features of the spectra of the mixture were different from that of the starting material, $Ni(acac)_2$. This shows that reaction had proceeded at these temperatures. In fact, the features (e.g. the shoulder on the edge) are very similar to those of an organometallic identified in a previous EXAFS study of a $Ni(acac)_2/AlEt_2(OEt)$/hex-1-ene mixture.[9,10]

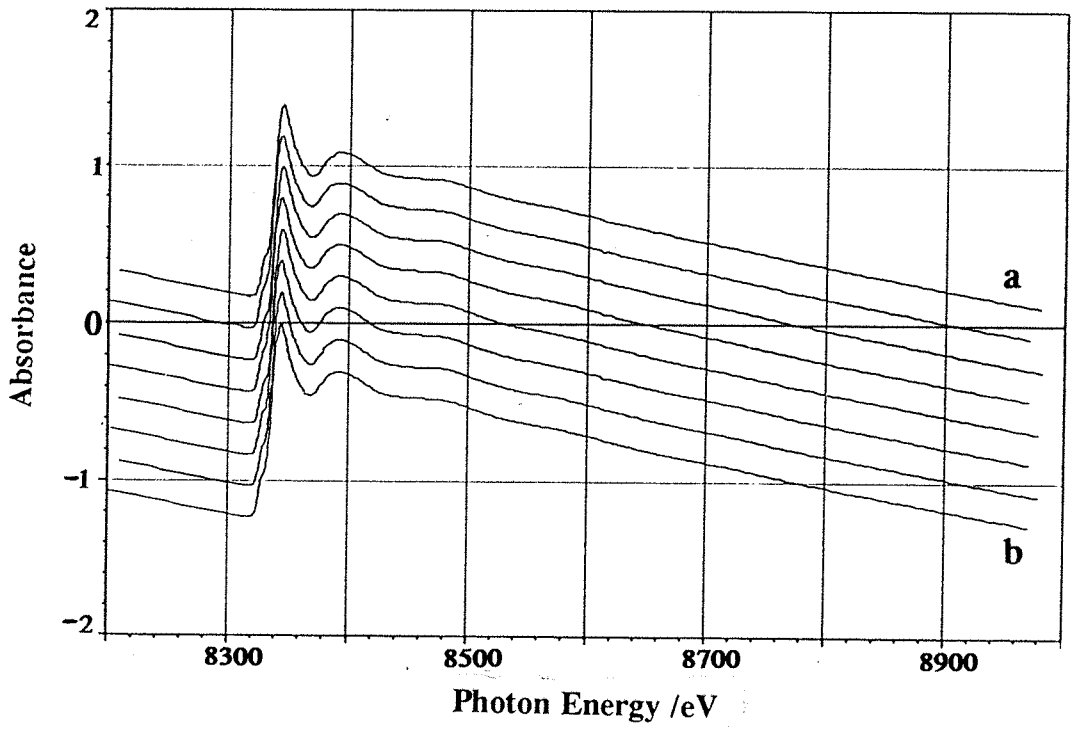

Figure 4.18. Figure showing a comparision of nine consecutive Ni-K-edge QUEXAFS spectra of $Ni(acac)_2/AlEt_3$/hex-1-ene (Ni:Al:hex-1-ene 1:2.5:20, [Ni]= 70mM) at 0°C taken from a) the point of mixing the reagents in situ up to b) twenty minutes after mixing the reagents.

Figure 4.19 shows the fitted Ni-K-edge QUEXAFS spectrum and Fourier transform of $Ni(acac)_2/AlEt_3$/hex-1-ene (Ni:Al:hex-1-ene 1:2.5:20, [Ni]= 70mM) mixture at 0°C. The spectrum is last one of the series shown in Figure 4.18.

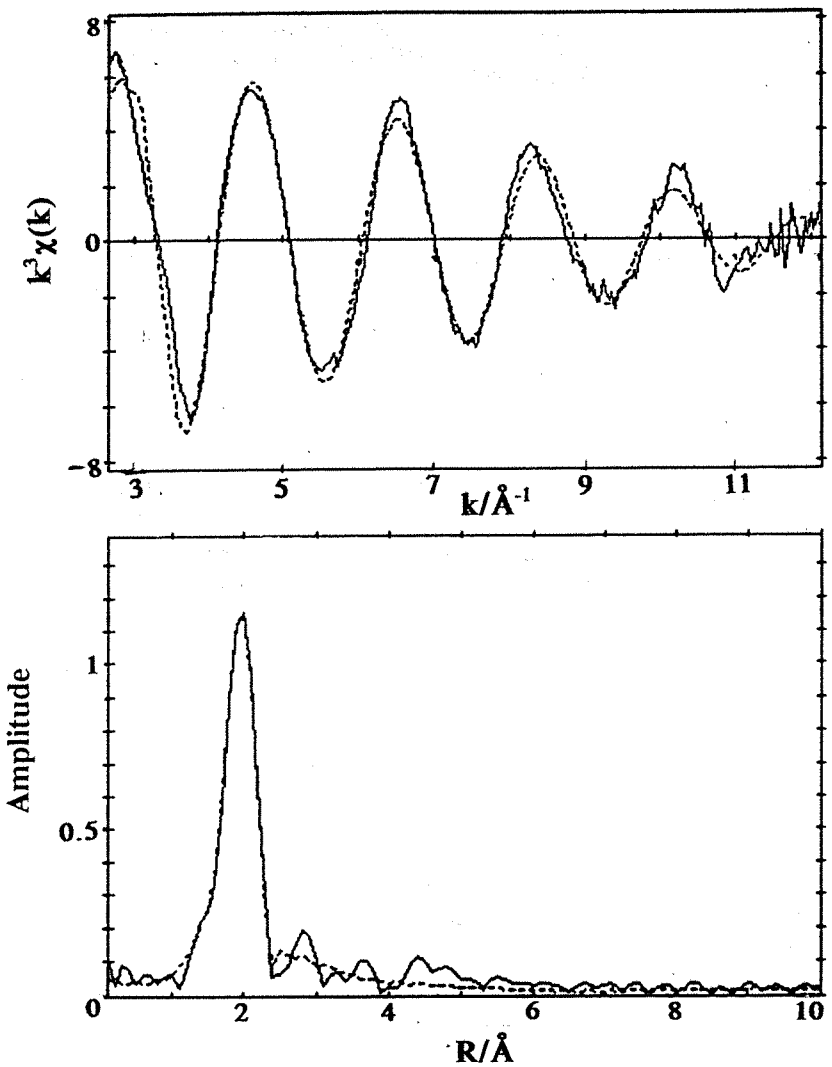

Figure 4.19. Figure showing the fitted Ni-K-edge QUEXAFS data (one scan, scan time= 2 minutes) of $Ni(acac)_2/AlEt_3$/hex-1-ene (Ni:Al:hex-1-ene 1:2.5:20, [Ni]= 70mM) at 0°C and its Fourier transform.

Table 4.6. Table showing the parameters obtained from the Ni-K-edge QUEXAFS spectrum (one scan, scan time= 2 minutes) of $Ni(acac)_2/AlEt_3$/hex-1-ene (Ni:Al:hex-1-ene 1:2.5:20, [Ni]= 70mM) at 0°C and its Fourier transform as shown in Figure 4.19.

EF= 3.7(2), AFAC= 0.9, R= 19.72%.

Atom type	Coordination number	R/Å	σ^2 /Å^{-1}
O	2.1(4)	1.943 (4)	0.006 (1)
C	2.6(5)	2.086 (5)	0.003 (1)

The parameters in the table show very clearly that there was no nickel coordination to the nickel atoms in the mixture. The coordination sphere consisted only of light atom shells. A single shell of four oxygen atoms gave a poorer R factor for the data, than a fit consisting of 2 oxygen atoms and 2 carbon atoms. The average structure of 2 oxygen atoms at 1.943 Å and 2.6 carbon atoms at 2.086 Å indicate the possibility of a structure as shown below:

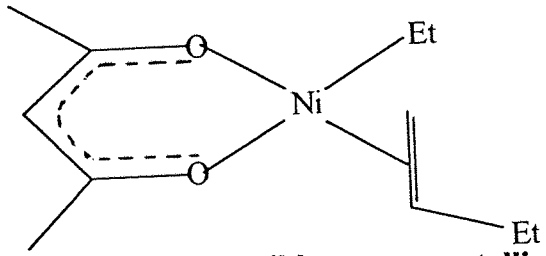

Figure 4.20. Figure showing a possible organometallic intermediate in the $Ni(acac)_2/AlEt_3$/hex-1-ene mixture at 0°C.

Such a structure has been indicated in previous EXAFS studies of such systems.[1] Previous papers on this catalyst system have suggested a catalytic intermediate with one acac group being retained by the nickel atom during catalysis.[16] Attempts to fit the shell at 2.9Å gave mainly negative Debye Waller factors. The methyl carbons of the acac group should be seen at this distance.

At -16°C, the reaction did not proceed at all and the QUEXAFS spectrum of the mixture fitted to the same parameters as the starting material i.e. $Ni(acac)_2$

c) Ni-K-edge QUEXAFS spectra of $Ni(acac)_2/AlEt_3$/hex-1-ene (Ni:Al:hex-1-ene 1:2.5:20, [Ni]= 70mM) mixture in toluene at room temperature (i.e. 20°C):

Figure 4.21 shows ten consecutive Ni-K-edge QUEXAFS spectra of the $Ni(acac)_2/AlEt_3$/hex-1-ene (Ni:Al:hex-1-ene 1:2.5:20, [Ni]= 70mM) mixture in toluene at room temperature (i.e. 20°C), taken from the point of mixing the reagents in situ up to twenty minutes after mixing. The figure shows quite clearly the change in the EXAFS as the reaction proceeded. As well as the EXAFS changing, the figure also shows that the edge height of the spectrum also drops.

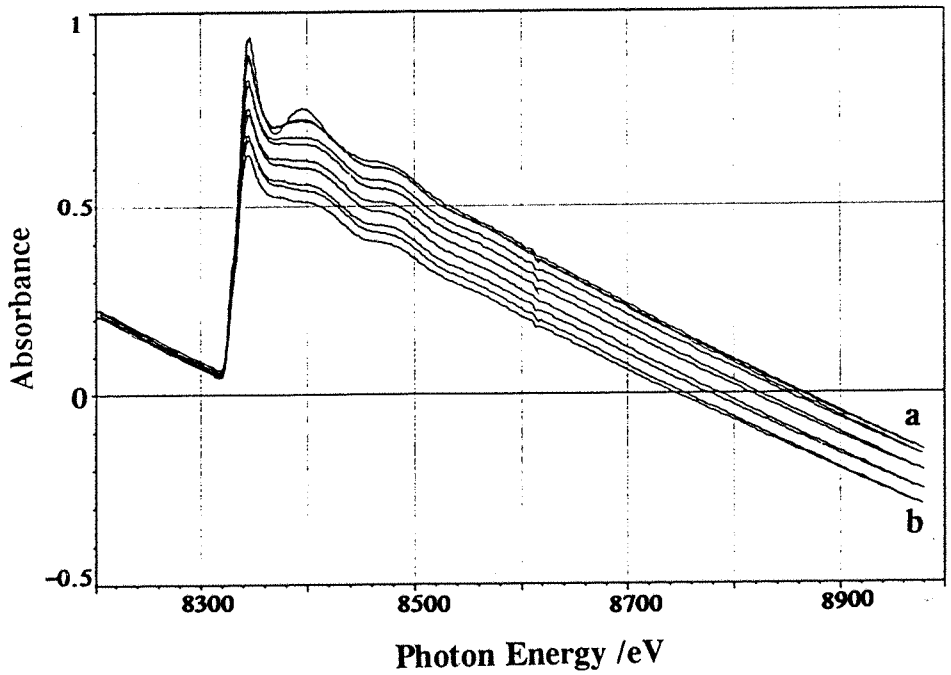

Figure 4.21. Figure showing a comparision between ten consecutive Ni-K-edge QUEXAFS spectra (scan duration= 2 minutes), of $Ni(acac)_2/AlEt_3$/hex-1-ene (Ni:Al:hex-1-ene 1:2.5:20, [Ni]= 70mM) mixture in toluene at room temperature (i.e. 20°C) taken from a) the point of mixing the reagents in situ up to b) 20 minutes after mixing.

Since the ten consecutive spectra showed numerous changes as the reaction proceeded, it was decided to analyse the first and last spectra after mixing to see the extent of the change in EXAFS. as the reaction proceeded at room temperature. Figure 4.22 shows the fitted QUEXAFS spectrum and Fourier transform of the first spectrum shown in figure 4.21 i.e the spectrum taken two minutes after mixing the reagents.

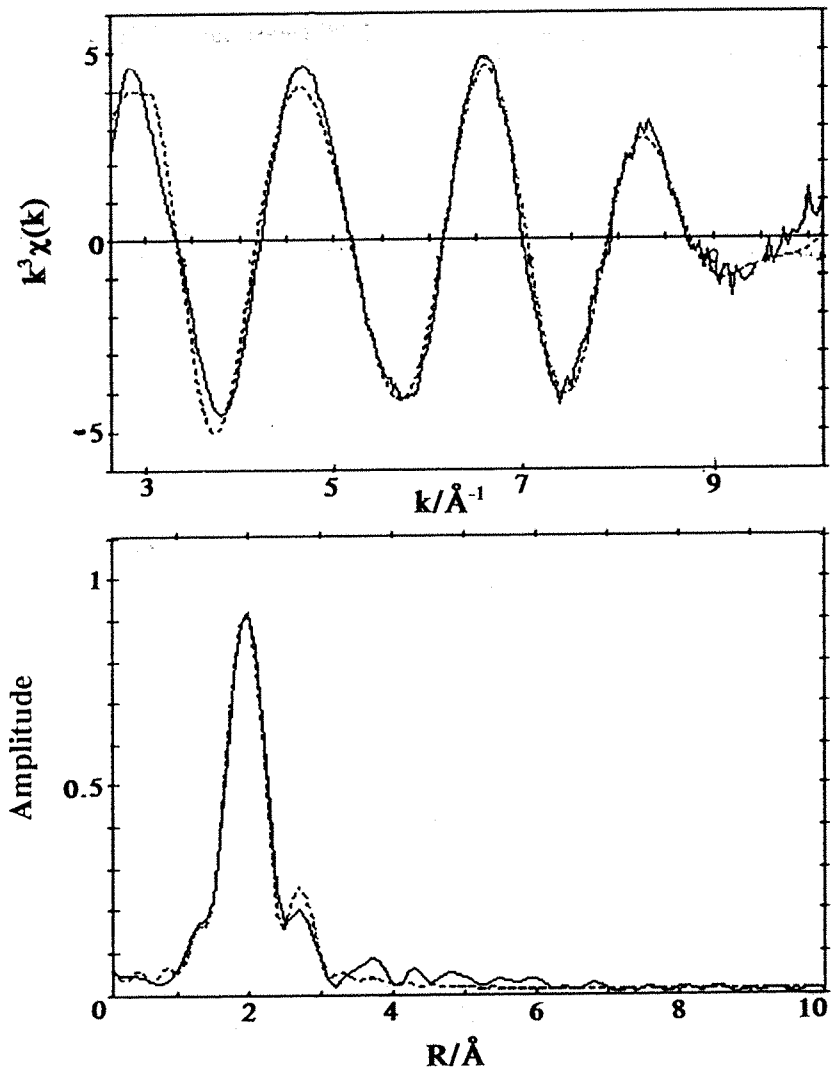

Figure 4.22. Figure showing the fitted Ni-K-edge QUEXAFS data (single scan, scan duration= 2 minutes) of $Ni(acac)_2/AlEt_3$/hex-1-ene (Ni:Al:hex-1-ene 1:2.5:20, [Ni]= 70mM) mixture in toluene at room temperature (i.e. 20°C) taken at t= 2 minutes after mixing the reagents.

Table 4.7. Table showing the parameters obtained from the fitted QUEXAFS data (single scan, scan duration=2 minutes) of $Ni(acac)_2/AlEt_3$/hex-1-ene (1:2.5:20, [Ni]= 70mM) mixture in toluene at room temperature, taken two minutes after mixing the reagents.

EF = 3.1(2), AFAC= 0.9, R= 15.8%.

Atom Type	Coordination number	R/Å	$\sigma^2/Å^{-1}$
O	2.85 (4)	1.965 (2)	0.0096 (4)
Ni	0.84 (4)	2.456 (2)	0.0138 (7)

The parameters in the Table 4.7 show that there was a nickel coordination sphere at 2.456 Å, once again indicating the formation of nickel metal particles. Thus, even in the presence of hex-1-ene, the solution did deteriorate at room temperature to give some nickel metal. From the data, it would seem that 2.85/6= 46% of the nickel was present as $Ni(acac)_2$, while the rest (54%) was present as nickel clusters with an average coordination number of 1.6 atoms.

The spectrum of the same mixture taken at 20 minutes after mixing was also analysed. Figure 4.23 shows the fitted EXAFS data and its Fourier transform. The table 4.8 shows the parameters obtained from the fitted data.

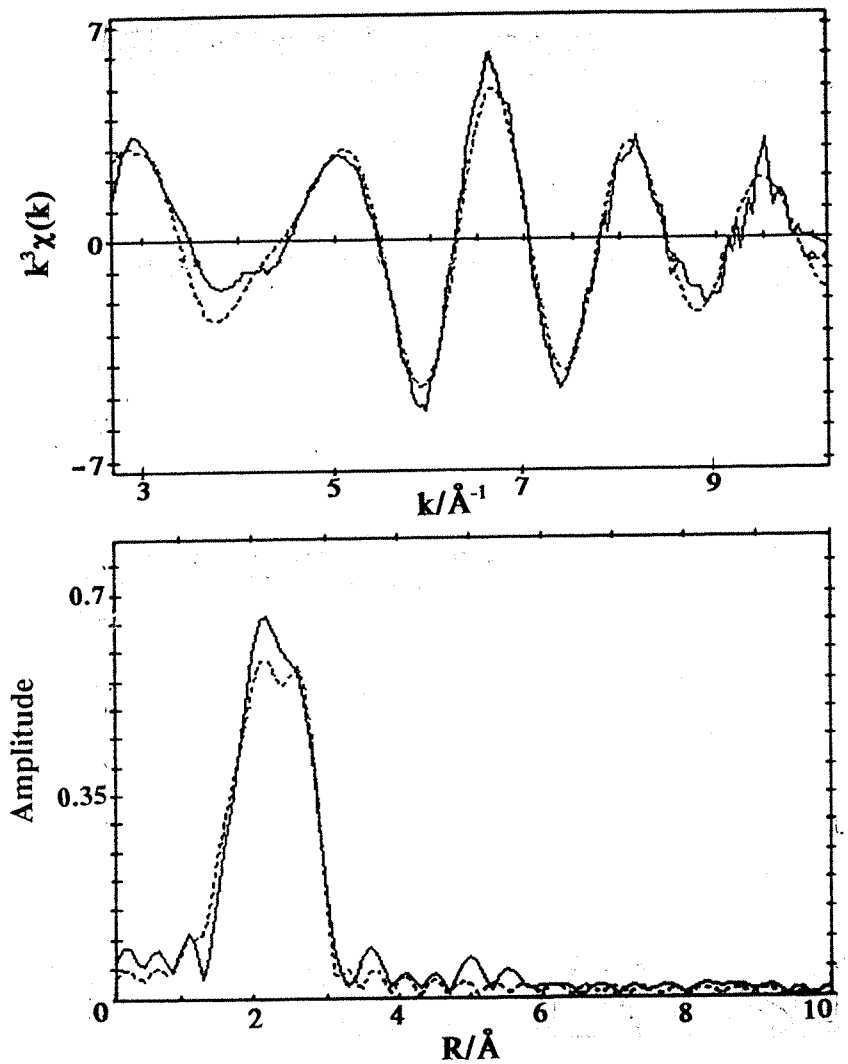

Figure 4.23. Figure showing the fitted Ni-K-edge QUEXAFS data (single scan, scan time= 2 minutes) of $Ni(acac)_2/AlEt_3$/hex-1-ene (1:2.5:20, [Ni]= 70mM) mixture in toluene at room temperature taken 20 minutes after mixing the reagents.

Table 4.7. Table showing the parameters obtained from the Ni-K-edge QUEXAFS data (single scan, scan duration= 2 minutes) of $Ni(acac)_2/AlEt_3$/ hex-1-ene (Ni:Al:hex-1-ene 1:2.5:20, [Ni]= 70mM) mixture in toluene at room temperature (i.e. 20°C) taken at t= 20 minutes after mixing the reagents as shown in figure 4.22.

EF= 3.8(5), AFAC= 0.9, R= 23.8%.

Atom Type	Coordination number	R/Å	σ^2 /Å^{-1}
O	1.98 (8)	1.925 (6)	0.024 (1)
Ni	3.26 (8)	2.447 (3)	0.0227 (4)

The data shows that the mixture contained some nickel species with Ni-O bonds and also some colloidal nickel as indicated by the coordination shell of 3 nickel atoms at 2.447 Å. From the oxygen coordination of 1.98 atoms it would seem that 1.98/6.1= 32% of the nickel was present as $Ni(acac)_2$, while the rest of the nickel (69%) was present as nickel metal clusters with an average coordination of 4.7 nickel atoms.

4.7 CONCLUSIONS:

The results show that at low temperatures (0°C) a mononuclear nickel organometallic species with 2 oxygen and 3 carbon bonds to the central nickel was present in the $Ni(acac)_2/AlEt_3$/hex-1-ene reaction mixture. A structure as shown on the next page is proposed.

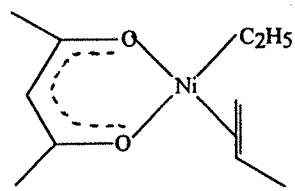

A similar species has been observed in mixtures of $Ni(acac)_2/AlEt_2(OEt)$/hex-1-ene at 0°C.[9,10] At room temperature, these reaction mixtures proceed further to give nickel metal.

In the absence of hex-1-ene, this reaction mixture resulted in the formation of nickel metal clusters. These clusters were formed from the starting material over the timescale of the QUEXAFS spectroscopy allowing some time resolution in the study of the process. Detailed EXAFS analysis indicated that the mean size of nickel particles in a reaction mixture of $Ni(acac)_2/AlEt_3$ (Ni:Al 1:5, [Ni]= 70mM) in toluene was 19 atoms. This result had to be interpreted with caution as it could mean the dominance of a 19 atom cluster or the presence of different sized clusters which averaged to 19 atoms. At lower temperatures, the reaction to give nickel metal particles proceeded to a lesser extent giving mixtures of nickel mononuclear species and also nickel metal particles.

It was also noted in all the spectra containing some nickel clusters that the nearest neighbour distance was consistently *ca.* 2.45 Å, which was less than the value expected from the metal foil (2.471 Å). Similar contractions of nearest neighbour distances were found in EXAFS studies of nickel metal vapour.[21] These contractions were considered as being due to the fact that in a cluster the total number of nearest neighbour atoms is significantly less than in bulk. This leads to a reduction in the repulsive interactions between non-bonded pairs. A contraction of nearest neighbour distances is therefore thought to be the result. The contraction in the nearest neighbour distances is thought to increase as the size of the cluster

decreases and could be seen in solvated nickel particles but to a lesser extent than in vapour phase.[21]

Electronic absorption spectroscopy data of $Ni(acac)_2/AlEt_3$ mixtures indicated that a species stable at room temperature (bands at 400nm and 500nm) was formed on the reaction between the $Ni(acac)_2$ and $AlEt_3$. Since the $AlEt_3$ is responsible for alkylating $Ni(acac)_2$, it was thought that this stable species observed at room temperature was a nickel alkyl species possibly stabilised by Ni-C-Al interactions as shown below.

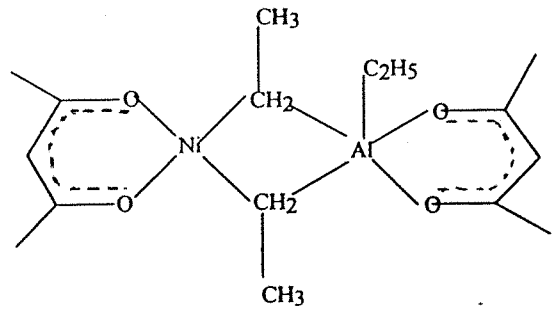

Such species have been indicated before in the reactions between nickel complexes and alkylaluminium reagents.[1,9]

The experiments performed using QUEXAFS and electronic absorption spectroscopy were not exactly the same as the concentrations of the nickel reagent required in each case was different.

The results overall show that the quality of data (up to 12k of data) obtained using QUEXAFS (scan duration= 2 minutes) spectroscopy was quite good and in some instances could provide some time resolution.

Recent theoretical studies of ethene oligomerisation by an organometallic nickel catalyst[28] have suggested that due to the mechanism of chain termination the actual catalyst is proposed as being $(acac)NiCH_2CH_3$ whereas (acac)NiH was proposed as the precursor or precatalyst. However, neither of these species have been identified using EXAFS spectroscopy as yet as they are very unstable in solution.

4.8. REFERENCES

1. K.Fischer, K.Jonas, P.Misbach, R.Stabba and G.Wilke, *Angew.Chem.Int.Ed.Engl.*, 1973, **12**, 943.
2. W.Keim, A.Behr, G.Kraus, *J.Organomet.Chem.*, 1983, **251**, 377.
3. P.W.Jolly and G.Wilke, The Organic Chemistry of Nickel., Vol 1, Academic Press, New York, 1975.
4. P.W.Jolly and G.Wilke, The Organic Chemistry of Nickel., Vol 2, Academic Press, New York, 1975.
5. B.Bogdanovic, B.Henc, A.Lösler, B.Meister, H.Pauling and G.Wilke, *Angew.Chem.Int.Ed.Engl.*, 1973, **12**, 954.
6. J.J.Eisch and M.W.Foxton, *J.Organomet.Chem.*, 1968, **12**, 33.
7. L.Lardicci, G.P.Giacomelli, P.Salvadori and P.Pino, *J.Am.Chem.Soc.*, 1971, **93**, 5794.
8. "Comprehensive Inorganic Chemistry"., Eds. J.C.Bailar, H.J.Emeleus, R.Nyholm, A.F.Trotman-Dickenson, Pergamon Press, 1973., Vol 1, Chapter 12.
9. J.M.Corker and J.Evans, *J.Chem.Soc.Chem.Comm.*, 1991, 1104.
10. J.M.Corker, PhD Thesis, Southampton University, 1991.
11. R.Frahm and J.Wong, *Jpn.J.Appl.Phys.*, 1993, **32**, 188.
12. B.R.Dobson, S.S.Hasnain, M.Neu, C.A.Ramsdale and L.M.Murphy, *Jpn.J.Appl.Phys.*, 1993, **32**, 192.
13. G.Maki, *J.Chem.Phys.*, 1958, **29**, 162.
14. "Comprehensive Inorganic Chemistry", Eds. J.C.Bailar, H.J.Emeleus, R.Nyholm, A.F.Trotman-Dickenson, Pergamon Press, 1973, Vol 3, Chapter 42.
15. A.B.P.Lever, "Inorganic Electronic Spectroscopy", Elsevier, 1968.
16. J.R.Jones and T.J.Symes, *J.Chem.Soc,C.*, 1971, 1124.
17. J.Goulon, E.Georges, C.Goulon-Ginet, Y.Chauvin, D.Commereuc, H.Dexpert and E.Freund, *Chem.Phys.*, 1984, **83**, 357.

18. S.C.Davis and K.J.Klabunde, *J.Am.Chem.Soc.*, 1978, **100,** 5974.

19. K.J.Klabunde, H.F.Efner, T.O.Murdoch and R.Ropple, *J.Am.Chem. Soc.*, 1976, **98,** 1022.

20. B.A.Scott, R.M.Plecenik, G.S.Cargill III, T.R.McGuire and S.R.Herd, *Inorg.Chem.*, 1980, **19,** 1252.

21. G.Apai, J.F.Hamilton, J.Stohr, and A.Thompson, *Phys.Rev.Lett.*, 1979, **43,** 165.

22. G.H.Via, J.H.Sinfelt and F.W.Lytle, *J.Chem.Phys.*, 1979, **71,** 690.

23. P.A.Montano, G.K.Shenoy, E.E.Alp, W.Schulze and J.Urban, *Phys.Rev.Lett.*, 1976, **56,** 2076.

24. J.H.A.Martens, R.Prins and D.C.Koningsberger, *J.Phys.Chem.*, 1989, **93,** 3179.

25. M.Boudart and D.J.Sajkowski, *Faraday Discuss.*, 1991, **92.**

26. W.Niemann, B.S.Claussen and H.Topsoe, in Physics and Chemistry of Small Clusters, *ed.* P.Jena, B.K.Rao and S.N.Khanna, Plenum Press, New York, 1987, 909.

27. R.E.Benfield, J.Chem.Soc, *Faraday Trans.*, 1992, **88,** 1107.

28. L.Fan, A.Krzywicki, A.Somogyvary and T.Ziegler, *Inorg.Chem.*, 1996, **35,** 4003.

29. D.Richard, J.W.Couves and J.M.Thomas, *Faraday. Discuss.*, 1991, **92,** 109.

30. N.Binsted, M.J.Pack, M.T.Weller and J.Evans, *J.Am.Chem.Soc.*, 1996, **118,** 10200.

31. G.Wilke, *Angew.Chem.Int.Ed.Engl.*, 1963, **2,** 105.

CHAPTER 5. ELECTRONIC ABSORPTION AND EDEXAFS SPECTROSCOPIC STUDIES OF $Ni(acac)_2/AlEt_2(OEt)$ CATALYST MIXTURES.

5.1 Introduction:

This chapter is concerned with a study of mixtures of $Ni(acac)_2/AlEt_2(OEt)$ in the presence and absence of olefin i.e. hex-1-ene, where the $Ni(acac)_2$ is the catalyst and the $AlEt_2(OEt)$ is the cocatalyst. Such catalysts are known to catalyse the oligomerisation reaction.[1-3] As with most of such mixtures, at room temperature, the $Ni(acac)_2$ is alkylated by the aluminium cocatalyst and is further reduced to nickel metal possibly by homolytic cleavage and coupling of bonded alkyl groups.[1-3] It is expected that at low temperatures and in the presence of hex-1-ene, the alkylated species are stabilised by the olefin molecule to give an organometallic intermediate which is stable enough at room temperature to be studied using EXAFS spectroscopy.[4,5] Figure 5.1 shows such an organometallic intermediate.

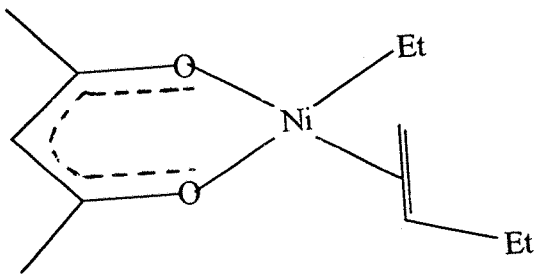

Figure 5.1. Figure showing an organometallic intermediate possibly formed in mixtures of $Ni(acac)_2/AlEt_2(OEt)$/hex-1-ene at 0°C.[4]

Studies by Jones and Symes[6] on the activity of this system (5mM of Ni complex-$AlEt_2(OEt)$ for propene dimerisation (at 40°C and 600 lb/sq in) and using toluene solvent have shown that the overall productivity g/g $Ni(acac)_2$ was 226. The initial activity g product/g $Ni(acac)_2$ equivalent/hr was 6.8. The major products were linear hexenes (78%).

The products expected from hex-1-ene dimerisation by this catalyst are dodecene (dimer 85%) and octadecene (trimer 10%). Overall productivity (g product/g $Ni(acac)_2$) was found to be 130. Activity (g product/g $Ni(acac)_2$/hr) for hex-1-ene dimerisation was found to be 5.2.

Keim *et al.*[7] studied the oligomerisation of 1-butene using 44 diketone and tetraketone ligands. In all cases, the formation of predominantly (>80%) linear dimers was favoured. The acidity of the diketone was the dominant influence on the properties of the catalyst and an almost linear correlation between pK_a and activity was observed.

The effect of solvent on the activity of this catalyst system for propene dimerisation showed that the highest activity was obtained using toluene solvent. Ether solvents gave slightly poorer results than toluene and coordinating solvents like N-methylpyrrolidone, carbon disulphide and dimethyl sulphoxide gave much poorer activities or none at all. Comparative kinetic experiments with hex-1-ene showed that the initial rate of dimerisation was faster in diglyme than in toluene but subsequent exponential loss of activity over a period of time was faster using diglyme than toluene with the result that the overall activity of both solvents was similar.

Jones and Symes[6] also studied the effect of the aluminium:nickel ratio on the activity of the system. It was found that the optimum molar ratio for hex-1-ene dimerisation by $Ni(acac)_2/AlEt_2(OEt)$ was 1:1. Further information of the effect of the Al:Ni ratio was found by IR observation of the absorbance frequency of 125mM solutions of $Ni(acac)_2$ at 1261 cm^{-1} when $AlEt_2(OEt)$ was added at concentrations of 0mM to 250mM. The reaction was observed at intervals for nearly 0.5 hr until the precipitation of nickel metal began to affect the absorbances. The graph showing the change in activity over a period of time and with Al:Ni ratio is shown in Figure 5.2.

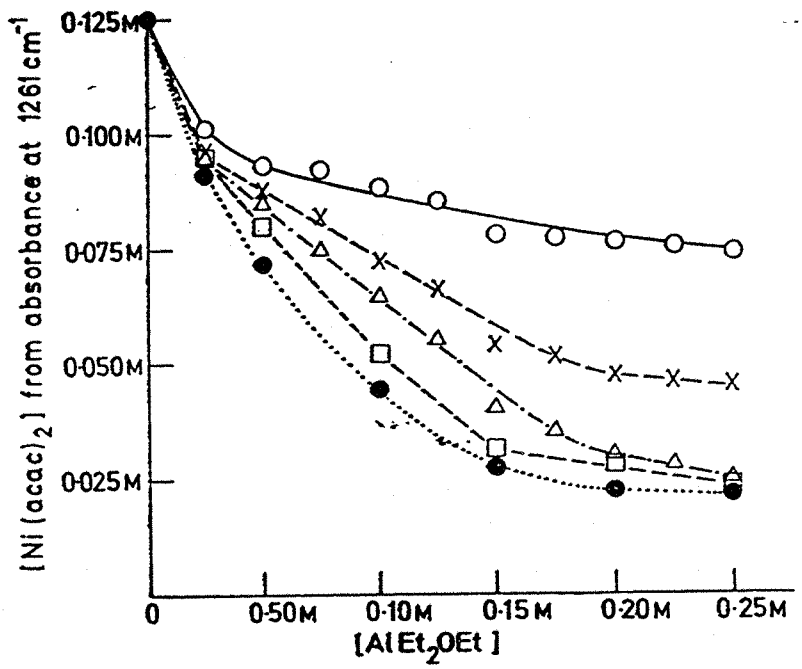

○ = 2 min, × = 6 min, △ = 10 min, □ = 16 min, ● = 24 min

Figure 5.2. Figure showing the change in absorbance of $Ni(acac)_2$ at 1261cm^{-1} over a period of time and with increasing Al:Ni ratio.[6]

Other interesting results[6] found were that there was absence of any ethane gas evolution during the catalysis using the $AlEt_2(OEt)$ suggesting that the ethyl groups are retained within the catalytic species. The IR investigation showed that complete exchange of alkyl groups with acetylacetonate ligands was not occurring at the point where the activity was the highest. In fact, the results at low Al:Ni ratios corresponded to the removal of only one of the chelating acac groups leaving the other one present during catalysis. The precise function of the acac group in catalysis was unclear, but the variation in performance between nickel complexes of various β-diketones confirmed that the ligand was actively involved in the catalytic species. It was thought that this involvement took the form of inductive and steric

effects. The IR study of this system also reported the formation of aluminium acetylacetonate (peak at 1288 cm^{-1}) in the reaction mixture.

5.2 Aims of this chapter:

The main objectives of this section were:

a) to study the reaction mixtures in the presence and absence of hex-1-ene using electronic absorption spectroscopy, in order to obtain information on any stable catalytic intermediates that may be formed.

b) To study the catalyst mixtures using EDE spectroscopy in order to follow any changes in the coordination sphere of the nickel atom e.g. loss of oxygen coordination from the starting material with consequent gain of carbon (formation of organometallic) or nickel coordination (formation of colloidal nickel which is thought to have a role in catalysis as a microheterogeneous catalyst).

c) To obtain some evidence for the rates of the reaction using EDE spectroscopy.

5.3 Electronic absorption spectroscopy studies of $Ni(acac)_2/AlEt_2(OEt)$ mixtures in the presence and absence of hex-1-ene:

a) Electronic absorption spectrum of the $Ni(acac)_2$, starting material:

An electronic absorption spectrum of $Ni(acac)_2$ (10mM in toluene) was presented in section 4.3. The spectrum shows clearly 2 bands in the visible and near IR region of the spectrum. These are at 655nm and 1135 nm, respectively. A detailed analysis of the spectrum[10] based on the octahedral coordination around the nickel atoms showed that the peak at 1135 nm (ε= 4 l mol^{-1} cm^{-1}) caused by a $^3A_{2g}$ to $^3T_{2g}$ transition and the peak at 655 nm (ε= 5 l mol^{-1} cm^{-1}) caused by a $^3A_{2g}$ to $3T_{ig}$ transition.

b) Electronic absorption spectra of $Ni(acac)_2/AlEt_2(OEt)$ catalyst mixture in the absence of hex-1-ene:

Electronic absorption spectra of a mixture of $Ni(acac)_2/AlEt_2(OEt)$ (Ni:Al 1:2, [Ni]= 8mM) were obtained at room temperature, in a spectrometer cell adapted for air-sensitive transfer of solutions (See appendix). The spectra were obtained at intervals from 0.5 minutes after mixing up to 20 minutes after mixing. The results are shown in Figure 5.3.

The results in the absence of hex-1-ene as shown in Figure 5.3, show the appearance of two new bands at 400 nm (ε= 100 l $mol^{-1}cm^{-1}$) and 500nm (ε= 200 l $mol^{-1}cm^{-1}$) as the reaction proceeds. There are no new bands above 800 nm. The lack of any bands at wavelengths> 1000nm indicates that this species was more likely to be a square planar species than an octahedral or tetrahedral species.[11,12] Square planar species usually exhibit bands (ε= 50-500 l $mol^{-1}cm^{-1}$) at 430-670 nm and 370-430 nm.

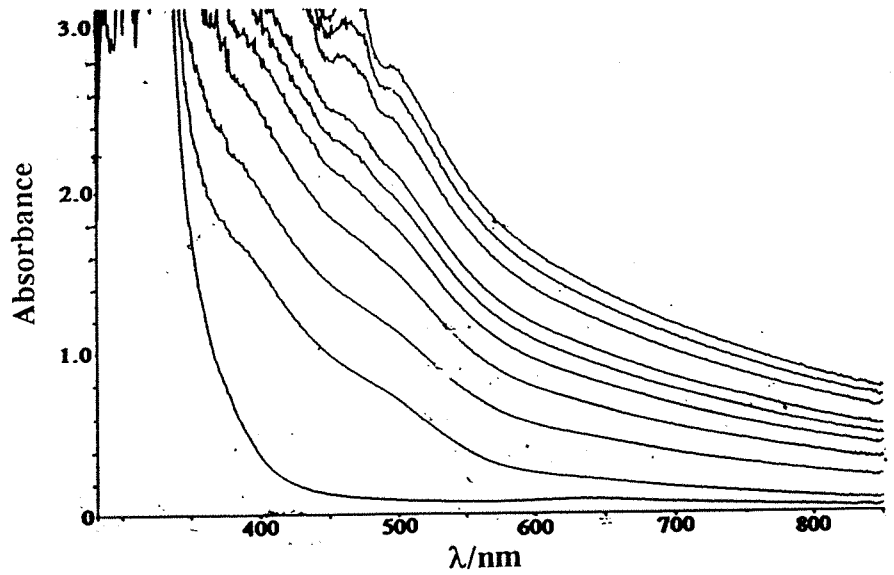

Figure 5.3. Figure showing the electronic absorption spectra of $Ni(acac)_2/AlEt_2(OEt)$ (Ni:Al 1:2, [Ni]= 8mM) at room temperature. The first spectrum was taken at 0.5 minutes after mixing and subsequent spectra were taken at 4 minute intervals after the first one.

The reaction involves alkylation and the resulting nickel alkyls are unlikely to be stable at room temperature. Similar changes in the electronic absorption spectrum were observed on using $AlEt_3$ co-catalyst (see chapter 4). As in that case, previous studies have shown that the reaction between the $Ni(acac)_2$ and $AlEt_2(OEt)$ should result in alkylation of the nickel centre with loss of one of the acac groups[2]. However, it is unlikely that such a mono-alkyl species could be stable enough to be observed at room temperature without any other stabilising ligands.

Therefore, as in the case of the reaction with $AlEt_3$, an alkyl species stabilised by Ni-C-Al interactions is proposed as shown in figure 5.4.

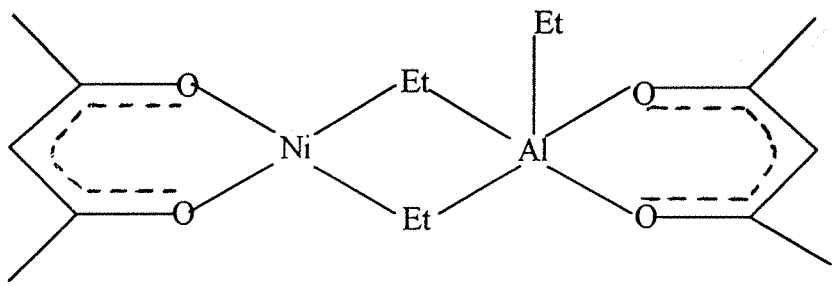

Figure 5.4. Figure showing a possible catalytic species observable in a mixture of $Ni(acac)_2/AlEt_2(OEt)$ (Ni:Al 1:2, [Ni]= 10mM) at room temperature.

Such a species shows good potential as a catalyst as it allows numerous sites for olefin coordination as it is square planar and therefore coordinatively unsaturated. The presence of both nickel and aluminium in such a species could explain why nickel is thought to restrict polymerisation by aluminium to oligomerisation (i.e. the nickel effect)[1,3,4,5] or even why the presence of both nickel and aluminium results in much higher catalytic activity for oligomerisation than either component on its own. Such structures involving multicenterbonding systems involving the alkylaluminium and the nickel complex have been proposed before.[4,5] EXAFS evidence for the occurrence of such Ni-C-Al interactions has been provided before by Corker and Evans[5] in the case of nickel halogenophosphine complexes and triethyaluminium.

c) Electronic absorption spectra of $Ni(acac)_2/AlEt_2(OEt)$/hex-1-ene i.e catalyst mixture <u>in the presence of hex-1-ene:</u>

Electronic absorption spectra of a mixture of $Ni(acac)_2/AlEt_2(OEt)$/hex-1-ene (Ni:Al:hex-1-ene 1:2:20, [Ni]= 8mM) were obtained at room temperature using a spectrometer cell adapted for air sensitive transfer of solutions. The spectra were once again obtained at intervals from 0.5 minutes up to 20 minutes after mixing. The results are shown Figure 5.5.

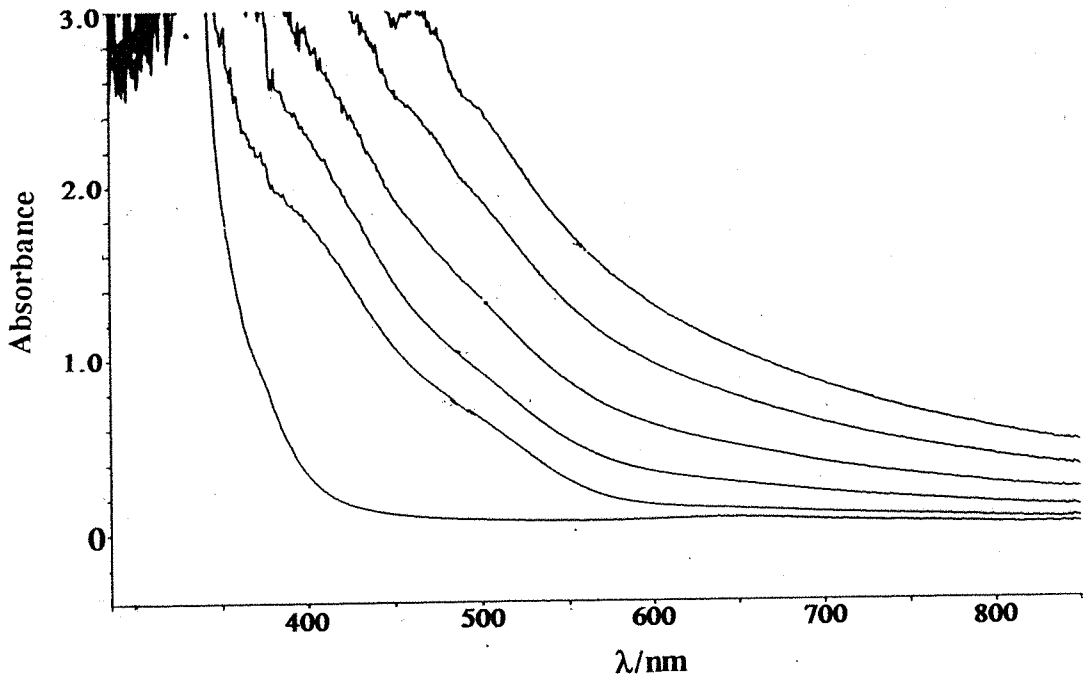

Figure 5.5. Figure showing the electronic absorption spectra of $Ni(acac)_2/AlEt_2(OEt)$/ /hex-1-ene (Ni:Al 1:2, [Ni]= 8mM) at room temperature. The first spectrum was in both figures was taken at 0.5 minutes and subsequent spectra at 4 minute intervals.

The spectra, once again, showed the appearance of two new peaks at 400 nm (ε= 100 l $mol^{-1}cm^{-1}$) and 500 nm (ε= 200 l $mol^{-1}cm^{-1}$). By the same reasoning as before a structure containing Ni-C-Al bridges can be proposed as shown in Figure 5.4. The spectra show that this structure was retained, even in the presence of olefin, suggesting that the structure with bands at 400 nm and 500 nm, may be part of the catalytic process. The spectrum at t= 0 minutes shows the starting material, $Ni(acac)_2$ spectrum (10mM in toluene) for comparision.

d) Electronic absorption spectra in time-drive following the progress of the reaction:

It is clear that as the alkylation reaction proceeded, the spectrum of the starting material, $Ni(acac)_2$, changed to give rise to the new peaks at 400nm and 500 nm showing a possible change from the octahedral symmetry of $Ni(acac)_2$ to a square planar product. Additionally, colloidal nickel particles may also have formed in the reaction mixture in the absence and presence of hex-1-ene. Colloidal nickel particles give rise to a large background absorbance.

It was therefore expected that as the reaction proceeded to give the product, the two bands from the octahedral starting material i.e. $Ni(acac)_2$, at 1160nm and 650nm would show a drop in absorbance. An attempt was made to follow this drop in the time-drive mode of the spectrometer using a mixture of $Ni(acac)_2$/ /$AlEt_2(OEt)$/hex-1-ene (Ni:Al:hex-1-ene 1:2:20, [Ni]= 70mM). The results are shown in Figure 5.6 a and b. That there is an initial drop in absorbance at both the wavelengths is clear from the figures. However, in both cases, the background absorbance caused by the formation of nickel metal particles in the mixture begins to overlap with the drops in absorbance resulting in stagnation of the drop followed by an increase in absorbance, as the background absorbance increases.

The gradient of the drop in absorbance could provide some idea of the initial rate of reaction however it is difficult to say at which stage this drop in absorbance begins to be affected by the increase in background absorbance.

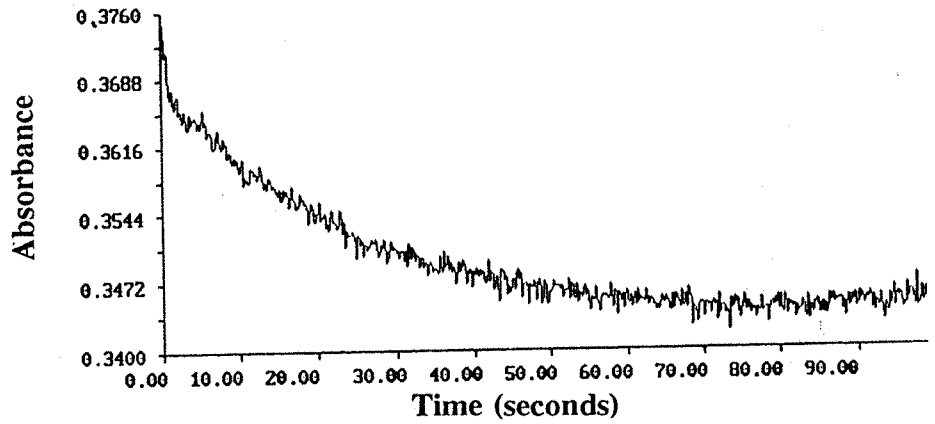

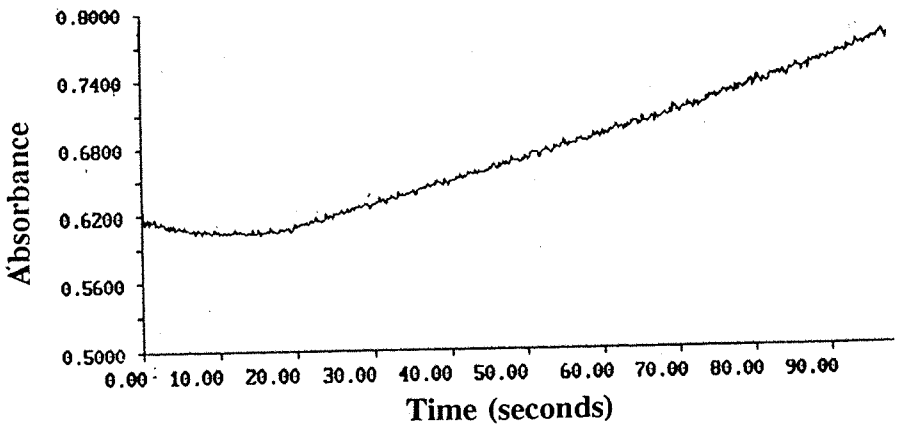

Figure 5.6. Figure showing the time drive electronic absorption spectra of $Ni(acac)_2/AlEt_2(OEt)$/hex-1-ene (Ni:Al:hex-1-ene 1:2:20, [Ni]= 70mM) mixture at a) 1160nm b) 650nm.

5.4 Time resolved second scale Energy Dispersive EXAFS[13-17] studies of the $Ni(acac)_2/AlEt_2(OEt)$/hex-1-ene at room temperature:

This section is concerned with a time resolved EDE study of the reaction between $Ni(acac)_2/AlEt_2(OEt)$/hex-1-ene at room temperature. An EXAFS spectum of the starting material, $Ni(acac)_2$ (70mM in toluene) is shown below in Figure 5.7.

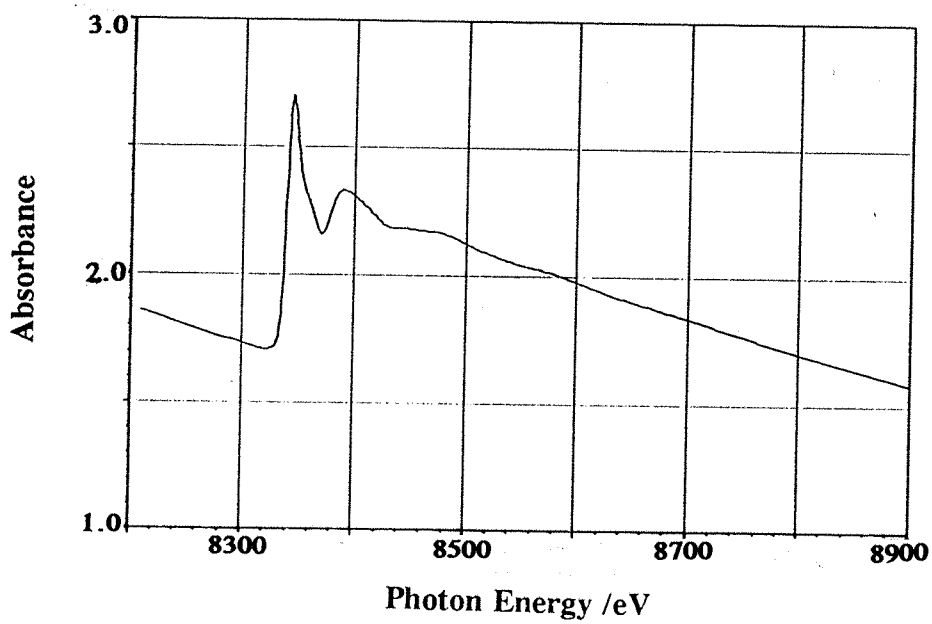

Figure 5.7. Figure showing the QUEXAFS spectrum of $Ni(acac)_2$ (70mM in toluene).

It can clearly be seen that the XANES region of the $Ni(acac)_2$ spectrum shows a high intensity peak at the position of the edge. As the concentration of the octahedral starting material i.e. $Ni(acac)_2$, in a reaction mixture decreased, it was expected that there would be a drop in the apparent edge height of the EXAFS as the square planar organometallic product (see Figure 5.9) would not have the same edge peak.

Equipment used for time resolved EDE spectroscopy: These EDE experiments were carried out at the ESRF (ID 24) at Grenoble. A rectangular shaped Si(111) Bragg monochromator was used for dispersion of the beam and subsequent focussing at the sample. The monochromator was cooled in a

gallium/indium bath. the detector consisted of a Thomson charged couple device camera. It had 1242 pixels. The other details of the EDE spectroscopy are as given in Section 2.4.2.c.

In order to perform a time resolved study of the reaction in the catalyst mixture, $Ni(acac)_2/AlEt_2(OEt)$/hex-1-ene (Ni;Al:hex-1-ene 1:4:12, [Ni]= 70mM) at the ESRF at Grenoble using high resolution EDE spectroscopy, specialised stopped-flow equipment was used, as detailed in Section 2.4.3 c along with a photograph of the equipment. The equipment involved two reagent syringes which pumped reagent solutions into a mixing chamber from where the freshly mixed solution was passed directly in to a 20μl stainless steel observation cell, with a 1cm path length enclosed on either side by kapton windows. (The numbers given in the brackets can be identified on the photograph). At the start of the next reaction, the used solution was emptied into a waste syringe before new reagent solutions were pumped in again for observation. The stopped-flow system was connected to a control box placed outside the X-ray hutch. The start button on the controller for the stopflow system was electronically connected to the point of acquisition of the EXAFS data such that the acquisition began at the same time as the mixing of the reagents was stopped. Further details of the stopflow system are given in Section 2.4.3.c of this thesis.

A photograph of the equipment as set up in the station ID24 of the ESRF at Grenoble is shown in Figure 5.8. As can be seen from the picture the main bulk of the equipment i.e. syringes and syringe driver- (1), was placed below the path of the evacuated beam pipe- (2). The actual observation cell- (3), was placed in the path of the beam. The syringe driver was connected to the observation cell via steel tubing-(4). The hemispherical grey area (containing a beryllium window-(5)) on the right of the picture hides the monochromator hutch. The spacially dispersed X-ray beam emerges from this hutch through the beryllium window, passes through the observation cell, and then passes through the evacuated beam pipe- (2), to reach the EDE detector- (6). The purpose of the steel tubing was to lessen the loss of photon energy by interaction with air.

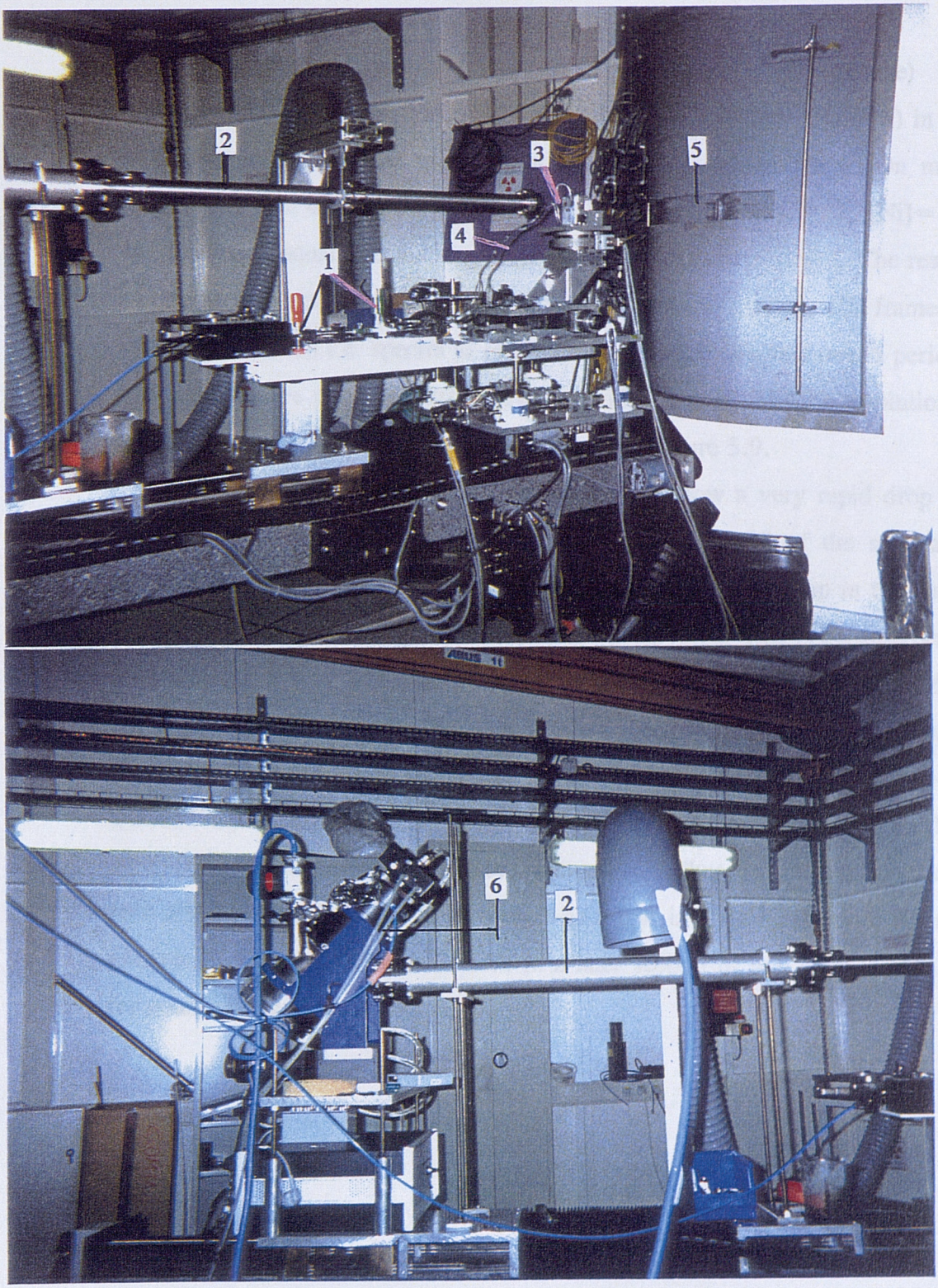

Figure 5.8. The experimental set-up at the ESRF, Grenoble, a) Figure showing the path the emerging beam takes after leaving the monochromator. b) the path the beam takes after passing through the observation cell to the EDE detector.

Two reagent solutions i) $Ni(acac)_2$ (140mM in toluene) and ii) $AlEt_2(OEt)$/hex-1-ene mixture ([Al]= 560mM, [hex-1-ene]= 1668mM) in toluene, were used in each of the two reagent syringes of the equipment. On mixing, a reagent solution with initial composition (Ni:Al:hex-1-ene 1:4:12, [Ni]= 70mM) was formed as equal injection rates were used for both the syringes. The reaction on mixing the two reagents was observed from the point of mixing. 100 frames (frame time= 13 seconds) i.e. spectra of reagent mixture were obtained over a period of 24 minutes from the point of mixing. This provided substantial time resolution of the reaction as can be seen from the results shown in Figure 5.9.

The series of spectra shown in Figure 5.9 show a very rapid drop in edge height along with other less clear changes in the EXAFS of the spectra as the reaction proceeded. The drop in edge height is related to the drop in the amount of starting material i.e. $Ni(acac)_2$ as the reaction progressed. This is because octahedral $Ni(acac)_2$ has a very large absorbance in the XANES region which coincides with the edge. The resulting square planar product species are not expected to have this characteristic feature of the $Ni(acac)_2$ spectrum based on previous studies of this system[4,5] and also the organometallic product formed when using $AlEt_3$ as the alkyl aluminium reagent in this thesis (see Figure 4.18). Thus, as the reaction proceeded with alkylation of the $Ni(acac)_2$, there was a loss in edge height over the first six minutes of the study. This will serve in a later section of this chapter as a marker for measuring the rate of this reaction.

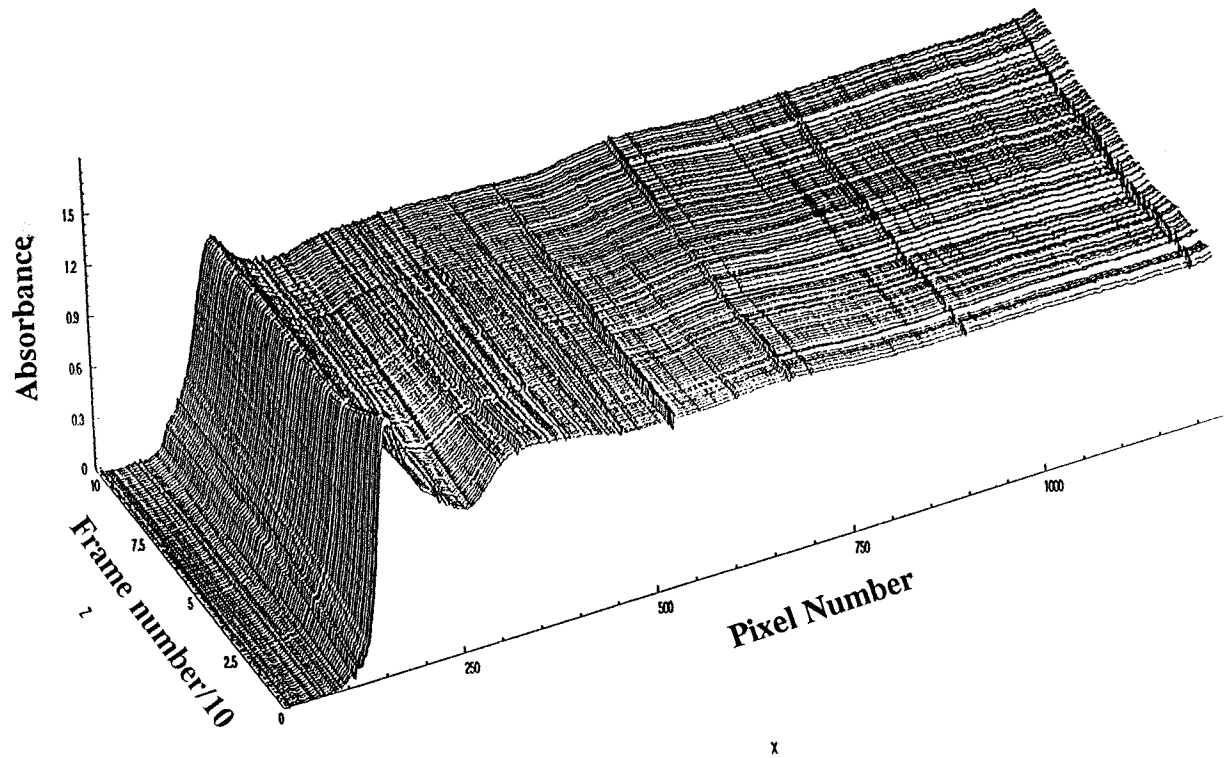

Figure 5.9. Figure showing the time resolved Ni-K-edge X-ray absorption spectra (100 frames, frame time= 13 seconds), following the reaction of $Ni(acac)_2/AlEt_2(OEt)$/hex-1-ene ([Ni]= 70mM, Ni:Al:hex-1-ene 1:4:12) mixture in toluene, at room temperature, starting from the point of mixing reagents up to 22 minutes after mixing reagents.

The Figure 5.9 also shows that after the initial part of the reaction was completed within the first six minutes after mixing the reagents, the edge height no longer dropped after that, showing that all the starting material was converted to product.

Figure 5.10 shows a two-dimensional overlay of the first 30 spectra obtained of the reaction mixture, from the point of mixing. This figure shows more clearly the change in the EXAFS as the reaction progressed, along with the 3 isobestic points at which the direction of change in absorbance reversed. It shows the drop in edge height and also a softenning of the EXAFS as the reaction progressed. In addition, there was the appearance of a shoulder on the edge which was not dissimilar to the spectra shown in Figure 4.18.

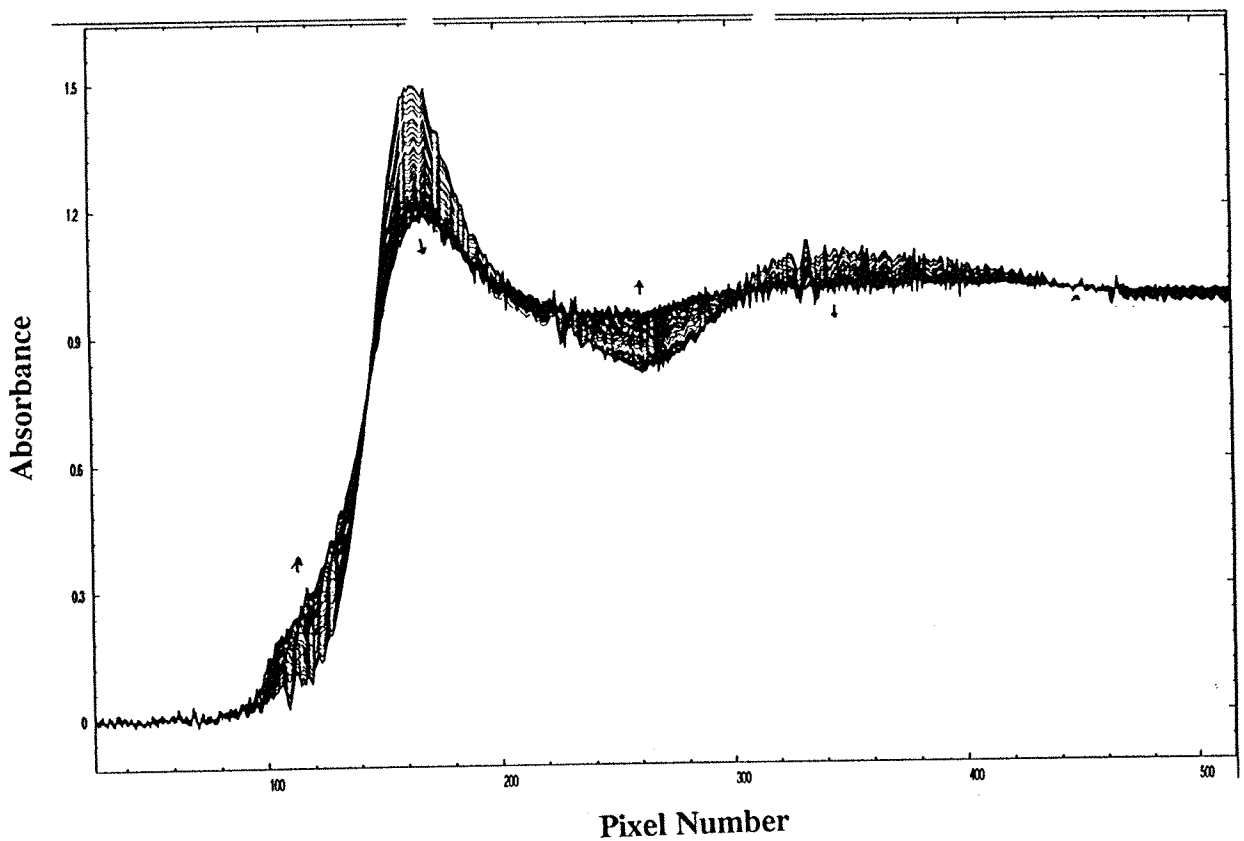

Figure 5.10. Figure showing an overlay of the time resolved Ni-K-edge X-ray absorption spectra (100 frames, frame time= 13 seconds), following the reaction of $Ni(acac)_2/AlEt_2(OEt)$/hex-1-ene ([Ni]= 70mM, Ni:Al:hex-1-ene 1:4:12) mixture in toluene, at room temperature, starting from the point of mixing reagents up to 22 minutes after mixing reagents.

Due to insufficient data length, it was not possible to analyse the spectra obtained in this experiment (there was less than 7k of EXAFS data). For this reason it was decided to compare the raw features of the product spectrum (Figure 5.11) obtained from this experiment with a scanning EXAFS spectrum[5] of the same mixture at 0°C (Figure 5.12) and the QUEXAFS spectrum of the organometallic catalytic product in the $Ni(acac)_2/AlEt_3$/hex-1-ene mixture (Figure 5.13). Although the mixtures used for the spectra in Figures 5.11 and 5.12 were identical, they were different in composition from the mixture used for Figure 5.13 as a different alkylaluminium species ($AlEt_3$) was used. It is not expected that this would have affected the nickel organometallic that was obtained. This can be seen from almost the same electronic absorption spectra obtained for both mixtures.

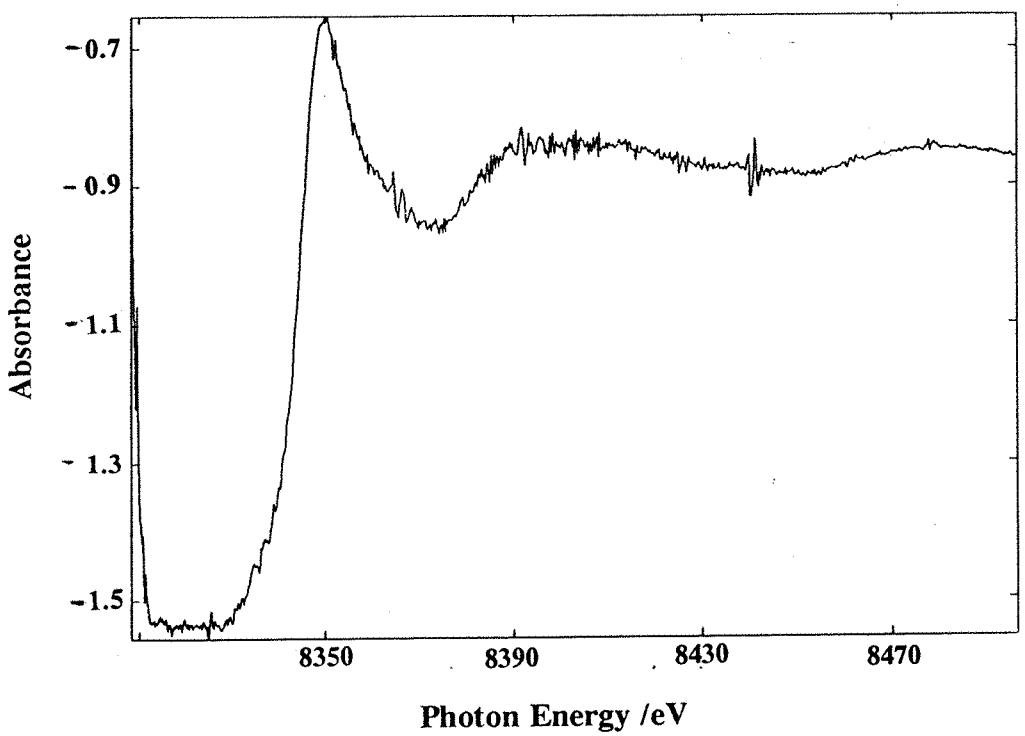

Figure 5.11. Figure showing the EDEXAFS spectrum number 30 from Figure 5.10 taken at 7 minutes and 36 seconds after mixing (scan duration= 13 seconds).

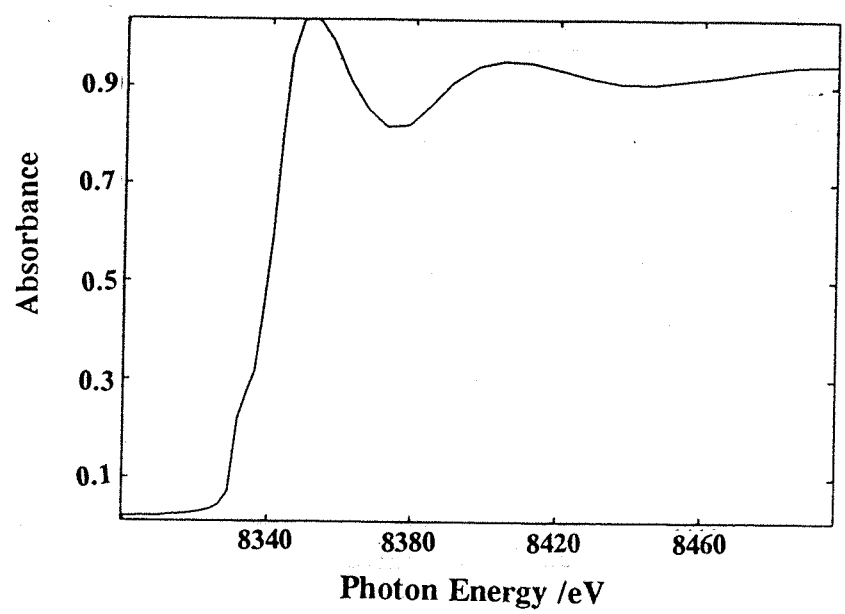

Figure 5.12. Figure showing an EXAFS spectrum (one scan, scan time= 40 minutes) of $Ni(acac)_2/AlEt_2(OEt)$/hex-1-ene (Ni:Al:hex-1-ene 1:2:20, [Ni]= 70mM) mixture taken at 0^0C.

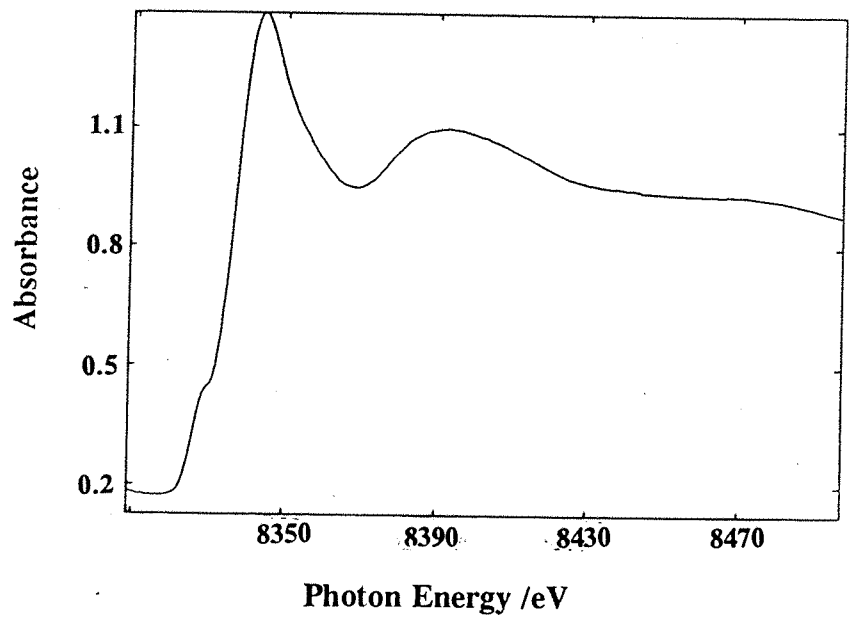

Figure 5.13. Figure showing a QUEXAFS spectrum (one scan, scan time= two minutes) of $Ni(acac)_2/AlEt_3$/hex-1-ene (Ni:Al:hex-1-ene 1:2:20, [Ni]= 70mM) measured at 0^oC.

As can be seen from the three spectra shown in Figures 5.11, 5.12, and 5.13, they are very similar and given the similarity of the starting materials it would seem that the same product was likely to have been formed. Although the EDEXAFS spectrum obtained in Figure 5.11 was too short to be analysed, the spectra in Figures 5.12 and 5.13 have been analysed and have been found to fit to a shell of 2 oxygen atoms and a second shell of three carbon atoms (See Section 4.6 b and Reference 4). No nickel shell could be fitted to the data showing that the trimeric structure of the starting material was lost and no nickel metal had formed in the mixture. Based on this qualitative study, it would seem that a structure similar to that shown below in Figure 5.14 was formed as the product in this study.

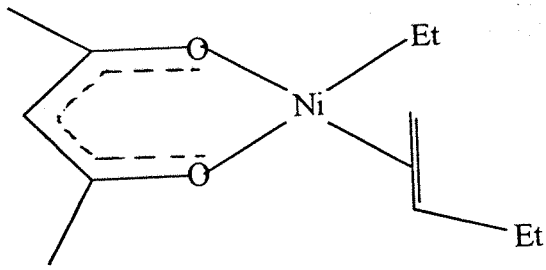

Figure 5.14. Figure showing a possible organometallic product formed in the time resolved spectra shown in Figure 5.9.

5.5 Rates of the reaction of $Ni(acac)_2$ catalyst with the $AlEt_2(OEt)$ cocatalyst in the presence of hex-1-ene:

As mentioned in the previous section, the rate of drop in edge height provided a marker for the rate of reaction between the octahedral nickel catalyst and the aluminium cocatalyst in the presence of hex-1-ene. It was therefore decided to obtain plots of the drop in edge height as the reaction progressed using varying ratios and concentration of the nickel and aluminium components. The different mixtures that were used were as follows:

a) $Ni(acac)_2/AlEt_2(OEt)$/hex-1-ene (Ni:Al:hex-1-ene= 1:2:12, [Ni] in mixture = 35mM, [Al] in mixture= 70mM).

b) $Ni(acac)_2/AlEt_2(OEt)$/hex-1-ene (Ni:Al:hex-1-ene= 1:8:12, [Ni] in mixture = 35mM, [Al] in mixture= 280mM).

c) $Ni(acac)_2/AlEt_2(OEt)$/hex-1-ene (Ni:Al:hex-1-ene= 1:4:12, [Ni] in mixture = 70mM, [Al] in mixture= 280mM).

The height of the edge was plotted as the reaction progressed for up to 10 minutes for all the three mixtures. A comparision of the edge height plots for all the three mixtures is shown on Figure 5.15.

From these graphs, a value was obtained for the rate of the reaction by measuring the slope of the three graphs over the first two minutes of the reaction using least squares analysis.

The rates of the reaction were found to be as follows:

Mixture a) $0.046(3)/\varepsilon$ mmol l^{-1} min^{-1}.

Mixture b) $0.087(9)/\varepsilon$ mmol l^{-1} min^{-1}.

Mixture c) $0.117(6)/\varepsilon$ mmol l^{-1} min^{-1}.

The order of the reaction between the nickel and aluminium components is not known. However, on increasing the aluminium concentration by 4 times, (*cf.* compositions of mixtures a and b) but keeping the concentration of nickel constant it was found that the rate increased 1.9 times. This could indicate that the reaction is of the order 0.5 in the aluminium reagent used.

On increasing the nickel concentration by 2 times and keeping the aluminium concentration constant, (*cf.* compositions of mixtures b and c) the rate of reaction increased by 1.4 times. This would indicate that the reaction is of the order 0.7 in nickel component.

The exact orders of the reaction would be difficult to say based on this single experiment, but an indication of the order of the reaction with respect to each of the components has been obtained.

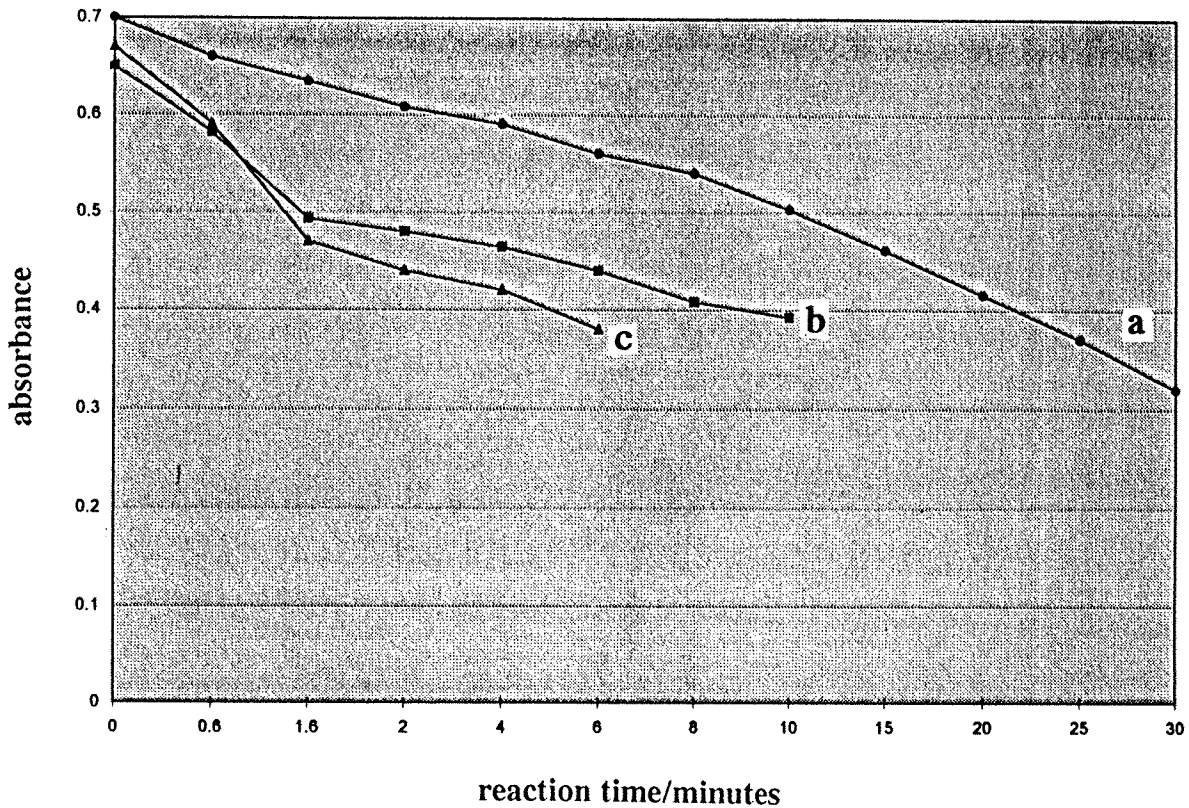

Figure 5.15. Figure showing the effect of a change in reagent concentration on the rate of the reaction of the mixture, $Ni(acac)_2/AlEt_2(OEt)$/hex-1-ene in toluene a) [Ni]= 35 mM, Ni:Al:hex-1-ene 1:2:12 b) [Ni]= 35mM, Ni:Al:hex-1-ene 1:8:12 c) [Ni]= 70mM, Ni:Al:hex-1-ene 1:4:12.

5.6 EDEXAFS spectra of the catalyst mixture in the absence of hex-1-ene:

It was next decided to study the reaction mixture in the absence of hex-1-ene. Such a reaction mixture should result in colloidal nickel metal particles.[6] $AlEt_2(OEt)$ is a weaker alkylating agent than $AlEt_3$.

The study of the mixture in the absence of hex-1-ene was carried out on Station 9.3, SRS at Daresbury. The variable temperature equipment detailed in Section 2.4.3.b was used for preparing the mixtures in-situ. Of the two reagent syringes used, both pumped in solutions into the observation cell (volume= 0.7ml) at the same rate (119 ml/hr) each. One of the syringes contained $Ni(acac)_2$ (140mM in toluene) and the second syringe contained $AlEt_2(OEt)$/ hex-1-ene (980mM/ 2800mM in toluene) solutions. On mixing in the observation cell, these concentrations would be halved as both syringes injected into the cell at the same rate. **The values given in the brackets in the rest of the chapter show the composition of the mixture after mixing.**

Figure 5.16 shows a comparision of the EDEXAFS spectra of a mixture of $Ni(acac)_2/AlEt_2(OEt)$ (Ni:Al 1:7; [Ni]= 70mM) in toluene, obtained over equal intervals of time from six minutes after mixing reagents up to 50 minutes after mixing the reagents.

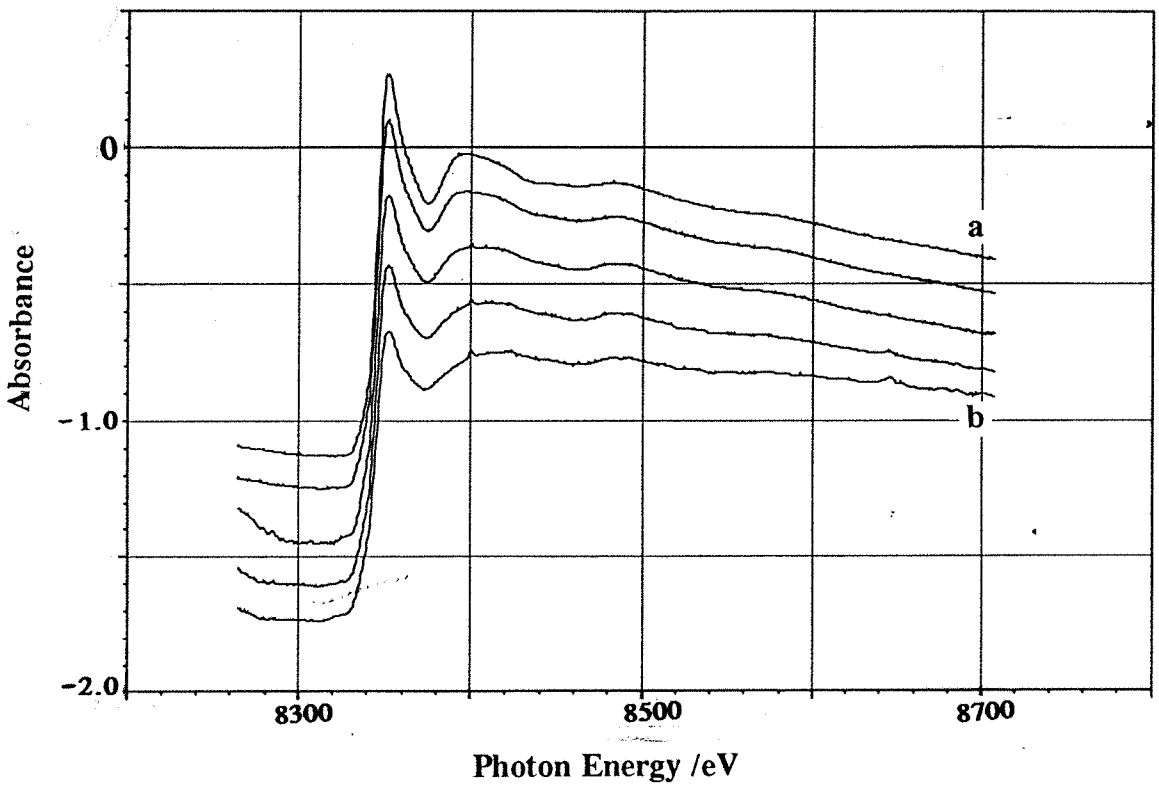

Figure 5.16. Figure showing a series of Ni-K-edge EDEXAFS spectra of a mixture of $Ni(acac)_2/AlEt_2(OEt)$ (Ni:Al 1:7, [Ni]= 70mM in toluene) taken from a) 6 minutes after mixing the reagents up to b) 50 minutes after mixing the reagents. The spectra were taken of the mixture at room temperature.

The spectra show a softening of the white line features from the sharp features of the octahedral $Ni(acac)_2$ to the smaller EXAFS features of colloidal nickel.

The first and last spectra of the above series of spectra were subjected to EXCURVE analysis. Figure 5.17 shows the fitted EDEXAFS spectra and Fourier transform of the mixture, $Ni(acac)_2/AlEt_2(OEt)$ (Ni:Al 1:7, [Ni]= 70mM) taken a) 6 minutes after mixing the reagents and b) 40 minutes after mixing the reagents.

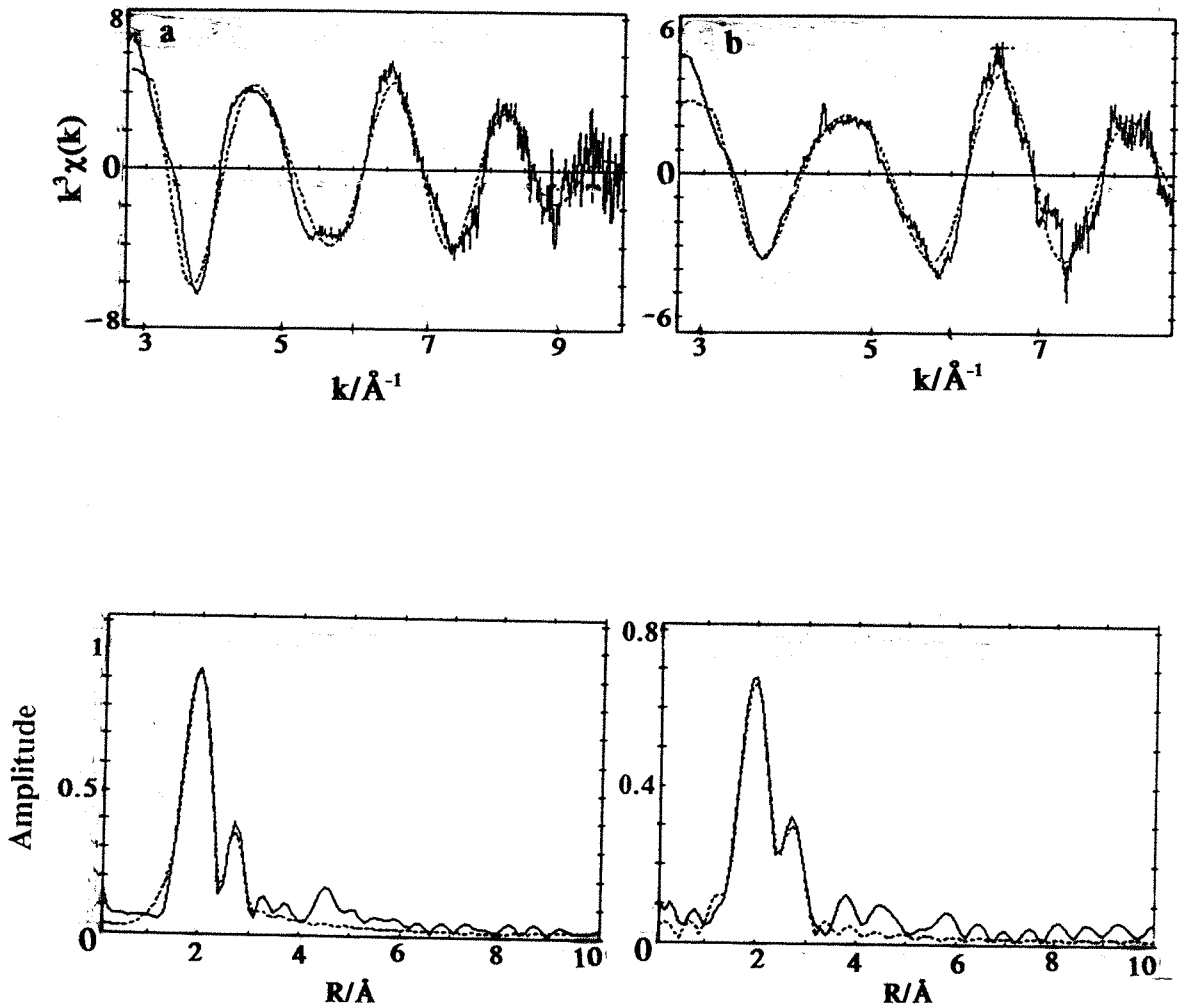

Figure 5.17. Figure showing the fitted EDEXAFS spectrum and Fourier transform of the mixture $Ni(acac)_2/AlEt_2(OEt)$ (Ni:Al 1:7, [Ni]= 70mM) taken at room temperature and a) 6 minutes after mixing reagents b) 40 minutes after mixing reagents.

Table 5.1. Table showing the parameters obtained from the fitted EDEXAFS spectrum shown on Figure 5.17a.

EF= 4.8(3), AFAC= 0.9, R= 32.0%.

	Coordination number	R/Å	$\sigma^2/Å^{-1}$
O	4.08 (8)	1.981 (3)	0.0202 (6)
Ni	1.41 (6)	2.440 (3)	0.0193 (7)

Table 5.2. Table showing the parameters obtained from the fitted EDEXAFS spectra shown in Figure 5.17b.

EF= 4.5(4), AFAC= 0.9, R= 26.8%.

	Coordination Number	R/Å	$\sigma^2/Å^{-1}$
O	2.01 (4)	1.960 (4)	0.0112 (6)
Ni	1.45 (4)	2.459 (3)	0.0173 (6)

The tables show that the oxygen coordination of the nickel dropped over a period of time as the mixture started to form nickel metal particles. This is shown by the coordination shell of nickel atoms at *ca.* 2.459 Å.[18] The low coordination numbers indicate that the clusters may be small in these mixtures. As with the metal particles formed when using $AlEt_3$, even here the exact values obtained from nickel metal foil for nearest neighbour distances and corresponding Debye Waller factors do not apply to small clusters.[19-22] Thus, as shown in the tables 5.3 and 5.4, the Ni-Ni distance was smaller than the expected 2.471 Å. As explained, before this is again due to a redistribution of charge and a decrease in repulsion between non-bonded pairs in the case of small clusters which have more surface atoms than in foil or bulk metal. As before, the Debye Waller factors were higher than expected

from the QUEXAFS spectrum of the foil (0.010). This is because of the larger vibrational amplitude available to the atoms in smaller clusters.

The oxygen coordination of 2 indicates that 2/3 of the nickel in the mixture existed as nickel particles rather than as $Ni(acac)_2$, as $Ni(acac)_2$ has an average coordination number of 6 oxygen atoms. Despite this, the mean value of the nickel coordination was only 1.4. The mean value of 1.4 nickel atoms does indicate that the clusters in this solution were very small.

5.7. CONCLUSIONS:

The results in this chapter show the current extent to which EDE can be used to follow a reaction as it occurs. By reducing the time required to acquire a spectrum, greater time resolution can be achieved but this can affect the quality and length of the data so that it can be difficult to analyse.

The EDE spectra of $Ni(acac)_2/AlEt_2(OEt)$/hex-1-ene mixture at room temperature indicated the formation of an organometallic intermediate shown below.

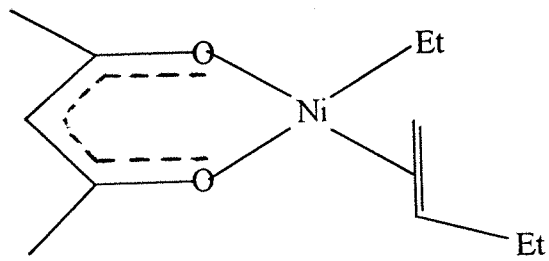

The result was based on a qualitative comparision of the spectra with those of the expected organometallic. Since the length of the data was $<7k$ a full analysis could not be carried out. However, the white line features of the spectra showed substantial changes as the reaction progressed showing the extent to which the acquisition time of 13 seconds/ spectrum allowed for time resolution of the progression of the reaction.

The EDEXAFS spectrum in the absence of hex-1-ene showed the formation of nickel metal clusters, as were formed when $AlEt_3$was used as the cocatalyst in Chapter 4. As in Chapter 4, the Ni-Ni distances of the clusters were smaller than

that of the metal foil and the Debye Waller factors higher. Once again, it would seem that the contractions in Ni-Ni distances seen in the clusters as compared to the foil is caused by the fact that there are fewer nearest neighbour atoms in a cluster as compared to the bulk. This leads to a reduction in the total repulsion between non-bonded electron pairs and therefore a contraction in bond distances. The increase in Debye Waller factors of the clusters is thought to be due to the larger vibrational amplitude at the surface of clusters, as compared to to the foil, which leads to a relaxation of coordinatively unsaturated surface nickel atoms at certain faces of the cluster.

The electronic absorption spectra of the mixture in the presence and absence of hex-1-ene, showed the formation of a nickel alkyl species possibly stabilised by Ni-C-Al interactions as shown below.

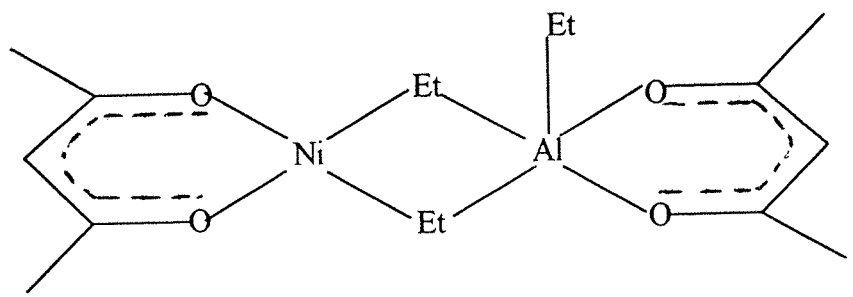

However, a similar species with aluminium coordination could not be seen at the expected 2.9 Å (expected Ni-C-Al distance) using EDEXAFS. This could be because the conditions of the electronic absorption spectroscopy and EXAFS experiments were different. This could mean that the reaction could have progressed to different extents in the two experiments.

5.8 REFERENCES

1. P.W.Jolly and G.Wilke, "The Organic Chemistry of Nickel"., Vol 1, Academic Press, New York, 1975.
2. P.W.Jolly and G.Wilke, "The Organic Chemistry of Nickel"., Vol 2, Academic Press, New York, 1975.
3. K.Fischer, K.Jonas, P.Misbach, R.Stabba and G.Wilke, *Angew.Chem. Int.Ed,Engl.*, 1973, **12**, 943.
4. J.M.Corker and J.Evans, *J.Chem.Soc.Chem.Comm.*, 1991, 1104.
5. J.M.Corker, PhD Thesis, Southampton University, 1991.
6. J.R.Jones and T.J.Symes, *J.Chem.Soc, C.*, 1971, 1124.
7. W.Keim, A.Behr and G.Kraus, *J.Organomet.Chem.*, 1983, **251**, 377.
8. G.J.Bullen, *Nature*, 1956, **177**, 537.
9. C.K.Jørgensen, *Acta.Chem.Scand.*, 1955, **9**, 1362.
10. G.Maki, *J.Chem.Phys.*, 1958, **29**, 162.
11. "Comprehensive Inorganic Chemistry", Eds. J.C.Bailar, H.J.Emeleus, R.Nyholm, and A.F.Trotman-Dickenson, Pergamon Press, 1973, Vol 3, Chapter 42, 1156.
12. A.B.P.Lever, "Inorganic Electronic Spectroscopy", Elsevier, 1968.
13. G.Salvini, D.Bogg, A.J.Dent, G.E.Derbyshire, R.C.Farrow, A.Felton and C.Ramsdale, *Physica B*, 1995, **209**, 229.
14. G.E.Derbyshire, W.I.Helsby, A.J.Dent, S.A.Wright, R.C.Farrow, G.N.Greaves, C.Morrell and G.J.Baker, *Adv.X-ray.Analysis.*, 1990, **34**.
15. M.Hagelstein, C.Ferrero, U.Hatje, T.Ressler and W.Metz, *J.Synchr.Rad.*, 1995, **2**, 174.
16. D.Bogg, A.J.Dent, G.E.Derbyshire, R.C.Farrow, C.A.Ramsdale and G.Salvini, *Nucl.Instr.Meth.*, 1993, **390**, 461.
17. J.Goulon, E.Georges, C.Goulon-Ginet, Y.Chauvin, D.Commereuc, H.Dexpert and E.Freund, *Chem.Phys.*, 1984, **83**, 357.

18. S.C.Davis and K.J.Klabunde, *J.Am.Chem.Soc.*, 1978, **100**, 5974.

19. K.J.Klabunde, H.F.Efner, T.O.Murdoch and R.Ropple, *J.Am.Chem.Soc.*, 1976, **98**, 1022.

20. B.A.Scott, R.M.Plecenik, G.S.Cargill III, T.R.McGuire and S.R.Herd, *Inorg.Chem*, 1980, **19**, 1252.

21. G.Apai, J.F.Hamilton, J.Stohr and A.Thompson, *Phys.Rev.Lett.*, 1979, **43**, 165.

22. D.Richard, J.W.Couves and J.M.Thomas, *Faraday.Discuss.*, 1991, **92**, 109.

CHAPTER 6. ELECTRONIC ABSORPTION AND EDEXAFS SPECTROSCOPIC STUDIES OF $NiX_2(PEt_3)_2$ (X= Br, Cl) /$AlEt_3$ MIXTURES.

6.1 INTRODUCTION:

This chapter is concerned with a study of $NiX_2(PEt_3)_2$ (X= Cl, Br) catalysts in the presence of $AlEt_3$ cocatalyst. The structure that a Ni(II) phosphine of the type $NiX_2(PR_3)_2$ (X= Cl, Br) usually takes depends on the phosphine. $P(aryl)_3$ complexes are usually tetrahedral while $P(alkyl)_3$ complexes are usually square planar and for mixed alkyl/aryl complexes planar-tetrahedral isomerism is usually exhibited.[1,2] $NiX_2(PEt_3)_2$ (X=Cl, Br) complexes are diamagnetic and trans-square planar in solid and in solution.[3-6]

$NiX_2(PEt_3)_2$ complexes have been used before as catalyst precursors for propene dimerisation.[7-9] Catalyst preparation involves adding an excess of the alkyl or alkyl aluminium halide reagent to the nickel complex dissolved in an aromatic or halohydrocarbon solvent.

Studies of the $NiCl_2(PEt_3)_2/AlEt_3$ catalyst for propene dimerisation have been performed previously. The catalyst mixture was prepared at -40°C in *p*-fluorotoluene. All the catalyst samples prepared were homogeneous in nature but were found to decompose if the temperature was maintained above *ca.* 5°C for any length of time. The results from this study were used to demonstrate that the catalysts are very active at the temperatures and conditions used in the study and to be employed in future XAS measurements.[1] GC-MS studies showed that the propene had oligomerised to form a variety of isomers of methylpentene of which 4-methylpent-2-ene was the dominant (44%) product.[1] The C_6 product composition identified was consistent with previously reported data on similar systems.[10] Previous studies of similar systems have also found that chlorobenzene and dichloromethane are excellent solvents for the catalysis studies but are extremely poor solvents for XAS measurements as they absorb at the Ni-K-edge.

EXAFS spectra of $NiX_2(PEt_3)_2$ (X= Cl, Br) in p-fluorotoluene have been recorded previously.[1] EXAFS spectra of $NiX_2(PEt_3)_2$ (X= Cl, Br) in the solid state in boron nitride have also been previously studied.[11] Distinguishing phosphorus from chlorine in EXAFS analysis presents difficulties because of the similarities in

the phaseshifts of the two elements.[1,2] A similar problem has not been experienced with $NiBr_2(PEt_3)_2$ because the phaseshifts of phosphorus and bromine are different.

In the presence of aluminium cocatalyst it is expected that alkylation will occur. It is not entirely certain whether alkylation will occur with loss of the halogen ions or phosphine ligands or a combination of both. EXAFS could confirm any loss of such atoms from the coordination sphere e.g. loss of bromine ions from $NiBr_2(PEt_3)_2$ on addition of alkylaluminium reagents is clear from bromine-K-edge data of the mixture.

It is thought that the main catalytic species consists of organometallic species formed from the alkylation of the nickel species followed by a step hydride elimination and subsequent olefin coordination.[13] However, the ease of formation of colloidal nickel in such species has lead to some speculation that catalysis may occur microheterogeneously on the surface of such colloidal particles. The exact role of the aluminium atom in the actual catalysis is difficult to say although it provides the carbon atoms for the alkylation of the nickel centre. Direct nickel to aluminium interactions have not been observed although interaction via carbon bridges have been observed.[14] Catalysis has previously been demonstrated to occur at the aluminium atom.[15] On its own, the aluminium atom can polymerise but not oligomerise,[16] while the nickel atom on its own can oligomerise at a rate much slower than in the presence of the aluminium cocatalyst.[17] Thus, a species involving both the nickel and aluminium atoms is thought to be responsible for oligomerisation.

This chapter will concentrate on the EDEXAFS, QUEXAFS and electronic absorption spectroscopy of mixtures of $NiX_2(PEt_3)_2/AlEt_3$ (X= Cl, Br) in the presence and absence of hex-1-ene. Both EDEXAFS[18-20] and QUEXAFS[20-22] allowed faster acquisition of data than scanning EXAFS. A problem which could be encountered in the EXAFS studies involving $NiX_2(PEt_3)_2$ complexes was the absorbance of X-rays at the Ni-K-edge by chlorine and bromine atoms. Increased acquisition times were required, in cases where chlorine and bromine atoms are present in the solution, for a better S/N ratio.

6.2 Aims of this chapter:

a) To study the catalyst mixtures using electronic absorption spectroscopy.

b) To obtain Ni-K-edge and where possible Br-K-edge EDEXAFS or QUEXAFS spectra of the following reaction mixtures:

i) $NiCl_2(PEt_3)_2/AlEt_3$ catalyst mixture at 0^oC and 20^oC in the presence and absence of olefin i.e. hex-1-ene.

ii) $NiBr_2(PEt_3)_2/AlEt_3$ catalyst mixture at 0^oC and 20^oC in the presence and absence of olefin i.e. hex-1-ene.

6.3. Electronic absorption spectra of $NiX_2(PEt_3)_2/AlEt_3$ (X= Cl, Br) mixtures:

i) $NiCl_2(PEt_3)_2$:

The complex has a trans-square planar structure. Figure 6.1 shows the electronic absorption spectrum of $NiCl_2(PEt_3)_2$ (4mM in *p*-fluorotoluene) obtained at room temperature.

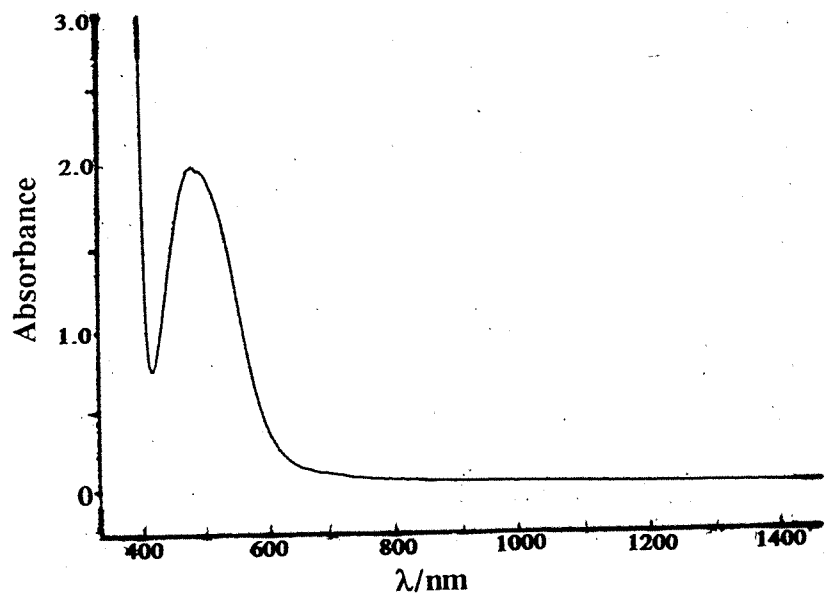

Figure 6.1. Figure showing the electronic absorption spectrum of $NiCl_2(PEt_3)_2$ (4mM in *p*-fluorotoluene) at room temperature.

ii) $NiCl_2(PEt_3)_2/AlEt_3$:

Figure 6.2 shows a series of electronic absorption spectra of the mixture $NiCl_2(PEt_3)_2/AlEt_3$ ([Ni]= 20mM, Ni:Al 1:2) obtained by adding $AlEt_3$ (2 ml, 80mM in *p*-fluorotoluene) to $NiCl_2(PEt_3)_2$ (2 ml, 40mM in *p*-fluorotoluene). The spectra were obtained at regular intervals from 0.5 minutes after mixing up to 32 minutes after mixing the reagents as shown in Figure 6.1. The spectrum of $NiCl_2(PEt_3)_2$ (20mM in *p*-fluorotoluene) is also shown for comparision.

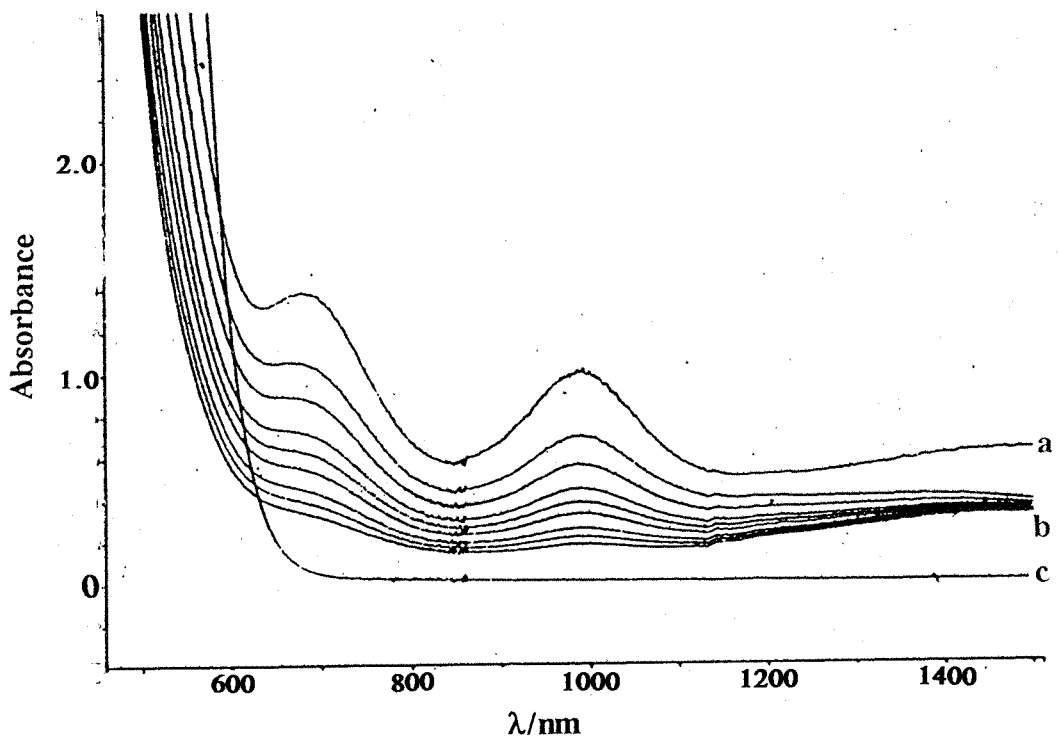

Figure 6.2. Figure showing the electronic absorption spectra of mixture $NiCl_2(PEt_3)_2/AlEt_3$ in *p*-fluorotoluene, ([Ni]= 20mM, Ni:Al 1:2) from a) 0.5 minutes after mixing up to b) 32 minutes after mixing the reagents. A spectrum of the starting material ($NiCl_2(PEt_3)_2$) is also included for comparision (see c).

From Figure 6.2, it can be seen that there was a clear change in the spectra on addition of the alkylaluminium reagent. Two new peaks appeared at 700nm (ε= 70 l mol^{-1} cm^{-1}) and 1000nm (ε= 50 l mol^{-1} cm^{-1}). While square planar d^8 nickel species generally exhibit two bands (ε= 50-500 l $mol^{-1}cm^{-1}$) at 430-670 nm and at 370-430 nm, tetrahedral species exhibit bands at 600-750 nm and 1000-1200nm.[23] Octahedral d^8 species generally[24] exhibit three bands at 1430-770 nm, 900–500 nm, and 526-370 nm. From the above data, it would seem that the complex formed was not a square planar d^8 species and is also unlikely to have been a tetrahedral d^8 species, as the ligand PEt_3 possesses too strong a field to give a tetrahedral species, except if only one PEt_3 group is present. Since there were no splittings of the bands it would seem that the complex was not a tetragonally distorted octahedron. However, it would be difficult to obtain a high spin regular octahedral d^8 structure from the donor sets present.

If the complex was not d^8, it was unlikely to be d^7 as $AlEt_3$ is a reducing agent. It could therefore be d^9 or d^{10} . It was unlikely to be d^{10} as such species do not give absorptions at low energy. Therefore, the species could have been a d^9 species of the type $P_2Ni(\mu\text{-}Cl)_2\ NiP_2$.

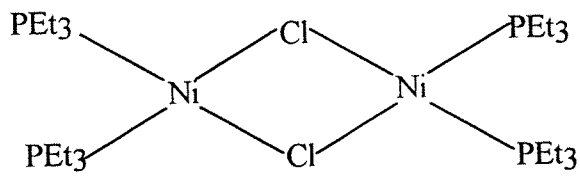

Figure 6.3. Possible dimer formed in a mixture of $NiCl_2(PEt_3)_2/AlEt_3$ in *p*-fluorotoluene at room temperature.

The dimer shown in Figure 6.3 is likely to form by the process of radical elimination shown in Figure 6.4.

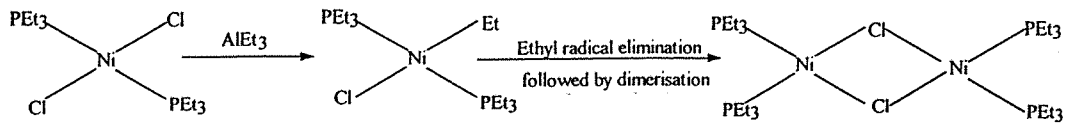

Figure 6.4 Figure showing the possible formation of Ni(I) species in a $NiCl_2(PEt_3)_2/AlEt_3$ solution.

As can be seen from Figure 6.4, the Ni(I) species could be formed from the loss of an alkyl radical from a nickel alkyl species leading to the formation of Ni(I) monomers.

The electronic absorption spectrum[25] of a square planar Ni(I) species ($Ni(Pcy_3)_2Cl$ - dimer) was found to show no bands at >500nm. The same study also showed that the Ni(0) (i.e. $Ni(P^nBu3)_4$ species formed, also showed no bands at >500 nm. However, tetrahedral Ni(I) species are known to show a band at 1000nm, as with $Ni(P_3)X$[26] involving the terdentate phosphine ligand, P_3= 1,1,1-tris(diphenyl phosphinomethyl)ethane.

Based on the above evidence, it was difficult to be precise about the nature of the species present in solution except to say that it could be a tetrahedral d^9 Ni(I) complex.

Low temperature electronic absorption spectra:

Figure 6.5 shows the electronic absorption spectra of the mixture $NiCl_2(PEt_3)_2/AlEt_3$ ([Ni]= 70mM, Ni:Al 1:2.5) obtained using the low temperature EXAFS equipment detailed in Chapter 2 adapted for electronic absorption

spectroscopy using mylar windows instead of kapton windows. The mixture was formed using equal volumes of $NiCl_2(PEt_3)_2$ (140mM in *p*-fluorotoluene) and $AlEt_3$ (350mM in *p*-fluorotoluene).

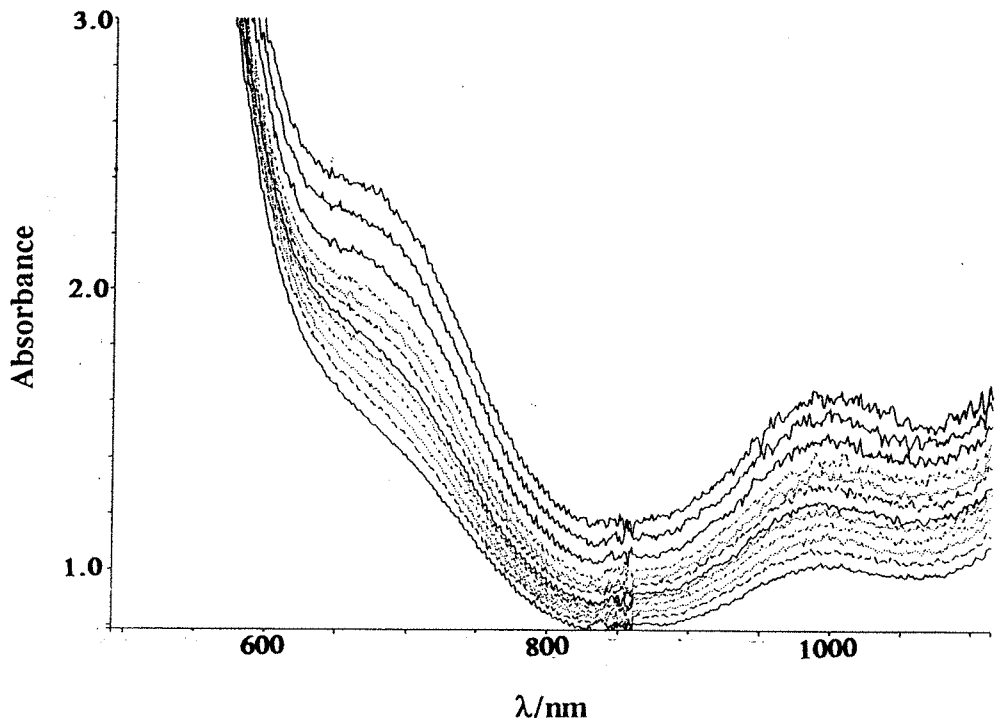

Figure 6.5. Figure showing the electronic absorption spectrum of $NiCl_2(PEt_3)_2$/ $AlEt_3$ ([Ni]= 70mM, Ni:Al 1:2.5) taken at -3°C.

The spectra in Figure 6.5 show the two bands at 700 nm and 1000 nm suggesting that as in the case of the room temperature experiment, a tetrahedral d^9 Ni(I) species may have formed.

This experiment involved higher concentrations of the nickel complex and could therefore be repeated using EDEXAFS, unlike the room temperature experiment using lower nickel complex concentrations.

A similar low temperature experiment was carried out using equal volumes of $NiBr_2(PEt_3)_2$ ([Ni]= 140mM solution in *p*-fluorotoluene) and $AlEt_3$ ([Al]= 840mM in *p*-fluorotoluene) to give a mixture with composition, ([Ni]= 70mM, Ni:Al 1:6). The low temperature EXAFS equipment detailed in Chapter 2, modified to include mylar windows for electronic absorption spectroscopy, was used. The results (Figure 6.6) once again showed the formation of a peak at 1000nm showing that the reaction followed a similar course to the chloro-analogue of the nickel species.

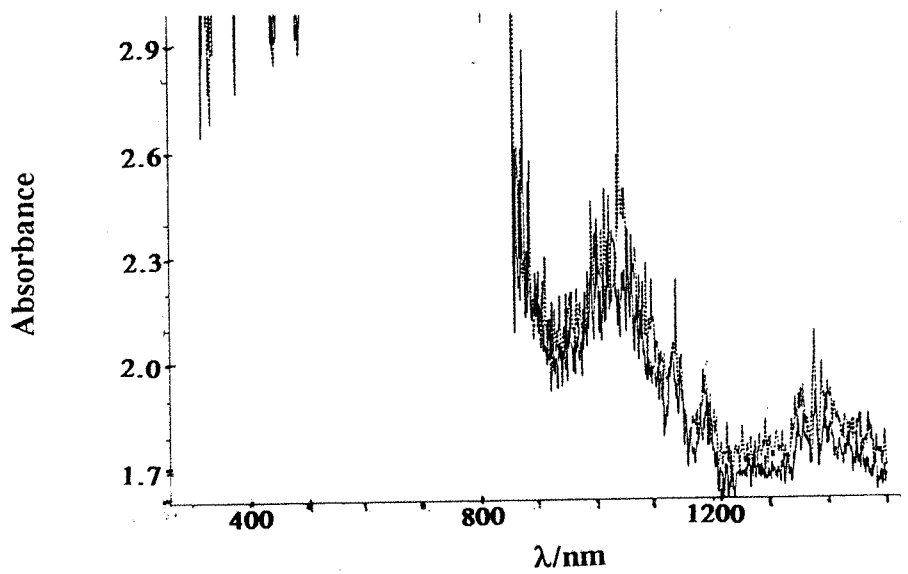

Figure 6.6. Figure showing the electronic absorption spectrum of $NiBr_2(PEt_3)_2/AlEt_3$ in *p*-fluorotoluene, ([Ni]= 70mM, Ni:Al 1:6) at -5°C.

6.4. Equipment used for EXAFS studies in this chapter:

In all cases, except where indicated otherwise, the variable temperature equipment described in Section 2.4.3 was used for the room temperature and low temperature EDEXAFS studies. As mentioned before, the equipment contained two reagent syringes connected by steel tubing to the observation cell where mixing occurred. **The compositions of the mixtures given henceforth in brackets are the compositions of the reagents in the observation cell.**

6.5. EDEXAFS spectra of $NiCl_2(PEt_3)_2/AlEt_3$ in the absence of hex-1-ene;

The fitted EDEXAFS and QUEXAFS spectra of the starting material $NiCl_2(PEt_3)_2$ are given in Chapter 3. The Ni-K-edge data was found to fit to a single shell of 4 phosphorus atoms at 2.23Å. It was difficult using these techniques to differentiate between the chlorine and phosphorus shells as they have very similar phase shifts.

The experiments in this section will be concerned with any changes in the nickel coordination sphere of this complex on addition of $AlEt_3$ both in the presence and absence of the olefin.

i) at low temperatures:

Figure 6.7 shows the Ni-K-edge EDEXAFS spectrum of $NiCl_2(PEt_3)_2/AlEt_3$ ([Ni]= 70mM, Ni:Al 1:2.5 in *p*-fluorotoluene) obtained at -2^{o}C.

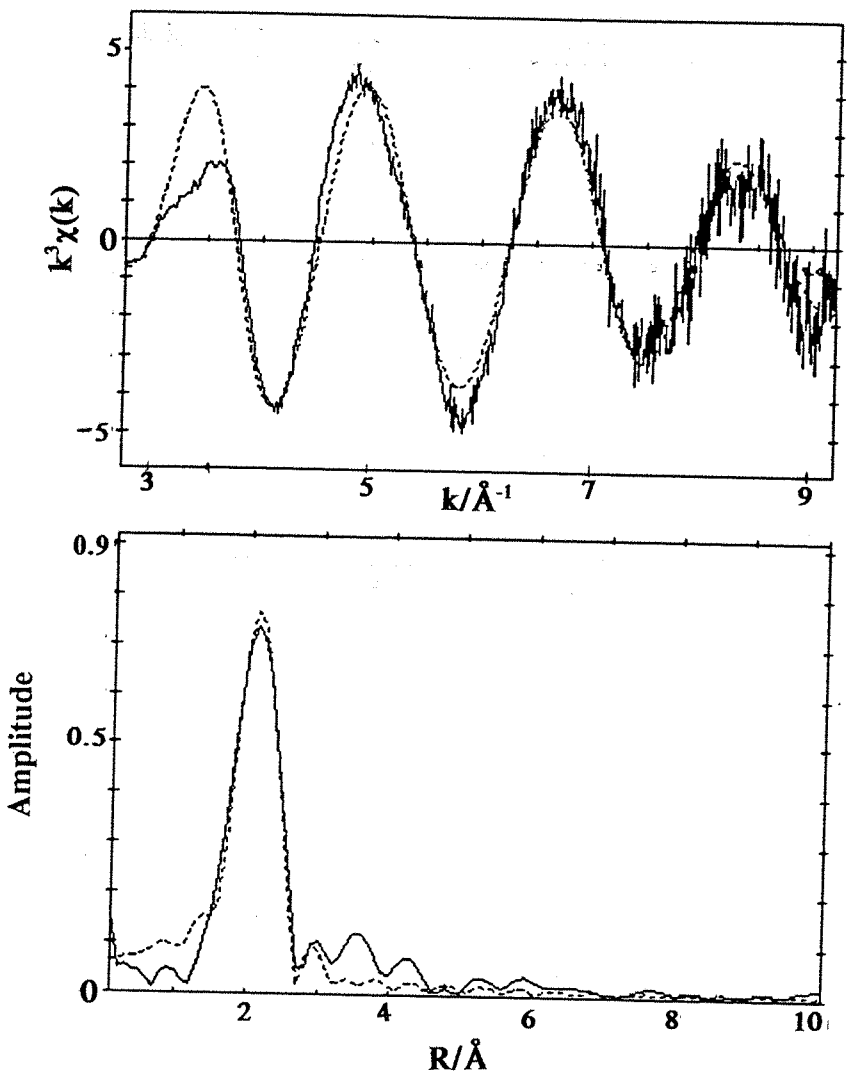

Figure 6.7. Figure showing the fitted Ni-K-edge EDEXAFS data (1000 scans, total scan time= 1020 ms) and Fourier transform of $NiCl_2(PEt_3)_2/AlEt_3$ (Ni:Al 1:2.5, [Ni]= 70mM) mixture in *p*-fluorotoluene at -2^oC.

Table 6.1. Table showing the parameters obtained from the fitted Ni-K-edge EDEXAFS data (1000 scans, scan time= 1020 ms) and Fourier transform of $NiCl_2(PEt_3)_2$ /$AlEt_3$ (Ni:Al 1:2.5, [Ni]= 70mM) at -2^{0}C.

EF= 2.3(3), AFAC= 0.7, R= 29.7%.

	Coordination number	R/Å	σ^2/A^{-1}
P	3.67 (6)	2.201 (2)	0.0191 (4)
Al	0.7 (2)	3.15 (2)	0.022 (6)

From the parameters shown it can be seen that the data could be fitted to 4 phosphorus atoms. As with the starting material (see Chapter 3), this shell of four phosphorus atoms could consist of 2 phosphorus atoms and two chlorine atoms which are difficult to distinguish between, due to the similarities in phase shifts of the two types of atom. An aluminium shell could be also fitted to the EXAFS data at a non-bonding distance of 3.15 Å. Such a shell could have arisen from the formation of Ni-Cl-Al bonds with some of the $AlEt_3$ attacking the chlorine atom. From the aluminium coordination of 0.7, it would seem that only part of the nickel halogenophosphine had reacted to form such an adduct. The rest is still likely to be starting material.

ii) at room temperature:

Figure 6.8 shows a fitted EDEXAFS spectrum and Fourier transform of $NiCl_2(PEt_3)_2$ /$AlEt_3$ (Ni:Al 1:4, [Ni]= 70mM) mixture which was taken at room temperature. The parameters obtained from the fit are shown in Table 6.2.

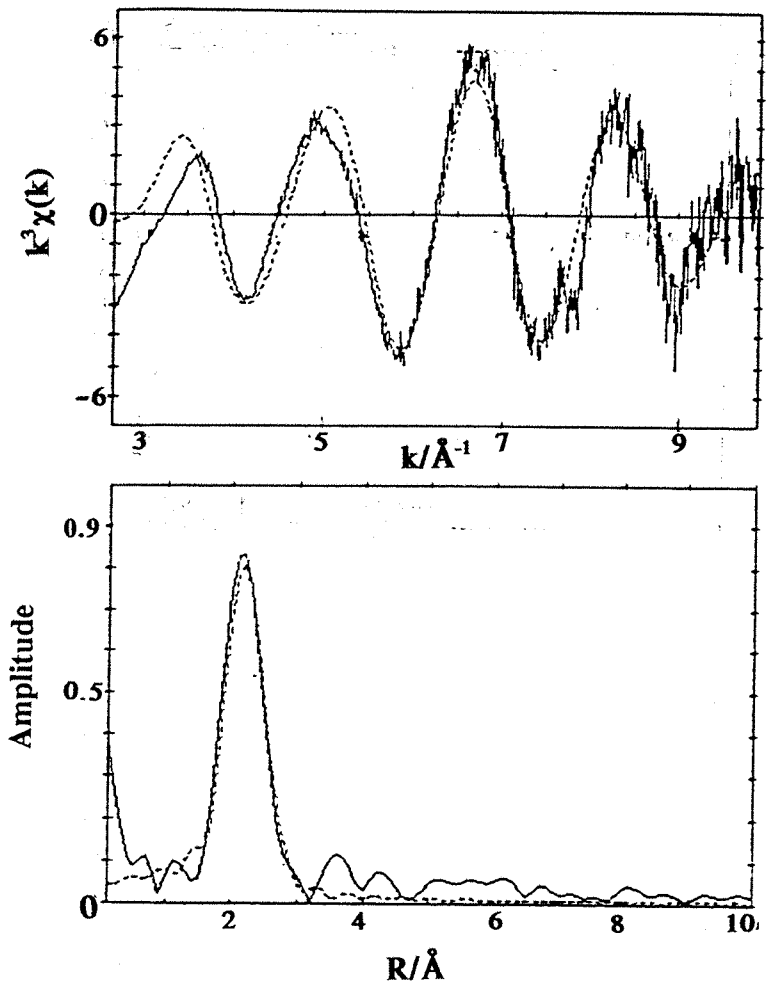

Figure 6.8. Figure showing the fitted Ni-K-edge EDEXAFS data (1000 scans, total scan time= 1420 ms) and Fourier transform of $NiCl_2(PEt_3)_2/AlEt_3$ (Ni:Al 1:4, [Ni]= 70mM) mixture in *p*-fluorotoluene at room temperature.

Table 6.2. Table showing the parameters obtained from the fitted Ni-K-edge EDEXAFS data (1000 scans, scan time= 1420 ms) and Fourier transform of $NiCl_2(PEt_3)_2/AlEt_3$ (Ni:Al 1:4, [Ni]= 70mM) at room temperature.

EF= 0.6(6), AFAC= 0.9, R= 39.1%

	Coordination number	R/Å	$\sigma^2/Å^{-1}$
P	2.11(6)	2.197 (5)	0.0121 (7)
Ni	1.5 (2)	2.460 (6)	0.024 (2)

As can be seen from the Table 6.2, the data at room temperature could be fitted to a first shell of 2P atoms showing, that there was still some material with Ni-P bonds present in the mixture. It is possible that this shell actually consisted of 1 P and 1 Cl atom as it is difficult to distinguish between phosphorus and chlorine atoms using EXAFS as they have very similar phaseshifts.

In addition, the data was also fitted to a shell of 1.5 nickel atoms at 2.460 Å. This shows that nickel clusters had formed in the reaction mixture. As in previous cases of the nickel clusters, the Ni-Ni first shell distance of 2.460(6) Å was shorter than the expected 2.471(2)Å from the foil. However, the contraction is less in this case, when *p*-fluorotoluene is used as solvent, than when toluene was used as the solvent, in the case of the $Ni(acac)_2$ experiments. Also the Debye Waller factor of this shell was higher (0.0242) than that expected from the foil (0.010). The increase in Debye Waller factors has been thought to be due to the large vibrational amplitude at the surface of the clusters and arises from the relaxation of coordinatively unsaturated surface nickel atoms at certain faces of the fine particle.

6.6. QUEXAFS of $NiCl_2(PEt_3)_2/AlEt_3$ in the presence of hex-1-ene:

i) at low temperatures:

The Ni-K-edge QUEXAFS (one scan, scan duration= 2 minutes) of $NiCl_2(PEt_3)_2/AlEt_3$/hex-1-ene (Ni:Al:hex-1-ene 1:3:20, [Ni]= 70mM) mixture in *p*-fluorotoluene was obtained at -3°C in order to find out the changes happening at the nickel centre. Figure 6.9 shows the fitted Ni-K-edge QUEXAFS spectrum and its Fourier transform.

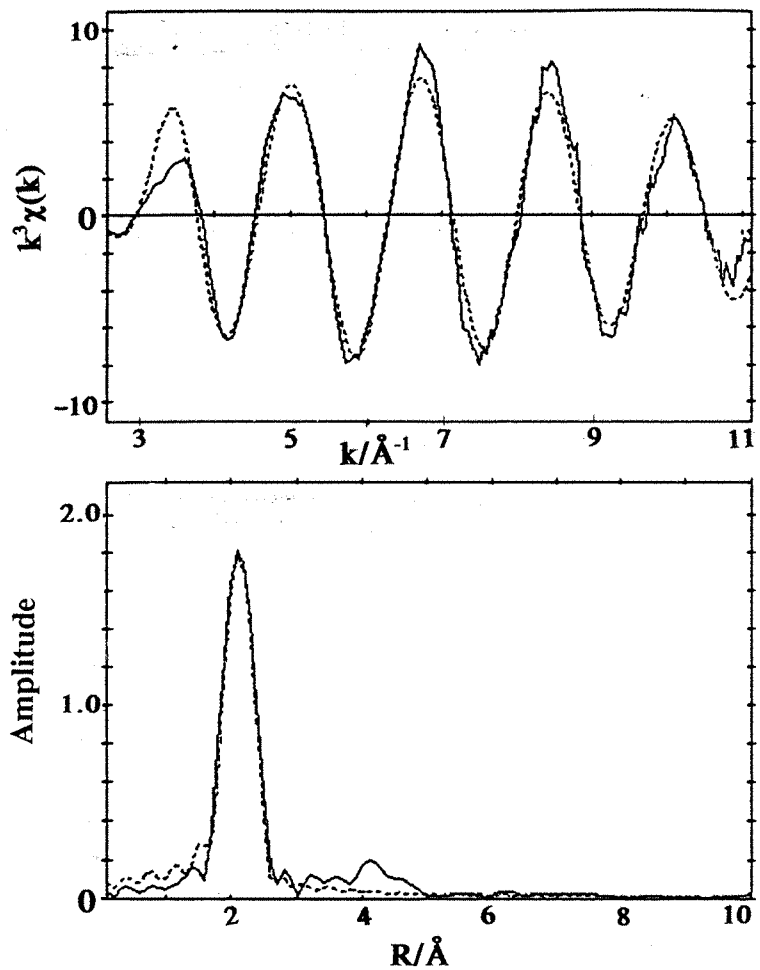

Figure 6.9. Figure showing the fitted Ni-K-edge QUEXAFS data (one scan, scan duration= 2 minutes) and Fourier transform of $NiCl_2(PEt_3)_2/AlEt_3$/hex-1-ene (Ni:Al:hex-1-ene 1:2:20, [Ni]= 70mM) mixture in *p*-fluorotoluene at -3°C.

Table 6.3. Table showing the parameters obtained from the fitted Ni-K-edge QUEXAFS spectrum (one scan, scan duration= 2 minutes) and Fourier transform of $NiCl_2(PEt_3)_2/AlEt_3$/hex-1-ene (Ni:Al:hex-1-ene 1:2:20, [Ni]= 70mM) mixture in *p*-fluorotoluene at -3°C.

EF= -0.8(4), AFAC= 0.8, R= 20.5%.

	Coordination number	R/Å	$\sigma^2/Å^{-1}$
P	4.04 (8)	2.184 (2)	0.014 (4)

At low temperatures, the data from the catalyst mixture in the presence of hex-1-ene, fitted to a single shell of four phosphorus atoms at 2.184 Å. It would seem that the reaction had not proceeded much from the starting material i.e. $NiCl_2(PEt_3)_2$. As with the mixture in the absence of hex-1-ene, it is possible that an adduct had formed between the $NiCl_2(PEt_3)_2$ and the $AlEt_3$ but since an aluminium shell could not be fitted at 3.1 Å, this is unlikely.

There was little evidence of a carbon shell from the fitted data, indicating that little or no alkylation had taken place at these low temperatures.

ii) at room temperature:

Figure 6.10 shows the fitted Ni-K-edge QUEXAFS data (one scan, scan duration= two minutes) and Fourier transform of $NiCl_2(PEt_3)_2/AlEt_3$/hex-1-ene (Ni:Al:hex-1-ene 1:2:20, [Ni]= 70mM) mixture in *p*-fluorotoluene, obtained at room temperature.

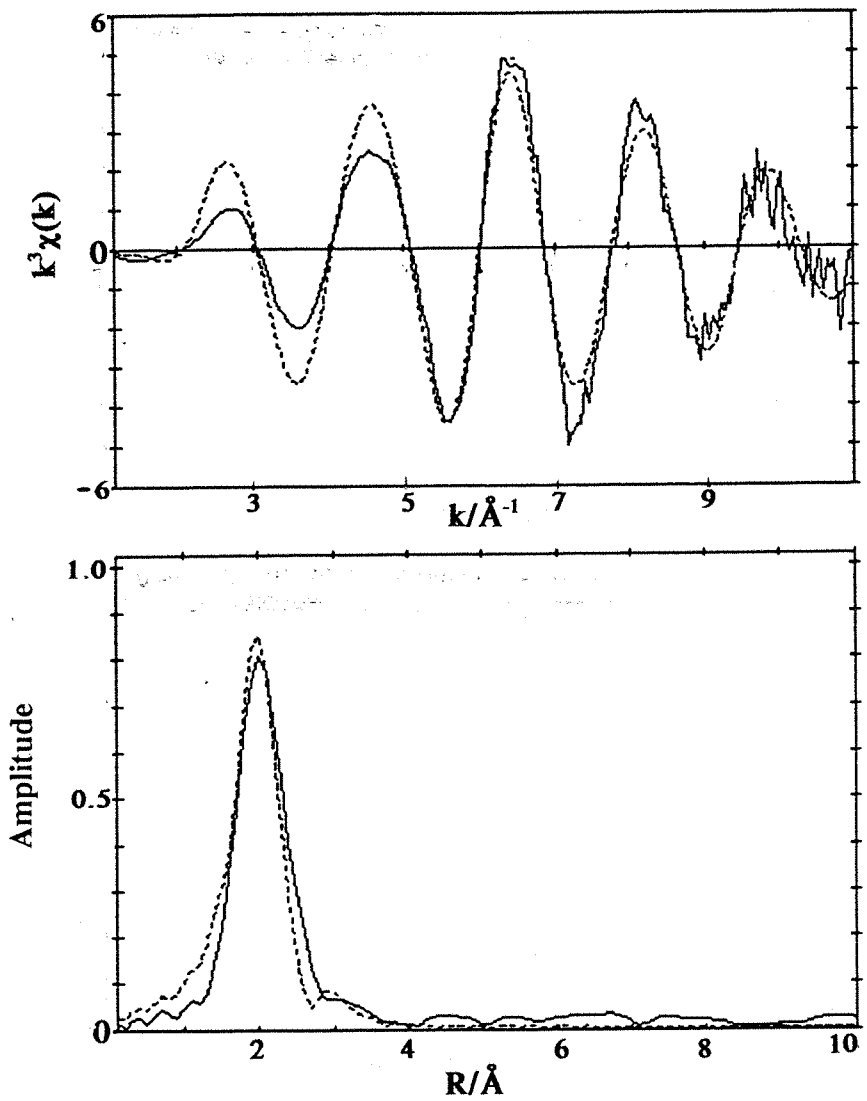

Figure 6.10. Figure showing the fitted Ni-K-edge QUEXAFS data (one scan, scan duration= two minutes) and Fourier transform of $NiCl_2(PEt_3)_2/AlEt_3$/ /hex-1-ene (Ni:Al:hex-1-ene 1:2:20, [Ni]= 70mM) mixture in *p*-fluorotoluene at room temperature.

Table 6.4. Table showing the parameters obtained from the fitted Ni-K-edge QUEXAFS data (one scan, scan duration= two minutes) and Fourier transform of $NiCl_2(PEt_3)_2/AlEt_3$/hex-1-ene (Ni:Al:hex-1-ene 1:2:20, [Ni]=, 70mM) mixture in *p*-fluorotoluene at room temperature.

EF= -3.7(6), AFAC= 0.8, R= 32.1%.

	Coordination number	R/Å	$\sigma^2/Å^{-1}$
P	3.8 (1)	2.198 (4)	0.0162 (5)
Al	1.2 (3)	3.25 (2)	0.023 (7)

The data in the above table shows that at room temperature the nickel atom had a first coordination shell 4 phosphorus atoms at 2.198Å. This phosphorus shell could, as in the starting material, have consisted of 2 phosphorus and 2 chlorine atoms. The resolution between the two was difficult due to similarities in the phase shifts of the two atoms and the length of data required for resolution.

A second shell of 1 aluminium atom at the non-bonding distance of 3.25 Å was also found to improve the fit. As in the absence of hex-1-ene, it could be that Ni-Cl-Al bonds had been formed as a result of the $AlEt_3$ attacking the chlorine atoms rather than the nickel centre to result in an adduct.

6.7. Ni- and Br-K-edge QUEXAFS and EDEXAFS of $NiBr_2(PEt_3)_2/AlEt_3$ at varying temperatures:

The fitted EDEXAFS and QUEXAFS spectra for the Ni- and Br-K edge of $NiBr_2(PEt_3)_2$ are given in Chapter 3. The Ni-K-edge data was found to fit to 2 phosphorus atoms at 2.23 Å and 2 bromine atoms at 2.32 Å. Unlike $NiCl_2(PEt_3)_2$ there was little difficulty in distinguishing between the shells of phosphorus and bromine atoms either in the EDEXAFS or the QUEXAFS data.

The Br-K-edge data was found to fit to a first shell of one nickel atom at 2.23Å , a second shell of 2 phosphorus atoms at 3.3Å and a shell of one *trans*-bromine at 4.5 Å.

In the next few sections we will look at the changes in the nickel and bromine coordination spheres of the starting material $NiBr_2(PEt_3)_2$ on addition of $AlEt_3$ both in the presence and absence of hex-1-ene.

i) at low temperature:

Figure 6.11 shows the fitted Ni-K-edge QUEXAFS data (one scan, scan duration= two minutes) and Fourier transform of $NiBr_2(PEt_3)_2/AlEt_3$ (Ni:Al 1:6, [Ni]= 70mM) mixture in *p*-fluorotoluene obtained at -5^{o}C.

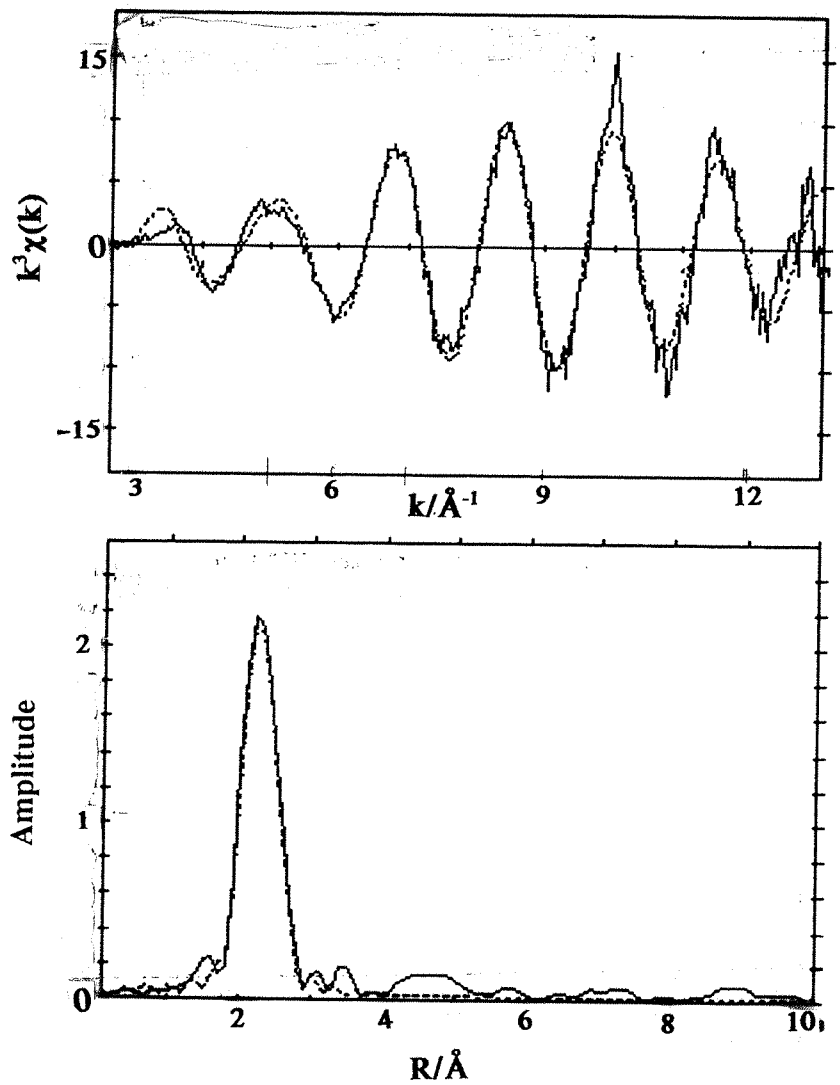

Figure 6.11. Figure showing the fitted Ni-K-edge QUEXAFS data (one scan, scan duration= two minutes) and Fourier transform of $NiBr_2(PEt_3)_2/AlEt_3$ (Ni:Al 1:6, [Ni]= 70mM) in *p*-fluorotoluene at -5^{0}C.

Table 6.5. Table showing the parameters obtained from the fitted Ni-K-edge QUEXAFS data (one scan, scan duration= two minutes) and Fourier transform of $NiBr_2(PEt_3)_2/AlEt_3$ (Ni:Al 1:6, [Ni]= 70mM) at -5°C.

EF= 1(1), AFAC= 0.80, R=29.3%.

	Coordination number	R/Å	σ^2/ $Å^{-1}$
P	2.0 (1)	2.190 (9)	0.005 (1)
Br	2.0 (1)	2.313 (3)	0.0080 (8)

The data in the table shows that, at -5°C, the nickel atom had an average coordination of 2 phosphorus atoms at 2.190 Å and 2 bromine atoms at 2.313 Å. This is the same as the fit which was obtained for the starting material i.e. $NiBr_2(PEt_3)_2$. Thus, at -5°C, it would seem that the reaction had not proceeded very far.

The bromine-K-edge spectrum of the same mixture was very difficult to analyse and has not been presented.

ii) at room temperature:

Figure 6.12 shows the Ni-K-edge fitted EDEXAFS spectrum (average of 10 frames, 99 scans, total scan duration= 250 ms) and Fourier transform of $NiBr_2(PEt_3)_2/AlEt_3$ (Ni:Al 1:6, [Ni]= 70mM) mixture in *p*-fluorotoluene as obtained at room temperature.

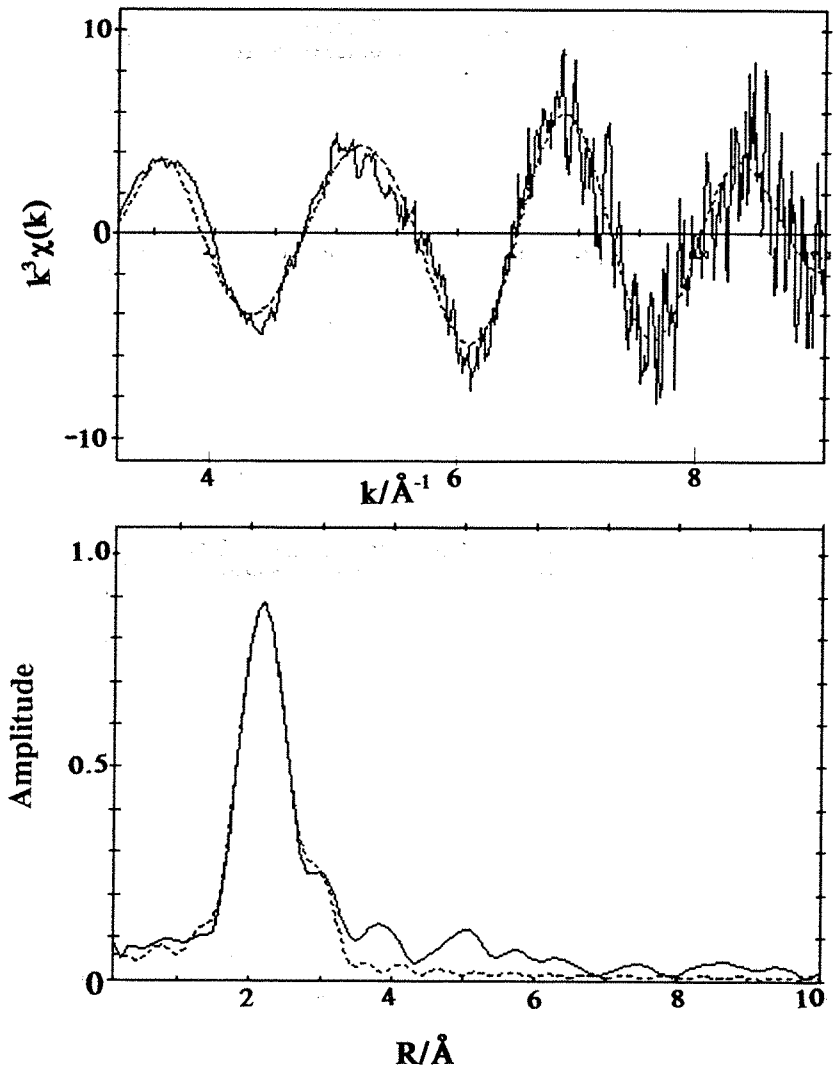

Figure 6.12. Figure showing the fitted Ni-K-edge EDEXAFS data (10 frames, 99 scans, total scan duration= 250 ms) and Fourier transform of $NiBr_2(PEt_3)_2/AlEt_3$ (Ni:Al 1:6, [Ni]= 70mM) in *p*-fluorotoluene at room temperature.

Table 6.6. Table showing the parameters obtained from the fitted Ni-K-edge EDEXAFS data (10 frames, 99 scans, total scan duration= 250ms) and Fourier transform of $NiBr_3(PEt_3)_2/AlEt_3$ (Ni:Al 1:6, [Ni]= 70mM) in *p*-fluorotoluene at room temperature.

EF= 2(1), AFAC= 0.9, R= 39.8%.

	Coordination number	R/Å	σ^2 /Å^{-1}
P	2.06 (9)	2.11 (1)	0.014 (1)
Br	2.0 (2)	2.364 (7)	0.017(1)
Al	1.2 (2)	3.06 (2)	0.015(5)

The data in the above table shows that on average, the nickel atoms in the mixture had a first coordination shell of 2 phosphorus atoms at 2.11Å, followed by a second coordination shell of 2 bromine atoms at 2.364 Å. In addition, an aluminium shell of 1.4 aluminium atoms was seen at 3.07 Å suggesting Ni-Br-Al bridges could have been present in the species in solution. The P, Br, and the Al shells were all found to improve the fit significantly at 1% probability. The solution may therefore contain an adduct species of the type shown in Figure 6.13, along with some starting material.

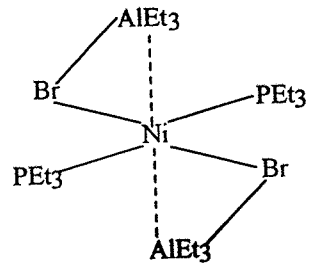

Figure 6.13. Figure showing a possible nickel species present in a solution of $NiBr_2(PEt_3)_2/AlEt_3$ (Ni:Al 1:6, [Ni]= 70mM) in *p*-fluorotoluene at room temperature.

The Br-K-edge spectrum of the same mixture at room temperature was obtained in a completely separate experiment. Figure 6.14 shows the fitted Br-K-edge EXAFS data (4000 scans, scan duration= 150 ms) of $NiBr_2(PEt_3)_2/AlEt_3$ (Ni:Al 1:6, [Ni]= 70mM) in *p*-fluorotoluene obtained at room temperature.

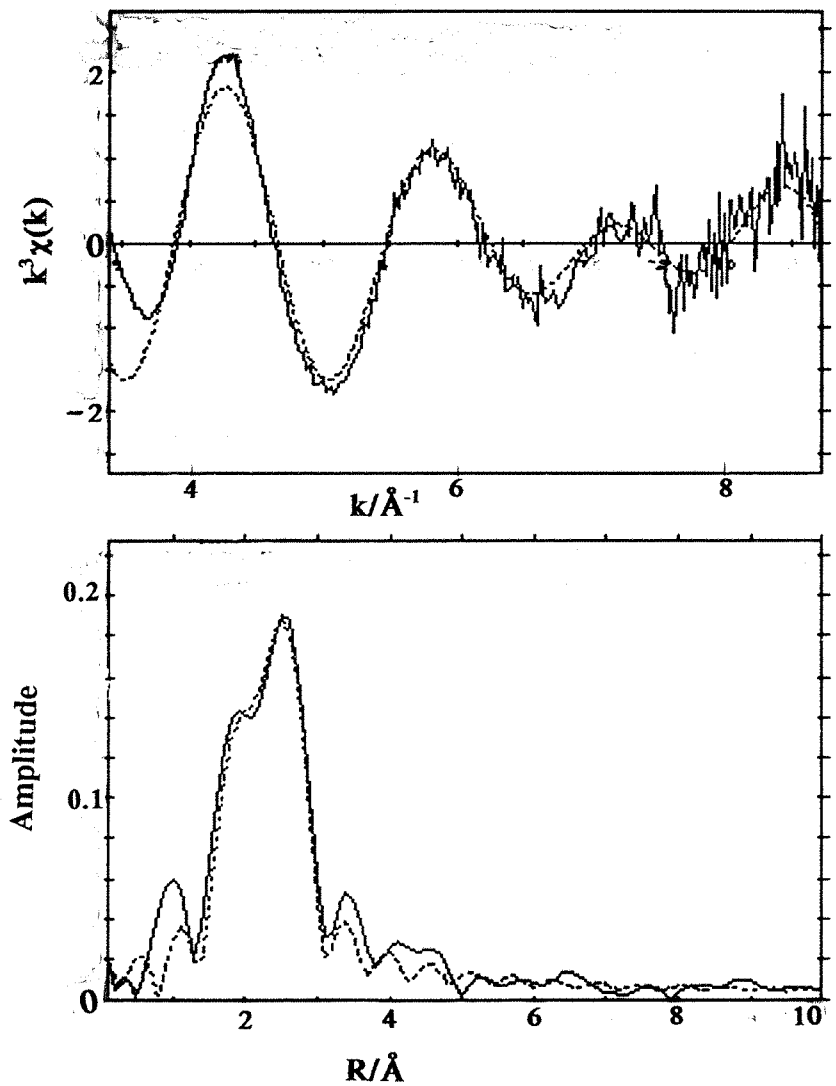

Figure 6.14. Figure showing the fitted Br-K-edge EDEXAFS data (4000 scans, scan duration= 150 ms) and Fourier transform of $NiBr_2(PEt_3)_2/AlEt_3$ (Ni:Al 1:6, [Ni]= 70mM) in *p*-fluorotoluene at room temperature.

Table 6.7. Table showing the parameters obtained from the fitted Br-K-edge EDEXAFS data (4000 scans, scan duration= 150 ms) and Fourier transform of $NiBr_2(PEt_3)_2/AlEt_3$ (Ni:Al 1:6, [Ni]= 70mM) in *p*-fluorotoluene at room temperature.

EF= 3.5(7), AFAC= 0.7, R= 37.6%.

	Coordination number	R/Å	$\sigma^2/Å^{-1}$
Al	0.92 (4)	2.197 (7)	0.005 (1)
Al	1.9 (1)	2.416 (7)	0.0111 (10)

As can be seen from the parameters in the above table, the average coordination around the bromine atom in the reaction mixture consisted of one aluminium atom at 2.197 Å and two further aluminium atoms at 2.416 Å. It is possible a number of aluminium bromide species with varying Al-Br distances may have been formed in solution as shown in Figure 6.15.

$$Al_2Br_6 \rightleftharpoons AlBr_4^- + AlBr_2^+$$

Figure 6.15. Possible aluminium bromide species formed in a solution of $NiBr_2(PEt_3)_2/AlEt_3$ (Ni:Al 1:6, [Ni]= 70mM) in *p*-fluorotoluene at room temperature.

It is clear from the EXAFS data, that whatever other species may have been present in the reaction mixture there was no large atom coordination, as the data could not be fitted to any atoms other than aluminium atoms.

A comparision of the raw spectra of the Br-K-edge of the $NiBr_2(PEt_3)_2/AlEt_3$ (Ni:Al 1:6, [Ni]= 70mM) in *p*-fluorotoluene obtained at room temperature (as

fitted in Figure 6.14 and Table 6.6) and the starting material ($NiBr_2(PEt_3)_2$ 140mM in *p*-fluorotoluene) is shown in Figure 6.16.

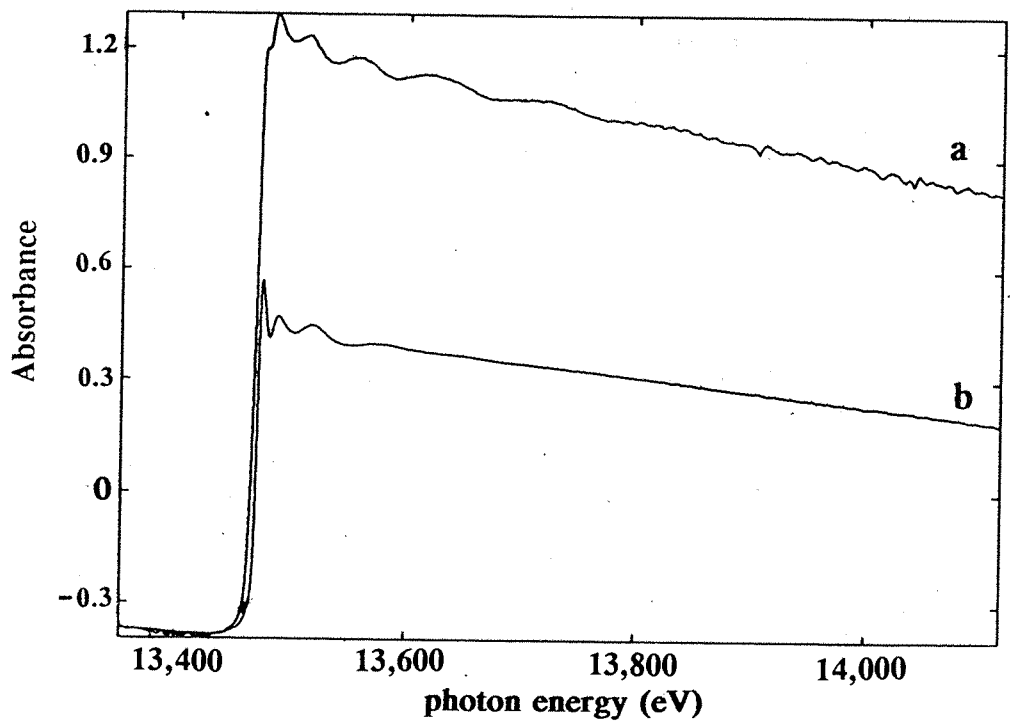

Figure 6.16. Figure showing a comparision of the Br-K-edge EDEXAFS spectrum of a) $NiBr_2(PEt_3)_2$ (140mM in *p*-fluorotoluene) with the Br-K-edge EDEXAFS spectrum of b) $NiBr_2(PEt_3)_2/AlEt_3$ (Ni:Al 1:6, [Ni]= 70mM) in *p*-fluorotoluene at room temperature.

As can be seen from the comparision of the bromine-K-edge before and after the addition of $AlEt_3$, there was a considerable change in the EXAFS and XANES region on addition of $AlEt_3$ showing that reaction had occurred. The lack of oscillations at higher energy after addition of $AlEt_3$ would indicate the loss of nickel coordination and replacement by lighter atoms.

6.8. Ni- and Br-K-edge QUEXAFS and EDEXAFS spectra of $NiBr_2(PEt_3)_2$/ $AlEt_3$ in the presence of hex-1-ene:

i) at low temperature:

Figure 6.17 shows the fitted Ni-K-edge EDEXAFS spectrum (10 scans, scan duration= 2 minutes) and Fourier transform of $NiBr_2(PEt_3)_2/AlEt_3$/hex-1-ene (Ni:Al:hex-1-ene 1:6:20, [Ni]= 70mM) mixture in *p*-fluorotoluene obtained at -5°C. Table 6.7 shows the parameters obtained from the fitted spectrum.

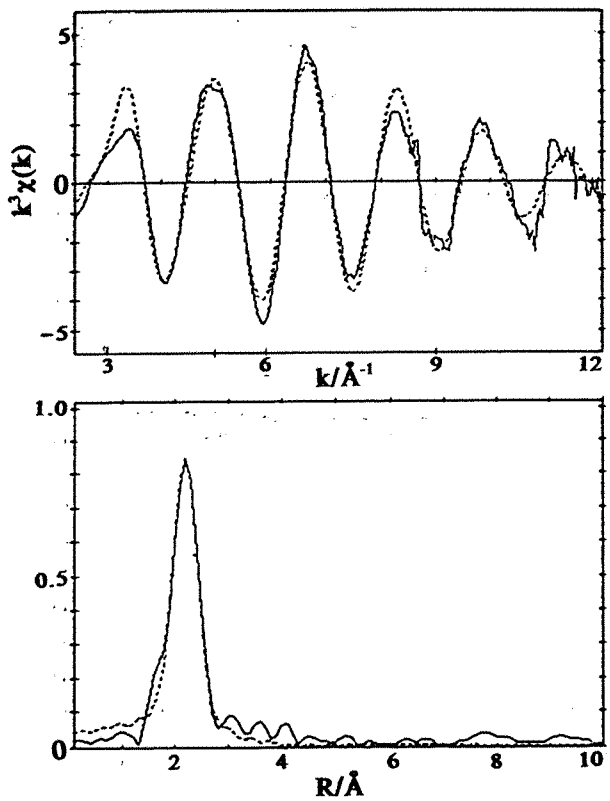

Figure 6.17. Figure showing the fitted Ni-K-edge QUEXAFS spectrum (10 scans, scan duration= 2 minutes) and Fourier transform of $NiBr_2(PEt_3)_2$/ $AlEt_3$/hex-1-ene (Ni:Al:hex-1-ene 1:6:20, [Ni]= 70mM) mixture in *p*-fluorotoluene obtained at -5°C.

Table 6.8. Table showing the parameters obtained from the fitted Ni-K-edge EDEXAFS spectrum (10 scans, scan duration= 2 minutes) and Fourier transform of $NiBr_2(PEt_3)_2/AlEt_3$/hex-1-ene (Ni:Al:hex-1-ene 1:6:20, [Ni]= 70mM) mixture in *p*-fluorotoluene obtained at -5^{0}C.

EF= -4.2(6), AFAC= 0.7, R= 23.3%.

	Coordination number	R/Å	σ^2/Å^{-1}
C	0.9 (2)	1.95 (1)	0.009 (3)
P	2.1(1)	2.209 (6)	0.0120 (8)
Br	1.08 (9)	2.367 (6)	0.021 (6)

The parameters in the above table show that the average coordination around the central nickel atom consisted of one carbon atom, two phosphorus atoms and one bromine atom. A possible intermediate species therefore indicated at low temperatures is as shown in Figure 6.18.

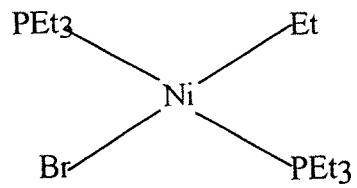

Figure 6.18. Figure showing a possible species present in solutions of $NiBr_2(PEt_3)_2/AlEt_3$/hex-1-ene at -5^{0}C.

Although it is clear that there was carbon coordination, the exact nature of the carbon shell i.e. length of alkyl group was difficult to ascertain. Since the coordination numbers were not integral values a mixture of species may have been present.

Figure 6.19 shows the fitted Br-K-edge EDEXAFS data of the same mixture obtained at -12^{o}C and its Fourier transform.

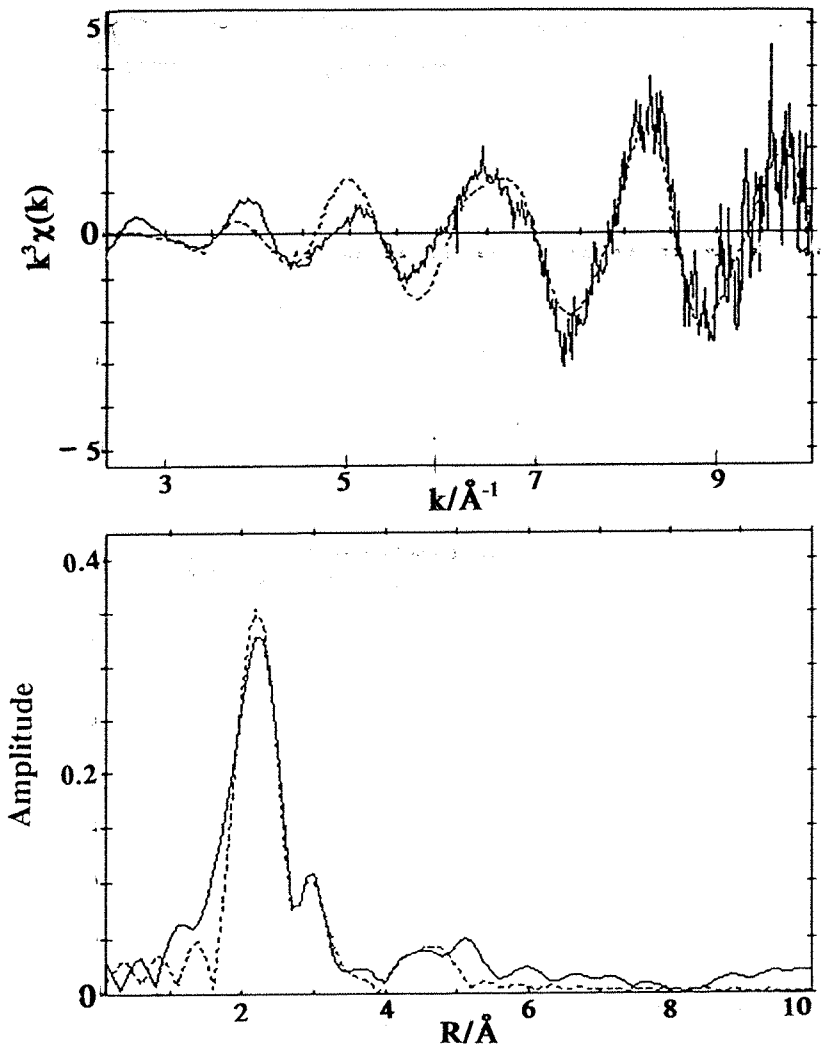

Figure 6.19. Figure showing the fitted Br-K-edge EDEXAFS data (4000 scans, scan time= 46 ms) and Fourier transform of $NiBr_2(PEt_3)_2/AlEt_3$/hex-1-ene (Ni:Al:hex-1-ene 1:6:20, [Ni]= 70mM) mixture in *p*-fluorotoluene obtained at -12^{o}C.

Table 6.9. Table showing the parameters obtained from the fitted Br-K-edge EDEXAFS data (4000 scans, scan time = 46 ms) and Fourier transform of $NiBr_2(PEt_3)_2/AlEt_3$/hex-1-ene (Ni:Al:hex-1-ene 1:6:20, [Ni]= 70mM) mixture in *p*-fluorotoluene obtained at -12^{0}C.

EF=-10.62 (1.04), AFAC= 0.9, R= 46.7%.

	Coordination number	R/Å	σ^2/ Å^{-1}
Ni	0.74 (2)	2.302 (5)	0.0095 (4)
P	0.66 (9)	3.24 (1)	0.010 (2)
Br	0.6 (1)	4.51(1)	0.010 (3)

The results show that the data could be fitted to a solution containing some $NiBr_2(PEt_3)_2$. Since the coordination numbers were lower than expected for a solution containing only starting material, it is possible that some of the bromine in the solution may have existed as another species e.g. bromide ions which have no EXAFS. The fit does not improve on adding aluminum atoms to the coordination sphere and it is therefore unlikely that there was any aluminium bromide in the solution. It was also difficult to fit the spectrum to any other combination of atoms. Also increasing the coordination numbers of the nickel, phosphorus and bromine atoms worsened the fit. It is therefore difficult to decide on the composition of this mixture except to say that it may have contained a mixture of some starting material and some bromide ions.

ii) *at room temperature*:

The bromine-K-edge EDEXAFS spectrum of the same mixture, at room temperature, revealed that there was virtually no EXAFS to the edge. This is shown

in Figure 6.20. It is possible that bromide ions had been formed from the nickel species subsequent to alkylation. This could be an explanation for the lack of any EXAFS.

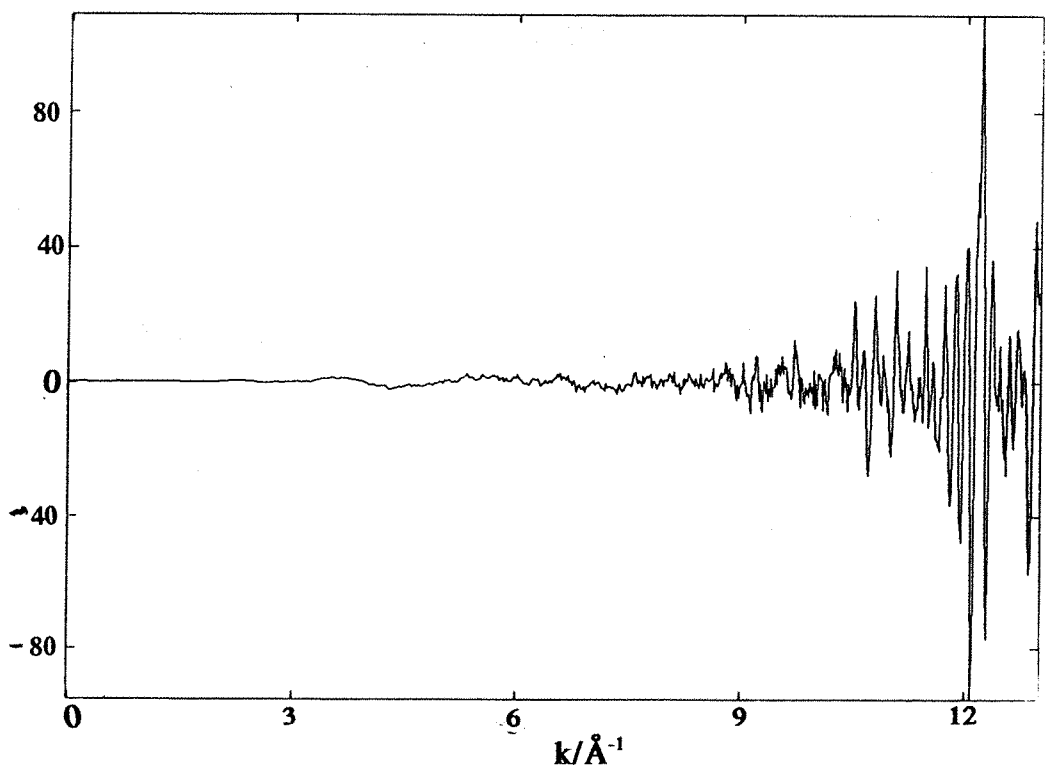

Figure 6.20. Figure showing the Br-K-edge EDEXAFS data (4000 scans, scan time= 24 ms) of $NiBr_2(PEt_3)_2/AlEt_3$/hex-1-ene (Ni:Al:hex-1-ene 1:6:20, [Ni]= 70mM) mixture in *p*-fluorotoluene obtained at room temperature.

6.9 CONCLUSIONS:

The electronic absorption spectroscopy results have shown that the reaction between $NiCl_2(PEt_3)_2/AlEt_3$ resulted in a stable new species with a possible oxidation state of Ni(I). This species could be tetrahedral. More evidence will be required to decide on the exact nature of this Ni(I) species. A similar Ni(I) species was indicated as having been formed in a solution of $NiBr_2(PEt_3)_2/AlEt_3$ despite the poor quality of the spectrum.

EDEXAFS data of $NiCl_2(PEt_3)_2/AlEt_3$ mixture at low temperatures indicated little change in the coordination sphere of the nickel atom compared to the starting material i.e. a first shell of 4 phosphorus atoms which could not be separated into two shells of 2 chlorine atoms and 2 phosphorus atoms. This was due to the similarity in phaseshifts of the two atoms. However, a shell of aluminium atoms was observed at the nonbonding distance of 3.15 Å. This is likely to be the result of Ni-Cl-Al bonds formed as a result of the $AlEt_3$ attacking the chlorine atoms of the starting material. Such a species is shown below.

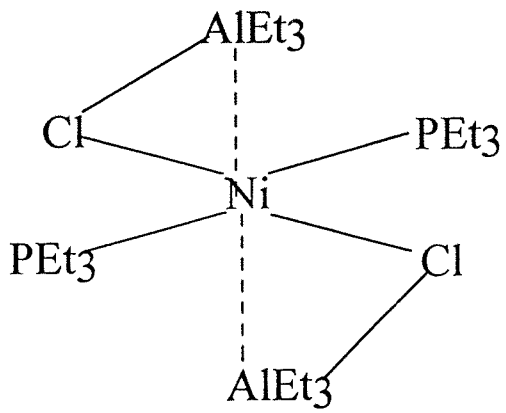

At room temperature this mixture was found to yield nickel metal clusters with nickel coordination seen at 2.460Å.

In the presence of hex-1-ene at $0^{o}C$, once again there was no change in the coordination sphere of the nickel atom compared to starting material. A shell of aluminium atoms could also not be identified indicating that the solution still contained mainly starting material. However, at room temperature, an aluminium shell was observed at 3.23 Å indicating that the $AlEt_3$ had begun attacking the halogenophosphine.

The reaction involving $NiBr_2(PEt_3)_2/AlEt_3$ did not proceed at all at low temperatures. At room temperature and within 4 minutes, it seemed from the Ni-K-edge that some adduct may have been formed between the nickel species and the aluminium species. This was clear from the coordination of one aluminium atom seen at 3.102 Å, in addition to a shell of two phosphorus atoms at 2.131 Å and two bromine atoms at 2.371 Å, indicating the presence of Ni-Br-Al bridges. A possible structure for the adduct is shown below:

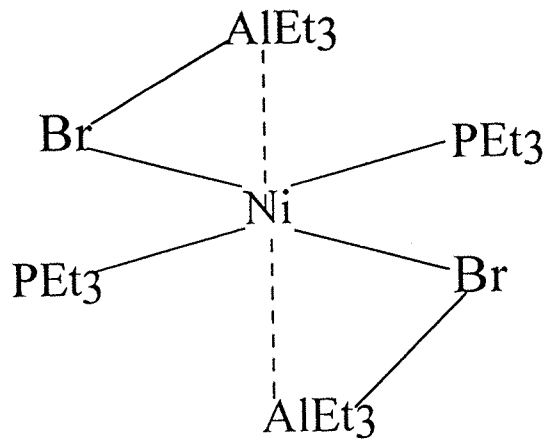

The reaction was not studied after 4 minutes and so any further loss of bromine atoms from the nickel coordination sphere could not be observed.

The bromine-K-edge spectrum of the mixture taken 15 minutes after the mixing of the reagents indicated loss of nickel from the bromine coordination sphere and the possible formation of an aluminium bromide species.

The Ni-K-edge spectra of the catalyst mixture, $NiBr_2(PEt_3)_2/AlEt_3$, in the presence of hex-1-ene and at low temperatures, indicated the formation of the species shown below:

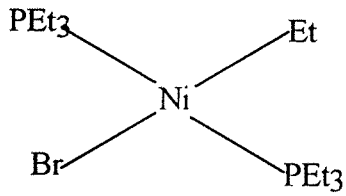

The bromine -K-edge of the same mixture at low temperature confirmed the presence of some nickel and phosphine coordination around the bromine atom. At room temperature, the formation of bromide ions was indicated by the lack of any oscillations in the Br-K-edge EXAFS of the mixture.

The results presented in this chapter indicated the extent to which EXAFS (EDEXAFS and QUEXAFS) can be used to obtain information about the coordination sphere of a metal atom in a catalyst mixture. Although mixtures are difficult to look at, still EXAFS provides considerable evidence as to the direction the reaction is taking by following any changes in the coordination sphere of the metal atom i.e. nickel in this case.

6.10. REFERENCES

1. J.M.Corker, PhD Thesis, University of Southampton, 1991.
2. W.Levason, 'The Chemistry of Organophosphorus Compounds', F.R.Hartley., Ed., Wiley, New York, Vol 1, 1990.
3. G.Booth, *Adv.Inorg.Chem.Radiochem.*, 1964, **61**, 1.
4. P.L.Goggin and R.J.Goodfellow, *J.Chem.Soc.A.*, 1966, 1462.
5. K.Shobotake and K.Nakamoto, *J.Am.Chem.Soc.*, 1970, **92**, 3332.
6. K.A.Jensen, P.H.Nielsen and C.Pedersen, *Acta.Chem.Scand.*, 1963, **17**, 1115.
7. M.Uchino, Y.Chauvin and G.Lefebvre, *C.R.Acad.Sc.Paris.*, 1967, **265**, C-103.
8. G.G.Eberhardt and W.P.Griffin, *J.Catal.*, 1970, **16**, 245.
9. G.G.Eberhardt and H.K.Myers, *J.Catal.*, 1972, **26**, 459.
10. J.R.Briggs, *J.Chem.Soc., Chem.Commun.*, 1989, 674.
11. H.Leach, PhD Thesis, University of Southampton, 1990.
12. J.Evans, J.T.Gauntlett and H.Leach, *J.Physique.*, 1986, **47**, C8-327.
13. P.W.Jolly and G.Wilke, 'The Organic Chemistry of Nickel', Academic Press, New York, 1974, Vol2, P21.
14. J.M.Corker and J.Evans, *J.Chem.Soc.Chem.Comm.*, 1991, **16**, 1104.
15. P.W.Jolly and G.Wilke, 'The Organic Chemistry of Nickel', Academic Press, New York, 1974, Vol2, P3.
16. P.W.Jolly and G.Wilke, 'The Organic Chemistry of Nickel', Academic Press, New York, 1974, Vol2, P1.
17. P.W.Jolly and G.Wilke, 'The Organic Chemistry of Nickel', Academic Press, New York, 1974, Vol2, P7,9.
18. G.E.Derbyshire, W.I.Helsby, A.J.Dent, S.A.Wright, R.C.Farrow, G.N.Greaves, C.Morrell and G.J.Baker, *Adv.X-ray.Analysis.*, 1990, **34.**
19. D.Bogg, A.J.Dent, G.E.Derbyshire, R.C.Farrow, C.A.Ramsdale and G.Salvini, *Nucl.Instr.Meth.*, 1993, **390**, 461.
20. G.Salvini, D.Bogg, A.J.Dent, G.E.Derbyshire, R.C.Farrow, A.Felton, and C.Ramsdale, *Physica B.*, 1995, **209**, 229.

21. R.Frahm and J.Wong, *Jpn.J.Appl.Phys.*, 1993, **32,** 188.

22. B.R.Dobson, S.Hasnain, M.Neu, C.A.Ramsdale and L.Murphy, *Jpn.J.Appl.Phys.*, 1993, **32,** 192.

23. `Comprehensive Inorganic Chemistry', Eds. J.C.Bailar, H.J.Emeleus, R.Nyholm, and A.F.Trotman-Dickenson, Pergamon Press, 1973, Vol3, Chapter 42.

24. A.B.P.Lever, "Inorganic Electronic Spectroscopy", Elsevier, 1968.

25. M.Aresta, C.F.Noble and A.Sacco., *Inorg.Chim.Acta.*, 1975, **12,** 167.

26. L.Sacconi and S.Midollini, *J.Chem.Soc., Dalton Trans.*, 1972, 1213.

CHAPTER 7. EXAFS AND QUEXAFS STUDIES OF THE PALLADIUM CATALYSTS FOR THE HECK REACTION.

7.1 Introduction to the Heck reaction:[1]

The palladium catalysed vinylation provides a convenient method of forming carbon-carbon bonds at unsubstituted vinylic positions. It is a useful method for the synthesis of a variety of olefinic compounds. The reaction generally does not require anhydrous or anaerobic conditions although limitation of the access of oxygen is advisable when arylphosphines are used as a component of the catalyst. The transformation is invaluable because it cannot be carried out in a single step by any other known method (except in certain Meerwein reactions).

The general reaction is as shown below:

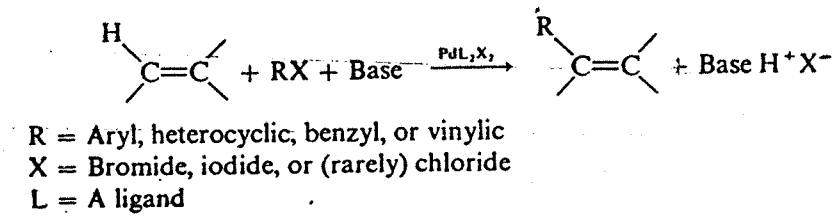

R = Aryl, heterocyclic, benzyl, or vinylic
X = Bromide, iodide, or (rarely) chloride
L = A ligand

Figure 7.1. Figure showing the general reaction for the palladium catalysed vinylation of organic halides.

During the seventies and eighties, a few research groups explored the scope and limitations of the method.[2,3,4,5,6] The organic halide employed is limited to aryl, heterocyclic, benzyl or vinyl types with bromides and iodides used most often[7,8,9]. Halides with easily eliminated β-hydrogen atoms (i.e. alkyl derivatives) cannot be used as they form olefins by elimination under normal conditions. The base needed may be a secondary or tertiary amine, sodium or potassium acetate, carbonate or bicarbonate.

When nucleophilic secondary amines are used as co-reactants with most vinylic halides, a variation occurs that often produces tertiary allylic amines as the major products. This is shown in Figure 7.2.

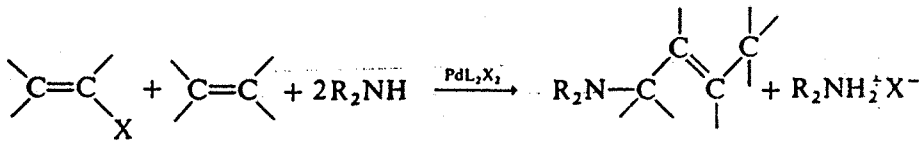

Figure 7.2. Figure showing the effect of nucleophilic secondary amines on the Heck reaction.

A range of olefins can be used in the Heck reaction. A primary factor in determining the reactivity of the olefin is the size and number of substituents on the double bond carbon atoms. Ethene is the most reactive olefin.[10]

The catalyst is commonly palladium acetate, although palladium chloride or preformed triarylphosphine palladium complexes, as well as palladium on charcoal have been used. A reactant, product or solvent may serve as ligand L in reactions involving organic iodides, but generally a triarylphosphine or a secondary amine is required when organic bromides are used.

The reaction occurs between 50°C and 160°C and proceeds homogeneously. Temperatures up to 160°C can be used before the reactions become heterogeneous and metal is precipitated.[11]

Amines are often used as bases as specific solvents are necessary to dissolve other inorganic bases e.g. dimethylformamide has been used to dissolve potassium carbonate[12] and methanol has been used to dissolve sodium acetate[13].

Solvents such as N-methylpyrrolidinone, acetonitrile, dimethylformamide, methanol, and hexamethylphosphoramide are used but are not necessary.

There are several other variations of the reaction in which the organic halide is replaced with reagents such as organometallics, diazonium salts or aromatic hydrocarbons

Other related reactions such as the palladium catalysed replacement of allylic substituents with carbanionic reagents[14], the palladium promoted nucleophilic substitution at olefinic carbons[15,16] and the palladium catalysed coupling reactions of halides and organometallics[17] have not been dealt with in this chapter.

7.2 Mechanism of the Heck reaction:

Stoichiometric reactions with organopalladium compounds indicate that they are involved in the vinylic substitution[7,18]. A possible scheme for the mechanism is shown in Figure 7.3. It is thought that under the reaction conditions, the palladium (II) complex is reduced to give finely divided palladium metal by oxidising some of the olefin present[19]. The finely divided metal then reacts with the organic halide intermediate. The organopalladium complex then adds to the double bond of the olefin. The resulting adduct is then thought to undergo elimination of a hydridopalladium halide if an sp^3-bonded hydrogen atom is present β to the palladium group. The reaction is catalysed in the presence of a base because the hydridopalladium halide dissociates reversibly and the base shifts the equilibrium to the palladium(0) species. This latter compound then rereacts with the organic halide and the cycle begins again.

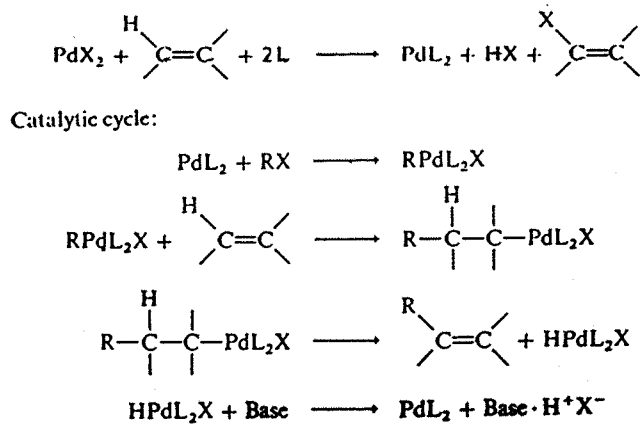

Figure 7.3. Figure showing a possible mechanism for the palladium catalysed vinylation of organic halides.

Today, a coordinatively unsaturated 14-electron palladium(0) species, usually coordinated with labile donor ligands (tertiary phosphines) is assumed to be the catalytically active complex[20]. This complex is normally generated in situ. Tetrakis(triphenylphosphine) palladium(0)[21], which forms a tris(triphenylphosphine) palladium(0) complex in solution, is frequently employed.[22]

A more detailed mechanism for the Heck reaction is given in Figure 7.4.[20]

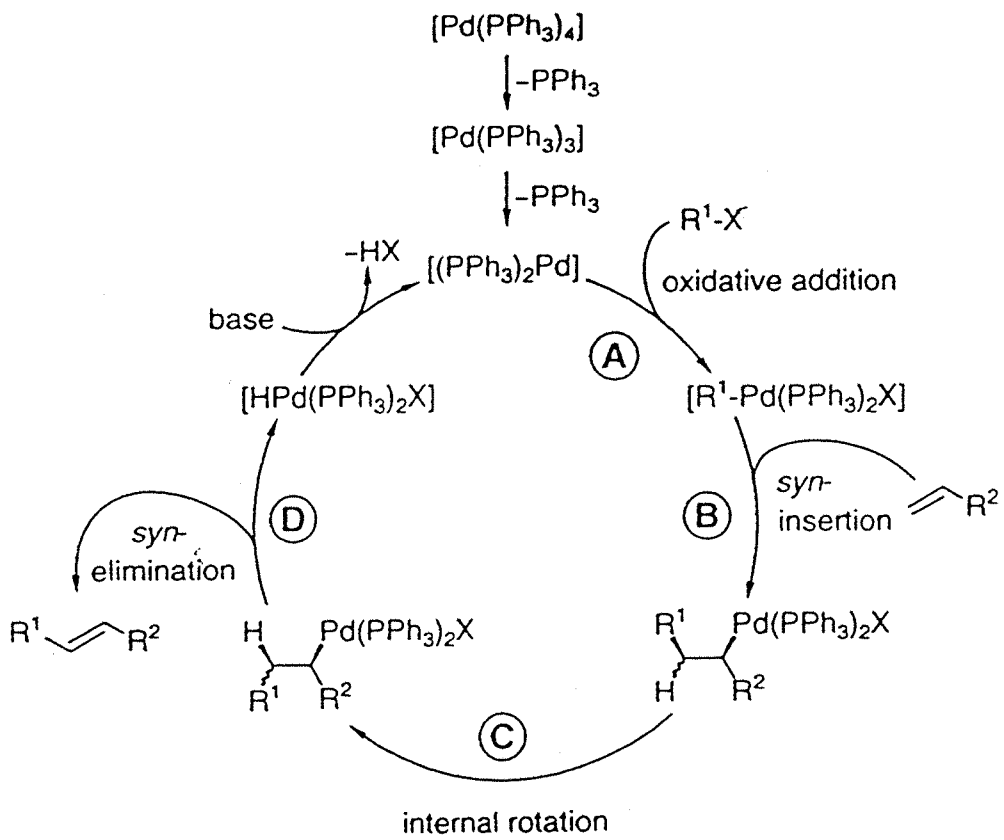

Figure 7.4. Figure[20] showing a schematic diagram of the mechanism of the Heck reaction. R^1= alkenyl, aryl, R^2= aryl, alkyl, alkenyl, CO_2R', R'= alkyl, X= I, Br(Cl), OSO_2CF_3.

As shown in the schematic diagram in Figure 7.4, the catalytically active species, bis(triphenylphosphine)palladium(0) is generated after endergonic loss of a phosphine ligand[23] from tris(triphenylphosphine)palladium(0) complex. The complex bis(triphenylphosphine)palladium (0) is a well characterised compound.[24,26]

Palladium(II) salts, such as palladium acetate or bis(triphenylphosphine) palladium dichloride, which can be reduced in the reaction medium are commonly used. A discussion of the reducing agent is further given by Hayashi *et al.*[25]

In the first step of the cycle shown in Figure 7.4, haloalkenes and haloarenes are commonly assumed to oxidatively add to bis(triphenylphosphine)palladium(0) generating a σ-alkenyl or σ-aryl palladium(II) complex. This reaction should lead to the thermodynamically stable[26,27] trans-σ–alkenyl or aryl palladium complex in several steps[28,29,30] probably via a cis-σ-alkenyl or arylpalladium(II) intermediate.

Next, the alkene molecule is coordinated possibly after elimination of another phosphine ligand.[31] This is followed by insertion of the alkene into the σ-alkenyl or σ-aryl palladium bond[32] to give a σ-alkylated complex via a 4-centre transition state.

After the cis addition of the alkene, the reaction terminating β-hydride elimination[33,34,35] can occur only after internal rotation in the alkylpalladium species. In this way, the essential syn orientation of a β-hydrogen is provided for elimination. The catalyst is regenerated after reductive elimination of HX in the presence of base. The base is known to have a rate increasing effect as a ligand.[36]

Recently, palladium dispersions containing small metal particles (20-80Å) have been of increasing scientific interest.[37] They have been found to have superior catalytic properties for some organic reactions e.g. hydrogenation and dehyrohalogenation compared with molecular complexes.[37,38,39] Different methods for preparing palladium colloids are available.[40,41]

Colloidal palladium only shows good activity for activated aryl bromides e.g. 4-bromoacetophenone where the high turnover factors can be compared with the fastest Heck reactions of activated aryl bromides reported in literature.[42,43] For

deactivated aryl bromides and chlorides, palladium colloids show only very low activity, if any at all. In general, irreversible agglomeration of the metal leading to deactivated palladium species is observed here instead.

It was again shown in 1996 by Beller *et al.*[44] that palladium colloids are effective and active catalysts for the olefination of aryl bromides. It was found that the addition of phosphines strongly retards the reaction rate of the colloid catalyst. As mentioned before the study once again showed that this type of catalyst is not suitable for the activation of non-activated substrates e.g. technically interesting aryl chlorides.

The direction of addition of the organopalladium species to unsymmetrically substituted double bonds appears to be largely sterically controlled. The organic group of the organopalladium complex goes on the less substituted carbon atom of the double bond[45]. When allylic alcohols are used as the olefinic compound, carbonyl compounds are usually obtained as significant or exclusive products[46,47,48] as shown in the Figure 7.5 below.

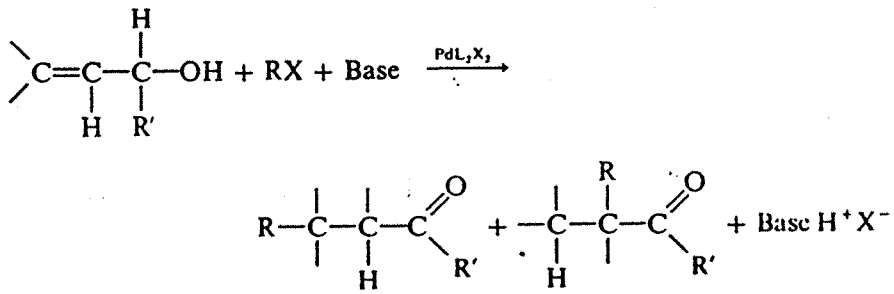

Figure 7.5. Figure showing the carbonyl products obtained from the palladium catalysed reaction between allylic alcohols and organic halides.

The carbonyl compounds result from palladium hydride elimination involving the β hydrogen atom on the hydroxyl bearing carbon atom. Rates of reaction of the allylic alcohols are generally higher than those of simple olefins, suggesting that hydroxyl coordination may be involved.

The mechanism of the reaction leading to carbonyl compounds is exemplified in the Figure 7.6 by the arylation of 3-buten-2-ol. A similar scheme was proposed for the olefin arylation reaction[7].

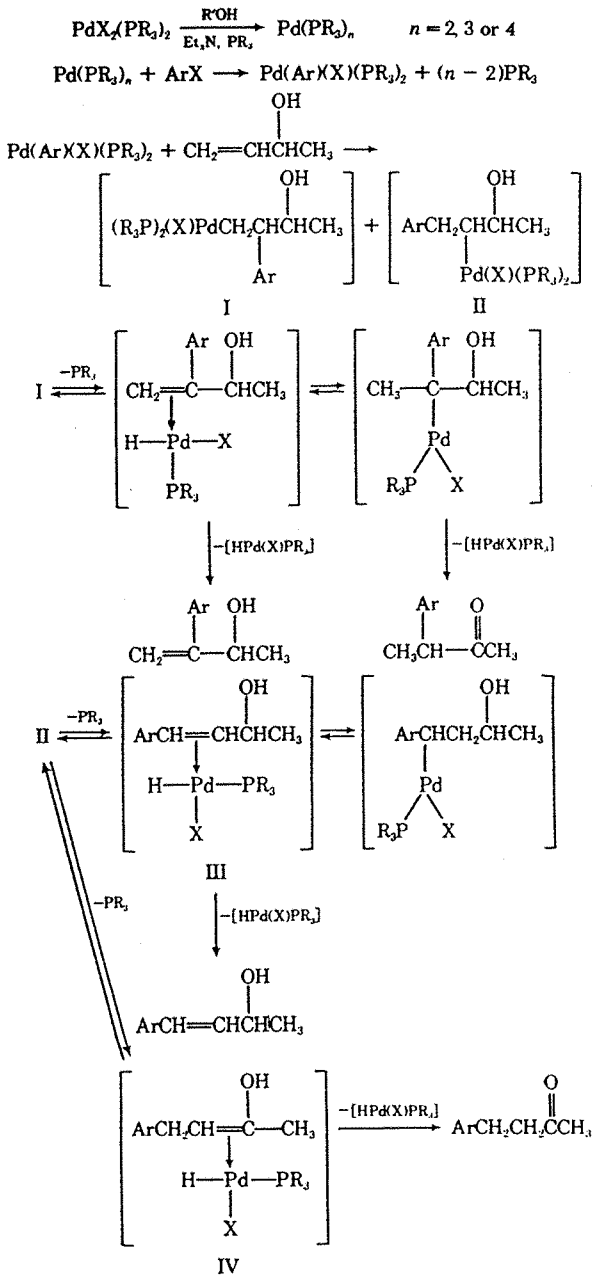

Figure 7.6. Figure showing a possible mechanism for the palladium catalysed arylation of 3-buten-2-ol.

Initially, the palladium(II) catalyst is thought to be reduced by the allylic alcohol to the true catalyst, a palladium(0)-triphenylphosphine complex or, in the case of palladium(II) acetate reactions, simply to finely divided palladium metal. In the latter reactions the precipitation of the palladium metal can be seen when the reactants are mixed together. The palladium(0) species then oxidatively adds the aryl halide to form an aryl palladium complex. The last complex then adds to the allylic double bond to give adducts I and II. These adducts then undergo elimination of the hydridopalladium group to form olefin π-complexes with the hydride. Dissociation at this stage produces the 2-aryl alcohol from I and either the 3-aryl alcohol or the 3-aryl carbonyl product from II. The presence of triphenylphosphine increases the rate of dissociation possibly by displacing the olefinic group from the metal in a second order reaction. If dissociation does not occur then readdition and elimination reactions of the hydride group occur leading ultimately to the carbonyl derivative at which point the reaction becomes irreversible. The dissociated free hydride rapidly decomposes, since once formed the unsaturated alcohols are generally stable in the reaction mixtures.

Chalk and Magennis[47,48] studied in detail the product distribution from reacting various isomers of methallylic alcohol and halobenzenes (X= I, Br) using a palladium chloride catalyst. The results are shown in Table 7.1. In all the cases shown in the Table 7.1, the halobenzene (50mmol) was reacted with of methallylic alcohol (75mmol) in the presence of sodium bicarbonate (60mmol) and palladium chloride (0.45mmol) in 20 ml of a solvent. This was NMP at 130°C when X= I and HMPA at 140°C for X= Br.

Table 7.1. Table showing the distribution of the products obtained by the reaction of iodobenzene and bromobenzene with various isomers of methallylalcohol.

Allylic alcohol	Time, hr	Halo-gen	Conversion, %	Product: 3-Aryl Carbonyl GC Yield, %	Product: 2-Aryl carbonyl GC Yield %	Other Products GC Yield %
$CH_2=C(CH_3)CH_2OH$	4	I	100	95	5	None
$CH_2=C(CH_3)CH_2OH$	4	Br	100	95	5	None
$CH_3CH=CHCH_2OH$	1	I	100	69	31	None
$CH_3CH=CHCH_2OH$	1.5	Br	93	69	31	None
$CH_2=CHCH(CH_3)OH$	2	I	100	100	---	None
$CH_2=CHCH(CH_3)OH$	2	Br	100	70	---	Unknown 30%.

Further work on the same reactants was carried out by Melpolder and Heck[46] this time using palladium acetate catalyst. The details are given in the Table 7.2. In all instances shown in the table the yields were determined using GLC and are based on the aryl halide used. All reactions were carried out in capped glass tubes under argon with acetonitrile as solvent and triethylamine as base. There was *ca.*400x excess of reactants (allylic alcohol and halobenzene) compared to palladium in these solutions.

Table 7.2. Table showing the products of the reaction between iodobenzene and bromobenzene with various isomers of methallylalcohol.

Allylic alcohol	Halo -gen	Time, Hr	Conversion, %	Product: 3-Aryl carbonyl Yield %	Product: 2-Aryl Carbonyl Yield %	Other Products Yield %
$CH_3CH=CHCH_2OH$	I	12	84	74	26	None
$(CH_3)_2C=CHCH_2OH$	I	96	51	62	3	Others 25.3%
$CH_2=C(CH_3)CH_2OH$	I	8	95	96	4	None
$CH_2=CHCHOHCH_3$	I	5	95	90	10	None
$CH_2=CHCHOHCH_3$	Br	35	95	50	2	Others 50%.

7.3 Objectives of this chapter:

In this chapter, we will be concerned primarily with EXAFS studies of catalyst structure in two main reaction mixtures. These are:

1) $Pd(OAc)_2$/methallylalcohol/iodobenzene/tri-n-butylamine/NMP

2) $Pd(OAc)_2/PPh_3$/bromobenzene/methallylalcohol/tri-n-Butylamine/NMP

The products expected from both these mixtures are detailed in the Table 7.2. The only difference between the mixtures used for the EXAFS experiments in this thesis and those detailed in Table 7.2 is that in the EXAFS experiments, NMP was used as solvent instead of acetonitrile and tri-n-butylamine was the base instead of triethylamine. In addition, the reactants i.e. methallylalcohol and halobenzene are only 50x in excess of the palladium complex compared to 400x in the catalytic runs

shown in Table 7.2. this was necessary to obtain a high enough concentration of the palladium complex to enable study by EXAFS.

Throughout this rest of this chapter the isomer of methallylalcohol that will be used is 2-methyl-2-propen-1-ol.

7.4 Equipment used for palladium catalyst studies:

The equipment shown in Figure 7.7 was used for all the EXAFS studies of palladium catalysts both in situ, in the reaction mixture and otherwise.

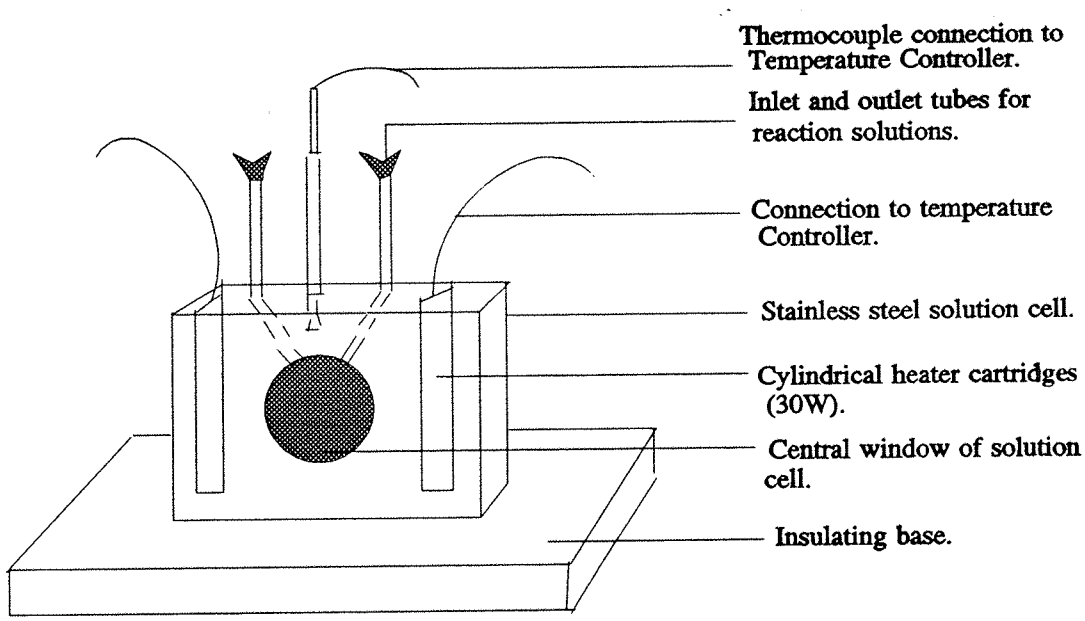

Figure 7.7. Figure showing the equipment required for in situ studies of palladium Heck reaction catalysts.

As can be seen from Figure 7.7, the equipment involved a cell consisting of kapton windows clamped against a central cell using clamping plates. The cell also had inlet and outlet tubes which allowed air sensitive transfer of solution into and out of the cell. The cell was heated using 30W heating cartridges placed in two cylindrical slots on either side of the central window. These could heat the solution in the cell to 65°C in *ca.*1 minute. The temperature of the cell was monitored by using a thermocouple located near the centre of the cell as shown in Figure 7.7. Both the heating cartridges and the thermocouple were connected to a central temperature controller. The cell was placed on an insulating plate which prevents heat loss from the cell. This setup was then placed in front of the X-ray beam for EXAFS studies. The cell could also be set at 45° for fluorescence EXAFS studies. The reaction solution could thus be studied at room temperature and then again at 65°C in the same cell.

7.5 Why fluorescence EXAFS and QUEXAFS ?

The studies of the palladium catalysts were carried out using fluorescence EXAFS and QUEXAFS. The reason for this is that the solubilty of the palladium acetate in most solvents was low and the low concentration of the palladium salt in solution was better suited for fluorescence studies than transmission EXAFS studies. This was because at low concentrations the absorption of the liquid (which contained bromine or iodine atoms) became important and this affected the quality of the EXAFS data obtained.

While QUEXAFS scans enabled fast acquisition of data, these scans could also be averaged to obtain better data quality . EDE was not yet possible on the palladium edge at Daresbury as palladium mirrors were used in the focussing of the beam for EDE experiments here. In addition, the Bragg geometry monochromator provided very poor resolution at the Pd-K-edge. So the studies had to be restricted to QUEXAFS and EXAFS.

All the EXAFS studies were carried out on Station 9.3 at the SRS in Daresbury. Although the ESRF at Grenoble has the facilities for carrying out palladium edge EDE studies these were not possible due to lack of time.

EXCALIB: This was the program used for averaging a number of QUEXAFS spectra of the same product. It can be accessed at Daresbury laboratory and involved the simple input of data e.g. file number, mode of acquisition and detector details. Once averaged, the data was background subtracted using PAXAS in the same way as described in Chapter 2.

7.6 EXAFS spectrum of palladium foil:

An EXAFS spectrum of palladium foil was run before starting the experiments on the Heck reaction. This enabled us to see the EXAFS parameters obtained using palladium foil. The spectrum consisted of a single scan obtained in thirty minutes. Upto 16 $Å^{-1}$ of data was obtained. The spectrum is shown in Figure 7.8.

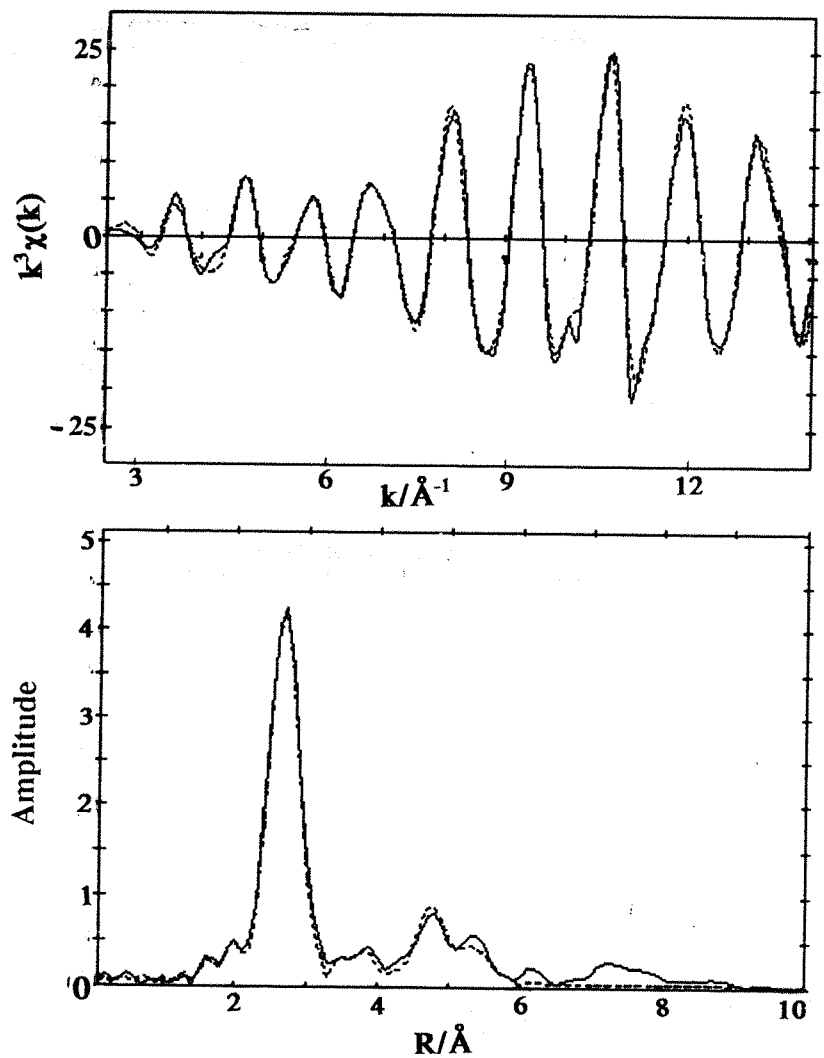

Figure 7.8. Figure showing the fitted palladium-K-edge EXAFS data (one scan, scan time= 31 minutes) of palladium foil and its Fourier transform.

Table 7.3. Table showing the parameters obtained from the fitted palladium-K-edge EXAFS spectrum of palladium foil.

EF= 1.1 (2), AFAC= 0.80, R= 13.7%.

Atom type	Coordination number	FCC Coordination number	R/Å	FCC R/Å	$\sigma^2/Å^{-1}$
Pd	12.1(1)	12	2.739 (1)	2.751	0.0096 (1)
Pd	6.7 (6)	6	3.854 (5)	3.890	0.019 (1)
Pd	21.3 (10)	24	4.765 (3)	4.764	0.0154 (4)
Pd	6.4 (4)	-	5.385 (4)	-	0.0064 (6)

Table 7.1 shows the parameters obtained from the EXAFS spectrum of palladium foil. The structural parameters obtained in the table compare well to values based on the FCC structure of palladium metal.

Thus, in future palladium edge study of reaction mixtures, the presence of a palladium shell at 2.75 Å, 3.89 Å, and 4.76 Å may indicate the formation of some palladium metal in solution.

7.7 EXAFS analysis of palladium acetate:

Palladium acetate is the starting material for all the catalyst mixtures looked at in this chapter. It is known to exist as a trimer in the solid state.[49] Figure 7.9 shows the trimeric structure.

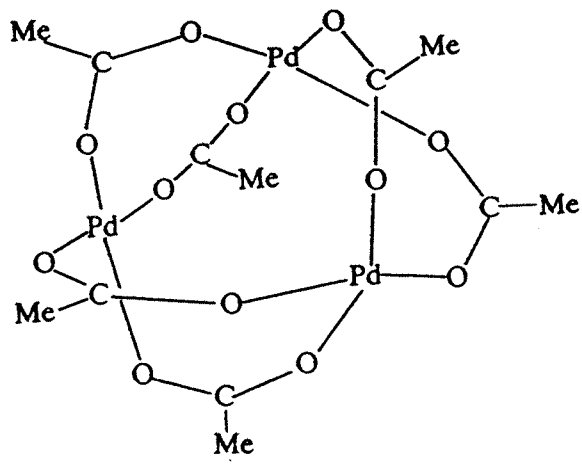

Figure 7.9. Figure showing the trimeric structure of palladium acetate.[49]

The molecules are known to consist of a nearly equilateral triangle of palladium atoms (*ca.* 3.15 Å apart) which are joined together by double acetate bridges such that the coordination at the metal atoms is approximately square planar. A certain amount strain is involved in the structure and this is a possible explanation for the relatively low stabilty of the trimeric molecule.[51] No metal-metal bonding is involved, the position of the metal atoms being a compromise between the square planar coordination and reasonable angles at the coordinating oxygen atoms. X-ray crystallography studies found that the Pd-Pd distances range between 3.105 Å and 3.203 Å (See Table 7.2). These ranges are thought to reflect the slight distortions caused by the packing requirements.

Table 7.4. Table showing the main X-ray crystallography parameters obtained on trimeric palladium acetate.[49]

	Range	σ	No. of independent values	Average
Pd-O	1.973-2.014 Å	0.009 Å	24	1.992 Å
Pd-Pd (non-bonded)	3.105-3.203 Å	0.001 Å		
Pd-O-C	127.8-133.2°	0.8°	24	130.3°
O-C-O	124.8-128.7°	1.1°	12	126.4°
O-Pd-*trans*-O	163.5-168.9°	0.4°	12	166.4°

It was decided as part of the initial experiments to obtain the EXAFS spectrum for palladium acetate in the solid state (as a 10% mixture with boron nitride). This is shown in Figure 7.10.

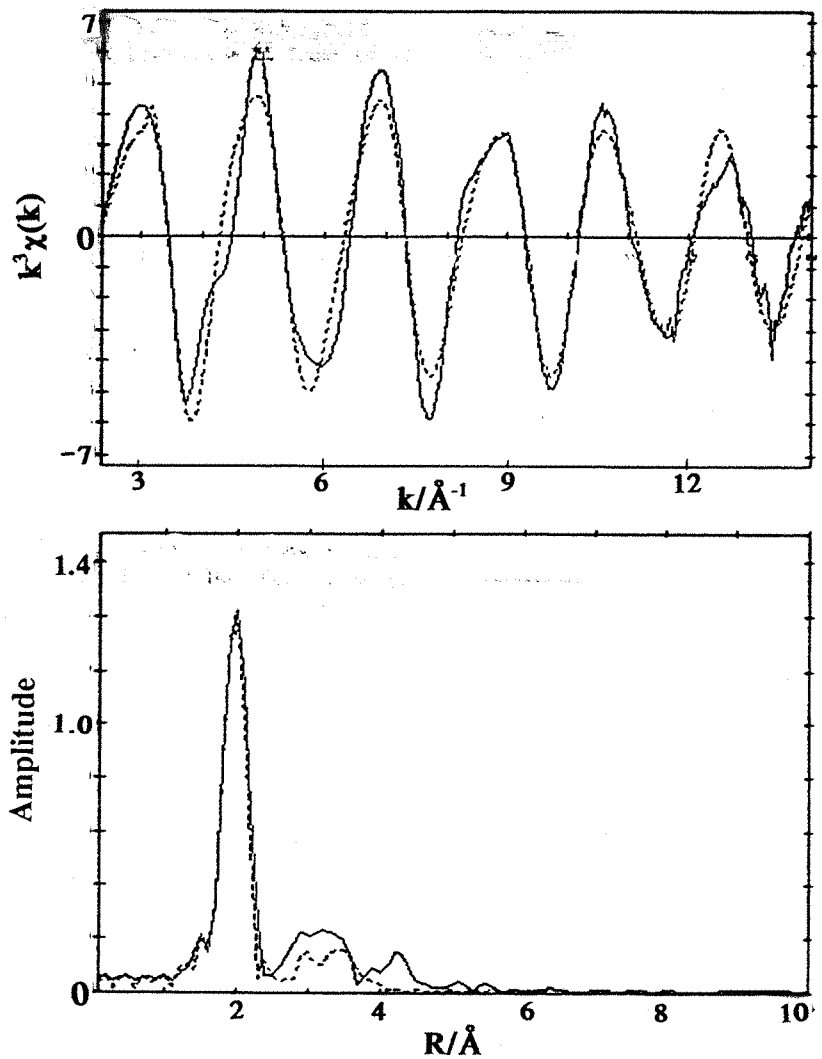

Figure 7.10. Figure showing the fitted Pd-K-edge EXAFS spectrum (one scan, scan time= 46 minutes) of $Pd(OAc)_2$ (10% in boron nitride), and its Fourier transform.

The parameters obtained from the fitted curves as shown in Figure 7.10 are given in Table 7.5.

Table 7.5. Table showing the parameters obtained from the fitted palladium-K-edge EXAFS spectrum of $Pd(OAc)_2$ (10% in boron nitride) shown Figure 7.10 and some corresponding X-ray crystallography data.

EF= -2.56 (28), AFAC= 0.8, R= 25.4%.

Shell Coordinates	O	Pd
EXAFS C.N	4.10 (7)	2.1 (3)
X-ray C.N[49]	4	2
EXAFS R/Å	1.995 (1)	3.113 (8)
X-ray R/Å[49]	1.973-2.014 (9)	3.105-3.203 (1)
$\sigma^2/Å^{-1}$	0.0028 (2)	0.022 (2)

As can be seen from the table above, the EXAFS data from the spectrum of palladium acetate in the solid state compare well with X-ray crystallographic data.[49] The data has confirmed the existence of palladium acetate as a trimer in the solid state. As expected, the palladium atoms had a first coordination shell four oxygen atoms at 1.995 Å, and two palladium atoms were seen at 3.113 Å.

Since all the experiments of the palladium acetate reaction mixtures were to be carried out in a solution of NMP, therefore a QUEXAFS spectrum of palladium acetate in NMP solvent was also obtained. The fitted QUEXAFS data is shown below in Figure 7.11 and the parameters obtained from it are given in Table 7.6.

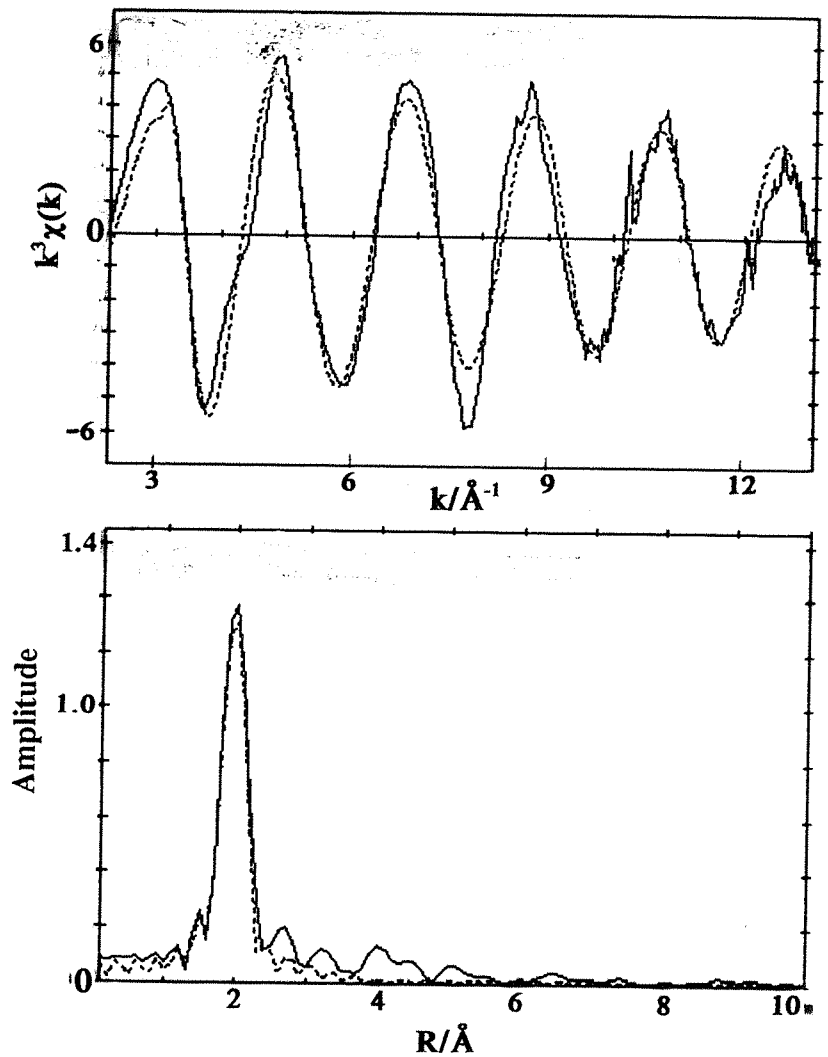

Figure 7.11. Figure showing the palladium-K-edge QUEXAFS data (one scan, scan time= 5 minutes) of $Pd(OAc)_2$ (70mM in NMP) and its Fourier transform.

Table 7.6. Table showing the parameters obtained from the fitted QUEXAFS data of $Pd(OAc)_2$ (70mM in NMP solvent).

EF= -1.1 (3), AFAC= 0.8, R= 24.6%.

Atom Type	C.N	R/Å	$\sigma^2/Å^{-1}$
O	4.37 (7)	1.998 (2)	0.0038 (3)

Generally, the acetate may exist in monomeric, dimeric, or trimeric forms in solution depending on the solvent used.[50] In a solution with NMP (N-methylpyrrolidinone), the QUEXAFS spectrum in Figure 7.6, showed a first coordination shell of only 4 oxygen atoms at 1.998 Å. A subsequent shell of two palladium atoms at 3.15Å was not seen indicating that the trimeric structure of palladium acetate had broken down in solution. As no palladium shell could be fitted to the data it is likely that the acetate existed as a monomer in NMP solvent. The presence of an oxygen coordination shell of four atoms suggested that a possible structure for the palladium acetate in solution could be as shown below in Figure 7.12.

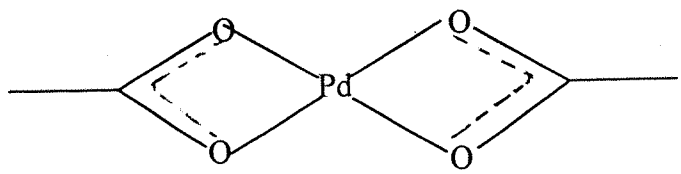

Figure 7.12. Figure showing a possible monomeric structure for palladium acetate in NMP solvent.

7.8. Studies of catalyst reaction mixture I: $Pd(OAc)_2$/NMP/ /iodobenzene/2-methyl-2-propen-1-ol /tri-n-butylamine :

i) Introduction:

A mixture of $Pd(OAc)_2$/NMP/iodobenzene/2-methyl-2-propen-1-ol/tri-n-butylamine using the molar ratio 1/60/50/50/36, [Pd]= 41mM, was prepared at room temperature using $Pd(OAc)_2$ (15mg) in NMP (4 ml), iodobenzene (4 ml), methallylalcohol (3 ml), tri-n-butylamine (6 ml). The acetate was first dissolved in NMP to give a light brown solution. On subsequent addition of iodobenzene, tri-n-butylamine and methallyl alcohol, to the acetate solution, in that order, a deep red solution resulted. On heating the red solution to 70°C for 5-10 minutes the deep red solution turned yellow in colour. On leaving the yellow solution to cool overnight it reverted back to the red colour. It is worth noting that when the methallyl alcohol was added to the palladium acetate/NMP solution prior to the addition of iodobenzene, colloidal palladium seemed to form which on subsequent addition of iodobenzene and on leaving overnight dissolved once again give the red solution. But in order to avoid complications, this reaction mixture was always prepared by adding the iodobenzene and tri-n-butylamine to the palladium acetate in NMP solution before adding the methallyl alcohol. It is known that the palladium acetate is reduced in the presence of the allyl alcohol to give palladium metal. It is likely, therefore, that the palladium metal therefore must be reacting with the iodobenzene and tri-N-butylamine to give the red product in solution.

ii) Electronic absorption spectroscopic studies of the reaction mixture:

Electronic absorption spectroscopic studies of the red reaction mixture at room temperature showed no peaks in the visible region of the spectrum. The absorption spectrum of palladium acetate in benzene/toluene solution shows a single

broad charge transfer band (ε=1000 1 mol^{-1} cm^{-1}) at 394 nm.[51] There was little change in the visible part of the spectrum on heating.

iii) X-ray crystal studies:

An attempt was made to separate the red product from the red reaction solution by washing the solution with n-pentane. Immediately, on addition of the n-pentane to the red solution, a deep red oil settled to the bottom of the reaction vessel and the clear organic solvent mixture remained at the top. This could be decanted off. This indicated the ionic nature of the red product. The red product was crystallised in two steps. First, any remaining NMP solvent still present in the red oil was removed by placing the red oil under vacuum for two days. The deep red oil became a deep red semi-solid. The semisolid was dissolved in methallylalcohol and placed in a enclosed beaker of n-pentane. Overnight deep red needle-like crystals formed. X-ray crystal analysis of the crystal and refinement of the data was performed by Mr.A.Genge, of the Department of Chemistry (Southampton University), using a Rigaku AFC X-ray Crystallography diffractometer.

The results showed that the crystals had the chemical formula $[NBu_3H]^+_2$ $[Pd_2I_6]^{2-}$. Thus, the deep red colour of the catalyst solution prior to heating was due to the formation of the ionic complex shown in Figure 7.13.

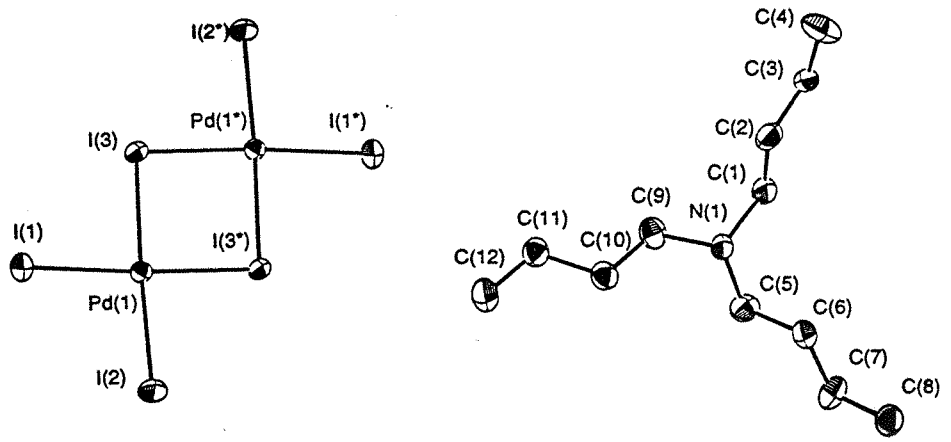

Figure 7.13. Figure showing the X-ray crystal structure of $[NBu_3H]^+_2[Pd_2I_6]^{2-}$

Although the hydrogen atom on the tributylammonium ion could not be detected it is thought to be present from the geometry at the central nitrogen atom. Selected X-ray crystal parameters obtained for $[NBu_3H]^+_2$ $[Pd_2I_6]^2$ are given in Table 7.7. Further details are given in the appendix. Similar species involving the $[Pd_2I_6]^2$ anion have been characterised before.[53.54.55] It will be noted later during this chapter, that during catalysis while the central Pd(μ^2-I)Pd bridges are retained the terminal iodines are lost and replaced by organic species e.g. olefin groups with consequent loss of $[NBu_3H^+I^-]$ from the crystal salt.

Table 7.7. Table showing selected X-ray crystal parameters obtained from $[Pd_2I_6]^{2-}[NBu_3H]^+_2$:

Parameter	**Value**
Bond distance: Pd-I (terminal)	2.611(2)-2.5931(8)
Bond distance: Pd-I(bridging)	2.604(2)-2.609(8)
Radial distance: Pd-Pd	3.840(1)
Bond angle: Pd-I-Pd	94.89(4)°
Bond angle: I-Pd-I (external to bridge)	91.30(4)°-92.10(4)°
Bond angle: I-Pd-I (inside bridge)	85.11(4)°

The X-ray crystal structure showed the extent of the reaction but did not provide evidence of the complexes actually present in the reaction solution at room temperature. In order to find out more about the complexes present in solution, in situ studies of the reaction solution were carried out using QUEXAFS spectroscopy.

Dissolving the red iodide salt in place of the palladium acetate in the various reagent solutions and heating, once again resulted in the yellow catalyst solution as before, which on cooling overnight reverted to the red solution.

iv) QUEXAFS spectrum of the reaction mixture 1 at room temperature:

Six fluorescence QUEXAFS spectra of the red reaction mixture 1 were taken at room temperature in the solution cell shown in Figure 7.7 . The fitted QUEXAFS data and its Fourier transform are shown in Figure 7.14.

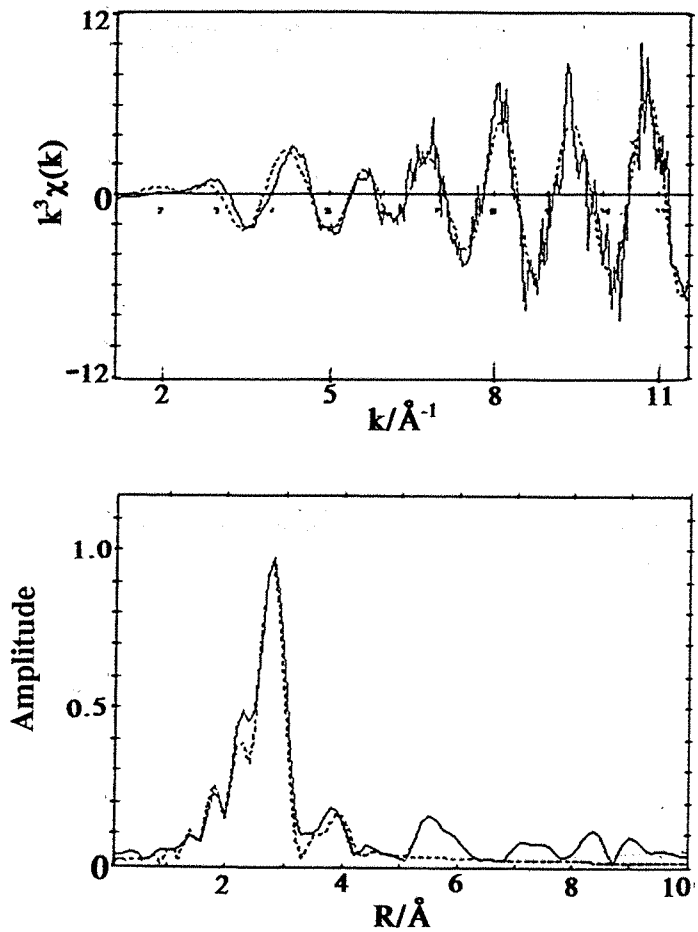

Figure 7.14. Figure showing the fitted in-situ Pd-K-edge data (average of six fluorescence QUEXAFS scans, scan time=5 minutes) of $Pd(OAc)_2$/ iodobenzene/methallylalcohol/tri-n-butylamine/NMP reaction mixture at room temperature.

Table 7.8. Table showing the parameters obtained from the fitted Pd-K-edge fluorescence QUEXAFS data of $Pd(OAc)_2$/iodobenzene/methallylalcohol/tri-n-butylamine/NMP reaction mixture.

EF= -4 (1), AFAC= 0.8, R= 40.4%.

Atom Type	C.N	R/Å	$\sigma^2/Å^{-1}$
C	2.1 (5)	2.11 (2)	0.0159 (5)
I	3.0 (1)	2.633 (4)	0.0086 (4)
Pd	1.0 (3)	3.82 (2)	0.008 (3)

The data show that the average coordination around a palladium atom in the mixture consisted of a shell of *ca.* 2 carbon atoms at 2.105 Å , and a shell of 3 iodine atoms at 2.633 Å and a third shell of a single palladium atom at 3.820 Å. (Despite using an average of six five minute scans the data were still very noisy and has led to a 40% fit). All the shells were found to be significant to the fit. A first shell of oxygen atoms was also tried but this led to a worse fit than using carbon atoms. The palladium shell was found to be significant to 1% probability.

It is clear solution from the iodine coordination, that an iodide was involved in the reaction. The formation of an organometallic was indicated by the carbon coordination shell. There was also clear indication of a species containing palladium atoms bridged by two iodine atoms as indicated by the non-bonding distance of 3.820 Å. This was similar to the iodine bridges found in the species which were crystallised out from the reaction solution (See Figure 7.13).

The data could on average fit the species shown in Figure 7.15.

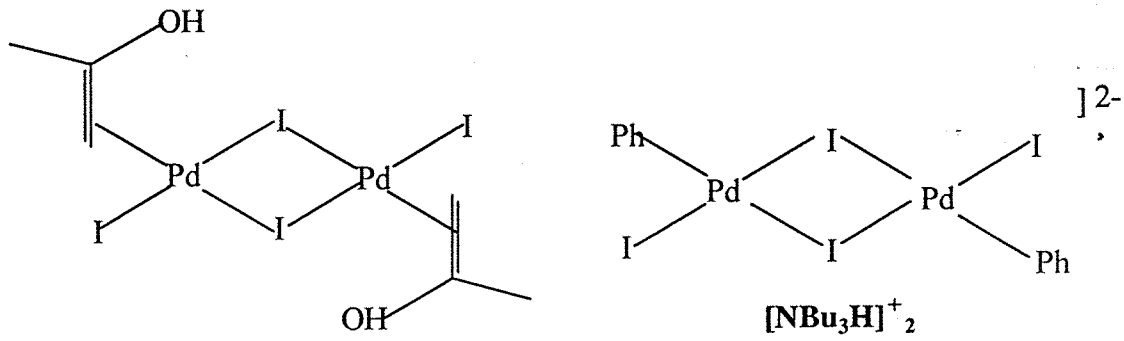

Figure 7.15. Figure showing two catalytic intermediates which could be formed in the $Pd(OAc)_2$/iodobenzene/methallylalcohol/tri-n-butylamine/NMP reaction mixture at room temperature.

The chloride analogue of a species similar to 1 i.e.di-μ-chlorodichlorobis (ethylene) dipalladium was synthesised before in 1967 by Ketley *et al.*[52] under similar reaction conditions by a method involving the reaction between a palladium chloride slurry in dichloromethane and ethene (10 atm) at 50°C.

However, given the data in Table 7.8, it is difficult to say which of the two species shown in Figure 7.15 could have been formed or whether a mixture of both was present in the reaction solution.

v) NMR studies of reaction solution 1:

In situ NMR studies of the catalyst reaction mixture were difficult to perform because of the large excess of organic reagents such as iodobenzene, methallyl alcohol and solvent NMP in the reaction mixture which diluted the signals from any organometallic palladium complex formed. Also, the concentration of the palladium in the reaction mixture used for the EXAFS experiments and in all the catalysis studies by other workers has been low (< 4mg in 0.5 ml) due to the poor solubility of palladium acetate in most solvents.

Further studies using a number of other techniques may have to be used to further characterise any species actually present in solution.

vi) QUEXAFS spectrum of the reaction mixture 1 on heating to 65°C:

On heating the reaction mixture 1 ($Pd(OAc)_2$/ iodobenzene/ methallylalcohol/ tri-n-butylamine/ NMP; 1/60/50/50/36, [Pd]= 41mM), in situ for 5 minutes at 65°C, the colour changed from deep red to yellow. Three fluorescence QUEXAFS scans (scan time= 5 minutes) and two fluorescence EXAFS scans (scan time= 30 minutes) of the reaction mixture were taken in succession and since they were later found to be identical they were then averaged. The fitted average data are shown in Figure 7.16.

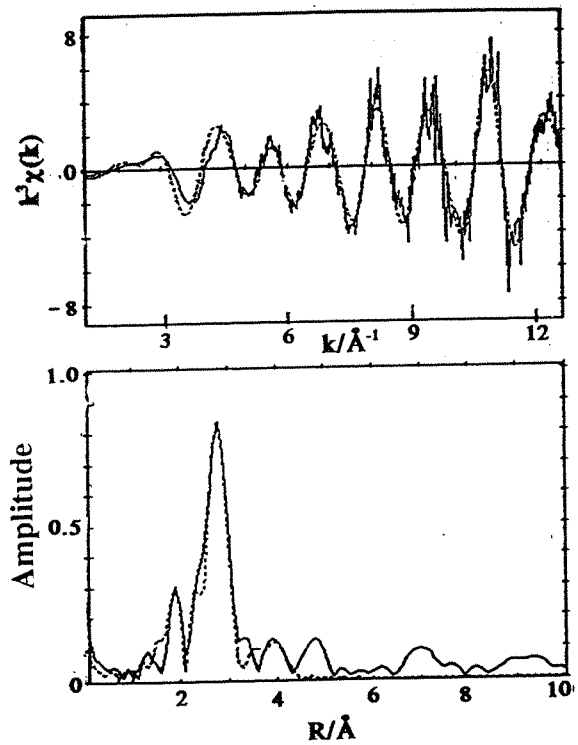

Figure 7.16. Figure showing the fitted average EXAFS data and Fourier transform of $Pd(OAc)_2$/iodobenzene/methallylalcohol/tri-n-butylamine/NMP; 1/60/50/50/36, [Pd]= 41mM) at 65°C using the average of three fluorescence QUEXAFS scans (scan time= 5 minutes) and two fluorescence EXAFS scans (scan time = 31 minutes).

Table 7.9 Table showing the parameters obtained from the fitted fluorescence EXAFS data and Fourier transform of $Pd(OAc)_2$/iodobenzene/methallylalcohol/ tri-n-butylamine/NMP; 1/60/50/50/36, [Pd]= 41mM) at 65°C using the average of three fluorescence QUEXAFS scans (scan time= 5 minutes) and two fluorescence EXAFS scans (scan time = 31 minutes).

EF= -6.7 (7), AFAC= 0.8, R= 38.2%.

Atom Type	C.N	R/Å	$\sigma^2/Å^{-1}$
C	1.7 (2)	2.035 (9)	0.008 (2)
I	3.0 (1)	2.647 (3)	0.0116 (4)
Pd	1.0 (2)	3.854 (9)	0.007 (2)

The table shows that the average coordination around a palladium atom in the reaction mixture involved a first coordination shell of 2 carbon atoms at 2.035 Å, and a second coordination shell of 3 iodide atoms at 2.65Å and a third coordination shell of a single palladium atom at 3.86Å. As before, the coordination shell of carbon atoms gave a better fit than when oxygen atoms were used suggesting the formation of an organometallic. The presence of palladium atoms at 3.854 Å indicates that Pd(μ-2I)Pd bridges were present in the species in solution (as in the crystal salt obtained from the same solution (see Figure 7.13).

The data could on average fit to the species shown in Figure 7.15. However, this is only one of the possibilities and other spectroscopic studies will have to be carried out to study all the species formed in the reaction solution.

7.9. A fluorescence EXAFS study of reaction mixture 1 in the absence of methallylalcohol:

In order to find out the reaction that occurred in the absence of methallyl alcohol, the following reaction mixture was studied using fluorescence EXAFS.

i) at room temperature:

A scanning fluorescence EXAFS spectrum (one scan, scan time= 30 minutes) was obtained of the yellow-brown mixture, $Pd(OAc)_2$ (0.15g)/iodobenzene(4ml)/tri-n-butylamine(6ml)/NMP(4ml) (molar ratio: 1/50/25/60, [Pd]= 50mM). The fitted EXAFS data and its Fourier transform is shown in Figure 7.17.

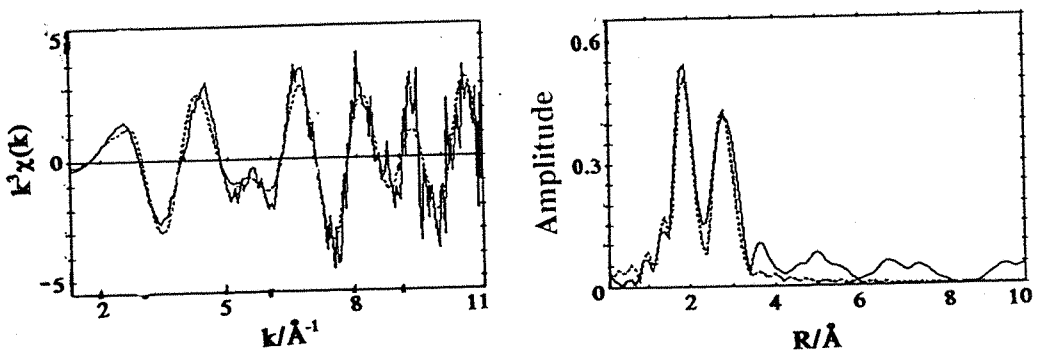

Figure 7.17. Figure showing the Pd-K-edge fluorescence EXAFS data (one scan, scan time=30 minutes) of $Pd(OAc)_2$/iodobenzene/tri-n-butylamine/NMP at room temperature.

Table 7.10. Table showing the parameters obtained from the fitted Pd-K-edge fluorescence EXAFS data (one scan, scan time= 30 minutes) of $Pd(OAc)_2$/ iodobenzene/tri-n-butylamine/NMP at room temperature.

EF= -7.04 (0.61), AFAC= 0.9, R= 41.9%.

Atom Type	Coordination Number	R/Å	$\sigma^2/Å^{-1}$
O	2.1 (1)	2.034 (6)	0.007 (1)
I	2.0 (1)	2.676 (5)	0.014 (1)

Table 7.10 shows the average coordination around a palladium atom in the reaction mixture, as being a shell of *ca.* 2 oxygen atoms at 2.034 Å and a shell of 2 iodine atoms at 2.676 Å. Since the main source of oxygen in this solution was the palladium acetate starting material, it is likely that the reaction solution either contained a mixture of 50% starting material and 50% palladium iodide salt (see Figure 7.12) in it or a single complex containing both acetate groups and iodide groups. The exact nature of such a complex if present would be difficult to decide upon at this stage.

ii) at 65°C:

A palladium-K-edge fluorescence EXAFS spectrum (one scan, scan time=30 minutes) of $Pd(OAc)_2$(0.15g)/iodobenzene(4ml)/tri-n-butylamine(6ml)/ NMP(4ml) (molar ratio: 1/50/25/60, [Pd]= 50mM) was obtained after heating the reaction mixture in-situ to 65°C. The fitted EXAFS data and its Fourier transform are shown in Figure 7.18.

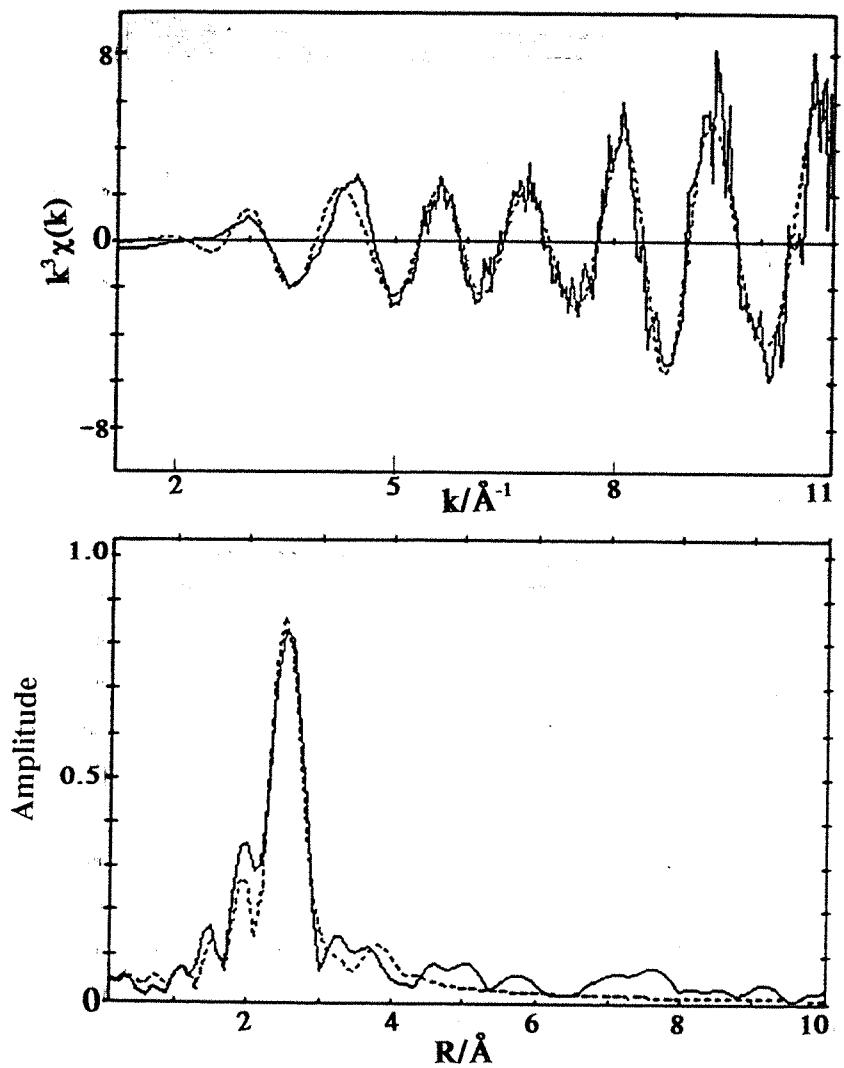

Figure 7.18. Figure showing the fitted Pd-K-edge fluorescence EXAFS data (one scan, scan time= 30 minutes) of $Pd(OAc)_2$/iodobenzene/tri-n-butylamine/NMP reaction mixture at 65°C, and its Fourier transform.

Table 7.11. Table showing the parameters obtained from the fitted Pd-K-edge fluorescence EXAFS data (one scan, scan time= 30 minutes) of $Pd(OAc)_2$/ iodobenzene/tri-n-butylamine/NMP reaction mixture at 65°C, and its Fourier transform.

EF= -6.2 (9), AFAC= 0.8, R= 35.5%.

Atom type	Coordination number	R/Å	$\sigma^2/Å^{-1}$
I	3.4 (1)	2.655 (4)	0.0105 (4)
Pd	1.0 (2)	3.82 (1)	0.003 (2)

The parameters in Table 7.8 show that the palladium atom in the catalyst reaction mixture in the absence of methallylalcohol and at 65°C, had on average a first coordination shell of 3.4 iodine atoms at 2.655 Å and a second coordination shell of one palladium atom at 3.82 Å. Although an oxygen/carbon shell was difficult to fit, it is possible that the reaction mixture contained some palladium iodide salt and possibly other species such as the starting material, palladium acetate or an organometallic.

7.10. Studies of the catalyst reaction mixture 2: $Pd(OAc)_2/PPh_3$/ bromobenzene/methallylalcohol/tri-n-butylamine mixture:

i) Introduction:

When bromobenzene was used instead of iodobenzene then in the presence of methallylalcohol, $Pd(OAc)_2$ was reduced to palladium metal which does not catalyse the reaction on its own. For this reason, when bromobenzene was used as the organic halide, PPh_3 had to be added to the catalyst mixture to prevent formation of palladium metal. In the presence of PPh_3, the catalyst precursor

formed was $Pd(OAc)_2(PPh_3)_2$.A QUEXAFS spectrum of the $Pd(OAc)_2/PPh_3$ in NMP is given in the following subsection.

ii) Fluorescence EXAFS spectrum of $Pd(OAc)_2/PPh_3$ in NMP:

A fluorescence scanning EXAFS spectrum (one scan, scan time= 31 minutes) of $Pd(OAc)_2/PPh_3$ in NMP (Pd:P 1:2, [Pd]= 70mM) was taken at room temperature. The fitted spectrum and its Fourier transform are shown below in Figure 7.19.

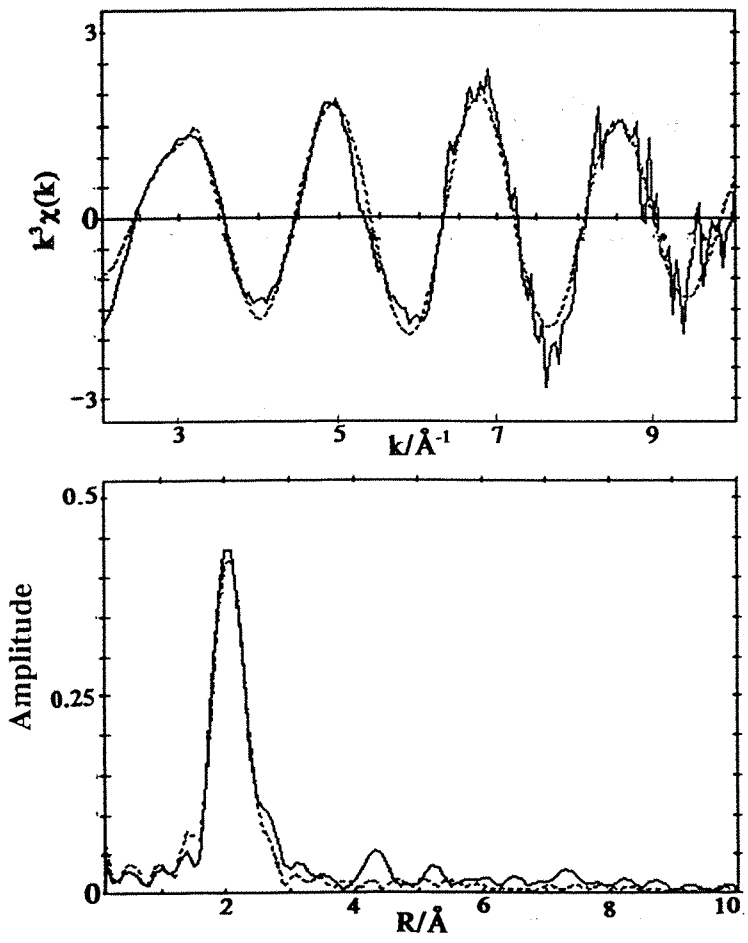

Figure 7.19. Figure showing the fitted Pd-K-edge fluorescence EXAFS data (one scan, scan time= 30 minutes) of $Pd(OAc)_2/PPh_3$ mixture (Pd:P 1:2, [Pd]=70mM) in NMP at room temperature.

Table 7.12. Table showing the parameters obtained from the fitted Pd-K-edge fluorescence EXAFS data (one scan, scan time= 30 minutes) of $Pd(OAc)_2/PPh_3$ mixture (Pd:P 1:2, [Pd]= 70mM) in NMP at room temperature and its Fourier transform.

EF= -7.9 (5), AFAC= 0.8, R= 24.2%.

Atom Type	Coordination number	R/Å	$\sigma^2/Å^{-1}$
O	2.0 (2)	2.09 (1)	0.013 (4)
P	1.8 (2)	2.218 (6)	0.019 (2)

The data in Table 7.8 show that the palladium atom in the $Pd(OAc)_2/PPh_3$ (Pd/P 1:2, [Pd]= 70mM) mixture in NMP on average had a first coordination shell of 2 oxygen atoms at 2.086 Å and a second coordination shell of two phosphorus atoms at 2.218 Å. Both shells were found to be significant in improving the fit. The data support the formation of the species shown below in Figure 7.20.

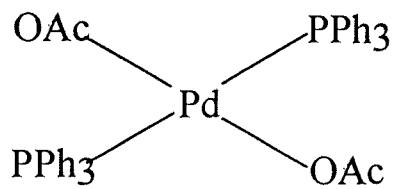

Figure 7.20. Square planar structure of $Pd(OAc)_2(PPh_3)_2$.

This species has been synthesised before by treating diacetatatopalladium(II) in benzene with an excess of triphenylphosphine in benzene to obtain lemon yellow crystals of the product - diacetatobis(triphenyphosphine)palladium(II)[51].

iii) Fluorescence EXAFS spectra of the catalyst reaction mixture 2 in situ catalyst ie. $Pd(OAc)_2/PPh_3$/bromobenzene/methallylalcohol/tri-n-butylamine:

a) at room temperature:

Fluorescence scanning EXAFS spectra (two scans, scan duration= 30 minutes) of the in situ catalyst mixture 2 i.e. $Pd(OAc)_2$(0.3g)/ PPh_3(0.7g)/bromobenzene(5.2ml)/methallylalcohol(6.2ml)/tri-n-butylamine (12ml) (molar ratio: 1/2/38/57/39 , [Pd]= 56mM) were obtained at room temperature. The fitted EXAFS data are shown in Figure 7.21.

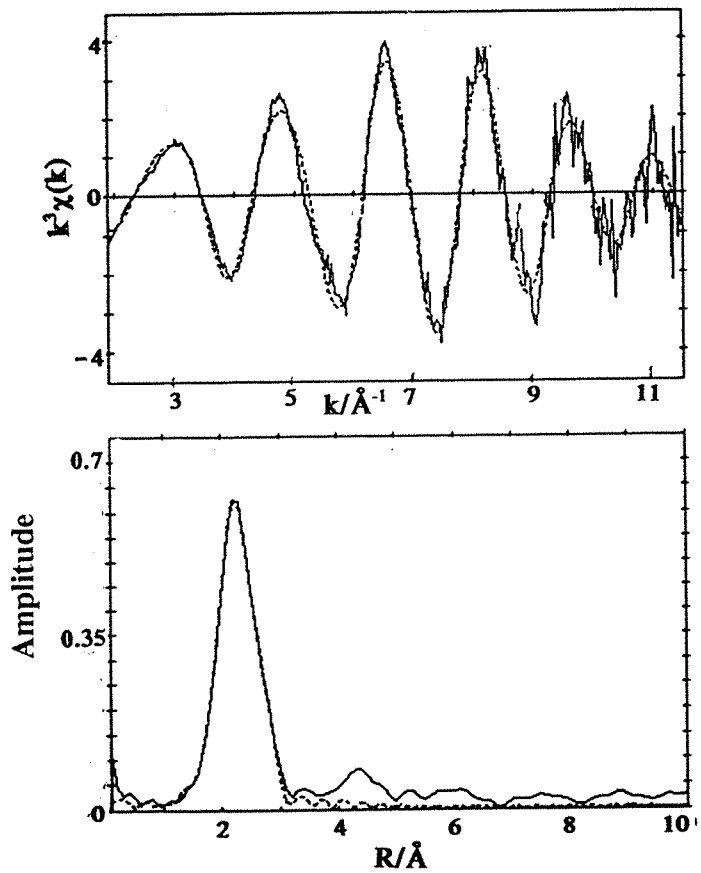

Figure 7.21. Figure showing the fitted fluorescence EXAFS data (two scans, scan time=30 minutes) of $Pd(OAc)_2/PPh_3$/bromobenzene/methallylalcohol/ tri-n-butylamine/NMP catalyst mixture at room temperature and its Fourier transform.

Table 7.13. Table showing the parameters obtained from the fitted fluorescence EXAFS data (two scans, scan time= 30 minutes) of $Pd(OAc)_2/PPh_3$/ bromobenzene/methallylalcohol/tri-n-butylamine/NMP catalyst mixture at room temperature and its Fourier transform.

EF= -11.9 (7), AFAC= 0.8, R= 25.38%.

Atom Type	Coordination number	R/Å	$\sigma^2/Å^{-1}$
O	1.91 (1)	2.097 (8)	0.014 (2)
P	1.04 (8)	2.305 (7)	0.009 (2)
Br	0.98 (6)	2.490 (4)	0.0089 (7)

The Table 7.9 shows that the average coordination around a palladium atom in the reaction mixture, $Pd(OAc)_2$/ PPh_3/ bromobenzene/ methallylalcohol/ tri-n-butylamine/ NMP, consisted of a first coordination shell of 1.91 oxygen atoms at 2.097 Å, a second shell of 1.04 phosphorus atom at 2.305 Å and a third coordination shell of 0.98 bromine atom at 2.490 Å. This data could indicate a mixture of products e.g. some $Pd(OAc)_2$ and also a $Pd(PPh_3)_2Br_2$ species given the oxygen, phosphorus and bromine coordination shells. The data could also indicate the presence of the species shown below in Figure 7.22.

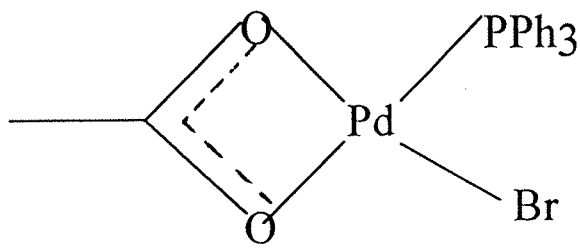

Figure 7.22. Figure showing a species possibly present in the catalyst reaction solution 2 at room temperature.

A similar species involving the dimethylphenylphosphine was prepared by Powell and Jack[56] in 1972. This species was a dimer involving 2 acetate bridges between the palladium atoms. It is shown more clearly in the Figure 7.23 below:

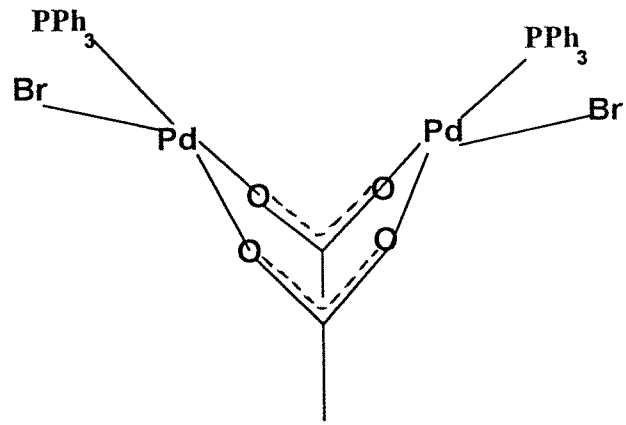

Figure 7.23. Figure showing a palladium complex with bridging carboxylate groups.

Such a species would have a very similar coordination sphere (upto three shells, O, P, Br) to its monomer . Thus, the fit shown in Figure 7.23 could relate to such a species as it has the relevant shells of 2 oxygen atoms, 1 phosphorus atom and 1 bromine atom.

However, as mentioned before a similar coordination fit would be obtained with an equimolar solution of $Pd(OAc)_2/Pd(PPh_3)_2Br_2$. As will be seen in the next section, the EXAFS of the above solution on heating fits to a solution containing $>90\%$ of $Pd(PPh_3)_2Br_2$.

b) at 60°C:

In situ fluorescence EXAFS spectra (2 scans, scan duration= 30 minutes) were taken of the catalyst mixture 2 i.e. $Pd(OAc)_2$/ PPh_3/ bromobenzene/ methallylalcohol/ tri-n-butylamine/ NMP at 60°C. The fitted EXAFS data is shown in Figure 7.24.

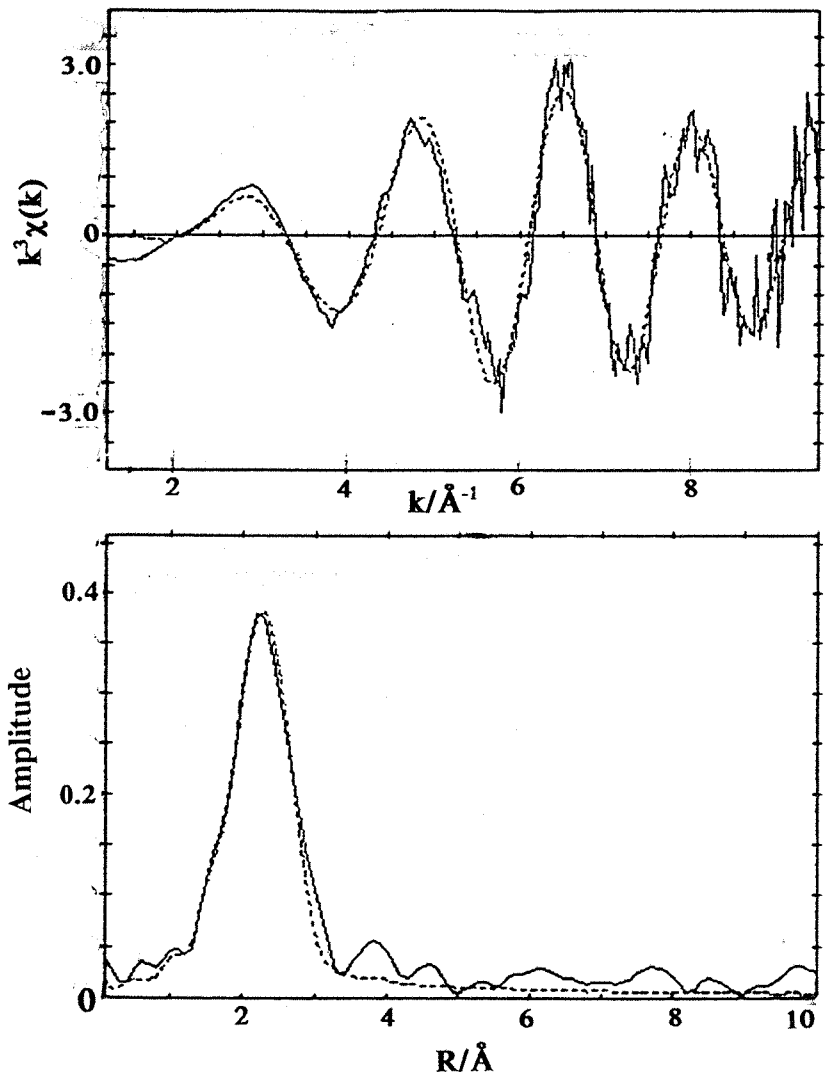

Figure 7.24. Figure showing the fitted fluorescence EXAFS data (2 scans, scan time =30 minutes) of $Pd(OAc)_2$/ PPh_3/ bromobenzene/ methallylalcohol/ tri-n-butylamine mixture at 60°C and its Fourier transform.

Table 7.14. Table showing the parameters obtained from the fluorescence EXAFS spectrum of $Pd(OAc)_2/PPh_3$/bromobenzene/methallylalcohol/tri-n-butylamine mixture at 60°C and its Fourier transform.

EF= -0.65 (1.80), AFAC= 0.80, R= 28.7%.

Atom Type	Coordination number	R/Å	$\sigma^2/Å^{-1}$
P	2.0 (1)	2.22 (2)	0.022 (2)
Br	2.0 (2)	2.47 (1)	0.016 (1)

The table shows that the palladium in the reaction mixture had a first coordination sphere of two phosphorus atoms at 2.22 Å and a second coordination sphere of two bromine atoms at 2.47 Å which could suggest the formation of structures as shown below in Figure 7.25.

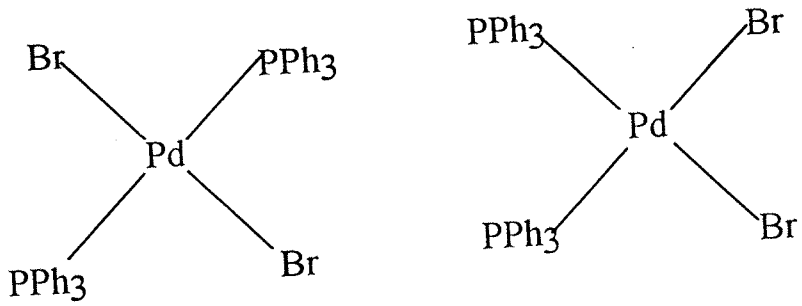

Figure 7.25. Figure showing the possible structures of the catalyst present, in the reaction solution 2 on heating to 65°C.

It is not possible to say from the EXAFS data if such a species is likely to be *cis* or *trans*.

7.11. Fluorescence EXAFS spectrum of catalyst mixture 2 in the absence of bromobenzene i.e. Pd(OAc)2/PPh3/methallylalcohol/tri-n-butylamine/NMP:

A fluorescence EXAFS spectrum of the catalyst mixture 2 in the absence of bromobenzene, was obtained using $Pd(OAc)_2$(0.032g)/ PPh_3(0.07g)/ methallyl alcohol(0.6ml)/ NMP(2ml) (molar ratio: 1:2:50, [Pd]= 54mM), first at a) room temperature and then at b) 65°C. The fitted fluorescence EXAFS data and their respective Fourier transforms are shown in Figure 7.26.

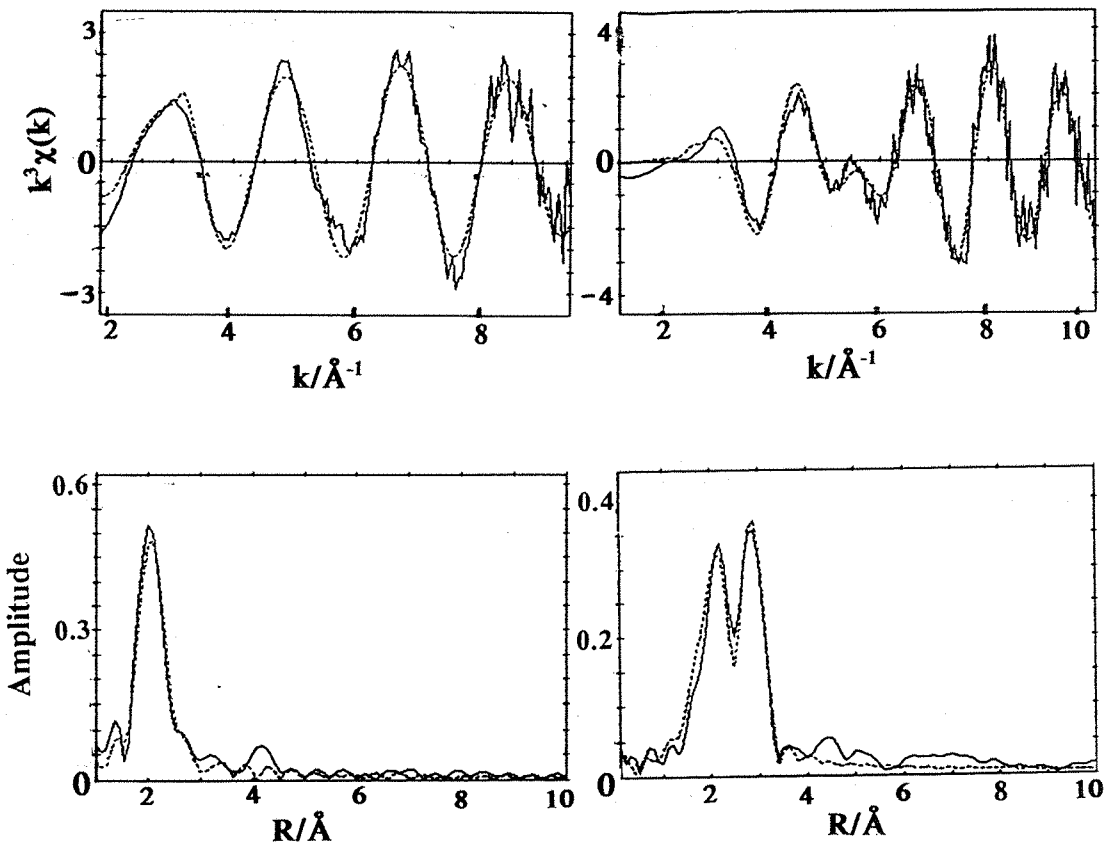

Figure 7.26. Figure showing the fitted fluorescence EXAFS spectra (one scan, scan duration= 30 minutes) of catalyst mixture 2 in the absence of bromobenzene, i.e. $Pd(OAc)_2$/ PPh_3/ methallylalcohol/ tri-n-butylamine/ NMP mixture at a) room temperature and b) in-situ at 65°C.

Table 7.15. Table showing the parameters obtained from fitted fluorescence EXAFS data (one scan, scan duration= 30 minutes) of catalyst mixture 2 in the absence of bromobenzene, i.e. $Pd(OAc)_2$/ PPh_3/ methallylalcohol/ tri-n-butylamine/ NMP mixture at room temperature.

EF= -7.7 (6), AFAC= 0.8, R= 21.6%.

Atom type	Coordination number	R/Å	$\sigma^2/Å^{-1}$
O	2.1 (2)	2.080 (8)	0.011 (4)
P	2.1 (2)	2.222 (8)	0.019 (3)

Table 7.16. Table showing the parameters obtained from fitted fluorescence EXAFS data (one scan, scan duration= 30 minutes) of catalyst mixture 2 in the absence of bromobenzene, i.e. $Pd(OAc)_2$/ PPh_3/ methallylalcohol/ tri-n-butylamine/ NMP mixture at 65°C.

EF= -2.13(8), AFAC= 0.8, R= 36.28%.

Atom Type	Coordination number	R/Å	$\sigma^2/Å^{-1}$
P	1.9 (1)	2.251 (7)	0.021 (2)
Pd	3.0 (1)	2.708 (5)	0.0163 (6)

The data from the tables show that at room temperature the methallylalcohol did not affect the $Pd(OAc)_2/PPh_3$ catalyst at all and the coordination around the palladium atom remained unaffected by the methallylalcohol. At 65°C, in the absence of bromobenzene, some palladium metal began to form in the mixture. This can be seen from the palladium shell which formed at 2.708Å which is at the same distance

as expected from palladium metal foil distances. The formation of the palladium metal is due to the reductive properties of the allyl alcohol, which reduced the palladium acetate triphenylphosphine to metal. The palladium particles were small and disordered as there were few peaks at larger R.

7.12 CONCLUSIONS:

The results obtained in this chapter show the extent to which EXAFS spectroscopy can provide information on the species present in some Heck reaction palladium catalyst solutions.

To start with, X-ray crystallography studies of the species which crystallised from catalyst mixture 1, i.e. $Pd(OAc)_2$/ iodobenzene/ methallylalcohol/ tri-n-butylamine/ NMP showed the formation of $[N\text{-}Bu_3H^+]_2[Pd_2I_6]^{2-}$ in the catalyst solution. EXAFS studies of the catalyst in-situ have indicated the presence of a $Pd(\mu^2\text{-}I)Pd$ structure, similar to that of the crystal salt along with some carbon coordination and a drop in iodide coordination. The exact nature of the carbon shell was not clear from EXAFS but it could be a result of olefin (methallylalcohol) coordination with loss of $[NBu_3H^+I^-]$ from the crystal salt. The carbon shell could also be due to phenyl coordination. Both possible structures are shown below.

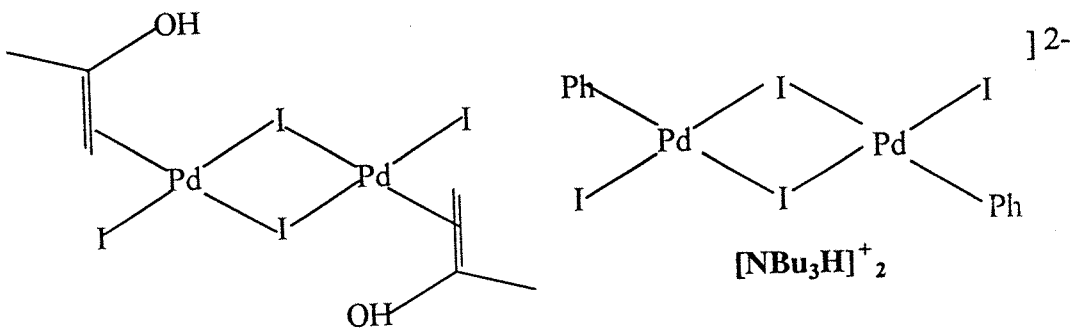

In the absence of the olefin i.e. methallylalcohol, the EXAFS of the reaction mixture fitted to a shell of 2 oxygen atoms and a second shell of 2 iodine atoms. It is possible that the reaction solution consisted of a mixture of the palladium acetate starting material and some palladium iodide salt. It is also possible that a single species with acetate bridges and Pd-I bonds may also be present with some of the acetate groups in the starting material being replaced by iodine atoms. It is difficult to be certain from the EXAFS. On heating this mixture, the oxygen shell disappeared and the coordination of the iodine shell increased indicating the increasing formation of the palladium iodide salt in the mixture.

Next the results from catalyst mixture 2 i.e. $Pd(OAc)_2/PPh_3$/bromobenzene/ methallylalcohol/tri-n-butylamine/NMP were studied. These results indicated that at room temperature the reaction mixture contained either an equimolar mixture of $Pd(OAc)_2$ and $Pd(PPh_3)_2Br_2$ or contained >90% of the species shown below.

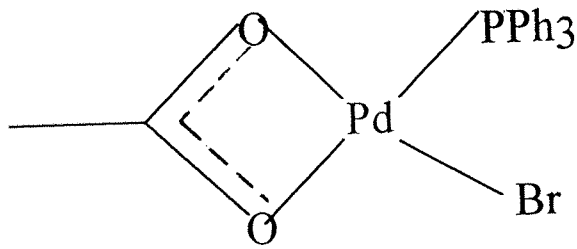

On heating EXAFS studies of the mixture indicated the formation of the species ($Pd(PPh_3)_2Br_2$) of the type shown below.

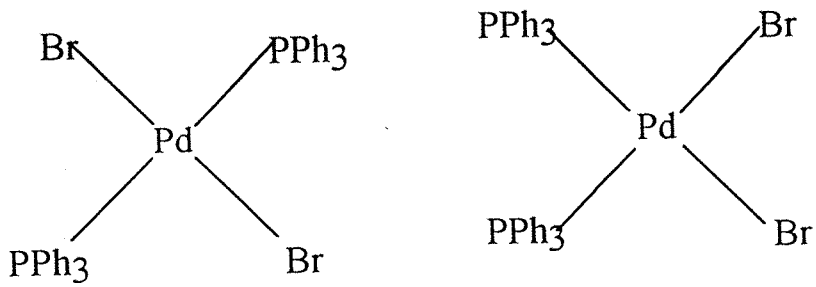

Such a species could take part in the catalysis by alkylation with loss of halogen atoms.

7.13. REFERENCES

1. R.F.Heck, *Organic Reactions.*, 1982, **27**, 344.
2. R.F.Heck, *Acc.Chem.Res.*, 1979, **12**, 146.
3. R.F.Heck, 'Palladium reagents in organic synthesis', Academic Press, London, 1985.
4. J.Tsuji, 'Organic Synthesis with palladium compounds', Springer, Berlin, 1980.
5. B.M.Trost and T.R.Verhoeven in 'Comprehensive Organometallic Chemistry', Vol 8, (*Ed.* G.Wilkinson), Pergamon Press, Oxford, 1982, 799.
6. R.F.Heck in 'Comprehensive Organic Synthesis', Vol 4, (Eds. B.M.Trost, I.Fleming), Pergammon, Oxford, 1991.
7. H.A.Dieck and R.F.Heck, *J.Am.Chem.Soc.*, 1974, **96**, 1133.
8. C.B.Ziegler Jr. and R.F.Heck, *J.Org.Chem.*, 1978, **43**, 2941.
9. B.A.Patel, L.Kao, N.A.Cortese, J.V.Minikiewicz and R.F.Heck, *J.Org.Chem.*, 1979, **44**, 918.
10. J.E.Plevyak and R.F.Heck, *J.Org.Chem.*, 1978, **43**, 2454.
11. B.A.Patel, C.B.Ziegler, N.Cortese, J.E.Plevyak, T.C.Zebovitz, M.Terpko and R.F.Heck, *J.Org.Chem.*, 1977, **42**, 3903.
12. Y.Tamaru, Y.Yamamda and Z.Yoshida, *Tetrahedron Lett.*, 1978, 919.
13. T.Mizoroki, K.Mori and A.Ozaki, *Bull.Chem.Soc.Jpn.*, 1971, **44**, 581.
14. B.M.Trost, L.Weber, P.E.Strege, T.J.Fullerton and T.J.Dietsche, *J.Am.Chem.Soc.*, 1978, **100**, 3416.
15. B.Akermark, J.E.Backvall, L.S.Hegedus and K.Zetterberg, *J.Organomet. Chem.*, 1974, **72**, 127.
16. T.Hosokawa, H.Ohkata, and I.Moritani, *Bull.Chem.Soc.Jpn.*, 1975, **48**, 1533.
17. N.Okuwado, D.E.Van Horn, W.L.Klima and E.Negishi, *Tetrahedron. Lett.*, 1978, 1027.
18. R.F.Heck, *J.Am.Chem.Soc.*, 1968, **90**, 5518.
19. R.F.Heck and J.P.Nolley Jr, *J.Org.Chem.*, 1972, **37**, 2320.
20. A.D.Meijere and F.E.Meyer, *Angew.Chem.Int.Ed.Engl.*, 1994, **33**, 2379.

21. D.R.Coulson, *Inorg.Synth.*, 1972, **13**, 121.

22. B.E.Mann and A.Musco, *J.Chem.Soc.Dalton Trans.*, 1975, 1673.

23. C.Amatore and F.Pfluger, *Organometallics.*, 1990, **9**, 2276.

24. E.-i.Negishi, T.Takahashi and K.Akiyoshi, *J.Chem.Soc.Chem.Comm.*, 1986, 1338.

25. T.Hayashi, A.Kubo and F.Oz, *Pure.Appl.Chem.*, 1992, **64**, 421.

26. C.Amatore, M.Azzabi, and A.Jutand, *J.Organomet.Chem.*, 1989, **363**, C4.

27. J.Low and W.A.Goddard III, *J.Am.Chem.Soc.*, 1986, **108**, 6115.

28. J.M.Brown and N.A.Goody, *Organometallics.*, 1990, **9**, 353.

29. P.Fitton and J.E.McKeon, *J.Chem.Soc.Chem.Comm.*, 1968.

30. J.M.Brown and N.A.Cooley, *J.Chem.Soc.Chem.Comm.*, 1988, 1345.

31. E.G.Samsel and J.R.Norton, *J.Am.Chem.Soc.*, 1984, **106**, 5505.

32. D.L.Thorn and R.Hoffman, *J.Am.Chem.Soc.*, 1979, **100**, 2079.

33. E.H.Brooks and F.Glockling, *J.Chem.Soc.A.*, 1967, 1030.

34. H.Munakata and M.L.H.Green, *J.Chem.Soc.Chem.Comm.*, 1970, 881.

35. C.Dibugno, M.Pasquali, P.Leoni, P.Sabatino, and D.Braga, *Inorg.Chem.*, 1989, **28**, 1390.

36. R.Benhaddou, S.Czernecki and G.Ville, *J.Chem.Soc.Chem.Comm.*, 1988, 247.

37. H.Bönnemann, W.Brijoux, R.Brinkmann, E.Dirijus, R.Fretzen, T.Joulsen and B.Korall, *J.Mol.Catal.*, 1992, **74**, 323.

38. L.N.Lewis, R.J.Griarte and N.Lewis, *J.Catal.*, 1991, **127**, 67.

39. L.A.Fowley, D.Michos, X.-L.Luo and R.H.Crabtree, *Tetrahedron Lett.*, 1993, **34**, 3075.

40. H.Bönnemann, W.Brijoux, R.Brinkmann, E.Dinjus, R.Fretzen, T.Joussen and B.Korall, *Angew.Chem.Int.Ed.Engl.*, 1991, **30**, 1312.

41. H.Bönnemann, W.Brijoux and T.Joussen, *Angew.Chem.Int.Ed.Engl.*, 1990, **29**, 273.

42. A.Spencer, *J.Organomet.Chem.*, 1983, **258**, 101.

43. W.A.Hermann, C.Brobmer, K.Ofele, C.-P.Reisinger, T.Priermeir, M.Beller and H.Fischer, *Angew.Chem.Int.Ed.Engl.*, 1995, **34**, 1844.

44. M.Beller, H.Fischer, K.Kühlein, C.-P.Reisinger, W.A.Hermann, *J.Organomet.Chem.*, 1996, **520**, 257.

45. R.F.Heck, *Acct.Chem.Res.*, 1979, **12**, 146.

46. J.B.Melpolder and R.F.Heck, *J.Org.Chem.*, 1976, **41**, 265.

47. A.J.Chalk and S.A.Magennis, *J.Org.Chem.*, 1976, **41**, 1206.

48. A.J.Chalk and S.A.Magennis, *J.Org.Chem.*, 1976, **41**, 273.

49. A.C.Skapski and M.L.Smart, *J.Chem.Soc.Chem.Comm.*, 1970, 658.

50. M.Tamura and T.Yasui, *J.Chem.Soc.Jpn., Ind.Chem.Sect.*, 1968, **71**, 1855.

51. T.A.Stephenson, S.M.Morehouse, A.R.Powell, J.P.Heffer and G.Wilkinson, *J.Chem.Soc.*, 1965, 3632.

52. A.D.Ketley, L.P.Fisher, A.J.Berlin, C.R.Morgan, E.H.Gorman and T.R.Steadman, *Inorg.Chem.*, 1967, **6**, 657.

53. F.Maasarani, M.Pfeffer and G.Le Borgne, *J.Chem.Soc.Chem.Comm.*, 1987,

54. F.Maasarani, M.Pfeffer and G.Le Borgne, *Organometallics.*, 1987, **6**, 2043.

55. S.Chan, S-M. Lee, Z. Lin, W-T. Wong, *J.Organomet.Chem.*, 1996, **510**, 219.

56. J.Powell and T.Jack, *Inorg.Chem.*, 1972, **11**, 1039.

APPENDIX

APPENDIX

A.1 Solvent Purification

Solvents were distilled under argon from the following,

solvent	drying agent
toluene, hex-1-ene	sodium/benzophenone
p-fluorotoluene	calcium hydride
iodobenzene, methallyl alcohol, tri-n-butylamine	molecular sieves (4 Å)

A.2 Compound Preparation and Reagents

$Ni(acac)_2$[1] and $NiX_2(PEt_3)_2$[2] were prepared according to literature methods, using dried and degassed solvents. All the complexes were vacuum dried and stored under nitrogen prior to use.

$AlEt_3$ (1.6M in toluene) and $AlEt_2(OEt)$ (1.9M in toluene) were purchased from Aldrich and used without further purification. All manipulations involving these reagents were performed using standard inert atmosphere techniques.[3]

$Pd(OAc)_2$ was purchased from Alfa chemicals (Johnson Mathey). NMP (anhydrous) was purchased from Fluka and used without further purification.

A.3 ELECTRONIC ABSORPTION SPECTROSCOPY

Solution spectra were recorded at room temperature on a Perkin Elmer Lambda 19 Spectrometer. Figure A.1. on the next page shows a 1cm quartz cell adapted for use with air-sensitive samples.

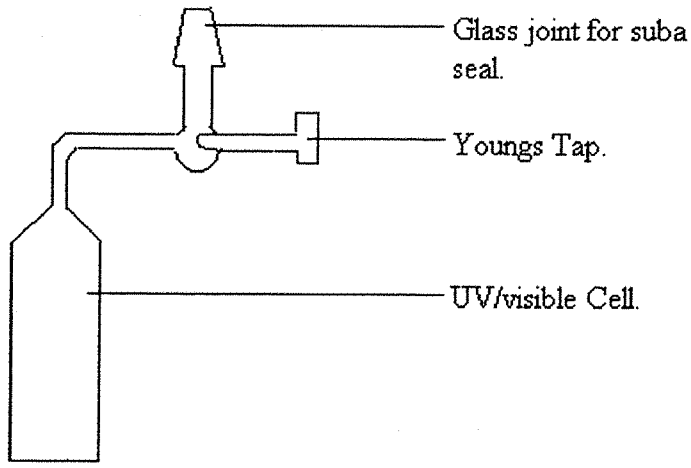

Figure A.I. Figure showing an electronic absorption spectrometer cell adapted for use with air-sensitive samples.

Molar absorption coefficients (ε_{mol} /$l^{-1}mol^{-1}cm^{-1}$) were calculated according to the Beer-Lambert law,

$$A = \log_{10}(I_0/I) = \varepsilon_{mol}Cl$$

Where, A is the absorbance, I_0 is the intensity of incident radiation, I is the intensity of transmitted radiation, c is the concentration (mol l^{-1}) and l is the sample path length (cm).

A.4 X-ray parameters of $[NBu_3H]_2^{1+}[Pd_2I_6]^{2-}$: These are given in detail on pages 261-268.

A.5 References to the appendix:

1. K.A.Jensen, P.H.Nielsen and C.Pedersen, *Acta.Chem.Scand.*, 1963, **17**, 1115.
2. R.G.Charles and M.A.Pawlikowski, *J.Phys.Chem.*, 1958, **62**, 440.
3. D.F.Shriver and M.A.Drezdon, "The Manipulation of Air-Sensitive Compounds", Wiley-Interscience, New York, 2nd Edition, 1986.

A. Crystal Data

Empirical Formula	$C_{12}H_{28}I_6Pd_2N$
Formula Weight	1160.59
Crystal Color, Habit	purple, plate
Crystal Dimensions	0.45 X 0.13 X 0.05 mm
Crystal System	triclinic
Lattice Type	Primitive
No. of Reflections Used for Unit Cell Determination (2θ range)	15 (19.7 - 22.8°)
Omega Scan Peak Width at Half-height	0.44°
Lattice Parameters	a = 11.779(8) Å b = 11.787(8) Å c = 8.690(5) Å α = 110.98(5)° β = 100.57(6)° γ = 61.67(4)°.
	V = 991(1) Å^3
Space Group	$P\bar{1}$ (#2)
Z value	2
D_{calc}	3.887 g/cm^3
F_{000}	1034.00
μ(MoKα)	111.56 cm^{-1}

B. Intensity Measurements

Diffractometer	Rigaku AFC7S
Radiation	MoKα ($\lambda = 0.71069$ Å) graphite monochromated
Attenuator	Zr foil (factor = 8.59)
Take-off Angle	6.0°
Detector Aperture	9.0 mm horizontal 13.0 mm vertical
Crystal to Detector Distance	400 mm
Temperature	-123.1°C
Scan Type	ω-2θ
Scan Rate	16.0°/min (in ω) (up to 4 scans)
Scan Width	$(1.47 + 0.35 \tan \theta)°$
$2\theta_{max}$	50.0°
No. of Reflections Measured	Total: 3668 Unique: 3479 ($R_{int} = 0.028$)
Corrections	Lorentz-polarization Absorption (trans. factors: 0.7914 - 1.0000)

C. Structure Solution and Refinement

Structure Solution	Patterson Methods (DIRDIF92 PATTY)
Refinement	Full-matrix least-squares
Function Minimized	$\Sigma w(\|Fo\| - \|Fc\|)^2$
Least Squares Weights	$\frac{1}{\sigma^2(Fc)} = \frac{4Fo^2}{\sigma^2(Fo^2)}$
p-factor	0.0220
Anomalous Dispersion	All non-hydrogen atoms
No. Observations (I>2.50σ(I))	2320
No. Variables	154
Reflection/Parameter Ratio	15.06

Residuals: R; Rw	0.030 ; 0.038
Goodness of Fit Indicator	1.26
Max Shift/Error in Final Cycle	0.01
Maximum peak in Final Diff. Map	1.16 $e^-/\AA^3$
Minimum peak in Final Diff. Map	-0.69 $e^-/\AA^3$

Table 1. Atomic coordinates and B_{iso}/B_{eq}

atom	x	y	z	B_{eq}
I(1)	0.81498(5)	0.69883(6)	0.70339(7)	2.94(1)
I(2)	0.55426(6)	0.60832(6)	0.72332(8)	3.70(1)
I(3)	0.62374(5)	1.04241(5)	0.99484(7)	2.56(1)
Pd(1)	0.59461(6)	0.82167(6)	0.85151(7)	2.10(1)
N(1)	0.2775(6)	0.3930(7)	0.7410(9)	3.0(2)
C(1)	0.2070(8)	0.5441(9)	0.832(1)	3.6(2)
C(2)	0.1863(8)	0.6350(9)	0.736(1)	3.6(2)
C(3)	0.1278(9)	0.7821(9)	0.843(1)	3.9(2)
C(4)	0.088(1)	0.882(1)	0.753(1)	5.6(3)
C(5)	0.2365(9)	0.3133(9)	0.800(1)	3.7(2)
C(6)	0.1050(8)	0.3246(9)	0.737(1)	3.3(2)
C(7)	0.0561(9)	0.258(1)	0.814(1)	4.0(2)
C(8)	-0.0715(9)	0.2621(10)	0.739(1)	4.1(2)
C(9)	0.4207(9)	0.3455(9)	0.750(1)	3.7(2)
C(10)	0.4987(9)	0.2103(9)	0.634(1)	3.5(2)
C(11)	0.6384(9)	0.1811(10)	0.636(1)	3.7(2)
C(12)	0.7217(10)	0.043(1)	0.522(1)	4.9(3)
H(1)	0.2568	0.5635	0.9275	4.3062
H(2)	0.1254	0.5625	0.8626	4.3062
H(3)	0.2668	0.6123	0.6964	4.3565
H(4)	0.1297	0.6228	0.6456	4.3565
H(5)	0.1899	0.7950	0.9246	4.6598
H(6)	0.0539	0.7998	0.8934	4.6598
H(7)	0.1607	0.8661	0.7002	6.7040

Table 1. Atomic coordinates and B_{iso}/B_{eq} (continued)

atom	x	y	z	B_{eq}
H(8)	0.0537	0.9715	0.8280	6.7040
H(9)	0.0241	0.8727	0.6714	6.7040
H(10)	0.2358	0.3464	0.9170	4.4772
H(11)	0.2978	0.2205	0.7648	4.4772
H(12)	0.0461	0.4180	0.7614	3.9307
H(13)	0.1090	0.2821	0.6213	3.9307
H(14)	0.0460	0.3043	0.9292	4.7720
H(15)	0.1180	0.1658	0.7970	4.7720
H(16)	-0.1339	0.3537	0.7556	4.9558
H(17)	-0.0993	0.2208	0.7910	4.9558
H(18)	-0.0620	0.2142	0.6248	4.9558
H(19)	0.4368	0.4105	0.7297	4.3939
H(20)	0.4476	0.3429	0.8589	4.3939
H(21)	0.4643	0.2074	0.5256	4.1795
H(22)	0.4940	0.1428	0.6643	4.1795
H(23)	0.6425	0.2481	0.6043	4.4222
H(24)	0.6716	0.1861	0.7455	4.4222
H(25)	0.8083	0.0302	0.5298	5.8386
H(26)	0.7188	-0.0255	0.5525	5.8386
H(27)	0.6908	0.0367	0.4118	5.8386
H(28)	0.2523	0.3803	0.6267	3.6883
Pd(1*)	0.40539(6)	1.17833(6)	1.14849(7)	2.10(1)
I(3*)	0.37626(5)	0.95759(5)	1.00516(7)	2.56(1)
I(1*)	0.18502(5)	1.30117(6)	1.29661(7)	2.94(1)

Table 1. Atomic coordinates and B_{iso}/B_{eq} (continued)

atom	x	y	z	B_{eq}
I(2*)	0.44574(6)	1.39168(6)	1.27668(8)	3.70(1)

$$B_{eq} = \frac{8}{3}\pi^2(U_{11}(aa^*)^2 + U_{22}(bb^*)^2 + U_{33}(cc^*)^2 + 2U_{12}aa^*bb^*\cos\gamma + 2U_{13}aa^*cc^*\cos\beta + 2U_{23}bb^*cc^*\cos\alpha)$$

Table 4. Bond Angles(°) (continued)

atom	atom	atom	angle	atom	atom	atom	angle
H(12)	C(6)	H(13)	109.5	C(6)	C(7)	C(8)	111.8(8)
C(6)	C(7)	H(14)	109.0	C(6)	C(7)	H(15)	108.8
C(8)	C(7)	H(14)	109.0	C(8)	C(7)	H(15)	108.8
H(14)	C(7)	H(15)	109.3	C(7)	C(8)	H(16)	109.5
C(7)	C(8)	H(17)	109.5	C(7)	C(8)	H(18)	109.7
H(16)	C(8)	H(17)	109.3	H(16)	C(8)	H(18)	109.6
H(17)	C(8)	H(18)	109.3	N(1)	C(9)	C(10)	116.3(8)
N(1)	C(9)	H(19)	107.8	N(1)	C(9)	H(20)	106.6
C(10)	C(9)	H(19)	108.2	C(10)	C(9)	H(20)	108.2
H(19)	C(9)	H(20)	109.6	C(9)	C(10)	C(11)	111.8(8)
C(9)	C(10)	H(21)	108.9	C(9)	C(10)	H(22)	108.8
C(11)	C(10)	H(21)	108.9	C(11)	C(10)	H(22)	108.9
H(21)	C(10)	H(22)	109.5	C(10)	C(11)	C(12)	113.4(8)
C(10)	C(11)	H(23)	108.4	C(10)	C(11)	H(24)	108.4
C(12)	C(11)	H(23)	108.6	C(12)	C(11)	H(24)	108.4
H(23)	C(11)	H(24)	109.5	C(11)	C(12)	H(25)	109.4
C(11)	C(12)	H(26)	109.6	C(11)	C(12)	H(27)	109.5
H(25)	C(12)	H(26)	109.4	H(25)	C(12)	H(27)	109.4
H(26)	C(12)	H(27)	109.5				